

Czech Technical University in Prague  
Faculty of Electrical Engineering  
Department of Electric Drives and Traction

# **Compact Matrix Converter Power and Control System Design and Verification**

**Doctoral Thesis**

**Jan Bauer**

Prague, August 2014

Ph.D. Programme: Electrical Engineering and Information Technology  
Branch of study: Electric Machines, Apparatus and Drives

**Supervisor: Prof. Ing. Jiří Lettl, CSc.**

Ph.D. Thesis



Czech  
Technical  
University  
in Prague

**F3**

Faculty of Electrical Engineering  
Department of Electric Drives and Traction

# COMPACT MATRIX CONVERTER POWER AND CONTROL SYSTEM DESIGN AND VERIFICATION

**Jan Bauer**

Electrical Engineering and Information Technology - Electric Machines,  
Apparatus and Drives

August 2014

Supervisor: Prof. Ing. Jiří Lettl, CSc.



## Acknowledgement / Declaration

This thesis is result of my doctoral study at Czech Technical University in Prague, Faculty of Electrical Engineering, Department of Electric Drives and Traction. The work was partly supported by internal student grants of the Czech Technical University in Prague. The subject of the thesis is design and development of the prototype of the matrix converter with power of approximately 20 kW. Part of the thesis is also focused on the development of control algorithm for the drive with an induction machine and the above mentioned matrix converter. I would like to thank to my supervisor prof. Ing. Jiri Lettl, CSc. for his support while conducting research on this work. My greatest gratitude belongs to Ing. Stanislav Fligl Ph.D. for his support and undying supply of knowledge, ideas and motivation. Many other thanks goes also to the staff of the K13114, namely M. Krausova, M. Lev, P. Vozenilek, J. Zdenek and V. Hlinovsky, for creation of pleasant place for my work. Similar gratitude belongs to other Ph.D. students, who studied at the department in the same time and, who literally help me back on my feet, when I slipped and fell on my way to knowledge. I would also like to thank my family for their support and understandings, while I was spending my time working on this thesis. Special thanks goes to the local filial of Starbucks, because without their coffee, the thesis would not exist. :-)

I hereby declare that I have written my thesis on my own.

In Čelákovice

.....



## Abstract

Matrix converter is a frequency converter, which does not contain a DC-link and therefore no bulky passive accumulation element are needed as it is common in indirect frequency converters. That makes matrix converter perfect candidate for applications, where the DC-link is not allowed because of the volume or where the weight of the device is more important than its price. On the other hand the absence of the DC-link has serious drawbacks under operations on distorted supply and it also places some restrictions on the matrix converter capabilities. It is to underline that this converter produces output voltage by direct switching of the proper input voltage to the output terminals. This fact limits maximal output voltage amplitude to 86.6% of the input voltage amplitude. In contrast this way of conversion offers abilities as regulation of input power factor and possibility of the work in all four quadrants.

This thesis deals in particular with the design and development of the matrix converter and its control strategy. The power of the converter is aprox. 20kW. Bidirectional switches are made of IGBTs. On the input of the converter there is placed an input filter with added damping circuit to increase immunity against oscillations. The control part of the converter is based on FPGA circuit and RTD single board PC platform. The PC platform offers enough computational power including floating point arithmetics support for testing of new control algorithms. PC platform was selected because it is standardized for long time and realization, organization and communication of particular HW peripheries as communication busses, VGA, serial line are well documented. Though because the PC is going to be used for execution of control algorithm, which requires hard real time execution, it was necessary to develop own RT kernel for PC, that ensures execution of all required tasks and services with defined period under hard real time conditions. Control part of the converter was completed with the circuits for fast detection of the current polarity trough the bidirectional switch. These circuits will help in future when designing faster commutation strategies, where the accurate and instant information about current polarity is essential.

In order to test the abilities of the designed converter and the induction motor drive as whole the following: scalar control, field oriented control and current PWM control were implemented. For the field oriented control strategies, the actual position of the rotor flux space vector and its amplitude is key information. Several methods that can be used for estimation are mentioned in this work. Finally the Luenberger observer for estimation of induction machine rotor flux was designed for this purpose. Because the drive is not equipped with the speed sensor the designed observer was extended to be able to estimate speed of the drive too. In the thesis simulation and experimental results of several control strategies and also accuracy of estimator are compared.

In the final part of the work by the means of simulation it is analysed the ability of the converter to work with an induction generator in stand alone application. Self excited induction generators are typically used as low power sources in the areas where inexhaustible prime mover is present e.g. as wind or water, and at the same time the public supply network is not available. The induction generator requires for its function source of reactive power (capacitor bank). The parameters of generated voltage and power are reliant on angular speed of generator's rotor. In contrast the matrix converter connected to the generator is able to control excitation of the induction motor and also control quality of generated voltage on its input without any additional capacitor bank.

**Keywords:** Matrix Converter; Induction Machine; Field Oriented Control, Self Excited Induction Generator

## Abstrakt

Maticový měnič je tzv. přímý měnič kmitočtu, který nepotřebuje pro svoji činnost stejnosměrný meziobvod. Proto je maticový měnič vhodným kandidátem pro aplikace frekvenčního měniče, kde je potřeba řešit úsporu místa, nebo kde má přímé spínání vstupního napětí ekonomické výhody. Na druhou stranu absence meziobvodu může činit problémy při práci měniče na nestabilní napájecí síti. Maticový měnič vytváří výstupní napětí připínáním vhodného napětí přímo ze vstupu. Tím je omezena amplituda výstupního napětí na 86,6% amplitudy vstupního napětí. Na druhou stranu umožňuje tento způsob generování napětí regulaci účinníku na vstupu měniče a práci měniče ve čtyřkvadrantovém módu.

Tato práce se zabývá návrhem a stavbou prototypu maticového měniče a jeho řízením. Výkon měniče byl vzhledem k vybavení laboratoří katedry stanoven na 20 kW. Obousměrné spínače jsou realizovány pomocí IGBT tranzistorů. Na vstupu měniče je umístěn navržený LC filtr s tlumícím obvodem tak, aby byla zvýšena odolnost filtru proti nežádoucím kmitům. Řídicí část měniče je založena na FPGA obvodu a jednodeskovém PC od firmy RTD. Použití jednodeskového PC poskytuje dostatek výpočetního výkonu s podporou výpočtů v plovoucí řádové čárce pro testování nových řídicích strategií. PC platforma byla pro řízení měniče zvolena z důvodu dlouho trvající stability standartizace a kvalitní dokumentace jejich periferií. Protože je zde ale PC využito k řízení měniče, což definuje požadavky na nasazení tzv. hard real time aplikaci, bylo nutné vyvinout vlastní jádro řídicí aplikace, které je schopné zaručit vykonávání jednotlivých úkonů s pevnou periodou tzv. RT-kernel. RT jádro se tak stará o samotné periodické vykonávání řídicí strategie a obsluhu periferií měniče.

Za účelem otestování chování měniče a jeho řídicí části byl k měniči připojen asynchronní motor a v řídicí části měniče byly implementovány tyto řídicí strategie: skalární řízení, vektorové řízení a proudové řízení PWM. Při vektorovém řízení asynchronního motoru je klíčovou informací pro kvalitu řízení aktuální poloha a modul prostorového vektoru rotorového magnetického toku ve stroji. Část metod, které lze pro výpočet toku použít, je též zmíněna v této práci. Pro realizaci řízení byla v případě této práce použita metoda založená na Luenbergerově observeru. Protože testovaný pohon neobsahuje čidlo otáček, byl observer také rozšířen o estimátor otáček pohonu. V práci jsou dále porovnány výsledky odhadu při simulaci a při reálném řízení na pohonu s maticovým měničem.

V závěru práce je pomocí simulací analyzována schopnost maticového měniče pracovat s asynchronním motorem v režimu generátoru. Samonabuzovací asynchronní generátory jsou obvykle používány jako zdroje malých výkonů v oblastech, kde je k dispozici zdroj hnací síly, jako vítr nebo voda, a napájecí síť není k dispozici. Asynchronní generátor vyžaduje pro svou funkci zdroj jalového výkonu (kondenzátory). Parametry generovaného napětí a výkonu jsou závislé na úhlové rychlosti rotoru generátoru. Při spojení maticového měniče s asynchronním generátorem je měnič schopen řídit nabuzení asynchronního motoru a také kvalitu generovaného napětí na jeho vstupu bez připojení dodatečných kondenzátorů.

**Klíčová slova:** maticový měnič; asynchronní motor; vektorové řízení, asynchronní generátor

# Contents /

<b>1 Introduction</b> .....	1
1.1 Motivation .....	2
1.2 Current State of Art and Possible Application .....	2
1.3 Goals Formulation .....	4
<b>2 Systematics and Description of Frequency Converters</b> .....	5
2.1 History of Direct Frequency Converters.....	5
2.2 Matrix Converter Fundamentals .....	7
2.3 Commutation .....	10
2.3.1 Simple Commutation Strategies.....	12
2.3.2 Output Current Direction Based Commutation Method.....	12
2.3.3 Input Voltage Polarity Based Commutation Method .....	14
2.3.4 Comparison of Voltage and Current Based Commutation Strategies .....	15
2.3.5 Soft Commutation .....	16
2.4 Power Part of the Matrix Converter .....	16
2.5 Bidirectional switch topologies .....	17
2.5.1 Diode Bridge Topology ..	18
2.5.2 IGBT with Anti-parallel Diode Topology .	18
2.5.3 Special Modules for the Matrix Converter .....	19
2.6 Input Filter .....	23
2.6.1 Start Up Resistor .....	26
2.6.2 Series Damped LC Filter .....	26
2.6.3 Parallel Damped LC Filter .....	27
2.7 Overvoltage Protection .....	28
<b>3 Modulation and Control Strategies for the Matrix Converter</b> .....	31
3.1 Scalar Techniques .....	32
3.1.1 Direct Method - Venturini .....	32
3.1.2 Scalar Method - Roy.....	34
3.2 Direct Torque Control .....	35
3.3 Predictive Current Control ....	36
3.4 Space Vector Modulation.....	38
3.4.1 Direct Space Vector Modulation.....	38
3.4.2 Indirect Space Vector Modulation.....	40
<b>4 Problems of the Induction Motor Mathematical Description</b> .....	49
4.1 IM Description Based on State Variables .....	49
4.1.1 Torque Equation .....	53
4.2 Flux Estimation.....	54
4.3 Speed Estimation .....	56
<b>5 Matrix Converter Induction Motor Drive Control Strategies</b> .	61
5.1 Scalar Control Methods for IM .....	61
5.2 Vector Control Methods for IM .....	62
5.2.1 Indirect Rotor Field Oriented Control.....	63
5.2.2 Direct Rotor Field Oriented Control .....	63
5.2.3 Direct Torque Control ...	64
5.2.4 Predictive Control .....	65
5.2.5 Current Regulated PWM.....	66
5.2.6 Calculation of Current Set Points .....	66
<b>6 Compact Matrix Converter Realization</b> .....	69
6.1 Power Part Design .....	69
6.2 Input Filter .....	71
6.2.1 High Frequency Filter ...	72
6.2.2 Low Frequency Filter ....	73
6.3 Protections .....	76
6.3.1 Circuit Breaker .....	76
6.3.2 Varistors.....	76
6.3.3 Clamp Circuit.....	76
6.3.4 Driver Board .....	77
6.3.5 SW Protections .....	79

6.4 Control Part .....	79	B.1 Matrix Converter Parameters .....	137
6.4.1 New Matrix Converter Controller .....	80	B.2 Induction Motor Parameters ..	137
6.4.2 New Matrix Converter Control SW .....	82	B.3 DC Motor Parameters .....	137
6.4.3 Development of SW and Simulation of the User Control Application .....	84	B.4 Simulation Settings .....	137
<b>7 Matrix Converter Drive - Results of Tests .....</b>	<b>87</b>	B.5 Luenberger Observer Settings .....	138
7.1 Outline .....	87	B.6 Current PWM Controllers Setting.....	138
7.2 Flux Oriented Control Simulation .....	87	B.7 DRFOC Controllers Setting..	138
7.2.1 Luenberger Observer Speed Estimation .....	88	B.8 Self Excited Generator Model Parameters .....	138
7.2.2 Scalar Control Measurement .....	94	<b>C Wiring Diagram .....</b>	<b>139</b>
7.2.3 Direct Rotor Flux Oriented Control Simulation .....	95	<b>D Space Vector Definition .....</b>	<b>141</b>
7.3 Direct Rotor Flux Oriented Control Realization .....	97	<b>E Representation of Induction Machine in Three Phase System .....</b>	<b>144</b>
7.4 Current PWM Control Simulation .....	101	E.1 IM Equations in Different Coordinate Systems.....	146
7.5 Current PWM Control Realization .....	103	<b>F List of Author's Publications ...</b>	<b>149</b>
<b>8 Application of Matrix Converter with Induction Generator .....</b>	<b>107</b>	F.1 Publications Related to Thesis .....	149
<b>9 Conclusion .....</b>	<b>121</b>	F.1.1 Publications in Journals with Impact Factor .....	149
9.1 Overview of the results .....	121	F.1.2 Publications in Reviewed Journals .....	149
9.2 Suggestions for the Future Work.....	123	F.1.3 Patents .....	149
9.3 Fullfillment of the Objectives Defined in Section 1.3 .....	124	F.1.4 Publications Excerpted in Web of Science....	149
<b>References .....</b>	<b>125</b>	F.1.5 Other Publications.....	150
<b>A Nomenclature .....</b>	<b>135</b>	F.2 Other Publications.....	150
A.1 Notation of Mathematical Symbols .....	135	F.2.1 Publications in Journals with Impact Factor .....	150
A.2 Glossary of Symbols and Variables .....	135	F.2.2 Publications in Reviewed Journals .....	151
A.3 Subscripts .....	136	F.2.3 Patents .....	151
A.4 Abbreviations .....	136	F.2.4 Publications Excerpted in Web of Science....	151
<b>B Parameters Set in Models.....</b>	<b>137</b>	F.2.5 Other Publications.....	151
		F.3 Responses to Published Works.....	153
		<b>G CV .....</b>	<b>155</b>

## Tables / Figures

<p><b>2.1.</b> Comparison of frequency converter topologies .....9</p> <p><b>2.2.</b> Loss comparison of RB-IGBT . 21</p> <p><b>2.3.</b> Summary of modules suitable for matrix converter ..... 22</p> <p><b>3.1.</b> Comparison of control and modulation strategies ..... 32</p> <p><b>3.2.</b> DSVM vectors and switching states ..... 38</p> <p><b>3.3.</b> Active vectors composition .... 39</p> <p><b>3.4.</b> Available vector combinations of virtual inverter stage.. 43</p> <p><b>3.5.</b> Available vector combinations of virtual rectifier stage.. 44</p> <p><b>3.6.</b> Switching table for ISVM..... 44</p> <p><b>3.7.</b> Optimized switching table for ISVM ..... 46</p> <p><b>4.1.</b> Recalculation coefficients for electromagnetic torque..... 53</p> <p><b>6.1.</b> Transistor Modules Parameters..... 70</p> <p><b>6.2.</b> 3ELF25ET parameters..... 72</p> <p><b>6.3.</b> Polarity detector states ..... 78</p> <p><b>6.4.</b> Software protection limits ..... 79</p> <p><b>E.1.</b> Coefficients used in Clark's transformation ..... 145</p>	<p><b>1.1.</b> Clasification of frequency converters.....2</p> <p><b>1.2.</b> Low power matrix converter by Yaskawa .....3</p> <p><b>1.3.</b> Medium power matrix converter by Yaskawa.....3</p> <p><b>2.1.</b> Soft starter .....5</p> <p><b>2.2.</b> Cycloconverter .....6</p> <p><b>2.3.</b> Principle of matrix converter ....6</p> <p><b>2.4.</b> Bidirectional switch topology ....7</p> <p><b>2.5.</b> Indirect matrix converter topology .....7</p> <p><b>2.6.</b> Rectifier side of matrix converter .....8</p> <p><b>2.7.</b> Multilevel matrix converter topology .....8</p> <p><b>2.8.</b> Example of switching combination RTS ..... 10</p> <p><b>2.9.</b> Synchronous switching combinations..... 11</p> <p><b>2.10.</b> Inverse switching combinations ..... 11</p> <p><b>2.11.</b> Active/pulsating switching combinations ..... 11</p> <p><b>2.12.</b> Zero switching combinations... 11</p> <p><b>2.13.</b> Matrix converter commutation ..... 12</p> <p><b>2.14.</b> Example of phase commutation ..... 13</p> <p><b>2.15.</b> Current polarity based commutation methods..... 14</p> <p><b>2.16.</b> Voltage polarity based commutation methods..... 15</p> <p><b>2.17.</b> Current polarity detection circuit ..... 16</p> <p><b>2.18.</b> Block diagram of the matrix converter..... 17</p> <p><b>2.19.</b> Bidirectional switch - diode bridge topology ..... 18</p> <p><b>2.20.</b> Bidirectional switch - common collector topology ..... 18</p> <p><b>2.21.</b> Bidirectional switch - common emitter topology ..... 18</p> <p><b>2.22.</b> Bidirectional switch - without central connection ..... 19</p>
--	--

2.23.	Bidirectional switch - reverse blocking IGBT topology .....	19
2.24.	IGBT packages .....	19
2.25.	Bidirectional switch DIM400PBM17-A000 .....	20
2.26.	Bidirectional switch SML150AT06 .....	20
2.27.	Bidirectional switch Econo-MAC .....	21
2.28.	Bidirectional switch based on JFET .....	21
2.29.	Bidirectional switch RB-IGBT .....	22
2.30.	Bidirectional switch RB-IGBT structure .....	22
2.31.	LC filter topologies .....	24
2.32.	LC filter phasor diagram .....	24
2.33.	Influence of filter damping .....	26
2.34.	LC filter with start up resistor ..	26
2.35.	LC filter with series damping ..	27
2.36.	Transfer function of series damped LC filter .....	27
2.37.	LC filter with parallel damping .....	28
2.38.	Transfer function of LC filter with parallel damping .....	28
2.39.	Multi section LC filter .....	29
2.40.	Clamp circuit .....	30
2.41.	Varistor protection .....	30
2.42.	Switch with integrated clamp ..	30
3.1.	Matrix converter modulation and control techniques summary .....	31
3.2.	Voltage ratio 50% .....	34
3.3.	Voltage ratio 86.6% .....	34
3.4.	Block diagram of the DTC ....	36
3.5.	Block diagram of the PCC .....	37
3.6.	Available voltage vectors common inverter SVM .....	39
3.7.	Output voltage and input current space vector hexagon ..	39
3.8.	Output voltage and input current space vector detail .....	39
3.9.	Matrix converter representation for indirect modulation ...	40

<b>3.10.</b>	Example of switching combination .....	42
<b>3.11.</b>	Example of switching combination .....	42
<b>3.12.</b>	Virtual inverter and virtual rectifier stages space vectors ...	43
<b>3.13.</b>	Example of ISVM switching sequence .....	47
<b>3.14.</b>	Example of optimized ISVM switching sequence .....	47
<b>4.1.</b>	Current model of IM .....	55
<b>4.2.</b>	Voltage model of IM .....	56
<b>4.3.</b>	Model reference adaptive system block diagram .....	57
<b>4.4.</b>	Block diagram of Luenberger observer .....	57
<b>5.1.</b>	Voltage type scalar control ....	61
<b>5.2.</b>	Current type scalar control ....	62
<b>5.3.</b>	Block diagram of the FOC.....	62
<b>5.4.</b>	Block diagram of the IRFOC ..	63
<b>5.5.</b>	Block diagram of the DRFOC .	64
<b>5.6.</b>	Block diagram of the DTC proposed by Takahashi .....	65
<b>5.7.</b>	Predictive current controller ...	66
<b>5.8.</b>	Current regulated PWM structure .....	67
<b>5.9.</b>	Current set point limit .....	67
<b>6.1.</b>	GD401-70-12 module.....	70
<b>6.2.</b>	Interconnections between IG-BT modules .....	70
<b>6.3.</b>	Interconnections boards.....	71
<b>6.4.</b>	Equivalent circuit modelling of the radiator .....	71
<b>6.5.</b>	High frequency filter topology .	72
<b>6.6.</b>	DM and CM interference suppression principle .....	73
<b>6.7.</b>	LC filter without damping .....	74
<b>6.8.</b>	LC filter with series damping ..	75
<b>6.9.</b>	LC filter with parallel damping .....	75
<b>6.10.</b>	Losses in damping circuit .....	76
<b>6.11.</b>	HCPL-316J connection .....	77
<b>6.12.</b>	Current polarity detection ....	78
<b>6.13.</b>	Former matrix converter controller .....	80

<b>6.14.</b>	Conception of proposed controller .....	81
<b>6.15.</b>	Matrix converter control part blocks .....	81
<b>6.16.</b>	CPU module and ADC module .....	82
<b>6.17.</b>	Real time application flowchart .....	83
<b>6.18.</b>	Real time application screenshot .....	84
<b>6.19.</b>	Compilation of parts of application .....	85
<b>6.20.</b>	Simulation testing .....	86
<b>7.1.</b>	Test bed for drive testing .....	87
<b>7.2.</b>	Simulation of Luenberger observer rotor flux estimation ....	90
<b>7.3.</b>	Speed estimator simulation ....	90
<b>7.4.</b>	Flux components estimator simulation .....	91
<b>7.5.</b>	Current components estimator simulation .....	92
<b>7.6.</b>	Comparison of observed and measured speed .....	93
<b>7.7.</b>	Results of the rotor flux estimation on real drive .....	93
<b>7.8.</b>	Measured input/output waveforms - scalar control ....	94
<b>7.9.</b>	Measured input/output waveforms - scalar control ....	95
<b>7.10.</b>	DRFOC control - flux and speed controller simulation ....	96
<b>7.11.</b>	DRFOC control - current component controllers reaction .....	97
<b>7.12.</b>	DRFOC control - $\Psi_r$ trajectory .....	97
<b>7.13.</b>	DRFOC control - flux and speed controller reaction .....	98
<b>7.14.</b>	DRFOC control - reaction to load step .....	99
<b>7.15.</b>	DRFOC control - current component controllers reaction .....	100
<b>7.16.</b>	DRFOC control - $\Psi_r$ trajectory .....	100

<b>7.17.</b>	Current PWM control - flux and speed controller simulation .....	101
<b>7.18.</b>	Current PWM control - current controllers reaction.....	102
<b>7.19.</b>	Current PWM control - $\Psi_r$ trajectory .....	103
<b>7.20.</b>	Current PWM control - current controllers reaction.....	104
<b>7.21.</b>	Current PWM control - flux and speed controller reaction .	105
<b>7.22.</b>	Current PWM control - $\Psi_r$ trajectory .....	105
<b>8.1.</b>	Self excited induction generator schematics .....	108
<b>8.2.</b>	Variation of magnetising inductance $L_m$ with phase voltage .....	109
<b>8.3.</b>	Equivalent circuit of the SEIG .....	109
<b>8.4.</b>	Block diagram of the proposed control structure for the SEIG .....	110
<b>8.5.</b>	Controllers reaction during SEIG operation.....	111
<b>8.6.</b>	Generator behaviour simulation .....	112
<b>8.7.</b>	Matrix converter output and input voltage and current waveforms .....	113
<b>8.8.</b>	Matrix converter output and input voltage and current waveforms details .....	114
<b>8.9.</b>	Controllers reaction during SEIG operation.....	115
<b>8.10.</b>	Matrix converter output and input voltage and current waveforms details .....	116
<b>8.11.</b>	Controllers reaction during SEIG operation.....	117
<b>8.12.</b>	Matrix converter output and input voltage and current waveforms details .....	118
<b>8.13.</b>	Harmonics analysis of generated current .....	119

<b>8.14.</b>	Harmonics analysis of generated current .....	119
<b>8.15.</b>	Harmonics analysis of generated current .....	120
<b>E.1.</b>	3 phase representation of IM..	144
<b>E.2.</b>	Stator current in three phase / orthogonal system.....	145

# Chapter 1

## Introduction

Electric drive is an electromechanical energy converter. The own transformation of electric energy to the mechanical one is ensured by the electric motor. For the demanded conversion of the energy the motor needs to be provided with proper voltages, currents and frequency on its input terminals. In case of greater demands as if the high dynamic of the motor is required, a converter is mostly connected in front of the motor.

The advantages of modern regulated electric drive can not be questioned. But the way to them lasted long time. The first usable electrical machine was introduced at the beginning of the 20<sup>th</sup> century. It was obvious from the beginning that especially their regulation is essential for their further effective application. First attempts were done with the assistance of mechanical converters like Ward – Leonard machine set.

With the development of the power electronics, these pure machine sets were slowly replaced. At first it were mercury rectifiers, which played the role of a successor. And later after the discovery of the transistor, the other upcoming semiconductor structures started to dominate.

The next important moment of the development was the replacing analogue regulators with microcontrollers. The last development progress can be dated to the year 1990, when the IGBT transistor was introduced for the first time. Since that time the IGBT transistors clearly prevail in power converters up to now. They are being manufactured in the wide range of powers, they endure a current of up to 2.4 kA and a voltage of up to 6.5 kV.

Similarly as the DC machine needs for its regulation a controlled rectifier, the induction machine requires an inverter or frequency converter, both including an appropriate control algorithm. The algorithms based on separated control of the motor flux and torque are used in order to gain the maximum performance from the induction machine.

Recently the drives with the asynchronous motors becomes to the most spread ones in the field of regulated drives[1–4]. The frequency converters needed in order to control the asynchronous motors can be constructed in various ways and thus split into various categories. E.g. according to the presence of the accumulation element the converters can be divided into following two groups [4–5]:

- Indirect frequency converters
- Direct frequency converters

The main drawback of the indirect frequency converters (Fig. 1.1) is that they contain a DC-link equipped with passive accumulation elements - inductors or capacitors. Since the corresponding operational frequency is typically in the range from 33 to 120 Hz, the passive elements are often very bulky and introduce additional power losses to the converter. Moreover the electrolytic capacitors used in the DC-links are subjects of ageing, therefore they are not suitable for all kinds of applications. That is why the research of pure semiconductor AC/AC converter topologies (direct frequency converters) has started.

Direct frequency converters (Fig. 1.1) could be also divided further into several subgroups. Among this group generally there are ranked all converter topologies converting

AC to AC energy without any DC-link accumulation elements. Also the conventional matrix converter belongs to this category. Such matrix converter is in general an array of bidirectional semiconductor switches that can connect directly the three phase source to the load and thereby create an output voltage system with an arbitrary output frequency.

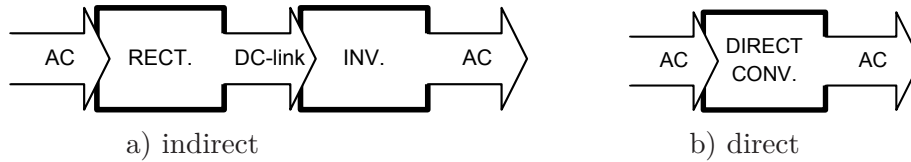


**Figure 1.1.** Classification of frequency converters

## 1.1 Motivation

The area of the regulated AC drives is very wide. But most of them are based on the induction machines and frequency converters. Compared to the indirect frequency converter matrix converter shows several advantages. At our department there had been already built one prototype of the matrix converter in 2003 and it was improved later in case of Ph.D. works defended in 2006 and 2010. But the rapid development in the field of the induction motor control strategies causes that more computational power is required from the converter's control part. The old prototype was not able to offer enough throughput to test new contemporary control strategies. That is why I have chosen to deal with the topics of the matrix converter drive in my Ph.D. thesis including the design and construction of the new compact prototype of the matrix converter. It is described in the first part of the thesis. The second part deals with the design of control algorithm for the induction machine based on vector control strategy.

## 1.2 Current State of Art and Possible Application

In former Czechoslovakia the Czech Academy of Science in Prague was dealing with the matrix converter topic in late eighties.

In late nineties and after year 2000 the research was conducted at the University of Žilina in the Slovakia. The results were published by Havrila and Dobrucký. The research was focused on building of the matrix converter with power of circa 200W loaded with a RL load.

In the Middle and East Europe many interesting articles were published by researches from the Ukraine, Latvia and Poland. Also in Germany there were created many publications, among others e.g. [6–7], a function sample of the matrix converter is at the University of Chemnitz. Several theses came from the University of Karlsruhe and the University of Hannover. Obligatorily, a couple of publications also come from the RWTH Aachen.

Recently, especially the modified topologies of the matrix converter as indirect, sparse and multilevel topologies have become popular. The Aalborg University in Denmark is dealing intensively with this issue [8–11] and also the Swiss Federal Institute of Technology in Zurich in Switzerland contributed significantly to this topic [12–15] At the University of Tampere there was written at least one Ph.D. thesis in the the field of matrix converters as well [16]. Matrix converter and its derived topologies e.g. multilevel, sparse, more phase topologies are also very popular in Asia [17–23].

The development and state of art of the matrix converter research are nicely described in [12, 24–26], therefore these publications are recommended as basics to interested readers in order to achieve the precognition necessary.

There is also a very active team in this field in Great Britain - PEMC Group at School of Electrical and Electronic Engineering University of Nottingham. They publish frequently in this field up to these days [27–31].

Nevertheless the matrix converter still does not seem to be widely in industrial use. As the main reason it can be assumed, that the topology incorporate too much power semiconductor devices and their price is still not negligible. Moreover the matrix converter is susceptible to input voltage disturbances, it requires unreliable over voltage protection, or complicated bidirectional switches with difficult commutation strategies. But, even nor the effort of one of the biggest semiconductor manufacturer Semikron to develop and introduce integrated MC modules, has not helped much [32]. However some of disadvantages of the MC can be possibly overcome with the utilisation of the new SiC devices. The PEMC group around P. Wheelner and other authors are already testing such topology with these devices and publishing results in articles [22, 27–28, 33–34]. This opinion is supported by the fact, that on EPE 2014 conference there will be held a dedicated tutorial session about "Matrix Converters: Implementation and Industrial Applications".

The company Yaskawa have already developed the very first serially produced matrix converters. Two product lines are offered at the market. A low voltage series Varispeed AC has been designed for 200 V and 400 V and power range from 5.5 kW to 75 kW (Fig. 1.2) [35]. A medium voltage series FSDrive-MX1S is available for rated voltages 2 kV and 6 kV and power range from 3 MVA to 6 MVA (Fig. 1.3) [36].



**Figure 1.2.** Low power matrix converter by Yaskawa



**Figure 1.3.** Medium power matrix converter by Yaskawa

At the Czech Technical University in Prague at the The Department of Electric Drives and Traction the research in field of matrix converter started at the beginning

of last decade. The first Ph.D. thesis was successfully defend by S. Fligl in 2006 [37]. Within this work a prototype of 12 kW matrix converter was built. The second Ph.D. thesis was defended by D. Kuzmanovic in 2010 [38], who was focusing on the DTC control strategy for the IM drive with matrix converter. During this period also several related bachelor and master theses were defended. They were dealing with the design of new prototype of the matrix converter, conducted under the supervision of J. Lettl and S. Fligl [39–42]. Recently a dissertation focusing on the modulator for the matrix converter compact prototype was submitted by P. Posta to the Office for research in fulfilment of the requirements for the degree of doctor of philosophy [43]. In this respect it is worth collecting the knowledge and experience together into one work and extend it with some application examples.

## 1.3 Goals Formulation

Main goal of the thesis are to summarize recent pieces of knowledge at our department in the area of matrix converters and based this knowledge to design and practically realise both power part and control part of a compact matrix converter including selection and implementation of control algorithms for three phase induction machine, whereas precise design and realization of the switching algorithm is part of other work. From this follows goals of the thesis:

- Design of whole circuit configuration of the compact matrix converter's power part and selection of its components with emphasis to predefined requirements.
- Selection of input filter topology, its components's parameters design, with the aim of minimization of the power losses of the filter damping circuit.
- Design of suitable protections for developed power part of the converter.
- Choice of the appropriate platform for control part of the converter and whole drive, with respect to required and further assumed computational power, with improved current polarity detection in the bi-directional switch.
- Analysis, comparison and implementation of appropriate control strategy for the induction machine drive.
- Analysis, design and implementation of convenient way of induction machine's speed and flux values identification.
- Integration of compact matrix converter power and control part; further implementation of control algorithms and consecutive verification of functionality of the realised system.
- Analysis of the possibilities of matrix converter deployment in an off grid system and induction generator.

## Chapter 2

# Systematics and Description of Frequency Converters

### 2.1 History of Direct Frequency Converters

The first direct frequency converters were introduced in 1960s after the invention of the thyristors. The first representative of AC/AC converters is depicted in Fig. 2.1. This topology is known as soft starter and is used for regulation of effective value of output voltage, but the output frequency remains unchanged [3, 5].

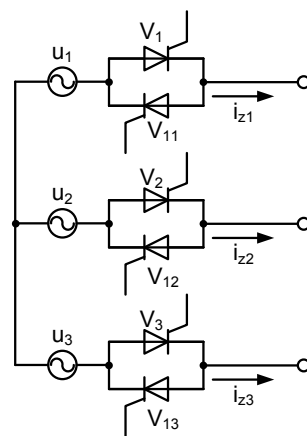
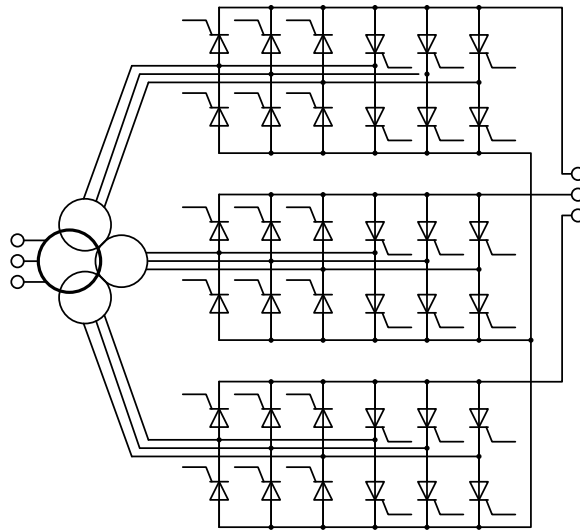


Figure 2.1. Soft starter

Another representative of this category, that in contrast to the previous one is able to change output frequency too is the cycloconverter Fig. 2.2 [3, 44–46]. A cycloconverter is made of two anti parallel six pulse rectifiers for each phase. The voltage on the output of the converter can be changed by control of the rectifiers output voltage. The output voltage and current waveforms are heavily distorted and the power factor is very low too. The main disadvantage is the amount of used thyristors and the fact, that maximal reachable output frequency is approximately one half of input frequency. The only advantage is robustness due to thyristor technology.

Therefore the research in the field of the direct frequency converters turns to the force commutated cycloconverters. The first attempts were done with thyristors with external force commutation circuits. But the power circuit with this solution was bulky and the efficiency was poor. The topology becomes more attractive when the power transistor was firstly introduced. But the real development of the matrix converter was kicked off by Venturini and Alesina in 1980 [47–48]. They presented the converter with bidirectional switches and they introduced the name „Matrix converter“.



**Figure 2.2.** Cycloconverter

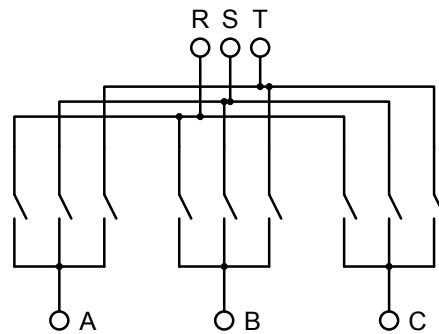


**Figure 2.3.** Principle of matrix converter

Fig. 2.3 shows schematics of the 3 x 3 matrix converter where each switch represents so called bidirectional switch that can conduct current and block voltage in both directions according to the control signal [25]. To permit the power flow in both directions the switches can be realized in several ways. The topologies in Fig. 2.4a, Fig. 2.4b are the spread ones. They are made of two transistors connected with common collector resp. emitter and two anti parallel diodes. The 3x3 MC in Fig. 2.3 has 9 bidirectional switches. That means 18 transistors and 18 diodes are required to realize power part of the converter. It can be said that the relatively large number of semiconductors is the reason of the converter's higher cost. That is why several topologies with reduced semiconductor numbers were developed too. Because of the reduced number of semiconductors they are sometimes called spares matrix converter topologies. Some of them will be listed now. The indirect matrix converter topology Fig. 2.5 is created by a direct connection of rectifier part and inverter part without DC-link element. Both parts of the converter can be then controlled separately and known control strategies can be applied on them. However because of the absence of the DC-link they must be synchronized precisely. Another drawback is higher conduction losses, since the current must flow through 3 semiconductors [16].



Figure 2.4. Bidirectional switch topology

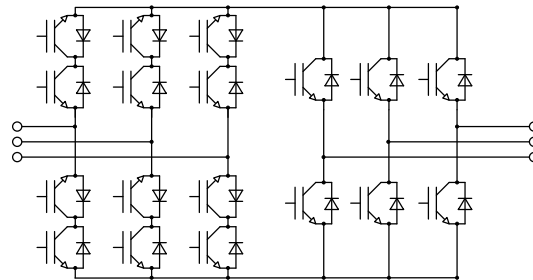


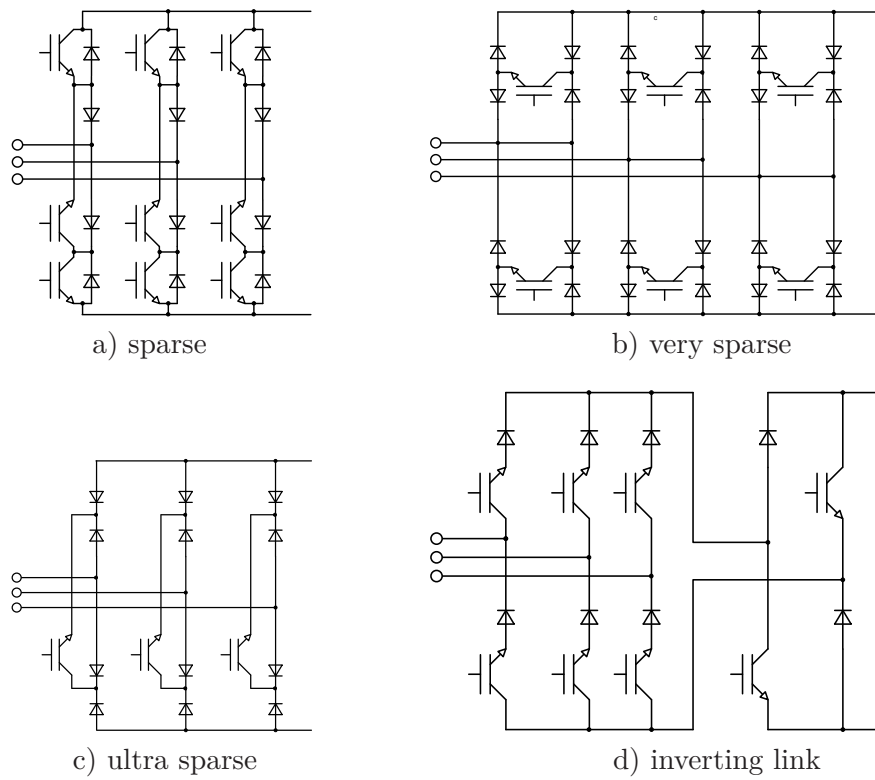
Figure 2.5. Indirect matrix converter topology

Fig. 2.6 shows several other „cost saving“ realizations of the input rectifier parts. The output is made as common two level inverter [25, 49–50]. Recently the so called multilevel converter topologies have become popular. They are eligible for operation on voltage levels that are not suitable for single semiconductor device. They are mostly realized as several transistors connected in series with some additional elements for voltage balancing between the transistors. These multilevel inverter topologies can be easily added to the sparse matrix converter instead of two level inverter. The classical matrix converter topology can be extended to multilevel as shown in Fig. 2.7a. The switches are then realized as shows Fig. 2.7b. There is therefore difference between the classical and multilevel matrix converter. The converter enables both increasing and decreasing of the voltage and frequency too. Each switching cell is clamped with capacitor, whose voltage can be regulated. The multilevel switches can be connected into series and used for generation of new voltage levels at the converter output. The commutation of the cell switches is also simpler than by conventional matrix converter. However with each additional cell it rises the amount of semiconductor devices and requirements on controller computational power.

There exists also other topologies named as matrix converter like single phase matrix converter or matrix converters with more output phases. But they are only distant relatives named because their power topology can be organized into sub blocks that form matrix shape. They are not listed here. To avoid misunderstandings, the term matrix converter means in this thesis three phase to three phase topology with bidirectional switches realized as in Fig. 2.4b. Just for comprehensible comparison the topologies mentioned above are summarized in Tab. 2.1.

## 2.2 Matrix Converter Fundamentals

The matrix converter uses nine bidirectional switches to transfer voltage from its input to the output, but compared to the indirect frequency converters it offers also some benefits among its features:



**Figure 2.6.** Rectifier side of matrix converter

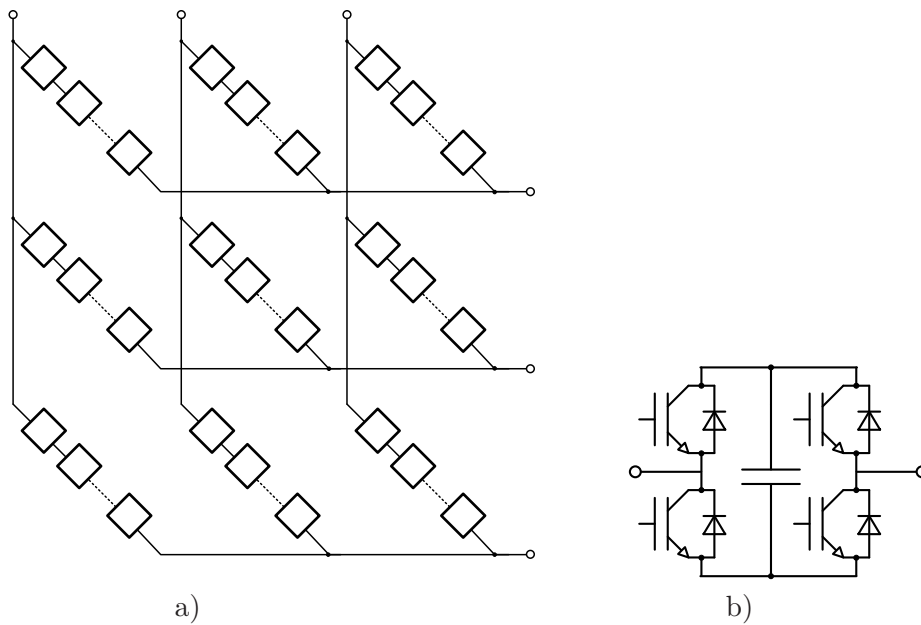


**Figure 2.7.** Multilevel matrix converter topology

- The output frequency is nearly without limits. The only limit is the maximal switching frequency of the used devices.
- It has relative simple power circuit, indirect frequency converters comprises of rectifier part, inverter part and DC-link with passive accumulation element. Matrix

		Passive semi-conductors	Active semi-conductors	Output frequency	Supply current	Number of Isolated gate potencial
Indirect frequency converter	CSC	12	12	Not restricted	Sinusoidal	8
	VSC	12	6	Not restricted	Distorted	4
Direct frequency converter	Softstarter	0	6 thyristor	$f_{out} = f_{in}$	Distorted	6
	Cycloconv.	0	36 thyristor	$f_{out} \leq \frac{2}{5} f_{in}$	Distorted	15
	DMC	18	18	Not restricted	Sinusoidal	9
	IMC	18	18	Not restricted	Sinusoidal	9
	SMC	18	15	Not restricted	Sinusoidal	7
	VSMC	30	12	Not restricted	Sinusoidal	10
	3 level MC	72	72	Not restricted	Sinusoidal	54

**Table 2.1.** Comparison of frequency converter topologies

converter has only 9 bidirectional switches. They are mostly realised from discreet semiconductor modules, but several manufactures already offers integrated compact IGBT based modules.

- The features of the matrix converter are the same as of a VSI with Active Front End on its input. But the drawback is, that because of the absence of the DC-link, the output voltage amplitude is limited to 86,6% of the input voltage amplitude if we wish to maintain sinusoidal input currents.
- Sinusoidal input and output currents.
- Power factor control.
- Operation in all four quadrants.
- Smaller proportion of pasive components

Each bidirectional switch of the converter can be either in on or off state. From this it follows that exists  $2^9 = 512$  possible switching combinations [24–25]. Because of the input and output behaviours the restrictions on the switching states can be expressed:

- The input of the matrix converter can be considered as voltage source, therefore in every switching moment none of the input phases shall be short circuited.
- The load connected to the output of the converter has mostly inductive character. None of the converter output phases may be disconnected.

When we follow these restrictions, from initially 512 possible combinations there remain  $3^3 = 27$  only. That means there are 27 voltage vectors that can be provided on the output of the converter. They can be further divided into:

- Synchronously rotating vectors
- Inversely rotating vectors
- Pulsing / active vectors
- Zero vectors

The orientation and the effects of the vectors are summarised in Fig. 2.9 - 2.12. In order to make the description of the state of each particular switch more transparent, we should develop an appropriate coding. When we take into account that each output

phase must be at every moment connected to only one input phase, the easiest way of designation is to write the symbols of the input phases to which output phase are connected (see example in the Fig. 2.8). This method of designating the switching combination will be used in this thesis.

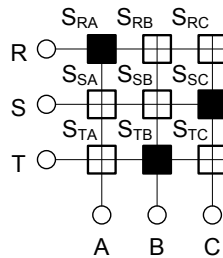


**Figure 2.8.** Switching combination RTS

The 6 rotating vectors are created by switching of each output phase to different input phase. This creates vector, that rotates with the frequency of mains, either in same direction as the input voltage vector for those synchronously rotating ones or in opposite direction for inversely rotating ones. They have the same module as the input voltage space vector and their displacement to input voltage space vector can be, depending on the combination of switches (RST, STR, TRS),  $0^\circ$ ,  $120^\circ$  or  $240^\circ$ .

The 18 active vectors have amplitude of the switched line to line voltage. The output voltage and input current have fixed directions. Their amplitude vary with the angle of input voltage and output current respectively. So when they are switched permanently their amplitude will be pulsating from maximal value with positive sign to maximal value with negative sign. They are produced, when two output phases are switched to one input phase. The last group of vector is made by switching all output phase to one input phase (free-wheeling the load current). Which switching combination will be selected to produce zero vector depends on a particular criterion chosen in order to minimise number of commutations, e.g. if a combination RRT is switched and zero vector shall follow, then RRR will be selected.

The output voltage of the matrix converter is synthesised from these vectors. The indirect modulation methods use only active and zero voltage vectors. In this way the modulation strategy is very similar to indirect frequency converters.

## 2.3 Commutation

Passing of the current from one switch to another is more difficult in matrix converter than in conventional VSI, because matrix converter lacks natural free-wheeling paths. Moreover due to the typical parameters of mains the input must be equipped with a LC filter. This guarantees the voltage source type input (filter capacitors) and enables to connect resistive or inductive load to the output of the converter. In other words there must always be conducting path on the load side of the converter and input cannot be ever short circuited. Otherwise it will cause voltage or current spikes, that should damage the semiconductors. The problems of short circuiting the input voltage or cutting off the output current can be avoided under normal operation conditions by controlling of device turn on and turn off switching separately. These methods are usually called commutation strategies. The aim of the commutation strategy is

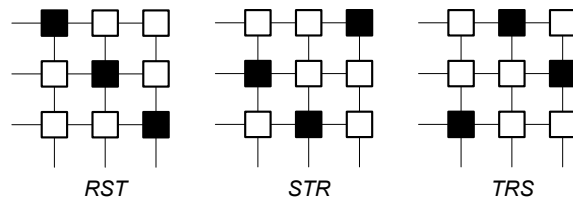


Figure 2.9. Synchronous switching combinations

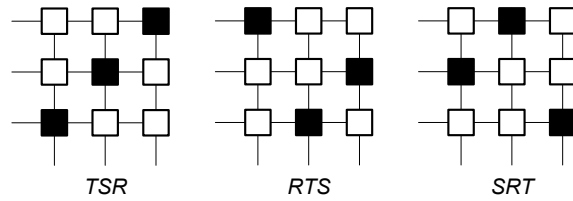


Figure 2.10. Inverse switching combinations

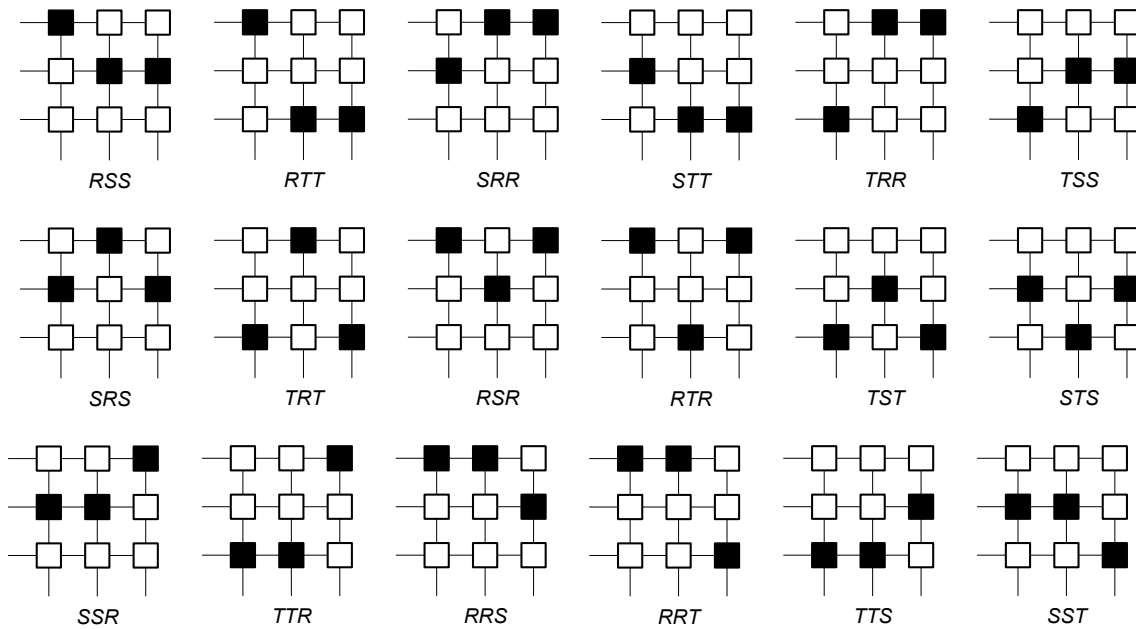


Figure 2.11. Active/pulsating switching combinations

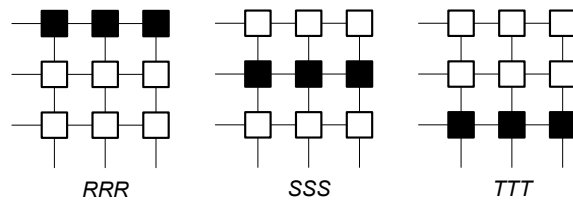


Figure 2.12. Zero switching combinations

to perform the commutation in steps, so the short- and open- circuit situations are avoided. Thus, the bidirectional switch have to be realised so that the direction of the current through the switch can be controlled. E.g. when using the transistor placed in a bridge of free-wheeling diodes the current cannot be controlled. It means when we turn on the bidirectional switch it will operate at all four quadrants and such bidirectional switch, despite of its simplicity, is not suitable for practical use.

Above that, the real semiconductor switch has some finite switch over time that must be taken into account too. When the current changes its sign the opposite diode will automatically start conducting. Therefore several commutation strategies based on the knowledge either of current or voltage polarity were developed [6–7, 51–59]. The brief summary of most used approaches follows in next subchapters.

### 2.3.1 Simple Commutation Strategies

Conventional VSI uses short time gap, also called deadtime, inserted between switching of upper and lower switch inside one leg in order to avoid short-circuit. In case of matrix converter the commutation with deadtimes will cause open-circuit of the load and thereby large voltage spikes Fig. 2.13b. These spikes can destroy the switches, therefore snubbers or clamp circuit are needed to ensure the current path during the deadtime. However this method will cause high power losses in snubber circuit during each commutation.

Another possible solution is to insert short overlap in the switching pulses. This will cause short-circuit during the overlap Fig. 2.13a, therefore extra line inductance should be added to slow the rise of the current. Of course this will be connected with the growth of the conduction losses, because the inductors are placed into main conduction path. Moreover there will be significant distortion of the output voltage waveform during the overlapping. Above discussed disadvantages caused that also advanced commutation methods were developed [7]. One is based on knowledge of output current direction and second on the knowledge of the input voltage polarities.

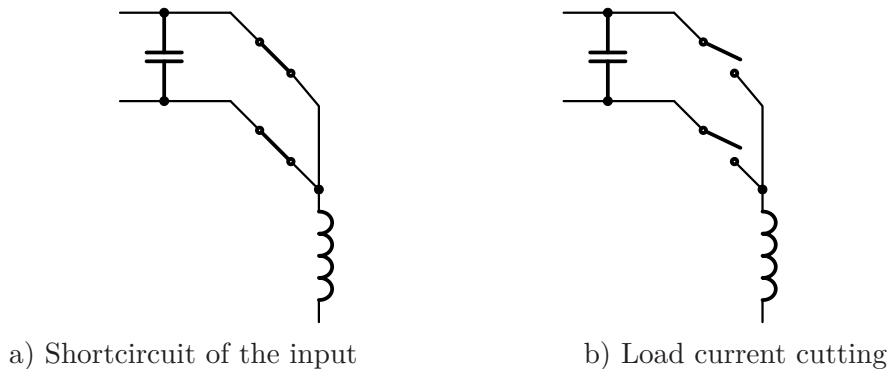


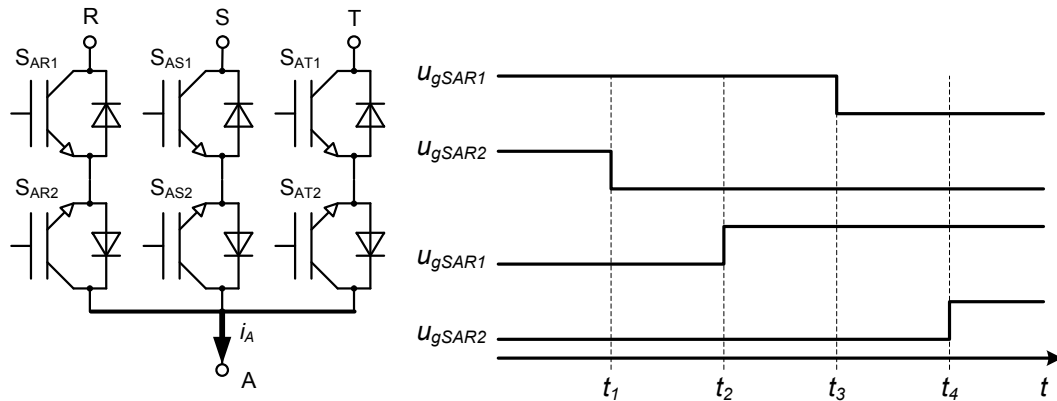
Figure 2.13. Matrix converter commutation

### 2.3.2 Output Current Direction Based Commutation Method

This method is based on the direction of the output current. Its principle is depicted in Fig. 2.14. Three bidirectional switches corresponding to the phase  $A$  are depicted in Fig. 2.14a. Fig. 2.14b shows gate signals for the transistors during the commutation process of the current  $i_A$  from phase R to phase S. Before the procedure starts  $S_{AR1}$  and  $S_{AR2}$  are on and  $S_{AR1}$  conducts current. The commutation procedure starts at  $t_1$  when non-conducting switch  $S_{AR2}$  is switched off. Next step is performed in  $t_2$  when switch  $S_{AS1}$  that conducts in direction of  $i_A$  in the next phase is switched on. In  $t_3$  the presently conducting switch  $S_{AR1}$  is turned off. The commutation is finished in  $t_4$  when the non-conducting transistor of the bidirectional switch  $S_{AS}$  is switched on. The instant of the current commutation presented in Fig. 2.14 depends on the polarity of the line to line voltage  $u_{RS}$ . If the  $u_{RS} \geq 0$  then the commutation occurs at  $t_3$  otherwise if

$u_{RS} \leq 0$  then the commutation occurs at  $t_2$ . When the commutation appears at the  $t_3$  the turn off of  $S_{AR1}$  is hard turn off and other switching are soft, because the positive  $u_{RS}$  is held by non-conducting anti parallel diode of  $S_{AR1}$ . In case of commutation process in  $t_2$  the turn off of the  $S_{AR1}$  is soft and both turn on of the  $S_{AS1}$  and turn off of the anti parallel diode of the  $S_{AR2}$  are hard, because of reverse recovery current. To better explain meaning of hard- and soft- commutation let us define:

- commutation is hard (forced), when it is driven by turn off of the switch
- commutation is soft (natural), when it is driven by turn on of some switch



a) Phase A bidirectional switches b) Control signals for transistors during commutation

**Figure 2.14.** Example of phase commutation

The so called four step commutation method allows the change of the direction of output current automatically. After the end of commutation process both switches are turned on. However, the turn on and turn off operations of non-conducting devices are useless and costs time. That is why also less time demanding commutation strategies were developed.

When we take into account direction of the current through the bidirectional switch the two step commutation strategy can be derived from the four step method (remain steps 2 and step 3 from 2.14b). The detection of the current direction becomes hard task near current zero crossings. The start up of the converter is problematic too, thus current direction is undefined. Therefore the two step commutation method requires additional circuits to take care of zero crossing and start up. One way is to introduce threshold levels into modulator. When current crosses the threshold level, the conducting transistor is turned off and the opposite transistor is turned on after deadtime. In this way the start up of the converter is also ensured. When the current does not start to flow after the first transistor is turned on, the controller switches on the opposite one after the blanking time. In order to summarize the current based two step commutation method, let us state, it significantly saves time, the resulting switching is more precise in time, but it requires more sophisticated logic in modulator and in addition information about the actual current sign is also needed.

Second alternative is to reduce the four step commutation method about one step and make commutation in three steps. The reduction is made by turning off and turning on of the conducting and non-conducting device in same time instant. In Fig. 2.14b it means  $t_2 = t_3$ . When we take into account also the condition, that current path at the load side of the converter shall not be interrupted, then the three step commutation

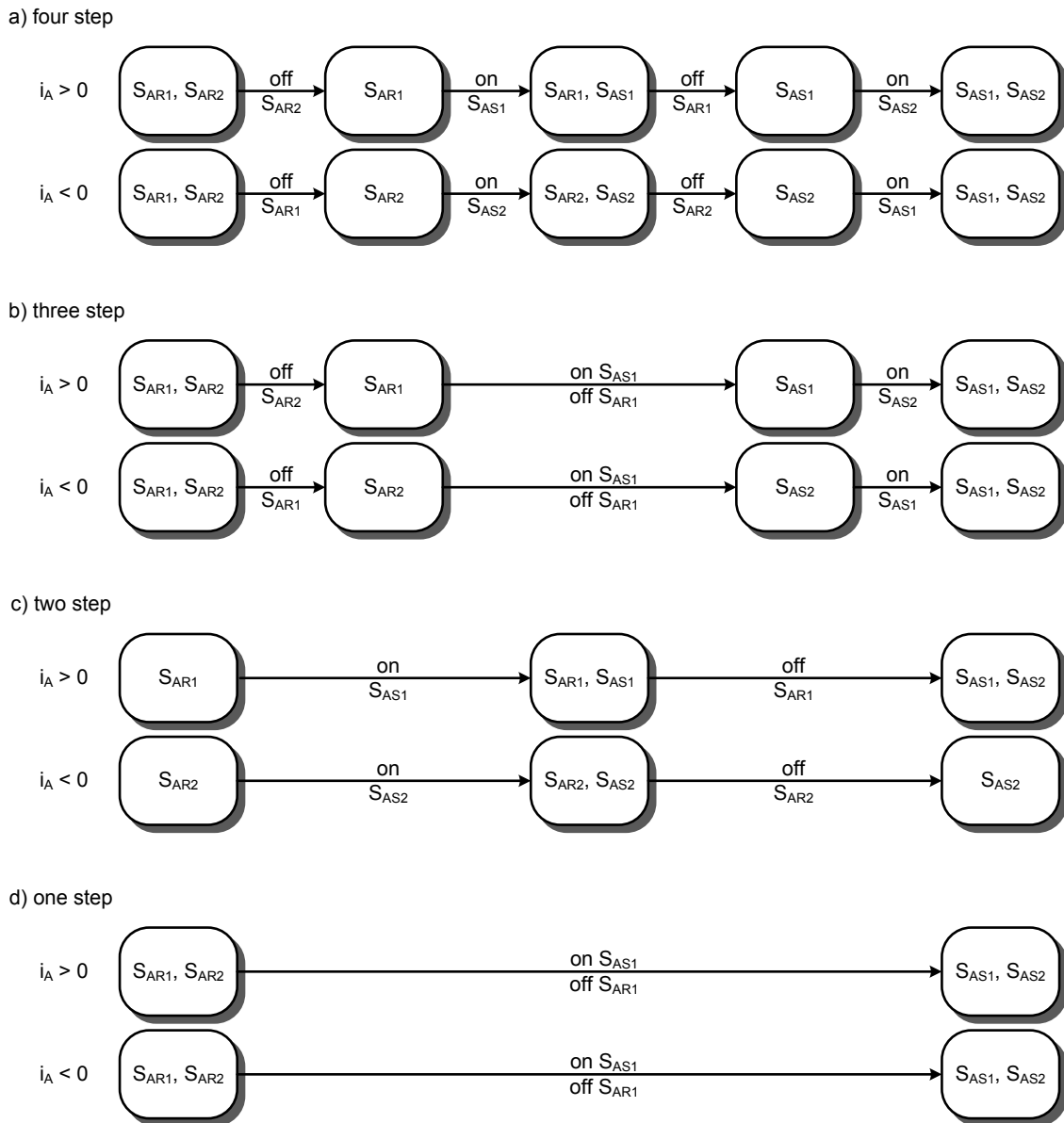


Figure 2.15. Current polarity based commutation methods

method can be used only with the devices that have longer turn off time than turn on time under all operation conditions. The overlapping of turn on and off will ensure, that the current path will be never interrupted.

In a similar manner also one step commutation strategy can be introduced, when we apply this reduction on the two step commutation method [60]. The reduced commutation strategies need not so much commutation time as the two and four step ones. All current polarity based commutation methods mentioned above are depicted in Fig. 2.15.

### 2.3.3 Input Voltage Polarity Based Commutation Method

Same as for current the commutation strategy can be based on the information about line-to-line voltage polarity. In the four step voltage based commutation method the commutation occurs after the step 2 or step 3 too. Because the device that is turn

on at step 1 is always blocking and the device turned on at step 3 is always forward biased. Therefore the commutation is soft at step 2 when  $i_A \geq 0$  and hard at step 3 when  $i_A \leq 0$  [61].

The input voltage polarity based two step method does not have same switching procedure as the current based [56, 62]. In two step commutation strategy only devices that prevent short circuit are turned off. The implementation of this method requires very accurate information about input line-to-line voltage polarity.

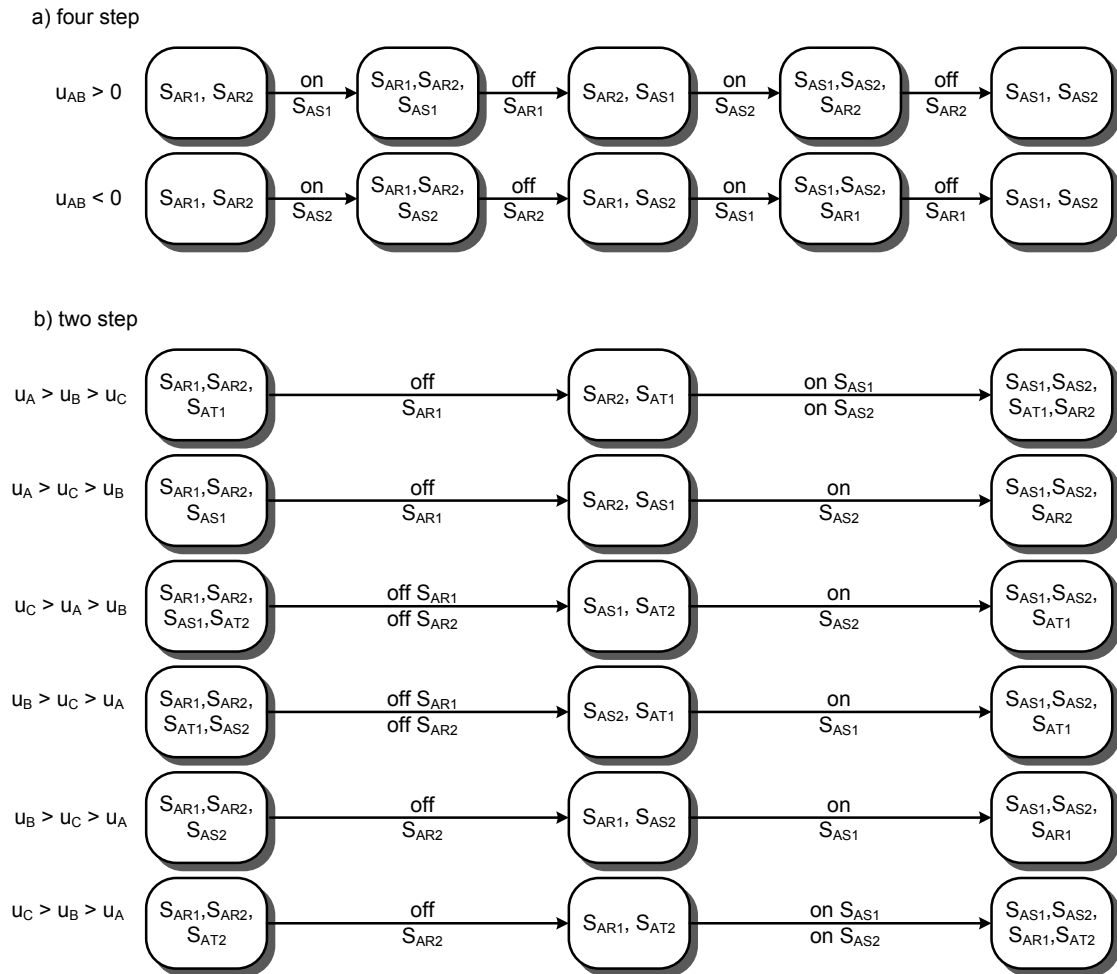


Figure 2.16. Voltage polarity based commutation methods

### 2.3.4 Comparison of Voltage and Current Based Commutation Strategies

The wrong detection of the input voltage sign may be fatal for the voltage based commutation strategies, because the wrong sign will cause short circuiting of input phases (input filter capacitor) that can be neither detected from the output waveforms nor input current sensors. The current based commutation method failure will disconnect the output. This will cause the over voltage spike, that can be caught by additional over voltage protection. Since the wrong sign detection will probably occur near current zero crossing, luckily the energy stored in the load leakage inductances is going to be low. In both cases anyway, wrong sign assumption will arise problems during the

commutation. Thus an additional logic has to be always implemented, to solve this problem.

As for the four step current based method we can solve this problem by latching of current sign information during the commutation process. This can cause only short interruption of current path. However in the voltage based commutation method, the latching of polarity can short circuit the input. Therefore the voltage based commutation strategy needs the information about polarity change immediately. The cutting off the current path and corresponding over voltage can be handled easier than over currents caused by short-circuiting the input filter.

Input voltage measurement in voltage based commutation strategy looks easier and is more cost effective than output current measurement. However, when only the information about the current polarity at the output is required, it can be obtained indirectly. Two possible solutions are depicted in Fig. 2.17. The variant in Fig. 2.17a is based on measurement of the voltage drop on the transistors. When we assume that current flows as showed in Fig. 2.17a the voltage drop  $u_1$  is going to be 0,7 V and  $u_2$  is going to be 1,2 V depending on devices used. This method is very accurate, but it requires voltage **probes** that withstands peak of line-to-line voltage, when the device is in blocking state. The topology depicted in Fig. 2.17b evaluates voltage drop on the two anti-parallel diodes that are connected in series with the bidirectional switch. This solution will increase conduction losses, because the current must flow trough another semiconductor p-n junction.

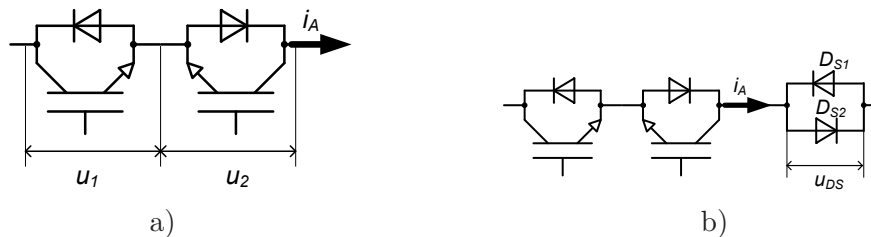


**Figure 2.17.** Current polarity detection circuit

### ■ 2.3.5 Soft Commutation

The resonant switching technique has been proposed for many converter topologies with purpose of reducing of the switching losses. In matrix convert resonant techniques also positively influence the current commutation. Developed approaches can be divided into two categories:

- resonant switch circuits [63–64]
- auxiliary or resonant circuits [7]

All these solutions further increase amount of the components in the matrix converter and also the conduction losses. Therefore despite the reduction of switching losses, their application might be considered as questionable.

## ■ 2.4 Power Part of the Matrix Converter

Power part of the matrix converter (Fig. 2.18) does not have any accumulation element. Therefore the output voltage is synthesized from the input voltage by the means of direct switching of the inputs to the output. That is why semiconductor switches that

have to conduct current and block voltage in both power flow directions are necessary. On the other hand it enables the operation of the converter in all four quadrants. Generally matrix converter consists of  $m \times n$  bidirectional switches that serve to connect  $m$ -input phase system to  $n$ -output phases. Nine bidirectional switches are employed to create most spread  $3 \times 3$  topology of the matrix converter. Practicable realizations of bidirectional switches are discussed in Section 2.5.

The converter is mostly connected between the inductive load and power grid. In order to reduce harmonics content in the input current caused by switching of the matrix converter it is good to add the converter with input filter. Design of such a filter will be discussed in Section 2.6.

The switches of the converter are vulnerable to over voltages. That is why the switching matrix is sometimes protected by some over voltage protection, see Section 2.7 for more details.

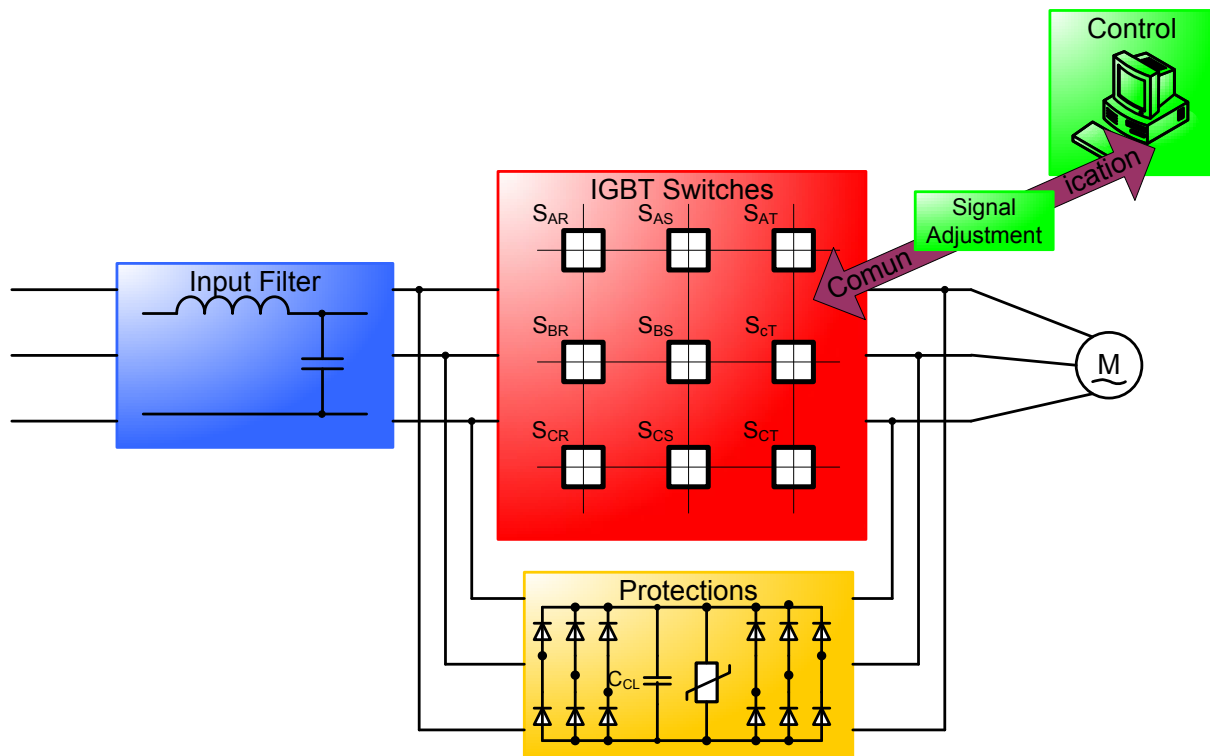


Figure 2.18. Block diagram of the matrix converter

## 2.5 Bidirectional switch topologies

Bidirectional switch for the matrix converter must be capable of conducting current and blocking voltages in both directions. Unfortunately the bidirectional switches are not yet usually available at the market. Therefore discrete semiconductor devices are being mostly used for the realization of these switches [24, 65–66]. As was briefly mentioned above there are several topologies of the bidirectional switch. Each topology has some special features like requirements on driver circuits or commutation method that can be used. Let us now describe some of them. It is silently assumed that as a switching device will be used IGBT, but also other devices like MOSFET or IGCT can be used.

### 2.5.1 Diode Bridge Topology

The topology is depicted in Fig. 2.19. It consists of one IGBT and four diodes. Main advantage of this solution is that only one active device is needed that lowers costs and also requirements on the gate circuit. The main drawback is that the direction of the current can not be changed without its termination and that is why advanced commutation strategies can not be used. The conduction losses are increased too, because the current must flow through three semiconductors.

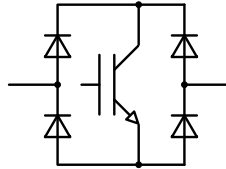


Figure 2.19. Bidirectional switch - diode bridge topology

### 2.5.2 IGBT with Anti-parallel Diode Topology

There are two solutions how to realize switch with IGBT and anti-parallel diodes. Compared to the diode bridge topology of the bidirectional switch this solution enables independent control of current flow. They are mentioned below.

- Common collector bidirectional switch - the arrangement of the two IGBTs with anti-parallel diodes is in Fig. 2.20. Anti-parallel diodes are included to provide reverse blocking capability. Compared to diode bridge topology the conduction losses are reduced because only two devices are conducting current at any time. Another advantage of the configuration with the common collector is that only six isolated sources are required for providing gate signals. However the inductances between the devices with the same isolated gate signal supply must be low. This is case for integrated matrix converter modules where more bidirectional switches are integrated together. With the increasing power become more important stray inductances of the individual bidirectional switches, therefore another configuration of bidirectional switch with common emitter is usually used for high powers.

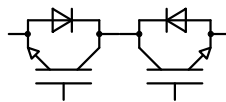


Figure 2.20. Bidirectional switch - common collector topology

- Common emitter bidirectional switch - the arrangement of the switch is similar to previous one. Only difference is that the IGBTs are arranged with common emitter Fig. 2.21. Same as the diode bridge switch each bidirectional switch in configuration with common emitter requires its own isolated power supply.

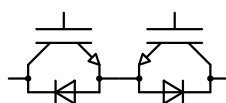
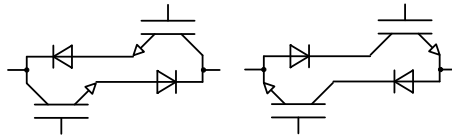


Figure 2.21. Bidirectional switch - common emitter topology

- Series IGBT diode configuration - Both configurations with common emitter and with common collector can be also realized without central connection as shown in Fig. 2.22. However this solution will remove especially in the configuration with common emitter the possibility to drive both transistors of the bidirectional switch with one power supply.



**Figure 2.22.** Bidirectional switch - without central connection

- Anti-parallel reverse blocking IGBTs - if the devices used for the bidirectional switch have integrated reverse voltage blocking capability the bidirectional switch can be realized as shown in Fig. 2.23. This leads to very compact solution of the matrix converter power part and improvement of efficiency. However until now the devices shows poor reverse recovery characteristics which increases the switching losses and has prevented spreading of this configuration.

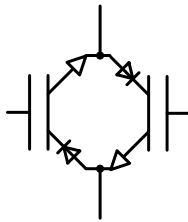


**Figure 2.23.** Bidirectional switch - reverse blocking IGBT topology

### ■ 2.5.3 Special Modules for the Matrix Converter

As was discussed above the bidirectional switches are mostly realized from discrete semiconductor devices. They can be simply divided into two groups:

- IGBT devices with collector current  $i_C \leq 50$  A - mostly realized with non isolated metallic case, with package designed for soldering through holes or by SMD into PCB (TO220, TO247 or TO263, TO268)
- modules, with transistor and anti-parallel diode, with collector current  $i_C \geq 50$  A - realized with inner ceramic insulation between the Si chip and copper base plate. This simplifies mounting of the devices and their cooling (SOT227, Square package, ECOPACK)



**Figure 2.24.** IGBT packages

The use of modules for matrix converter has several advantages. The integration of transistor and fast recovery diode into one module decrease the stray inductances between the devices, thereby the switching losses. The number of components required for the power stage also decrease. Several offers from various manufacturers will be presented.

First example is module of bidirectional switch offered by Dynex [67]. Offered module DIM400PBM17-A000 Fig. 2.25 is realized in configuration with common emitter, it has  $U_{CE} = 1700\text{ V}$  and  $I_{C_{max}} = 400\text{ A}$ . Nine of these modules are required for realization of 3x3 matrix converter.



**Figure 2.25.** Bidirectional switch DIM400PBM17-A000

More improvements can be achieved by implementing of more switches together. Semelab offers integrated module with three bidirectional switches in common emitter topology (Fig. 2.26) [32]. Such module can be used to build one phase of the matrix converter, therefore three modules are required for whole converter. They are available in two versions SML300AT06 and SML150AT12 for 600 V and 1200 V respectively, collector current that can flow through the module is  $I_C = 300\text{ A}$ .

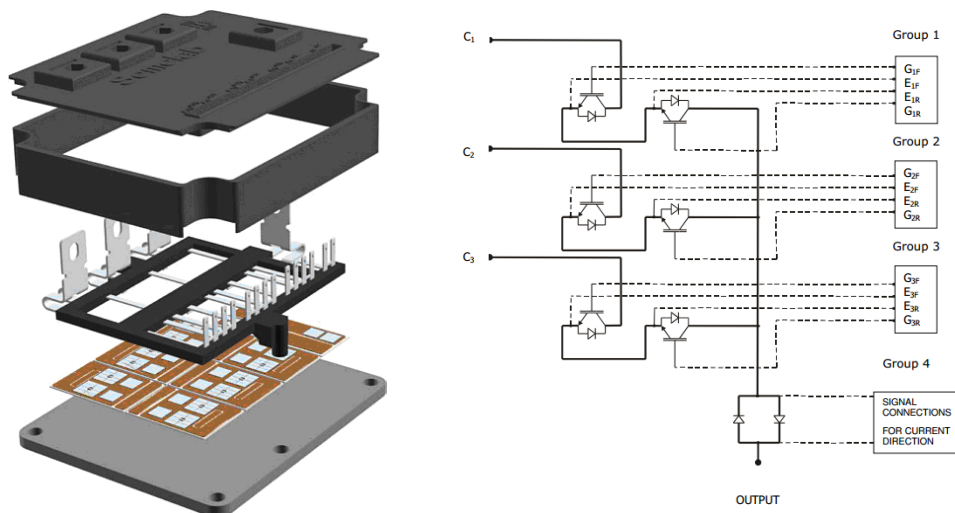


**Figure 2.26.** Bidirectional switch SML300AT06 [32]

Next integrated module is (EconoMAC Fig. 2.27) from INFINEON [68]. This is all-in-one module for matrix converter with nominal power 7,5 kW. The bidirectional switches are realized in configuration with common collector. Continuous current of the module is  $I_C = 30\text{ A}$ . Connection of the inputs, outputs and control signals is done

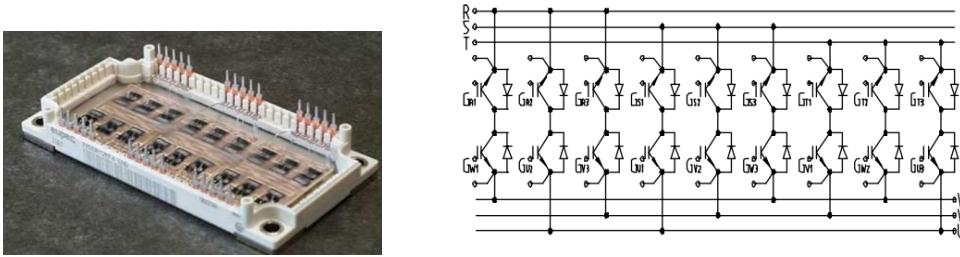


**Figure 2.27.** Bidirectional switch EconoMAC [68]

by soldering of the EconoMAC to the PCB, this ensures the high compactness of the converter.

In [27] is mentioned the another experimental all-in-one module from INFINEON based on the SiC JFET with intrinsic free wheeling diode in its structure. JFETs used in this modules has 10 times lower gate charge (aprox. 30 nC) compared to IGBT. This offers possibility to increase module switching frequency up to 50 kHz and also the power loses in the control part of the converter are greatly decreased, therefore more compact converter can be built.

One step further is the module offered by Mitsubishi. It is all-in-one matrix converter module based on the reverse blocking IGBT (RB-IGBT) SiC chips (Fig. 2.29) [69]. Nominal power of the module is approximately 22 kW with dimensions of 152 mm x 109 mm. RB-IGBT has symmetrical blocking voltage characteristic. It can block both forward or reverse voltage Fig. 2.30 in turned off state. This capability simplifies the bidirectional switch because there is no need of anti-parallel diode, which greatly decreases power loses in the module. The structure of RB-IGBT is in Fig. 2.30, the structure is similar to IGBT except it has deep diffusion collector wall. This collector isolation ensures the blocking capabilities of the transistor.

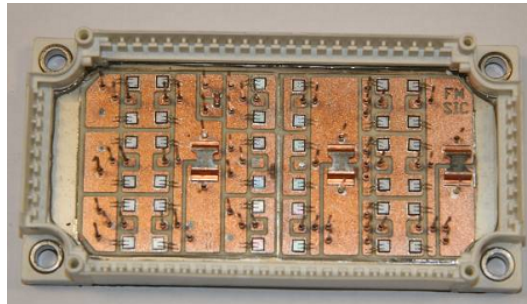


**Figure 2.28.** Bidirectional switch based on JFET [27]

Comparison of RB-IGBT with 4<sup>th</sup> generation of IGBT with free wheeling diode from point of losses is in Tab. 2.2. Low value of recovery and turn off loses shows that RB-IGBT structure is good for applications with high switching frequency.

	RB-IGBT	4 <sup>th</sup> IGBT+diode
$V_{on}(V)$	3.06	3.80
$E_{sw}(mJ/p)$	11.6	19.1
$E_{rr}(mJ/p)$	11.7	12.2

**Table 2.2.** Loss comparison of RB-IGBT

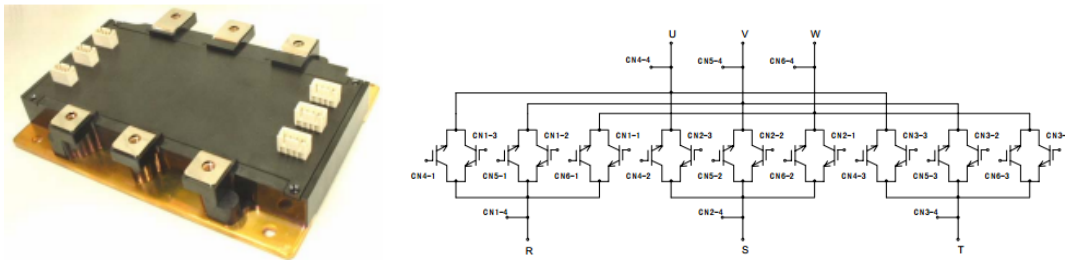


Figure 2.29. Bidirectional switch RB-IGBT [69]

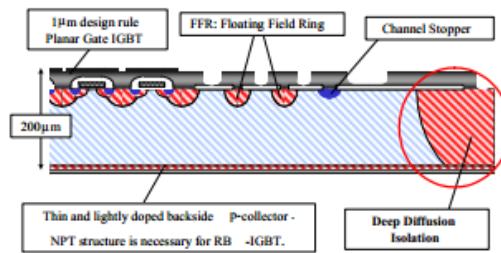


Figure 2.30. Bidirectional switch RB-IGBT structure [69]

Bidirectional switch in single module			
Manufacturer	Reference	Parameters	Configuration
DYNEX	DIM400PBM17	1700 V, 400 A	Common emitter
DYNEX	DIM200MBS12-A	1700 V, 200 A	Common emitter
SEMIKRON	SK60GM123	1200 V, 60 A	Common emitter
IXYS	FIO50-12BD	1200 V, 50 A	Diode bridge + IGBT
IXYS	IXRH50N120	1200 V, 60 A	RB IGBT
IXYS	IXRH50N100	1000 V, 60 A	RB IGBT
Output phase in single module			
Manufacturer	Reference	Parameters	Configuration
SEMELAB	SML300MAT06	600 V, 300 A	Common emitter
SEMELAB	SML300MAT12	1200 V, 150 A	Common emitter
Matrix converter in single module			
Manufacturer	Reference	Parameters	Configuration
FUJI	18MBI100W-120A	1200 V, 100 A	RB IGBT
FUJI	18MBI50W-120A	1200 V, 50 A	RB IGBT
FUJI	18MBI200W-060A	600 V, 200 A	RB IGBT
FUJI	18MBI100W-060A	600 V, 100 A	RB IGBT
EUPEC	FM35R12KE3 (EconoMac)	1200V, 35 A	Common collector

Table 2.3. Summary of modules suitable for matrix converter

Most significant special modules for the matrix converter are once more summarized in Tab. 2.3.

## 2.6 Input Filter

Another important part of the matrix converter is input filter. Power converters switch on and off large amounts of electric energy thereby generate unwanted electric signals (harmonics) that can affect other electric devices. The production of these negative side effects is also affected by the non-linearities of the devices and current spikes caused by finite slopes of the switching actions. These side effects are common to all converters driven by PWM:

- high harmonics content in the supply current
- influence on other devices - EMI

That is why the filter has to be connected in front of each power converter. Main task of the filter is to attenuate harmonics in the input current caused by the switching of the semiconductors. Secondly, the filter can also shield the converter from the transients that should appear in the input voltage.

From the other point of view the filter should have minimal impact on the input of the converter, in other words it should produce maximal current ripple reduction with minimum dissipated energy on the reactive elements. Moreover the filter should produce minimal phase shift between the input voltage and input current. Typically such filter is made of inductors and capacitors connected to Y /  $\Delta$  (Fig. 2.31). This solution of the LC filter is frequently presented as final and without problems, however especially the absence of the DC-link in the matrix converter can introduce high oscillations into filter. Sometimes more complex filter topologies are recommended in the literature in order to achieve better attenuation of the filter, however they are not practical from the component or economical point of view. Design of the filter is described in [70–72]. Following will be introduced only simplified procedure of the design.

Designed input filter should fulfill following conditions:

- Act as a low pass filter with cut off frequency lower then switching frequency

$$L_f C_f = \frac{1}{\omega_0^2} \quad (2.1)$$

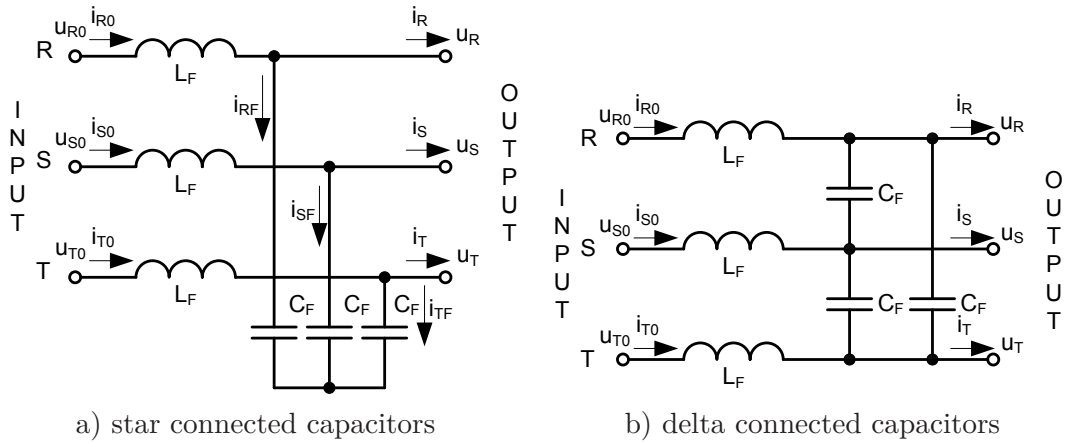
where  $L_f$ ,  $C_f$  are values of the inductor and capacitor of the input filter and  $\omega_0 = 2\pi f_0$  defines resonance frequency of the filter

- Introduce minimal displacement angle  $\varphi_{in}$  between the input voltage and input current
- Minimize volume of the input filter for given reactive power
- Minimize the voltage drop on the filter inductance at rated current to provide maximal voltage transfer ratio

The cut-off frequency of the filter  $f_0$  is selected to provide enough attenuation at the switching frequency and it must have enough distance from the input source frequency, too. Therefore during the design of the filter we can look on the filter parameters from two points:

- filter is LC combination that loads supply network
- filter frequency behaviour (transfer function)

Form the mains point of view, the filter can be analysed using harmonic steady state and phasors. If we consider non loaded filter we can expressed the current consumed by the filter as:


**Figure 2.31.** LC filter topologies

$$\underline{I}_{Cf} = \frac{\underline{U}_{R0}}{j\omega_{\text{mains}}L_f - \frac{1}{j\omega_{\text{mains}}C_f}} \quad (2.2)$$

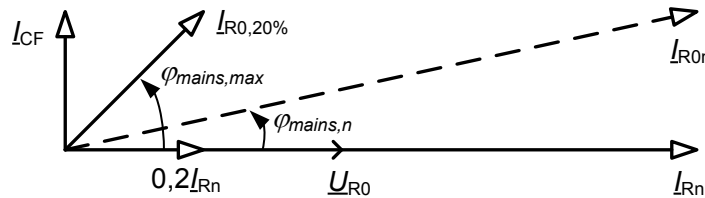
When we assume that the converter operates with unity power factor at its input and we neglect the losses we can express the rated value of the current flow through the filter as:

$$\underline{I}_{Rn} = \frac{S_{MCn}}{3(\underline{U}_{R0} - j\omega_{\text{mains}}L_f I_{R0n})^*} \quad (2.3)$$

Because we try to use inductance with the minimal voltage drop the (2.3) can be simplified

$$\underline{I}_{Rn} \approx \frac{S_{MCn}}{3\underline{U}_{R0}^*} \quad (2.4)$$

However the converter will not operate always on its rated values. Because the current consumed by the capacitor  $C_f$  is constant, therefore the lower converter's current the higher angle  $\varphi_{\text{mains}}$  will appear. That is why when designing the value of  $C_f$  it is good to comprise also the limit of the maximal allowable angle between the mains voltage and current  $\varphi_{\text{mains,max}}$  Fig. 2.32.


**Figure 2.32.** LC filter phasor diagram

$$C_f \leq \frac{S_{MC} \tan \varphi_{\text{mains,max}}}{3\underline{U}_{R0} \omega_{\text{mains}}} \quad (2.5)$$

Second important property of the filter is cut off frequency

$$f_0 = \frac{1}{2\pi\sqrt{L_f C_f}} \quad (2.6)$$

The  $f_0$  should have enough distance from the switching frequency to ensure enough attenuation of the filter. This can be expressed as safety frequency ratio

$$k_f = \frac{f_{sw}}{f_0} \quad (2.7)$$

when substituting (2.7) into (2.6) we obtain

$$L_f \geq \frac{f_{sw}^2}{4\pi^2 f_0^4 C_f} \quad (2.8)$$

From (2.8) and (2.5) follows, that the design of the filter has to be compromise between the inductor and capacitor size. A small capacitor ensures a high power factor  $\cos \varphi_{mains}$  on the input of the filter, however large inductor is required to reach demanded cut off frequency of the filter. Moreover the size of the inductor is limited by the voltage drop across it. Some authors tends to use  $\Delta$  connection of the filter's capacitors instead of Y. The effect of this solution is same as for induction machine. The same capacitors connected to  $\Delta$  will produce trice higher reactive power than capacitors connected to Y. Therefore filter with capacitor of three times smaller capacity will have same behaviour if the capacitors will be connected to  $\Delta$ . One of the side effects of this solution is that the capacitors will be exposed to line-to-line voltage. Moreover the behaviour of the whole filter will be slightly different with respect of the 3<sup>rd</sup> harmonics and its multiples. Solution depicted in Fig. 2.31 is also called as undamped. It is damped only by the resistance of the load and the gain of the filter is limited only by the internal resistances of the real components. The transfer function can be expressed as

$$F_{LC}(\omega) = \frac{U_{LC,out}}{U_{LC,in}} = \frac{1}{1 + j\omega \frac{L_f}{R_{load}} + (j\omega)^2 L_f C_f} \quad (2.9)$$

In (2.9) we can define damping behaviour of the  $R_{load}$  as damping factor

$$\zeta = \frac{L_f}{2R_{load}\sqrt{L_f C_f}} \quad (2.10)$$

Transfer function of the filter can be then rearranged with the help of (2.1) and (2.10) to

$$F_{LC}(\omega) = \frac{1}{1 + j2\zeta \frac{\omega}{\omega_0} - \frac{\omega^2}{\omega_0^2}} \quad (2.11)$$

The influence of the damping factor  $\zeta$  on the attenuation of the filter is depicted in Fig. 2.33. It can be seen that  $\zeta$  influence the behaviour of the filter around its cut off frequency. This shall not be problem in the steady state, however the converter shall operate under transients or under periodic disturbances too, therefore the the filter must be supplemented with some damping [70]. Moreover the filter is vulnerable to oscillations especially at the converter start up. In order to hold damping factor more under control own damping of the filter is being connected to the filter. Several solution used for the filter will be discussed now.

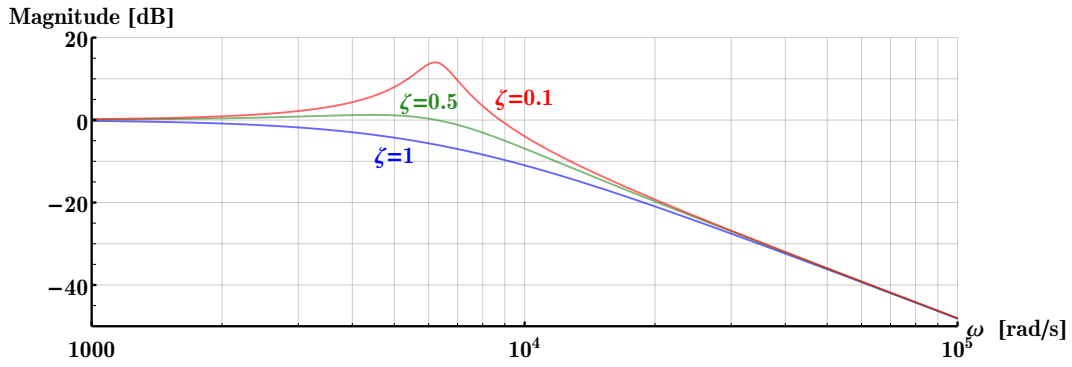


Figure 2.33. Influence of the  $\zeta$  on the behaviour of the filter

### 2.6.1 Start Up Resistor

Simple solution that is often used to suppress transient phenomenon during start up, is connection of the resistor in series with the filter. The resistor damps oscillations of the filter during the converters start up and then it is spanned by the contactor Fig. 2.34. This solution is simple and cheap. It limits the currents charging the capacitor  $C_F$ , then the resistor is shorted out by the contacts, therefore it has no effect on the filter during the operation of the converter.

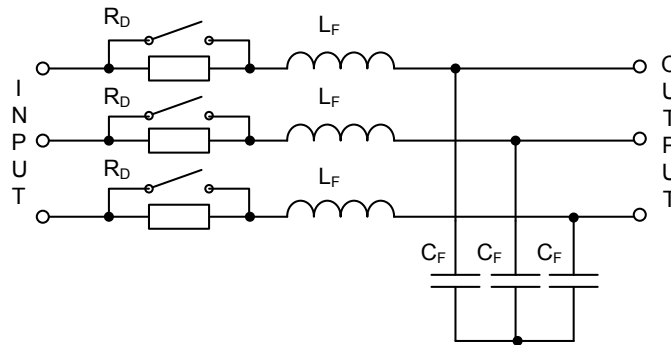


Figure 2.34. LC filter with start up resistor

### 2.6.2 Series Damped LC Filter

Another way to obtain a damped filter is Fig. 2.35 a resistance  $R_{SD}$  in series with an inductor  $L_{SD}$ , all connected in parallel with the filter inductor  $L_F$ . At the cut off frequency, the resistance  $R_{SD}$  has to have a higher value than the  $L_{SD}$  impedance.

The transfer function of series damped filter can be expressed as

$$F_{LC,SD}(\omega) = \frac{U_{LC,SDout}}{U_{LC,SDin}} = \frac{R_{SD} + j\omega(L_F + L_{SD})}{R_{SD} + j\omega(L_F + L_{SD}) + (j\omega)^2 L_F C_F R_{SD} + (j\omega)^3 L_F L_{SD} C_F} \quad (2.12)$$

The damping factor of the filter can be expressed as

$$\zeta = \frac{1}{2} \frac{R_{SD}}{(n+1)} \frac{\sqrt{C_F}}{\sqrt{L_F}} \quad (2.13)$$

where  $n = \frac{L_{SD}}{L_F}$ . From the analysis of the filter follows that peaking of the filter is minimized for  $n = 15$ . The values of the components in the damping circuit can be then calculated as

$$R_{SD} = \sqrt{\frac{L_F}{C_F}} \quad (2.14)$$

$$L_{SD} = nL_F = \frac{2}{15}L_F \quad (2.15)$$

The disadvantage of this damped filter is that the high frequency attenuation is degraded, see Fig. 2.36

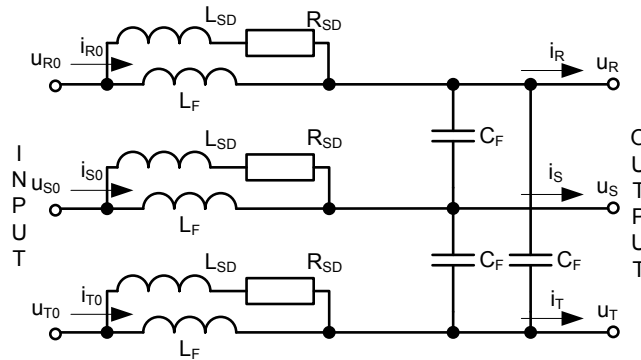


Figure 2.35. LC filter with series damping

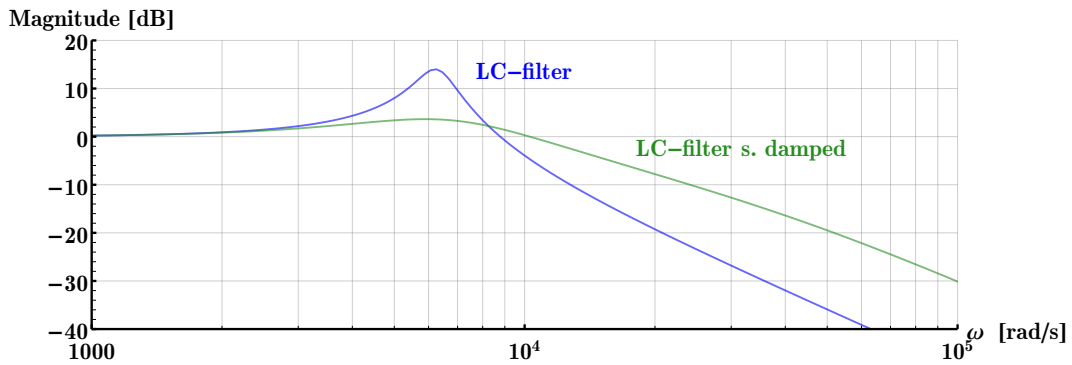


Figure 2.36. Transfer function of series damped LC filter

### 2.6.3 Parallel Damped LC Filter

The filter Fig. 2.37 is complemented with resistor  $R_{PD}$  in series with capacitor  $C_{PD}$ . All are connected parallel with the filter's capacitor  $C_F$ . The purpose of resistor  $R_{PD}$  is to reduce the output peak impedance of the filter at the cut off frequency. The capacitor  $C_{PD}$  blocks the DC component of the input voltage and avoids the power dissipation on  $R_{PD}$ . The capacitor  $C_{PD}$  should have lower impedance at the resonance frequency than  $R_{PD}$  and has to be bigger than  $C_F$  otherwise damping will have influence on the cut off frequency of the filter.

The transfer function of the filter can be expressed as

$$F_{LC,PD}(\omega) = \frac{1 + j\omega R_{PD}C_{PD}}{1 + j\omega R_{PD}C_{PD} + (j\omega)^2 L_F (C_F + C_{PD}) + (j\omega)^3 L_F C_F R_{PD} C_{PD}} \quad (2.16)$$

The damping factor of the filter is

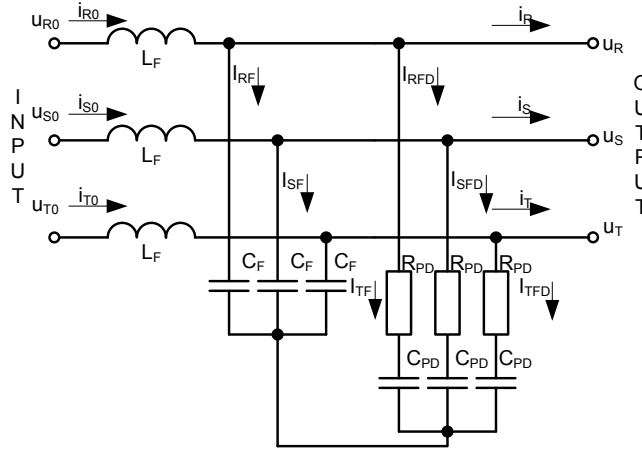


Figure 2.37. LC filter with parallel damping

$$\zeta = \frac{n + 1}{n} \frac{L_F}{2R_{PD}\sqrt{L_F C_F}} \quad (2.17)$$

where  $n = \frac{L_{PD}}{C_F}$ . From the analysis of the filter follows that peaking of the filter is minimized for  $n = 4$ . The values of the components in the damping circuit can be then calculated as

$$R_{PD} = \sqrt{\frac{L_F}{C_F}} \quad (2.18)$$

$$L_{PD} = nC_F = 4C_F \quad (2.19)$$

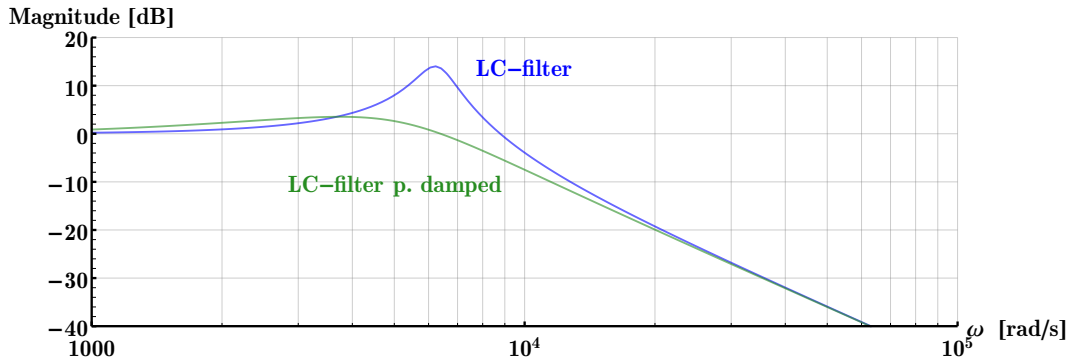


Figure 2.38. Transfer function of LC filter with parallel damping

There are also another topologies of the input filter with better attenuating characteristic, however they are complicated or consists of many components. One of the sophisticated topologies is multi section LC filter in Fig. 2.39.

## 2.7 Overvoltage Protection

The overvoltage protection circuit is not implicitly important part of the converter when we assume proper function of the converter's modulator. However, there always exists

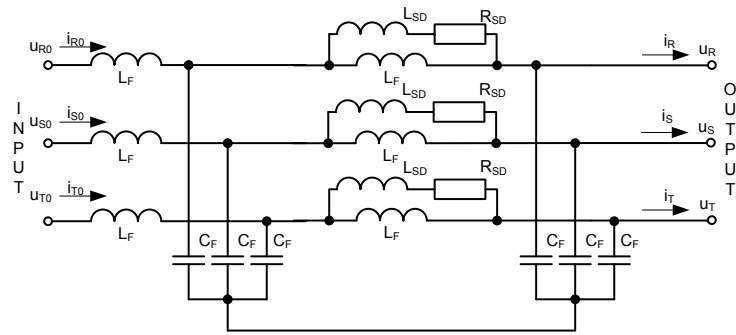


Figure 2.39. Multi section LC filter

possibility of commutation failure due some EMI or power failure. Moreover when the converter supply inductive load the overvoltage can appear when the output current path is accidentally cut. A typical solution of this protection is clamp circuit presented in [73–75]. It consists of two diode bridges connected to the input and output side of the switching matrix (Fig. 2.40). Between diode rectifiers is connected capacitor that forms small DC-link. Such formed floating protection protects bidirectional switches against quick  $dI/dt$  caused by leakage inductance of the switching matrix interconnections and also it must be capable of accepting the energy from the load in case of some bad switching.

After connecting of the converter to the mains the capacitor in clamp circuit  $C_{CL}$  is charged to the value of mains line to line voltage maximum and then is continuously charged due to the leakage inductances of the converter. That is why discharging of the capacitor must be ensured. Simplest way is to connect discharging resistor  $R_{CL}$  in parallel to the  $C_{CL}$ , on the other hand continuous discharging will add another power losses in the converter. The resistor  $R_{CL}$  can excite the input filter oscillations too. Next solution is replacing of the resistor with varistor, that will limit the voltage across the  $C_{CL}$ . Last solution is to replace the passive elements with active semiconductor switch with resistor as is known from the DC-links of the VSI.

Another approach to the overvoltage protection of the converter is to use separate protection devices for every switch [76–77]. In presented solution with  $\Delta$  connected varistors on the input and output terminals of the converter Fig. 2.41. When overvoltage appears the corresponding varistor turns on and dissipates energy of the voltage spike. When a varistor is used in protection circuit it requires careful design. Firstly the voltage of the varistor must be chosen so that varistor protects the semiconductor switches. Mainly when selecting varistors on the input side of the switching matrix the selectivity of short-circuit protections have to be respected carefully. Also the maximal allowable energy of the varistor is important parameter when the inductive load as IM is supposed. The way how to calculate rough value of the energy stored in leakage inductances of the IM can be found in [37].

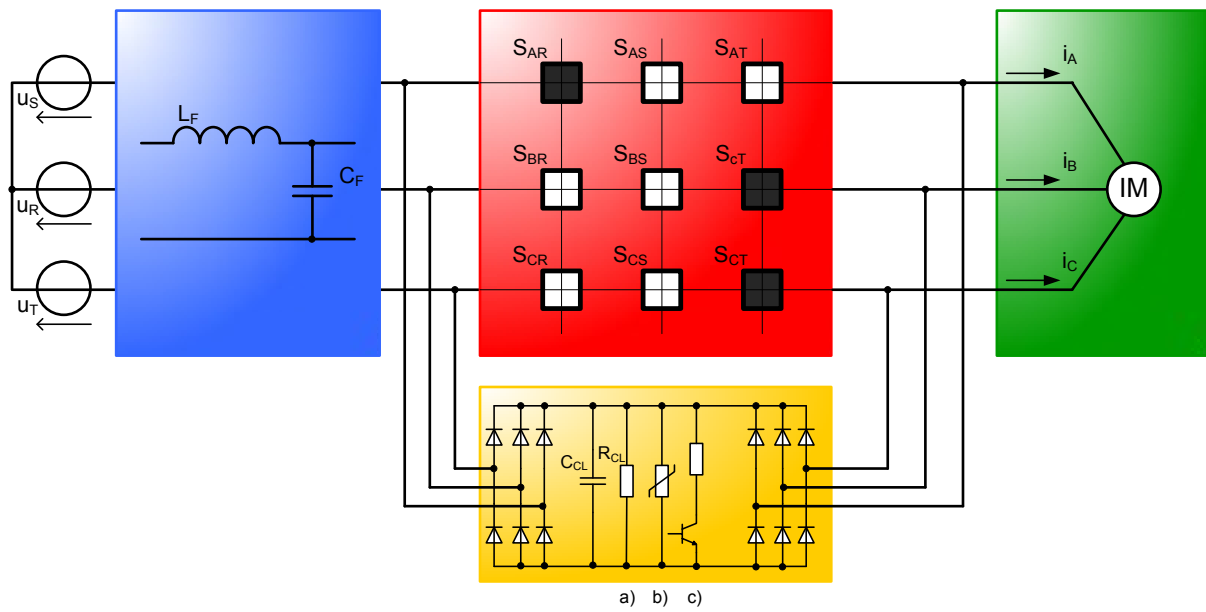


Figure 2.40. Clamp circuit protection for matrix converter

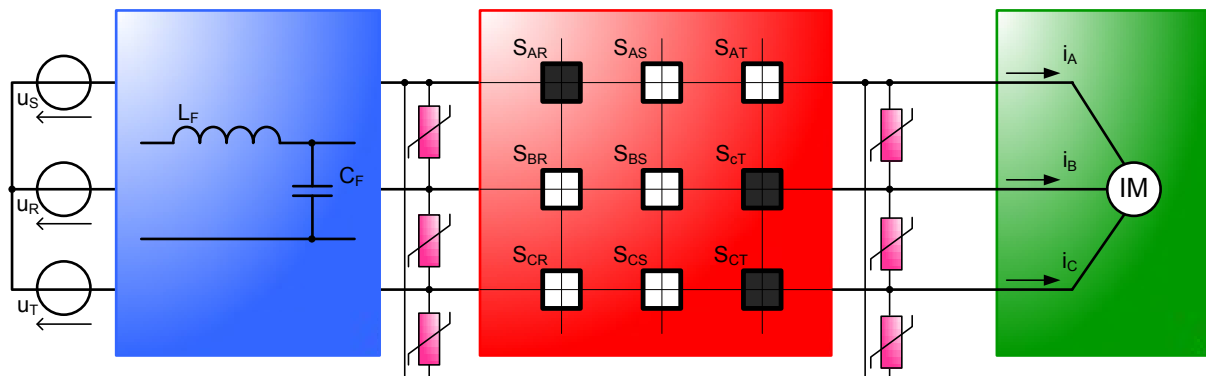


Figure 2.41. Varistor protection for matrix converter

There are also another solutions, that can be used in the area of low power applications. Semiconductor switches based on FET or IGBT transistors often contains clamp made by zener diode connected between gate and collector of the transistor Fig. 2.42. Contrary to the common operation of the IGBT as a switching device (ON/OFF operation), here during the turn off of the transistor with the inductive load diode holds the transistor partly open and with it the load is turned off with constant  $dI/dt$ . In other words the energy from the load is dissipated on the transistor and hereby transistor warms up.

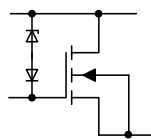
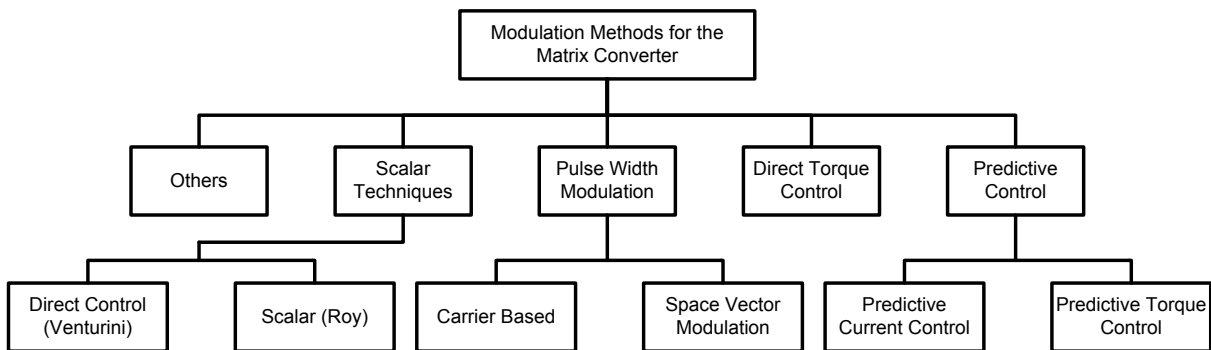


Figure 2.42. Switch with integrated clamp

## Chapter 3

# Modulation and Control Strategies for the Matrix Converter

Modulation is the procedure used to produce proper firing pulses to each of the nine bidirectional switches ( $S_{ij}$ ). The most relevant modulation and control strategies for the matrix converter are summarized in [26]. They are visualized in Fig. 3.1. The first method is called the direct transfer function approach and is also known as Venturini method [47]. The output voltage is obtained as the product of the input voltage and the transfer matrix representing the converter. Another strategy is scalar method developed by Roy [78]. This method uses instantaneous voltage ratio of converter's input phases to generate zero or active states of the switches. Other control strategies are based on the pulse width modulation PWM technique originally developed for the voltage source inverters. Very powerful solution that is recently in use is application of space vector modulation (SVM) [79–80] or indirect space vector modulation (ISVM) [45–46]. Alternatively can be employed strategies based on direct torque control, recently predictive control has been proposed for the control of IM fed by matrix converter. In this chapter a description and comparison of these techniques will be presented.



**Figure 3.1.** Matrix converter modulation and control techniques summary

Performance of all methods can be compared from many points of view, for example:

- complexity
- quality of output current
- dynamic response
- sampling frequency
- switching frequency
- resonance of input filter

This comparison is summarized in Tab. 3.1. From the complexity point of view carrier based techniques involve many equations, however compared to other methods the generation of the switching signals from them is very simple. Main difference is

	Venturini	Scalar	Carrier Based PWM	Space Vector Modulation	DTC	Predictive Current Control
Complexity	low	low	very low	very high	high	low
Sampling frequency	very low	very low	low	low	very high	high
Switching frequency	very low	very low	low	low	high	high
Dynamic response	good	good	good	good	fast	very fast
Resonance of input filter	low	low	medium	low	very high	from very high to low

**Table 3.1.** Comparison of control and modulation strategies

that some methods work with the fixed switching frequency and other strategies like DTC work with variable switching frequency, which can cause resonances of the input filter. Some form the mentioned strategies will be briefly discussed in this chapter.

## 3.1 Scalar Techniques

### 3.1.1 Direct Method - Venturini

Method proposed by Venturini in [47]. The aim of this modulation is to generate variable frequency and variable amplitude sinusoidal output voltage from the fixed frequency and fixed amplitude of the input voltage. The instantaneous input voltages are used to synthesize a signal whose low frequency component is the desired output voltage. When we define  $t_{ij}$  as time during which the switch  $S_{ij}$  is switched on and  $T_S$  is the sampling interval, then the proposed modulation can be expressed as

$$\bar{u}_j = \frac{t_{Rj}u_R + t_{Sj}u_S + t_{Tj}u_T}{T_S} \quad (3.1)$$

where  $\bar{u}_j$  is the low frequency component (mean value calculated over one sampling interval) of the  $j^{\text{th}}$  output phase and it changes in each sampling interval. In this way the high frequency voltage is generated, but the fundamental component has desired waveform. It is clear that  $T_S = t_{Rj} + t_{Sj} + t_{Tj}$  with  $j = A, B, C$  and therefore we can define the individual modulation indexes as

$$m_{Rj}(t) = \frac{t_{Rj}}{T_S} \quad m_{Sj}(t) = \frac{t_{Sj}}{T_S} \quad m_{Tj}(t) = \frac{t_{Tj}}{T_S} \quad (3.2)$$

Combining (3.1) and (3.2) for each output phase leads to the following equation

$$\bar{u}_o(t) = \mathbf{M}(t)\bar{u}_i(t) \quad (3.3)$$

where  $\bar{u}_o(t)$  is low frequency output voltage vector,  $u_i(t)$  is instantaneous input voltage vector and  $\mathbf{M}(t)$  is the transfer matrix of the converter defined as

$$\mathbf{M}(t) = \begin{bmatrix} m_{RA} & m_{SA} & m_{TA} \\ m_{RB} & m_{SB} & m_{TB} \\ m_{RC} & m_{SC} & m_{TC} \end{bmatrix} \quad (3.4)$$

Similarly can be derived equation for the input current

$$\bar{i}_i(t) = \mathbf{M}^T(t)\bar{i}_o(t) \quad (3.5)$$

where  $\bar{i}_i(t)$  is the input current vector and  $\bar{i}_o(t)$  is the instantaneous output current vector and  $\mathbf{M}^T(t)$  is the transpose of  $\mathbf{M}(t)$ . The Venturini modulation is then based on (3.3) and (3.5). The low frequency output voltage components are produced from instantaneous values of the input voltage and in a similar way the low frequency components of the input currents are synthesised from the instantaneous values of the output currents. Supposing the input voltages  $u_i$  are given by

$$u_i(t) = \begin{bmatrix} U_i \cos(\omega_i t) \\ U_i \cos(\omega_i t - 2\pi/3) \\ U_i \cos(\omega_i t + 2\pi/3) \end{bmatrix} \quad (3.6)$$

because the load of the converter has mostly low pass characteristic, the output currents can be expressed as

$$i_o(t) = \begin{bmatrix} I_o \cos(\omega_o t + \phi_o) \\ I_o \cos(\omega_o t - 2\pi/3 + \phi_o) \\ I_o \cos(\omega_o t + 2\pi/3 + \phi_o) \end{bmatrix} \quad (3.7)$$

where  $\omega_i$  and  $\omega_o$  corresponds to the input and output phasor angular speeds respectively,  $U_i$  is the input voltage amplitude and  $I_o$  is the output current amplitude. The input currents and output voltages can be defined likewise

$$i_i(t) = \begin{bmatrix} I_i \cos(\omega_i t + \phi_i) \\ I_i \cos(\omega_i t - 2\pi/3 + \phi_i) \\ I_i \cos(\omega_i t + 2\pi/3 + \phi_i) \end{bmatrix} \quad (3.8)$$

$$u_o(t) = \begin{bmatrix} qU_i \cos(\omega_o t) \\ qU_i \cos(\omega_o t - 2\pi/3) \\ qU_i \cos(\omega_o t + 2\pi/3) \end{bmatrix} \quad (3.9)$$

Also the following active power balance must be valid

$$P_o = \frac{3qU_i I_o \cos(\phi_o)}{2} = \frac{3U_i I_i \cos(\phi_i)}{2} = P_i \quad (3.10)$$

with  $P_o$  and  $P_i$  are output and input active powers, respectively,  $\phi_i$  is displacement angle between input voltage and input current and  $q$  is the voltage gain between the input and output of the MC. From the previous definitions we can reduce the modulation problem to simple finding a transfer matrix  $\mathbf{M}(t)$  such the (3.3) and (3.5) are satisfied. More detailed description can be found in [47], where can be also found simplifying expression

$$m_{ij}(t) = \frac{1}{3}(1 + 2u_i(t)\frac{\bar{u}_j}{U_i^2}) \quad (3.11)$$

where  $i = R, S, T$  and  $j = A, B, C$ .

The drawback of this solution is that maximal gain of the output voltage is limited to  $q = 0,5$  due to the employment of the mean value in the modulation Fig. 3.2. In order to increase the voltage gain to the  $q = \sqrt{3}/2 = 0,866$ , Venturini proposed injection of the third harmonics (Fig. 3.3) into (3.9) [73].

$$u_o(t) = qU_{i,\max} \begin{bmatrix} \cos(\omega_o t) - \frac{1}{6} \cos(3\omega_o t) + \frac{1}{2\sqrt{3}} \cos(3\omega_i t) \\ \cos(\omega_o t - 2\pi/3) - \frac{1}{6} \cos(3\omega_o t) + \frac{1}{2\sqrt{3}} \cos(3\omega_i t) \\ \cos(\omega_o t + 2\pi/3) - \frac{1}{6} \cos(3\omega_o t) + \frac{1}{2\sqrt{3}} \cos(3\omega_i t) \end{bmatrix} \quad (3.12)$$

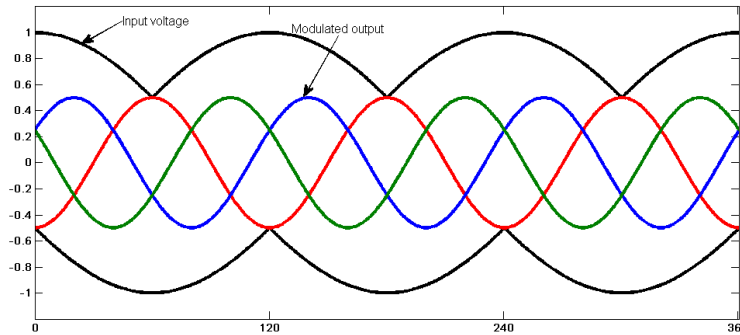


Figure 3.2. Voltage ratio 50%

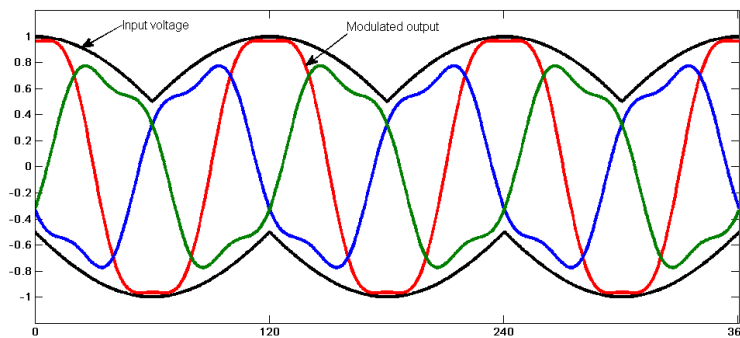


Figure 3.3. Voltage ratio 86.6%

### 3.1.2 Scalar Method - Roy

Another scalar modulation method was proposed in 1989 by Roy and April in [78]. This method uses instantaneous voltage ratio of input phase voltages to generate active or zero states for the switches of the converter. The value of any instantaneous output phase voltage is:

$$u_j = \frac{1}{T_S} (t_K u_K + t_L u_L + t_M u_M) \quad (3.13)$$

where  $j = A, B, C$  and  $T_S = t_K + t_L + t_M$ . The subscript M is assigned to the phase whose voltage has different sign than voltages of two other phases and subscript L is assigned to one of the other phases whose voltage has smaller magnitude. The equation (3.13) is same as Venturini's (3.1), however here the modulation depends on the scalar

comparison of the input phase voltages with the instantaneous value of the desired output voltage. The duty cycles can be expressed as:

$$\begin{aligned} m_{Lj} &= \frac{(u_j - u_M)u_L}{3/2U_i^2} \\ m_{Kj} &= \frac{(u_j - u_M)u_K}{3/2U_i^2} \\ m_{Mj} &= 1 - (m_{Lj} + m_{Kj}) \end{aligned} \quad (3.14)$$

where  $j = A, B, C$ . However this modulation method offers only  $q \leq 0.5$ . To improve the voltage transfer ratio the third harmonics must be also added. This leads to:

$$m_{ij}(t) = \frac{1}{3}(1 + 2u_i u_j / U_i^2 + 2/3\zeta) \quad (3.15)$$

where  $\zeta = \sin(\omega_i t + \beta_i) \sin(3\omega_i t)$  and  $\beta_i = \{0, 2\pi/3, -2\pi/3\}$ . The difference between the Roy's method and Venturini's method is only in the term  $q$  which is for the Roy's fixed at its maximum value.

According to [78] by shifting of the timing sequence with the respect to the zero crossing of the input phase voltage, it is possible to control the phase shift of the current on the input of the converter  $i_i$  relative to  $u_i$ . We can define the virtual phase voltages at the input of the converter as:

$$\begin{aligned} u'_R &= U_i \sin(\omega_i t + \Delta\phi) \\ u'_S &= U_i \sin(\omega_i t + \Delta\phi - \frac{2\pi}{3}) \\ u'_T &= U_i \sin(\omega_i t + \Delta\phi + \frac{2\pi}{3}) \end{aligned} \quad (3.16)$$

where  $\Delta\phi$  is the displacement angle between measured input voltage vector  $u_i$  and input current vector  $i_i$ . The virtual voltages from (3.16) can be substituted into (3.11) and (3.15) this will produce new duty cycles. In this way the displacement angle between the input voltage and input current can be controlled. However this control will as its side effect produce reduction of the voltage transfer ratio.

## 3.2 Direct Torque Control

The direct torque control (DTC) belongs to the one of the high performance control strategy for the IM drive fed by VSI [1]. This strategy is based on the direct flux and torque control. The DTC rather belongs to the control algorithm not to the modulation strategy, but because the switching patterns are direct product of the algorithm it can be treated as the modulation strategy too. The torque equation of the IM can be expressed as a function of the angle between rotor and stator flux (3.17).

$$T_e = \frac{3}{2}pP \frac{L_m}{L_r L_s - L_m^2} (\psi_{r\alpha} \psi_{s\beta} - \psi_{r\beta} \psi_{s\alpha}) \quad (3.17)$$

The flux control is based on the fact that changes in the voltage delivered by the converter affect behavior of the IM stator flux.

$$\underline{\psi}_s(k+1) = \underline{\psi}_s(k) + T_s \underline{u}_s(k+1) - R_s T_s i_s(k) \quad (3.18)$$

The DTC control of the MC is described in [81]. Block diagram of this method is in Fig. 3.4. It uses hysteresis comparators for controlling the torque  $c_T$ , flux  $c_\psi$  and the

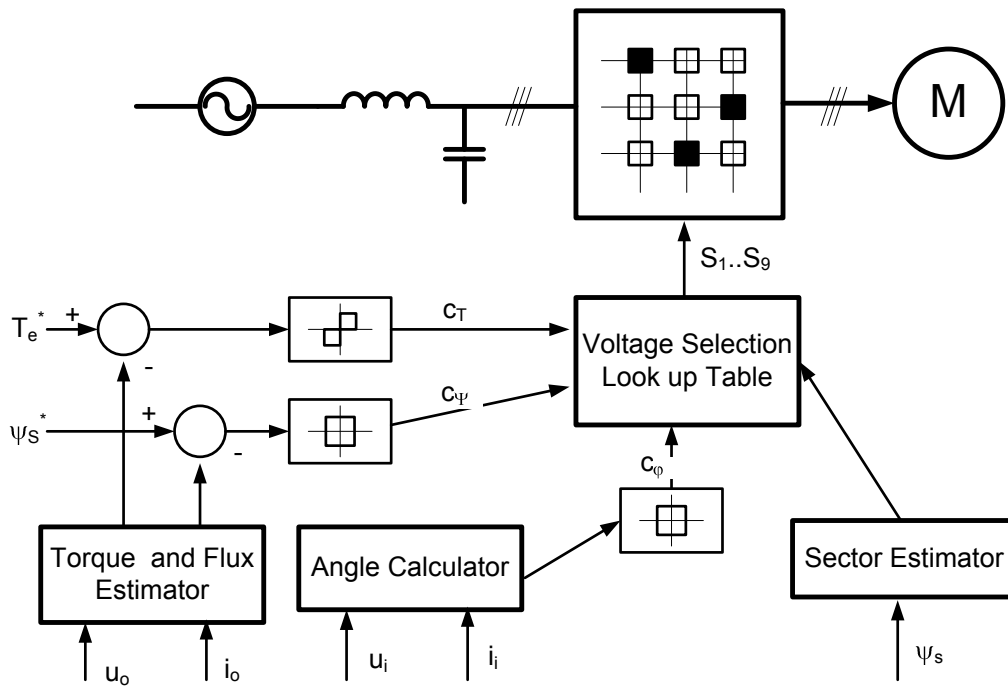


Figure 3.4. Block diagram of the DTC

input current displacement  $c_\varphi$ . These three variables and the position of the stator flux  $\psi_s$  determines which switching combination will be selected from the look-up table.

Look up table for selecting the voltage vector for the DTC algorithm is well known. However the combination with the matrix converter rises the complexity of the algorithm. The selection of the switching state is not exclusively based on the state of the torque and flux, but the selection must also take into account effects on the input current. Moreover the variable switching frequency produced by the algorithm excites high oscillations in the input filter. Therefore the DTC algorithm for the matrix converter is a subject of the intensive study.

### 3.3 Predictive Current Control

Because the processors offers more computational power the predictive current control methods recently emerge feasible approaches [82], [83]. The control strategy is depicted in Fig. 3.5. According to the Fig. 3.5 the algorithm selects the switching state that produces controlled variables closest to their references at the end of sampling period. Strategy uses models of the converter and load to predict the future behaviour of load currents and reactive power.

Simple model of the load side can be expressed as

$$\frac{di_o}{dt} = \frac{1}{L_1}u_o - \frac{R_1}{L_1}i_o \quad (3.19)$$

The state variable model of the input side of the converter is according to Fig. 3.5 as:

$$\frac{di_s}{dt} = \frac{1}{L_f}(u_s - u_i - R_f i_s) \quad (3.20)$$

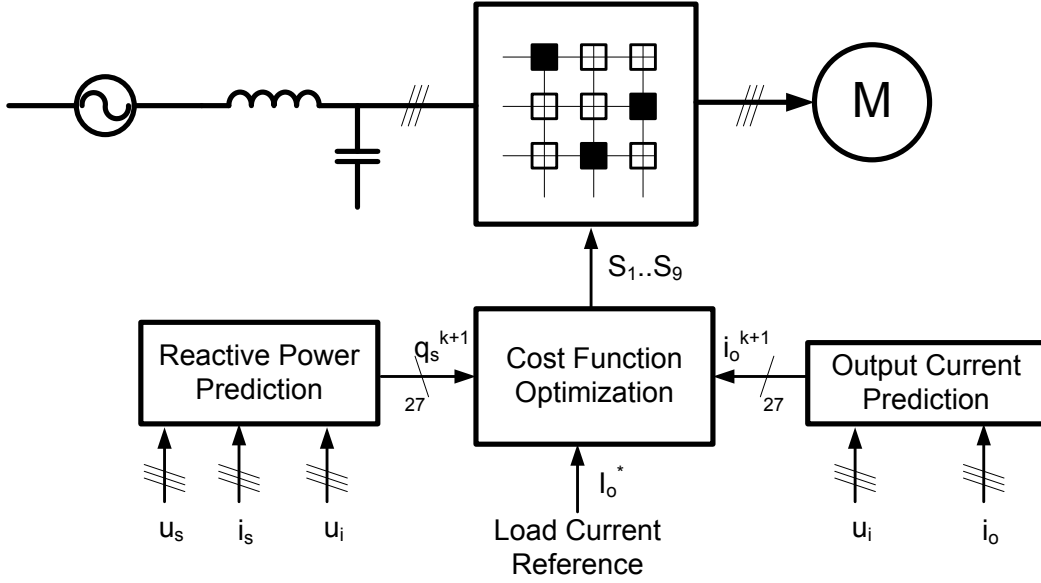


Figure 3.5. Block diagram of the PCC

$$\frac{du_i}{dt} = \frac{1}{C_f}(i_s - i_i) \quad (3.21)$$

When we assume the load as first order system a first order discrete approximation allows to predict the future of the output current as:

$$i_o(k+1) = \frac{T_S u_o(k+1) + L_1 i_o(k)}{L_1 + R_1 T_S} \quad (3.22)$$

Because the input described by (3.20) and (3.21) forms second order system the best solution is to search for the future of the supply current  $i_s(k+1)$ . Two conditions must be fulfilled for the stable operation of the converter: First, the line side of the converter must minimize the instantaneous reactive power, and second, the load current must follow the reference with good accuracy. Both requirements can be merged to the single quality function  $g$  as:

$$g = \delta i_o(k+1) + A \delta q_s(k+1) \quad (3.23)$$

where

$$\Delta i_o(k+1) = |i_{o\alpha}^* - i_{o\alpha}(k+1)| + |i_{o\beta}^* - i_{o\beta}(k+1)| \quad (3.24)$$

$$\Delta q_s(k+1) = |u_{s\alpha}(k+1)i_{s\beta}(k+1) - u_{s\beta}(k+1)i_{s\alpha}(k+1)| \quad (3.25)$$

The (3.24) respects comparison between the reference load currents and predicted ones. The (3.25) corresponds to the predicted input reactive power. The control method operates on the following principle: At each sampling period all 27 possible switching combinations are used to calculate the predicted input and output current values. All values are then evaluated by the quality function  $g$  (3.23). A switching combination that produces minimal value of  $g$  is then selected for the next sampling period. The quality of this control strategy is influenced by the value of the weighting factor  $A$  in (3.23). More information about this control strategy can be found in technical literature.

## 3.4 Space Vector Modulation

### 3.4.1 Direct Space Vector Modulation

The space vector modulation (SVM) principle is well known from the modulation of the conventional inverters [1, 84]. However, its employment in matrix converter is more complex. The output voltage of the conventional inverter is generated combining two from the six active voltage vectors and one from the two zero vectors Fig. 3.6. SVM of the matrix converter offers 18 active voltage vectors and 3 zero Fig. 2.9-2.12 and Tab. 3.2 [79]. Input current space vectors with output voltage space vectors form together two hexagons. These two hexagons limits any reference vector that can be generated by the MC Fig. 3.7. Composition of the output voltage vector is depicted in Fig. 3.8. Vector is formed combining of two surroundings vectors of the sector. The input current vector is formed identically, besides it is forced to the sector where lies the input voltage vector. Combining the sectors of the output voltage and input current sectors we obtain Tab. 3.3, that presents switching combinations that have to be used in order to modulate input current and output voltage vectors at the same time.

State		Switched Switches	$ u_{out} $	$\angle u_{out}$	$ i_{in} $	$\angle i_{in}$
RSS	+1	$S_{RA}S_{SB}S_{SC}$	$\frac{2}{3}u_{RS}$	0	$\frac{2}{\sqrt{3}}i_A$	$-\frac{\pi}{6}$
SRR	-1	$S_{SA}S_{RB}S_{RC}$	$-\frac{2}{3}u_{RS}$	0	$-\frac{2}{\sqrt{3}}i_A$	$-\frac{\pi}{6}$
STT	+2	$S_{SA}S_{TB}S_{TC}$	$\frac{2}{3}u_{ST}$	0	$-\frac{2}{\sqrt{3}}i_A$	$\frac{\pi}{2}$
TSS	-2	$S_{TA}S_{SB}S_{SC}$	$-\frac{2}{3}u_{ST}$	0	$-\frac{2}{\sqrt{3}}i_A$	$\frac{\pi}{2}$
TRR	+3	$S_{TA}S_{RB}S_{RC}$	$\frac{2}{3}u_{TR}$	0	$\frac{2}{\sqrt{3}}i_A$	$\frac{7}{6}\pi$
RTT	-3	$S_{RA}S_{TB}S_{TC}$	$-\frac{2}{3}u_{TR}$	0	$-\frac{2}{\sqrt{3}}i_A$	$\frac{7}{6}\pi$
SRS	+4	$S_{SA}S_{RB}S_{SC}$	$\frac{2}{3}u_{RS}$	$\frac{2}{3}\pi$	$\frac{2}{\sqrt{3}}i_B$	$-\frac{\pi}{6}$
RSR	-4	$S_{RA}S_{SB}S_{RC}$	$-\frac{2}{3}u_{RS}$	$\frac{2}{3}\pi$	$-\frac{2}{\sqrt{3}}i_B$	$-\frac{\pi}{6}$
TST	+5	$S_{TA}S_{SB}S_{TC}$	$\frac{2}{3}u_{ST}$	$\frac{2}{3}\pi$	$\frac{2}{\sqrt{3}}i_B$	$\frac{\pi}{2}$
STS	-5	$S_{SA}S_{TB}S_{SC}$	$-\frac{2}{3}u_{ST}$	$\frac{2}{3}\pi$	$-\frac{2}{\sqrt{3}}i_B$	$\frac{\pi}{2}$
RTR	+6	$S_{RA}S_{TB}S_{RC}$	$\frac{2}{3}u_{TR}$	$\frac{2}{3}\pi$	$\frac{2}{\sqrt{3}}i_B$	$\frac{7}{6}\pi$
TRT	-6	$S_{TA}S_{RB}S_{TC}$	$-\frac{2}{3}u_{TR}$	$\frac{2}{3}\pi$	$-\frac{2}{\sqrt{3}}i_B$	$\frac{7}{6}\pi$
SSR	+7	$S_{SA}S_{SB}S_{RC}$	$\frac{2}{3}u_{RS}$	$\frac{4}{3}\pi$	$\frac{2}{\sqrt{3}}i_C$	$-\frac{\pi}{6}$
RSS	-7	$S_{RA}S_{SB}S_{SC}$	$-\frac{2}{3}u_{RS}$	$\frac{4}{3}\pi$	$-\frac{2}{\sqrt{3}}i_C$	$-\frac{\pi}{6}$
TTS	+8	$S_{TA}S_{TB}S_{SC}$	$\frac{2}{3}u_{ST}$	$\frac{4}{3}\pi$	$\frac{2}{\sqrt{3}}i_C$	$-\frac{\pi}{2}$
SST	-8	$S_{SA}S_{SB}S_{TC}$	$-\frac{2}{3}u_{ST}$	$\frac{4}{3}\pi$	$-\frac{2}{\sqrt{3}}i_C$	$-\frac{\pi}{2}$
RRT	+9	$S_{RA}S_{RB}S_{TC}$	$\frac{2}{3}u_{TR}$	$\frac{2}{3}\pi$	$\frac{2}{\sqrt{3}}i_C$	$\frac{7}{6}\pi$
TTR	-9	$S_{TA}S_{TB}S_{RC}$	$-\frac{2}{3}u_{TR}$	$\frac{2}{3}\pi$	$-\frac{2}{\sqrt{3}}i_C$	$\frac{7}{6}\pi$
RRR	$0_1$	$S_{RA}S_{RB}S_{RC}$	0	—	0	—
SSS	$0_2$	$S_{SA}S_{SB}S_{SC}$	0	—	0	—
TTT	$0_3$	$S_{TA}S_{TB}S_{TC}$	0	—	0	—

Table 3.2. DSVM vectors and switching states

		Output voltage vector sector											
		I. or IV.				II. or V.				III. or VI.			
Input current	I. or IV.	9	7	3	1	6	4	9	7	3	1	6	4
vector	II. or V.	8	9	2	3	5	6	8	9	2	3	5	6
sector	III. or VI.	7	8	1	2	4	5	7	8	1	2	4	5
		$d_\alpha$	$d_\beta$	$d_\gamma$	$d_\delta$	$d_\alpha$	$d_\beta$	$d_\gamma$	$d_\delta$	$d_\alpha$	$d_\beta$	$d_\gamma$	$d_\delta$

Table 3.3. Active vectors composition

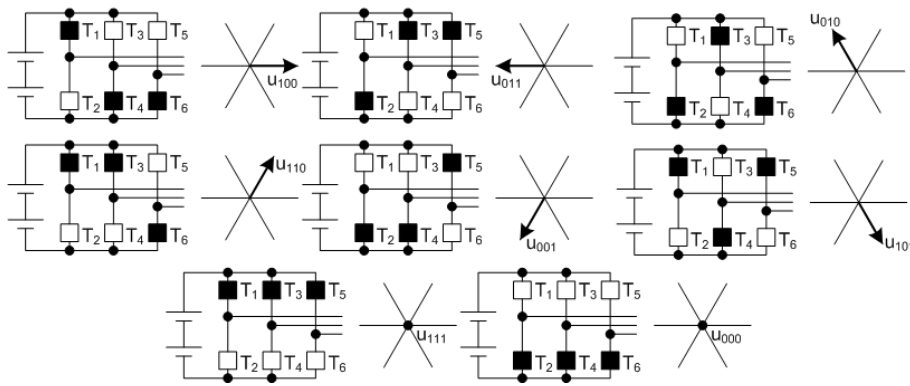


Figure 3.6. Available voltage vectors common inverter SVM

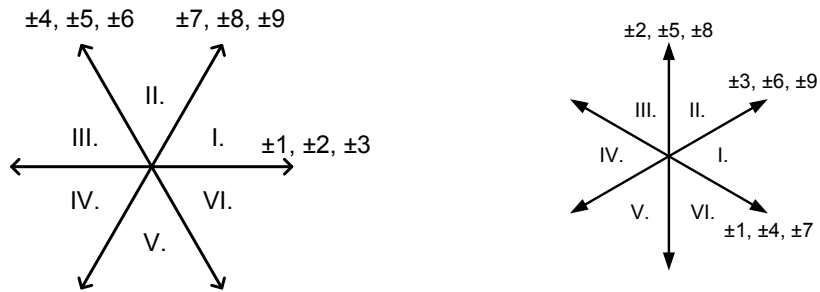


Figure 3.7. Output voltage and input current space vector hexagon

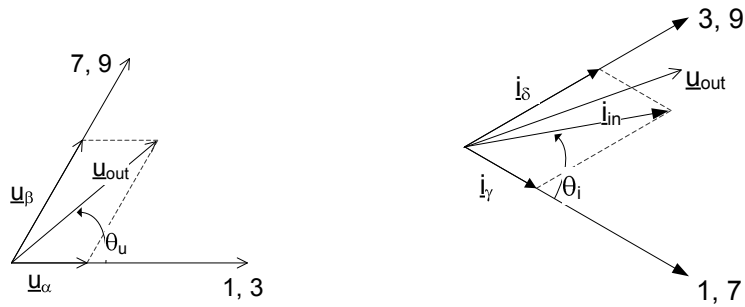


Figure 3.8. Output voltage and input current space vector detail

Output voltage of the matrix converter with employed direct space vector modulation is created by selection of 4 active vectors from the 18 available and 1 zero vector from 3 available during each switching period  $T_S$  [85]. Duty cycles of each switching combination are calculated according to

$$\begin{aligned}
 d_\alpha &= (-1)^{K_u+K_i} \frac{2}{\sqrt{3}} m \frac{\cos(\Theta_u - \frac{\pi}{3}) \cos(\Theta_i - \frac{\pi}{3})}{\cos \varphi_i} \\
 d_\beta &= (-1)^{K_u+K_i+1} \frac{2}{\sqrt{3}} m \frac{\cos(\Theta_u - \frac{\pi}{3}) \cos(\Theta_i + \frac{\pi}{3})}{\cos \varphi_i} \\
 d_\gamma &= (-1)^{K_u+K_i+1} \frac{2}{\sqrt{3}} m \frac{\cos(\Theta_u + \frac{\pi}{3}) \cos(\Theta_i - \frac{\pi}{3})}{\cos \varphi_i} \\
 d_\delta &= (-1)^{K_u+K_i} \frac{2}{\sqrt{3}} m \frac{\cos(\Theta_u + \frac{\pi}{3}) \cos(\Theta_i + \frac{\pi}{3})}{\cos \varphi_i} \\
 d_0 &= 1 - d_\alpha - d_\beta - d_\gamma - d_\delta
 \end{aligned} \tag{3.26}$$

where  $K_u$  is sector where lies output voltage vector,  $K_i$  is sector where lies input current vector,  $m$  is modulation index,  $\Theta_u$  and  $\Theta_i$  are phase angles of the vectors within the sectors and  $\varphi_i$  is the displacement angle between the input voltage and current vectors [79].

### 3.4.2 Indirect Space Vector Modulation

There are several indirect space vector modulation (ISVM) methods. The most used is method proposed by Huber and Borojevic [45]. The principle of ISVM can be easily comprehend when we split the converter into two parts according to the function that they perform.

- Generates output voltages (same as VSI)
- Directs output currents to the input phases to consume sinusoidal currents with defined power factor (input current modulation)

It is easier to analyse the both processes separately. The matrix converter can be taken as a combination of virtual current source rectifier and virtual voltage source inverter connected by virtual DC link Fig. 3.9. This enables to use conventional modulation strategies known for indirect AC-DC-AC converters. However, this approach decreases allowable switching combinations from 27 to 21, because direct switching combinations can not be used.

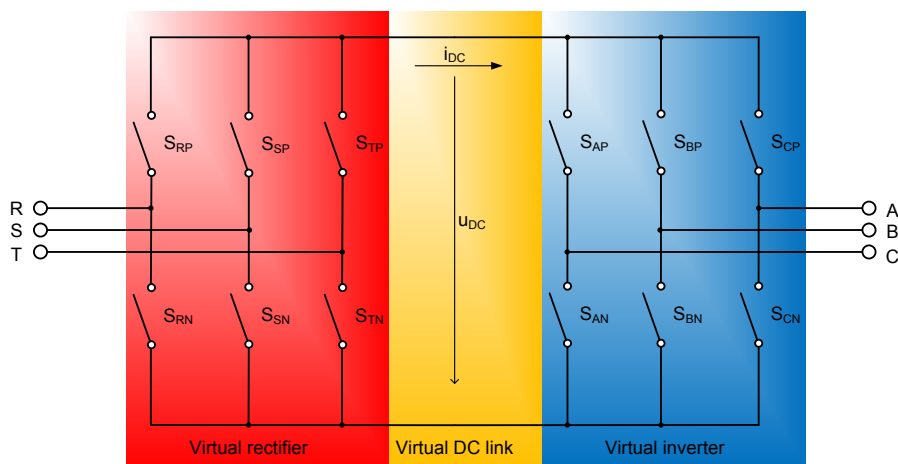


Figure 3.9. Matrix converter representation for indirect modulation

Due to the assumptions mentioned above, the transfer matrix of the MC splits into  $\mathbf{M}_R$  and  $\mathbf{M}_I$

$$\mathbf{M}_R = \begin{bmatrix} S_{RP} & S_{SP} & S_{TP} \\ S_{RN} & S_{SN} & S_{TN} \end{bmatrix} \quad (3.27)$$

$$\mathbf{M}_I = \begin{bmatrix} S_{AP} & S_{BP} & S_{CP} \\ S_{AN} & S_{BN} & S_{CN} \end{bmatrix} \quad (3.28)$$

For the voltages and currents of the virtual rectifier stage can be written

$$\underline{u}_{DC} = \mathbf{M}_R \underline{u}_{in} \quad \begin{bmatrix} u_{DCP} \\ u_{DCN} \end{bmatrix} = \begin{bmatrix} S_{RP} & S_{SP} & S_{TP} \\ S_{RN} & S_{SN} & S_{TN} \end{bmatrix} \begin{bmatrix} u_R \\ u_S \\ u_T \end{bmatrix} \quad (3.29)$$

$$\underline{i}_{in} = \mathbf{M}_R^T \underline{i}_{DC} \quad \begin{bmatrix} i_R \\ i_S \\ i_T \end{bmatrix} = \begin{bmatrix} S_{RP} & S_{RN} \\ S_{SP} & S_{SN} \\ S_{TP} & S_{TN} \end{bmatrix} \begin{bmatrix} i_{DCP} \\ i_{DCN} \end{bmatrix} \quad (3.30)$$

and for the virtual inverter stage

$$\underline{u}_{out} = \mathbf{M}_I^T \underline{u}_{DC} \quad \begin{bmatrix} u_A \\ u_B \\ u_C \end{bmatrix} = \begin{bmatrix} S_{AP} & S_{AN} \\ S_{BP} & S_{BN} \\ S_{CP} & S_{CN} \end{bmatrix} \begin{bmatrix} u_{DCP} \\ u_{DCN} \end{bmatrix} \quad (3.31)$$

$$\underline{i}_{DC} = \mathbf{M}_I \underline{i}_{out} \quad \begin{bmatrix} i_{DCP} \\ i_{DCN} \end{bmatrix} = \begin{bmatrix} S_{AP} & S_{BP} & S_{CP} \\ S_{AN} & S_{BN} & S_{CN} \end{bmatrix} \begin{bmatrix} i_A \\ i_B \\ i_C \end{bmatrix} \quad (3.32)$$

Combining (3.29) with (3.31) and (3.30) with (3.32) final transfer equations for voltage and current

$$\underline{u}_{out} = \mathbf{M}_I^T \underline{u}_{DC} = \mathbf{M}_I^T \mathbf{M}_R \underline{u}_{in} = \begin{bmatrix} S_{AP} & S_{AN} \\ S_{BP} & S_{BN} \\ S_{CP} & S_{CN} \end{bmatrix} \begin{bmatrix} S_{RP} & S_{SP} & S_{TP} \\ S_{RN} & S_{SN} & S_{TN} \end{bmatrix} \underline{u}_{in} = \mathbf{M} \underline{u}_{in} \quad (3.33)$$

$$\underline{i}_{in} = \mathbf{M}_R^T \underline{i}_{DC} = \mathbf{M}_R^T \mathbf{M}_I \underline{i}_{out} = \begin{bmatrix} S_{RP} & S_{RN} \\ S_{SP} & S_{SN} \\ S_{TP} & S_{TN} \end{bmatrix} \begin{bmatrix} S_{AP} & S_{BP} & S_{CP} \\ S_{AN} & S_{BN} & S_{CN} \end{bmatrix} \underline{i}_{out} = \mathbf{M}^T \underline{i}_{out} \quad (3.34)$$

$$\mathbf{M} = \begin{bmatrix} S_{RA} & S_{SA} & S_{TA} \\ S_{RB} & S_{SB} & S_{TB} \\ S_{RC} & S_{SC} & S_{TC} \end{bmatrix} = \mathbf{M}_I^T \mathbf{M}_R = \begin{bmatrix} S_{AP} & S_{AN} \\ S_{BP} & S_{BN} \\ S_{CP} & S_{CN} \end{bmatrix} \begin{bmatrix} S_{RP} & S_{SP} & S_{TP} \\ S_{RN} & S_{SN} & S_{TN} \end{bmatrix} \quad (3.35)$$

Equation (3.35) defines every switching combination for the ISVM and it can be easily reassigned to the real MC switching combination. As a simple example lets suppose, that switches  $S_{RP}$  and  $S_{SN}$  are closed on the virtual rectifier stage and switches  $S_{AP}$  and  $S_{BN}$  and  $S_{CN}$  are closed at the virtual inverter stage. This can be represented as

$$\mathbf{M} = \mathbf{M}_I^T \mathbf{M}_R = \begin{bmatrix} 1 & 0 \\ 0 & 1 \\ 0 & 1 \end{bmatrix} \begin{bmatrix} 1 & 0 & 0 \\ 0 & 1 & 0 \end{bmatrix} = \begin{bmatrix} 1 & 0 & 0 \\ 0 & 1 & 0 \\ 0 & 1 & 0 \end{bmatrix} \quad (3.36)$$

Visualization of the example situation by the means is in Fig. 3.10. Due to the bidirectionality of the switches the sign of the voltage in the virtual DC-link is not important. Therefore the situations depicted in Fig. 3.10 and Fig. 3.11 are equal. However, in most cases it is silently assumed that two phases with highest line-to-line voltage are always used on the input stage of the converter, so the condition  $u_{PN} \geq 0$  is fulfilled. Modulation of the both parts must be synchronized together because the MC lacks DC-link accumulation elements. Synchronization is achieved by selection of correct switching pattern of the MC.

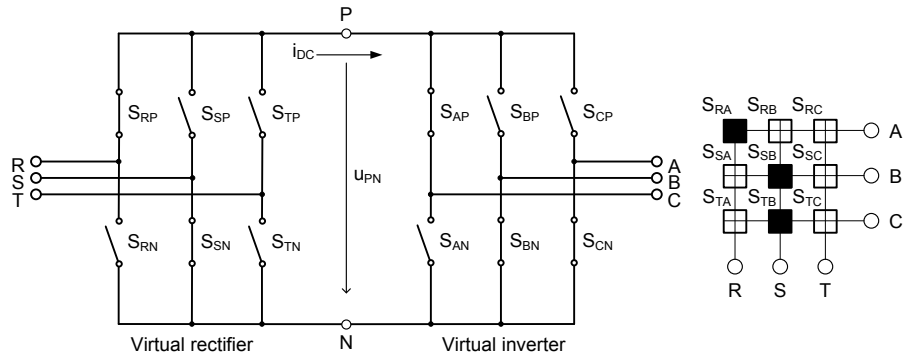


**Figure 3.10.** Example of switching combination of (3.36)

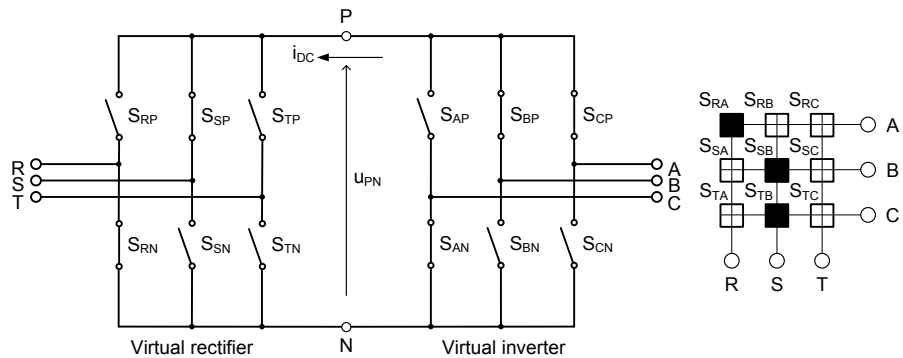


**Figure 3.11.** Example of switching combination of (3.36)

Output voltage SVM is implemented like classical space vector modulated VSI. Available vectors are summarized in Tab. 3.4. The output voltage vector is generated as two nearest active voltage vectors and zero vector Fig. 3.12.

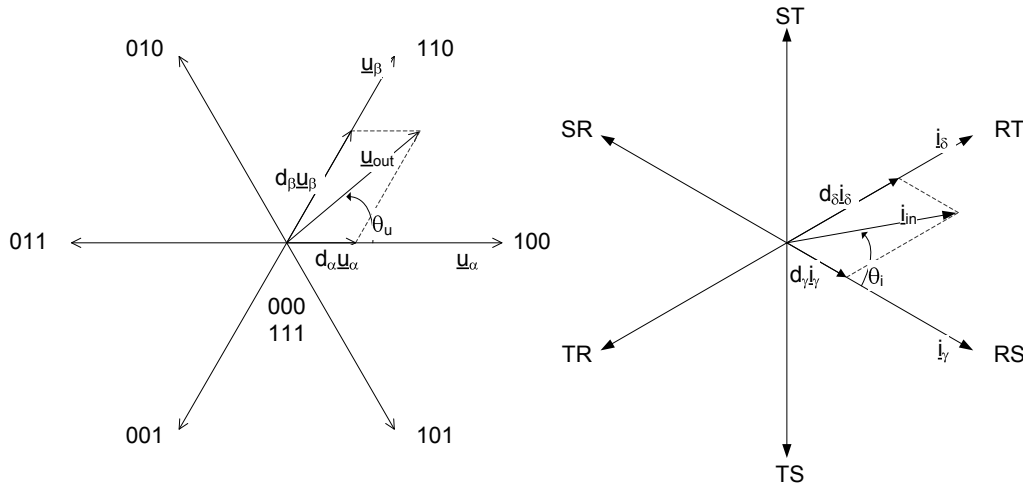
According to Fig. 3.12 the  $d_\alpha$  and  $d_\beta$  represents duty times of both active vectors. The output voltage vector can be then defined as

$$\underline{u}_{\text{out}} = u_\alpha d_\alpha + u_\beta d_\beta \quad (3.37)$$

The sum of the duty times during one switching period  $T_S$  is equal to 1, therefore  $d_0$  is duty time of zero voltage vector

$$d_\alpha + d_\beta + d_0 = 1 \quad (3.38)$$

Vector	Switched combination	$\angle u_{out}$	$i_{DC}$
000	$S_{NA}S_{NB}S_{NC}$	—	0
100	$S_{PA}S_{NB}S_{NC}$	0	$i_A$
110	$S_{PA}S_{PB}S_{NC}$	$\frac{\pi}{3}$	$-i_C$
010	$S_{NA}S_{PB}S_{NC}$	$\frac{2}{3}\pi$	$i_B$
011	$S_{NA}S_{PB}S_{PC}$	$\pi$	$-i_A$
001	$S_{NA}S_{NB}S_{PC}$	$\frac{4}{3}\pi$	$i_C$
101	$S_{PA}S_{NB}S_{PC}$	$\frac{5}{3}\pi$	$-i_B$
111	$S_{PA}S_{PB}S_{PC}$	—	0

**Table 3.4.** Available vector combinations of virtual inverter stage

**Figure 3.12.** Virtual inverter and virtual rectifier stages space vectors

With the help of Fig. 3.12 duty time for the active vectors are obtained by solving (3.37) and (3.38)

$$d_\alpha = m_I \sin\left(\frac{\pi}{3} - \theta_I\right) \quad (3.39)$$

$$d_\beta = m_I \sin(\theta_I) \quad (3.40)$$

$$d_0 = d_\alpha - d_\beta \quad (3.41)$$

where  $\theta_I$  is angle of generated voltage vector within the sector Fig. 3.12 and  $m_I$  is modulation index of the output voltage. It can be defined as

$$m_I = \frac{\frac{|u_{out}|}{k_{\alpha\beta}}}{\frac{\sqrt{3}}{2}u_{DC}} = \frac{\sqrt{3}|u_{out}|}{u_{DC}} \quad (3.42)$$

Same as for VSI when  $m_1 \leq 1$  matrix converter operates in linear range, the generated voltage vector copies circular path. When modulation index  $m_1 \geq 1$  then the converter operates in over modulation. The input current reference vector can be generated analogously as voltage reference vector combining two adjacent active current vectors and zero vector Fig. 3.12. Available combinations of the virtual rectifier are presented in Tab. 3.5.

Vector	Switched combination	$\angle i_{in}$	$u_{DC}$
RS	$S_{RP}S_{SN}$	$-\frac{\pi}{6}$	$u_{RS}$
RT	$S_{RP}S_{TN}$	$\frac{\pi}{6}$	$-u_{TR}$
ST	$S_{SP}S_{TN}$	$\frac{\pi}{2}$	$u_{ST}$
SR	$S_{SP}S_{RN}$	$\frac{5}{6}\pi$	$-u_{RS}$
TR	$S_{TP}S_{RN}$	$-\frac{5}{6}\pi$	$u_{TR}$
TS	$S_{TP}S_{SN}$	$-\frac{\pi}{2}$	$-u_{ST}$
RR	$S_{RP}S_{RN}$	—	0
SS	$S_{SP}S_{SN}$	—	0
TT	$S_{TP}S_{TN}$	—	0

**Table 3.5.** Available vector combinations of virtual rectifier stage

In order to make modulator design more simple we can define table that summarizes all possible switching combinations based on Fig. 3.12 and Tab. 3.4 and 3.5. Modulation algorithm then selects proper switching pattern based on the actual input current vector sector and required output voltage vector sector.

		Output voltage vector sector					
		1	2	3	4	5	6
Input current vector sector	1	RS,RT 100, 110, 111	RS,RT 110, 010, 000	RS,RT 010, 011, 111	RS,RT 011, 001, 000	RS,RT 001, 101, 111	RS,RT 101, 100, 000
	2	RT,ST 100, 110, 111	RT,ST 110, 010, 000	RT,ST 010, 011, 111	RT,ST 011, 001, 000	RT,ST 001, 101, 111	RT,ST 101, 001, 000
	3	ST,SR 100, 110, 111	ST,SR 110, 010, 000	ST,SR 010, 011, 111	ST,SR 011, 001, 000	ST,SR 001, 101, 111	ST,SR 101, 100, 000
	4	SR,TR 100, 110, 111	SR,TR 110, 010, 000	SR,TR 010, 011, 111	SR,TR 011, 001, 000	SR,TR 001, 101, 111	SR,TR 101, 001, 000
	5	TR,TS 100, 110, 111	TR,TS 110, 010, 000	TR,TS 010, 011, 111	TR,TS 011, 001, 000	TR,TS 001, 101, 111	TR,TS 101, 100, 000
	6	TS,RS 100, 110, 111	TS,RS 110, 010, 000	TS,RS 010, 011, 111	TS,RS 011, 001, 000	TS,RS 001, 101, 111	TS,RS 101, 001, 000

**Table 3.6.** Switching table for ISVM

$$\underline{i}_{in} = k_{\alpha\beta}(i_R + i_S \mathbf{e}^{j\frac{2}{3}\pi} + i_T \mathbf{e}^{-j\frac{2}{3}\pi}) \quad (3.43)$$

The  $d_\gamma$  and  $d_\delta$  represents duty times of both active vectors. The input current vector can be then defined as

$$\underline{i}_{\text{in}} = i_{\gamma}d_{\gamma} + i_{\delta}d_{\delta} \quad (3.44)$$

The sum of the duty times during one switching period  $T_S$  is equal to 1, therefore  $d_{0R}$  is duty time of zero voltage vector

$$d_{\gamma} + d_{\delta} + d_{0R} = 1 \quad (3.45)$$

With the help of Fig. 3.12 duty time for the active vectors are obtained by solving (3.44) and (3.45)

$$d_{\gamma} = m_R \sin\left(\frac{\pi}{3} - \theta_R\right) \quad (3.46)$$

$$d_{\delta} = m_R \sin(\theta_R) \quad (3.47)$$

$$d_{0R} = 1 - d_{\gamma} - d_{\delta} \quad (3.48)$$

where  $\theta_R$  is angle of input current vector within the sector Fig. 3.12 and  $m_R$  is current modulation index. It can be defined as

$$m_R = \frac{\frac{|\underline{u}_{\text{in}}|}{k_{\alpha\beta}}}{\frac{\sqrt{3}}{2}\sqrt{3}i_{\text{DC}}} = \frac{|\underline{i}_{\text{in}}|}{i_{\text{DC}}} \quad (3.49)$$

From (3.49) is obvious that current modulation index is ratio between input current vector module and radius of the inner circle of hexagon with side length of  $\sqrt{3}i_{\text{DC}}$ . Virtual rectifier stage with employed SVM generates voltage of the virtual DC-link. Average value of the  $\bar{u}_{\text{DC}}$  can be calculated from power balance of the converter

$$\begin{aligned} P_{\text{DC}} &= P_{\text{in}} \\ u_{\text{DC}}i_{\text{DC}} &= \frac{2}{3}u_{\text{in}}i_{\text{in}} = \frac{2}{3}|\underline{u}_{\text{in}}||\underline{i}_{\text{in}}|\cos\varphi_{\text{in}} \\ u_{\text{DC}} &= \frac{2}{3}|\underline{u}_{\text{in}}|\frac{|\underline{i}_{\text{in}}|}{i_{\text{DC}}}\cos\varphi_{\text{in}} \end{aligned} \quad (3.50)$$

Finally substituting (3.49) into (3.50)

$$u_{\text{DC}} = \frac{2}{3}|\underline{u}_{\text{in}}|m_R\cos\varphi_{\text{in}} \quad (3.51)$$

From (3.51) can be seen that parameters  $m_R$  and  $\cos\varphi_{\text{in}}$  has direct influence on the DC-link voltage value. Maximal transfer ratio of the matrix converter is achieved when

$$\begin{aligned} m_R &= 1 \\ \cos\varphi_{\text{in}} &= 1 \end{aligned} \quad (3.52)$$

The current modulation is usually set to 1 and output voltage module is controlled by changing of the output voltage modulation index  $m_I$ . Second condition shows that maximum voltage transfer ratio can be achieved when matrix converter consumes zero reactive power. Combining presented SVM strategy for virtual inverter stage and for virtual rectifier stage we receive final algorithm for ISVM modulation of the matrix converter [86]. It is obvious, that combination of six and six sectors of the rectifier and inverter hexagons leads to  $6 \cdot 6 = 36$  duty cycle combinations. Voltage in virtual DC-link  $u_{\text{DC}}$  is equal to voltage of two active phases during the times  $d_{\gamma}$ ,  $d_{\delta}$ . The output voltage is modulated from the fictive  $u_{\text{DC}}$  applying  $u_{\alpha}$  and  $u_{\beta}$  for times  $d_{\alpha}$ ,  $d_{\beta}$ . This leads to formation of new duty cycles

$$\begin{aligned}
 d_{\alpha\gamma} &= m_R m_I \sin\left(\frac{\pi}{3} - \Theta_I\right) \sin\left(\frac{\pi}{3} - \Theta_R\right) \\
 d_{\alpha\delta} &= m_R m_I \sin\left(\frac{\pi}{3} - \Theta_I\right) \sin(\Theta_R) \\
 d_{\beta\gamma} &= m_R m_I \sin(\Theta_I) \sin\left(\frac{\pi}{3} - \Theta_R\right) \\
 d_{\beta\delta} &= m_R m_I \sin\left(\frac{\pi}{3} - \Theta_I\right) \sin(\Theta_R)
 \end{aligned} \tag{3.53}$$

Rest time of the switching period is switched zero vector

$$d_0 = 1 - d_{\alpha\gamma} - d_{\alpha\delta} - d_{\beta\gamma} - d_{\beta\delta} \tag{3.54}$$

Different sequence of the duty times can optimize switching from the point of power losses or harmonics content of consumed current [80, 87]. Example of one rules set:

- Input switching combination is always  $d_\gamma d_\delta d_0$
- When sum of input current and output voltage sectors is odd, then the switching sequence is  $d_\alpha d_\beta d_\beta d_\alpha d_0$
- When sum of input current and output voltage sectors is even, then the switching sequence is  $d_\beta d_\alpha d_\alpha d_\beta d_0$
- When the number of input current sector is odd, then output zero vector is 000
- When the number of input current sector is even, then output zero vector is 111

In [38] can be found optimized switching table for the ISVM modulation of the matrix converter. Optimization uses idea of switching of the virtual rectifier stage in time instants when is switched on zero output voltage vector (no current is flowing in virtual DC-link). The switching sequence of the virtual inverter is optimized in order to minimize number of switchings too.

		Output voltage vector sector					
		1	2	3	4	5	6
Input current vector sector	1	RS,RT 100, 110, 111	RS,RT 010, 110, 111	RS,RT 010, 011, 111	RS,RT 001, 011, 111	RS,RT 001, 101, 111	RS,RT 100, 101, 111
	2	RT,ST 110, 100, 000	RT,ST 110, 010, 000	RT,ST 011, 010, 000	RT,ST 011,001, 000	RT,ST 101, 001, 000	RT,ST 101, 001, 000
	3	ST,SR 100, 110, 111	ST,SR 010, 110, 111	ST,SR 010, 011, 111	ST,SR 001, 011, 111	ST,SR 001, 101, 111	ST,SR 100, 101, 111
	4	SR,TR 110, 100, 000	SR,TR 110, 010, 000	SR,TR 011, 010, 000	SR,TR 011,001, 000	SR,TR 101, 001, 000	SR,TR 101, 001, 000
	5	TR,TS 100, 110, 111	TR,TS 010, 110, 111	TR,TS 010, 011, 111	TR,TS 001, 011, 111	TR,TS 001, 101, 111	TR,TS 100, 101, 111
	6	TS,RS 110, 100, 000	TS,RS 110, 010, 000	TS,RS 011, 010, 000	TS,RS 011,001, 000	TS,RS 101, 001, 000	TS,RS 101, 001, 000

**Table 3.7.** Optimized switching table for ISVM

Idea of optimization is obvious from Fig. 3.13 and Fig. 3.14. In both cases we suppose that required output voltage vector is in sector 1 and input current vector is in sector 6. Figures shows only first half of switching period, because the second half is symmetric. It is obvious that when we change order of switching of output vectors we can save one switching in the interval of zero vector combination thus switching losses decrease.

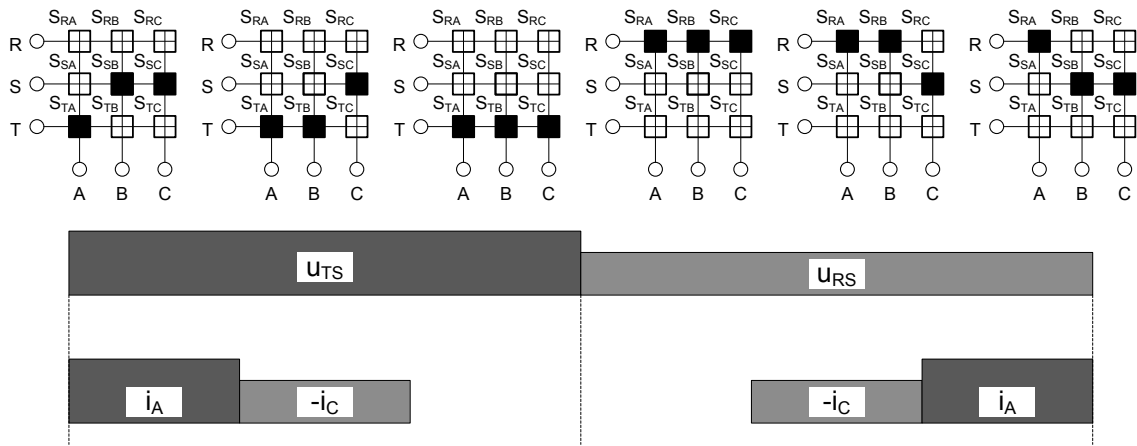


Figure 3.13. Example of ISVM switching sequence

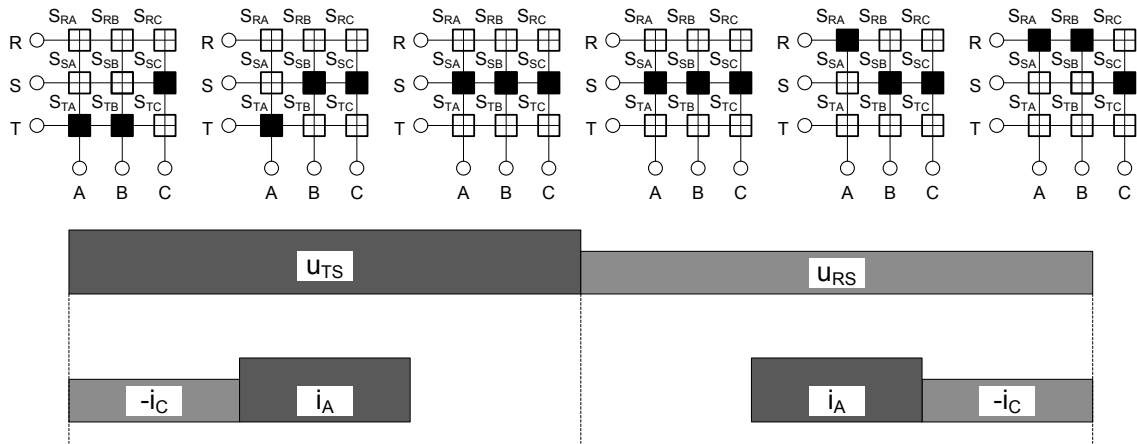


Figure 3.14. Example of optimized ISVM switching sequence



## Chapter 4

# Problems of the Induction Motor Mathematical Description

Nowadays induction machines (IM) are widely used in variable speed drives [1–3]. For an understanding and clear specification of the electromagnetic processes in induction machines different equivalent circuits can be employed [88]. In order to reduce the complexity of the mathematical model, resistances and inductances are represented as concentrated components and the 3-phase winding system is assumed to be symmetrical. The equivalent circuits are also used as a starting point for the design of a drive controller. For the satisfactory functioning of a controller or model of a machine, designed on the basis of the machine's equivalent circuit, the parameters of the equivalent circuit must be known with sufficient accuracy.

In order to obtain maximum performance from the drive, a precise regulation algorithm is needed. These algorithms are based mostly on the regulation of machine flux, that can not be measured directly. For an estimation of the inner machine flux, the models based on machine equations, machine parameters from an equivalent circuit and measured values are used. The final accuracy of the equivalent circuit and hereby controller as well depend on an exact knowledge of the equivalent circuit values. Another important asset of the equivalent circuit is the fact that, from the mathematical description of the equivalent circuit, the behaviour of the machine including a stable operation area or a maximal reachable torque etc. can be analytically derived [89].

### 4.1 IM Description Based on State Variables

The IM can be mathematically described by set of higher order differential equations. The state space representation, where the system is described by the set of first order differential equations is advantageous. It is considered as a good starting point for design of controllers and system observers [90].

The time continuous system can be represented as

$$\begin{aligned}\dot{\mathbf{x}}(t) &= \mathbf{A}(t)\mathbf{x}(t) + \mathbf{B}(t)\mathbf{u}(t); \mathbf{x} \in \mathbb{R}^n; \mathbf{u} \in \mathbb{R}^m; \mathbf{x}_0 = \mathbf{x}(t_0) \\ \mathbf{y}(t) &= \mathbf{C}(t)\mathbf{x}(t); \mathbf{y} \in \mathbb{R}^p\end{aligned}\tag{4.1}$$

where  $\mathbf{A}$  represents system matrix,  $\mathbf{B}$  represents input matrix,  $\mathbf{C}$  represents output matrix,  $\mathbf{x}$  is vector of state variables and  $\mathbf{u}$  is input vector.

However the control algorithm and estimator are processed by a computer, it means in discrete time. So the system receives information at definite equidistant points after sampling and A/D conversion. That is why the model of the IM have to be discretised. The discretisation is quite simple when the electrical transient processes settles faster

than mechanical ones, the system can be then treated as time invariant over sampling period  $T$  and thus discrete representation of the (4.1) is after integration expressed as

$$\begin{aligned}\mathbf{x}(k+1) &= \mathbf{\Phi}\mathbf{x}(k) + \mathbf{H}\mathbf{u}(k) \\ \mathbf{y}(k) &= \mathbf{C}\mathbf{x}(k)\end{aligned}\quad (4.2)$$

where input vector  $\mathbf{u}(k)$  is given by controller and has step shape. The transition matrix  $\mathbf{\Phi}$  and input matrix  $\mathbf{H}$  depends on sampling period. They can be calculated from matrix exponential function  $\mathbf{e}^{\mathbf{A}T}$ . Solution of this function can be found as series expansion (4.3). For the systems with sampling period lower than  $500\mu s$  the first order approximation is usually enough.

$$\mathbf{\Phi} = \mathbf{e}^{\mathbf{A}T} = \sum_{\nu=0}^{\infty} (\mathbf{A})^{\nu} \frac{T^{\nu}}{\nu!}; \quad \mathbf{H} = \int_{kT}^{(k+1)T} \mathbf{e}^{\mathbf{A}(T-\tau)} \mathbf{B} d\tau = \sum_{\nu=0}^{\infty} (\mathbf{A})^{\nu-1} \frac{T^{\nu}}{\nu!} \mathbf{B} \quad (4.3)$$

Derivation of the IM model for the control will proceed from continuous state space model of the IM, afterwards this model will be discretised. As a starting point for the derivation of the model are used stator and rotor voltage equations. Under assumption that rotor and stator windings of IM are symmetrical we can apply (9.1) to (9.16), thus we get representation of IM by space vectors

$$\begin{aligned}\underline{u}_s^s &= R_s \underline{i}_s^s + \frac{d}{dt} \underline{\Psi}_s^s \\ 0 &= \underline{u}_r^r = R_r \underline{i}_r^r + \frac{d}{dt} \underline{\Psi}_r^r\end{aligned}\quad (4.4)$$

where superscript  $s$  resp.  $r$  represents quantities in stator resp. rotor reference system. Lets assume arbitrary rotating system denoted as  $k$  then (4.4) is

$$\begin{aligned}\underline{u}_s^k \mathbf{e}^{j\theta_k} &= R_s \underline{i}_s^k \mathbf{e}^{j\theta_k} + \frac{d}{dt} \underline{\Psi}_s^k \mathbf{e}^{j\theta_k} \\ 0 &= \underline{u}_r^k \mathbf{e}^{j\theta_k - \theta_r} = R_r \underline{i}_r^k \mathbf{e}^{j\theta_k - \theta_r} + \frac{d}{dt} \underline{\Psi}_r^k \mathbf{e}^{j\theta_k - \theta_r}\end{aligned}\quad (4.5)$$

where  $\theta_r$  means rotor angle and  $\theta_k$  is selected reference frame angle. After derivation of (4.5) we obtain

$$\begin{aligned}\underline{u}_s^k &= R_s \underline{i}_s^k + \frac{d}{dt} \underline{\Psi}_s^k + j\omega_k \underline{\Psi}_s^k \\ 0 &= \underline{u}_r^k = R_r \underline{i}_r^k + \frac{d}{dt} \underline{\Psi}_r^k + j(\omega_k - \omega_r) \underline{\Psi}_r^k\end{aligned}\quad (4.6)$$

and space vectors of the stator and rotor fluxes

$$\begin{aligned}\underline{\Psi}_s^k &= L_s \underline{i}_s^k + L_m \underline{i}_r^k \\ \underline{\Psi}_r^k &= L_r \underline{i}_r^k + L_m \underline{i}_s^k\end{aligned}\quad (4.7)$$

Splitting of the space vector to its components (real and imaginary part)  $\underline{x} = x_u + jx_v$  in (4.6) and (4.7) will produce final equation system for modelling of IM

$$\begin{aligned}u_{su} &= R_s i_{su} + \frac{d}{dt} \Psi_{su} - \omega_k \Psi_{sv} \\ u_{sv} &= R_s i_{sv} + \frac{d}{dt} \Psi_{sv} + \omega_k \Psi_{su} \\ 0 = u_{ru} &= R_r i_{ru} + \frac{d}{dt} \Psi_{ru} - (\omega_k - \omega_r) \Psi_{rv} \\ 0 = u_{rv} &= R_r i_{rv} + \frac{d}{dt} \Psi_{rv} + (\omega_k - \omega_r) \Psi_{ru} \\ \Psi_{su} &= L_s i_{su} + L_m i_{ru} \\ \Psi_{sv} &= L_s i_{sv} + L_m i_{rv} \\ \Psi_{ru} &= L_r i_{ru} + L_m i_{su} \\ \Psi_{rv} &= L_r i_{rv} + L_m i_{sv}\end{aligned}\quad (4.8)$$

As was stated before we can select coordinate system with arbitrary angular speed  $\omega_k$ . In praxis only 3 angular speeds are used. Here will be presented only coordinate system connected with stator (stationary) where  $\omega_k = 0$ , that is used in realisation of control algorithm. This system is noted with  $\alpha, \beta$  coordinates.

$$\begin{aligned}u_{s\alpha} &= R_s i_{s\alpha} + \frac{d}{dt} \Psi_{s\alpha} \\ u_{s\beta} &= R_s i_{s\beta} + \frac{d}{dt} \Psi_{s\beta} \\ 0 = u_{r\alpha} &= R_r i_{r\alpha} + \frac{d}{dt} \Psi_{r\alpha} + \omega_r \Psi_{r\beta} \\ 0 = u_{r\beta} &= R_r i_{r\beta} + \frac{d}{dt} \Psi_{r\beta} - \omega_r \Psi_{r\alpha} \\ \Psi_{s\alpha} &= L_s i_{s\alpha} + L_m i_{r\alpha} \\ \Psi_{s\beta} &= L_s i_{s\beta} + L_m i_{r\beta} \\ \Psi_{r\alpha} &= L_r i_{r\alpha} + L_m i_{s\alpha} \\ \Psi_{r\beta} &= L_r i_{r\beta} + L_m i_{s\beta}\end{aligned}\quad (4.9)$$

Equations describing IM in other coordinate systems can be found in Appendix E.

Not all electrical quantities e.g rotor current space vector  $\underline{i}_r$  or stator flux space vector  $\underline{\Psi}_s$  in the systems (4.9) - (9.24) need to be known. These quantities are usually eliminated from the system of equations with the help of following equations

$$\begin{aligned} \underline{i}_r &= \frac{1}{L_r} (\underline{\Psi}_r - L_m \underline{i}_s) \\ \underline{\Psi}_s &= L_s \underline{i}_s + \frac{L_m}{L_r} (\underline{\Psi}_r - L_m \underline{i}_s) \end{aligned} \quad (4.10)$$

Substituting the (4.10) into (4.9) and defining  $T_s = L_s/R_s$  and  $T_r = L_r/R_r$  and total leakage factor as  $\sigma = 1 - L_m^2/(L_s L_r)$  and leads to final state equation set of IM in stator coordinate system

$$\begin{aligned} \frac{d}{dt} i_{s\alpha} &= - \left( \frac{1}{\sigma T_s} + \frac{1-\sigma}{\sigma T_r} \right) i_{s\alpha} + \frac{1-\sigma}{\sigma T_r} \Psi'_{r\alpha} + \frac{1-\sigma}{\sigma} \omega_m \Psi'_{r\beta} + \frac{1}{\sigma L_s} u_{s\alpha} \\ \frac{d}{dt} i_{s\beta} &= - \left( \frac{1}{\sigma T_s} + \frac{1-\sigma}{\sigma T_r} \right) i_{s\beta} - \frac{1-\sigma}{\sigma} \omega_m \Psi'_{r\alpha} + \frac{1-\sigma}{\sigma} \Psi'_{r\beta} + \frac{1}{\sigma L_s} u_{s\beta} \\ \frac{d}{dt} \Psi'_{r\alpha} &= \frac{1}{T_r} i_{s\alpha} - \frac{1}{T_r} \Psi'_{r\alpha} - \omega_m \Psi'_{r\beta} \\ \frac{d}{dt} \Psi'_{r\beta} &= \frac{1}{T_r} i_{s\beta} + \omega_m \Psi'_{r\alpha} - \frac{1}{T_r} \Psi'_{r\beta} \end{aligned} \quad (4.11)$$

where  $\underline{\Psi}'_r = \underline{\Psi}_r/L_m$ . Considering (4.1) the vectors  $\mathbf{x}$  and  $\mathbf{u}$  can be defined as

$$\mathbf{x}^T = [i_{s\alpha}, i_{s\beta}, \Psi'_{r\alpha}, \Psi'_{r\beta}]; \mathbf{u}^T = [u_{s\alpha}, u_{s\beta}] \quad (4.12)$$

and the system input and state matrices as

$$\mathbf{A} = \begin{bmatrix} - \left( \frac{1}{\sigma T_s} + \frac{1-\sigma}{\sigma T_r} \right) & 0 & \frac{1-\sigma}{\sigma T_r} & \frac{1-\sigma}{\sigma} \omega_m \\ 0 & - \left( \frac{1}{\sigma T_s} + \frac{1-\sigma}{\sigma T_r} \right) & - \frac{1-\sigma}{\sigma} \omega_m & \frac{1-\sigma}{\sigma} \\ \frac{1}{T_r} & 0 & - \frac{1}{T_r} & - \omega_m \\ 0 & \frac{1}{T_r} & \omega_m & - \frac{1}{T_r} \end{bmatrix} \quad (4.13)$$

$$\mathbf{B} = \begin{bmatrix} \frac{1}{\sigma L_s} & 0 \\ 0 & \frac{1}{\sigma L_s} \\ 0 & 0 \\ 0 & 0 \end{bmatrix} \quad (4.14)$$

Based on (4.3) matrices (4.13) and (4.14) can be discretised as

$$\Phi = \begin{bmatrix} 1 - \frac{T}{\sigma} \left( \frac{1}{\sigma T_s} + \frac{1-\sigma}{\sigma T_r} \right) & 0 & \frac{1-\sigma}{\sigma T_r} \frac{T}{T_r} & \frac{1-\sigma}{\sigma} \omega_m T \\ 0 & 1 - \frac{T}{\sigma} \left( \frac{1}{\sigma T_s} + \frac{1-\sigma}{\sigma T_r} \right) & -\frac{1-\sigma}{\sigma} \omega_m T & \frac{1-\sigma}{\sigma} \frac{T}{T_r} \\ \frac{T}{T_r} & 0 & 1 - \frac{T}{T_r} & -\omega_m T \\ 0 & \frac{T}{T_r} & \omega_m T & 1 - \frac{T}{T_r} \end{bmatrix} \quad (4.15)$$

$$\mathbf{B} = \begin{bmatrix} \frac{T}{\sigma L_s} & 0 \\ 0 & \frac{T}{\sigma L_s} \\ 0 & 0 \\ 0 & 0 \end{bmatrix} \quad (4.16)$$

Because of the matrix description of IM we can now simply transform the system of variables into another one by multiplying it by recalculation matrix. The recalculation matrixes and discussion about equivalent circuit coequality is in [91]. Usage of the state variables when describing IM can be very helpful. As is shown in [89] it can be used to analyse analytically behaviour of the IM. Moreover system analyses known from the control theory can be used to analyse selected IM description from the point of stability, observability etc. The identification of the IM parameters can be based on the state variables description too.

#### ■ 4.1.1 Torque Equation

Important part of the IM model is the equation for calculation of electromagnetic torque. It can be calculated as vector multiplication of the flux and current space vectors [1–2].

$$T_e = K \cdot pP |\underline{\Psi}_s \times \underline{i}_s| = K \cdot p(\Psi_{su} i_{rmsv} - \Psi_{sv} i_{su}) \quad (4.17)$$

where  $p$  is number of pole pairs and  $K$  is constant that depends on selected Clark's transformation coefficient (Tab. E.1).

$$K = \frac{2}{3k_{\alpha\beta}^2} \quad (4.18)$$

It is also possible to calculate the torque by multiplication of arbitrary space vectors, however this is connected with another multiplication coefficients. They are summarised in Tab. 4.1.

Vector 1	$\underline{i}_r$	$\underline{\Psi}_s$	$\underline{\Psi}_\mu$	$\underline{\Psi}_r$	$\underline{\Psi}_s$	$\underline{\Psi}_\mu$	$\underline{\Psi}_r$	$\underline{\Psi}_r$
Vector 2	$\underline{i}_s$	$\underline{i}_s$	$\underline{i}_s$	$\underline{i}_s$	$\underline{i}_r$	$\underline{i}_r$	$\underline{i}_r$	$\underline{\Psi}_s$
Mult. Coeff	$L_m$	-	-	$\frac{L_m}{L_r}$	$\frac{L_m}{L_r}$	-	-	$\frac{L_m}{\sigma L_s L_r}$

**Table 4.1.** Coefficients used for torque calculation

## 4.2 Flux Estimation

The flux of the IM is crucial parameter required for IM control. There are several ways of the flux estimation and also the different control algorithms are based on the knowledge of the different flux spacevectors (stator, rotor). In the first method of field oriented control proposed by Blaschke [92] was the flux, in the air gap, of the IM measured directly by Hall sensors. Later several methods have tried to use taps of stator winding, to get information about flux space vector position. But both methods has proven to be ineffective, because they require HW modifications of the motor. Several methods that identify the flux position by injection of high frequency voltage signals and its response [93] have been developed. These methods are simple, but they require high computational power and they are sensitive to disturbances too. That is why the open loop observers were developed for estimation of the rotor flux of IM.

Open loop flux observers-motor models are based on the IM equations (4.8). The combination of variables that are easy to measure like voltage, current or speed are used to calculate the value and position of the rotor flux. The most used models are

- Current model I-n
- Voltage model U-I

Current model calculates rotor flux form stator current and rotor speed. The rotor flux is obtained by substituting rotor currents (4.9)

$$\begin{aligned} i_{r\alpha} &= \frac{\Psi_{r\alpha} - L_m i_{s\alpha}}{L_r} \\ i_{r\beta} &= \frac{\Psi_{r\beta} - L_m i_{s\beta}}{L_r} \end{aligned} \quad (4.19)$$

into rotor voltage equation in system (4.9)

$$\begin{aligned} \frac{d\Psi_{r\alpha}}{dt} &= \frac{R_r L_m}{L_r} i_{s\alpha} - \frac{R_r}{L_r} \Psi_{s\alpha} - \omega_m \Psi_{r\beta} \\ \frac{d\Psi_{r\beta}}{dt} &= \frac{R_r L_m}{L_r} i_{s\beta} - \frac{R_r}{L_r} \Psi_{s\beta} + \omega_m \Psi_{r\alpha} \end{aligned} \quad (4.20)$$

The block diagram of the model based on (4.20) is in Fig. 4.1. The main advantage of the current model is, that it is stable also in areas of low speed  $\omega_m$ . But the requirement of the speed sensor increases cost of the drive.

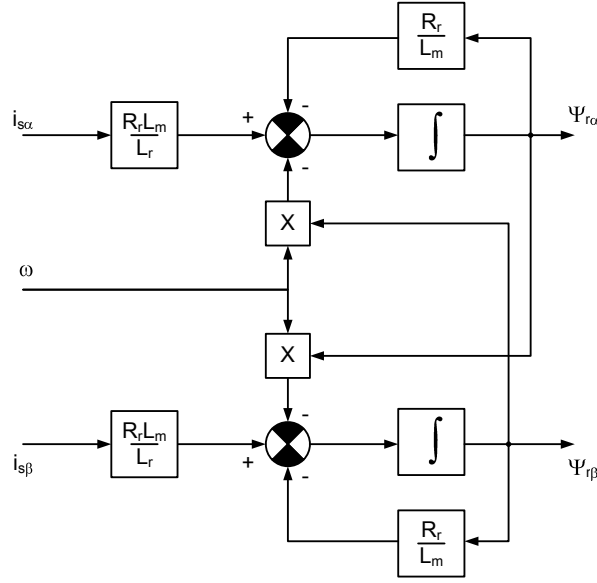


**Figure 4.1.** Current model of IM

Voltage model calculates the value of the rotor flux from stator voltage and stator current, that means speed sensor is not required. The model is accurate for high speeds where the voltage drop on the stator resistance can be neglected. The method of calculation of the flux space vector, by the means of integration of measured voltage, cause that the model is sensitive to DC drift errors. Moreover during the low speeds the voltage drop across the stator resistance can not be neglected. The stator resistance depends on the temperature, therefore the temperature characteristic of the stator resistance have to be respected.

Derivation of the model is based on expression of the dependency between rotor and stator flux from (4.9).

$$\underline{\Psi}_s = \sigma L_s i_s + \frac{L_m}{L_r} \underline{\Psi}_r \quad (4.21)$$

where

$$\sigma = 1 - \frac{L_m^2}{L_s L_r} \quad (4.22)$$

After substituting (4.21) into (4.9) and integration we reach the final equation of U-I model

$$\begin{aligned} \Psi_{r\alpha} &= \frac{L_r}{L_m} \left( \int_0^t (u_{s\alpha} - R_s i_{s\alpha}) dt - \sigma L_s i_{s\alpha} \right) \\ \Psi_{r\beta} &= \frac{L_r}{L_m} \left( \int_0^t (u_{s\beta} - R_s i_{s\beta}) dt - \sigma L_s i_{s\beta} \right) \end{aligned} \quad (4.23)$$

The block diagram of the model based on (4.23) is in Fig. 4.2

To improve accuracy of the flux estimation close loop observers can be used [94–95]. However these observers require information about rotational speed too.

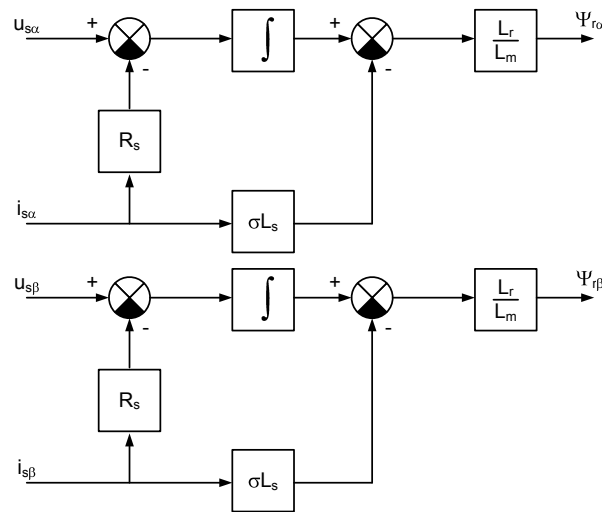


Figure 4.2. Voltage model of IM

### 4.3 Speed Estimation

The speed of IM required for control algorithm can be obtained either from rotational speed sensor or by estimation algorithm. The resolver or incremental encoder can be used for speed measurement. However these sensors increase cost of the drive and also decrease its reliability. That is why the algorithms for sensorless estimation of the speed has been developed in last decades [2, 90, 96]. Generally these methods can be divided into

- Methods that are oriented on control of stator flux and does not require speed sensor e.g DTC, NFO
- Estimation based on kalman filters, model adaptive reference systems of other observers
- Methods that estimates speed from specific effects e.g. unbalance, slot harmonics

But all of those listed methods suffer great inaccuracy in the area around standstill. This is caused by the fact, that the magnetisation of the slowly rotating rotor can be easily changed by standing rotor flux vector. If the rotational speed reaches specific level approx.  $\omega_{slip}$  these algorithms start estimates the speed correctly.

The model reference adaptive system (MRAS) estimator consists of two models - so called reference model, that does not require speed information and so called adjustable model, that has as one of the inputs estimated speed. Outputs of both models are processed in block of model adaptation. The estimated speed is adjusted based in the difference between the outputs of the reference and adaptive model. In most cases as reference model acts voltage model (Fig. 4.2) and as an adjustable model acts I-n model. The rotor flux is the output of the models and its deviation is processed in adaptation block (Fig. 4.3).

Main disadvantage of this method is, that both models requires information about stator resp. rotor resistance which is parameter with great temperature dependency. The reference model of the estimator will also suffer inaccuracy because of DC drift of the integrators. That is why also another more or less stable topologies of MRAS estimators based on reactive power, back EMF or another principles were developed [97–100]. Recently were also developed methods that tends to estimate on the MRAS

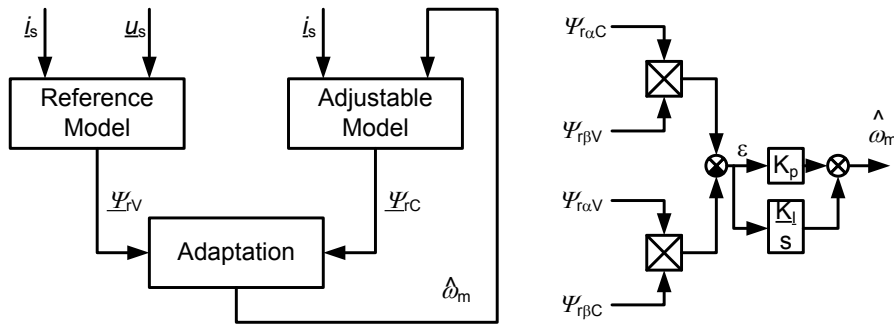


Figure 4.3. Model reference adaptive system block diagram

principle also resistance as second variable in order to make the speed estimator more accurate [101–104].

Another method for sensorless speed estimation is based on state variable model of IM (4.11). When we assume that the machine parameters are time invariant only parameter  $\omega_m$  in system matrix  $\mathbf{A}$  need to be updated. The Luenberger observer can be used to calculate actual values of the state vector  $\mathbf{x}$ . The observer is based on the (4.24)

$$\frac{d\hat{\mathbf{x}}}{dt} = \hat{\mathbf{A}}\hat{\mathbf{x}} + \mathbf{B}\mathbf{u} + \mathbf{K}(\mathbf{i}_s - \hat{\mathbf{i}}_s) \quad (4.24)$$

where superscript  $\hat{\phantom{x}}$  means estimated quantities and  $\mathbf{K}$  is correction matrix. In case when the speed sensor is present, the observer is used only for estimation of rotor flux. In this case there are many approaches how to design  $\mathbf{K}$  mostly based on method of pole placement. If the observer should be used also for estimation of the speed the structure must be extended like in Fig. 4.4.

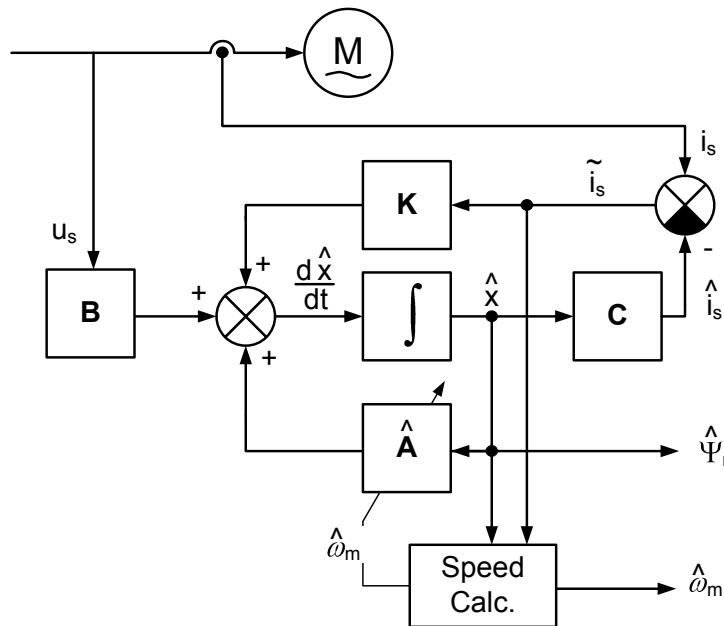


Figure 4.4. Block diagram of Luenberger observer

When we define the state error  $\mathbf{f}$  as

$$\mathbf{f} = \mathbf{x} - \hat{\mathbf{x}} \quad (4.25)$$

then when subtracting (4.11) and (4.24) the following error state equation is reached

$$\frac{d\hat{\mathbf{f}}}{dt} = (\mathbf{A} + \mathbf{KC})\mathbf{f} + \Delta\mathbf{A}\hat{\mathbf{x}} \quad (4.26)$$

where

$$\Delta\mathbf{A} = \mathbf{A} - \hat{\mathbf{A}} = \begin{bmatrix} \mathbf{0} & \Delta\omega \frac{1-\sigma}{\sigma} \mathbf{J} \\ \mathbf{0} & -\Delta\omega \mathbf{J} \end{bmatrix} \quad (4.27)$$

$$\mathbf{J} = \begin{bmatrix} 0 & 1 \\ -1 & 0 \end{bmatrix}; \Delta\omega = \omega - \hat{\omega} \quad (4.28)$$

Because IM is nonlinear system this fact must be included into observer design from the beginning [105]. The stability of the observer can be proved by Ljapunov method. The method will be here only briefly described. In more detail it can be found in [90, 106–107].

If the Ljapunov function  $V$  for the error equation (4.26) contains both the state error  $\mathbf{f}$  and parameter error  $\Delta\omega$ , it can be than defined as

$$V = \mathbf{f}^T \mathbf{f} + \frac{\Delta\omega_m^2}{\lambda} \quad (4.29)$$

The first derivation of the  $V$  is

$$\frac{dV}{dt} = \mathbf{f}^T [(\mathbf{A} + \mathbf{KC})^T + (\mathbf{A} + \mathbf{KC})] \mathbf{f} - 2\Delta\omega_m (\tilde{i}_{s\alpha} \hat{\Psi}'_{r\beta} - \tilde{i}_{s\beta} \hat{\Psi}'_{r\alpha}) \frac{1-\sigma}{\sigma} + 2\Delta\omega_m \frac{d\hat{\omega}_m}{dt} \frac{1}{\lambda} \quad (4.30)$$

where  $\tilde{i}_{s\alpha} = i_{s\alpha} - \hat{i}_{s\alpha}$ ;  $\tilde{i}_{s\beta} = i_{s\beta} - \hat{i}_{s\beta}$  are components of state error used to correct the estimated outputs of the observer.

The system is stable when (4.30):

- $\mathbf{K}$  is chosen in the way that the negative definiteness is ensured.
- Estimation algorithm is designed so that the second and third term on the right side of (4.30) compensate each other.

For this purpose supposes [106–107] correction matrix  $\mathbf{K}$  that depends on  $\omega_m$

$$\mathbf{K} = \begin{bmatrix} k_1 & k_2 & k_3 & k_4 \\ -k_2 & k_1 & -k_4 & k_3 \end{bmatrix} \quad (4.31)$$

$$k_1 = -\frac{k-1}{\sigma} \left( \frac{1}{T_r} + \frac{1}{T_s} \right); k_2 = (k-1)\hat{\omega}_m; k_3 = \frac{k-1}{1-\sigma} \left( \frac{1}{T_r} - \frac{k}{T_s} \right); k_4 = \frac{k-1}{1-\sigma} \hat{\omega}_m \sigma \quad (4.32)$$

Selection of  $k > 0$  should fix the poles of the observer proportionally to the motor so the observer remains stable. To satisfy second condition of stability the estimated speed  $\hat{\omega}_m$  have to fulfil following

$$\frac{d\hat{\omega}_m}{dt} = \lambda \frac{1-\sigma}{\sigma} (\tilde{i}_{s\alpha} \hat{\Psi}'_{r\beta} - \tilde{i}_{s\beta} \hat{\Psi}'_{r\alpha}) \quad (4.33)$$

This can be satisfied by proper selection of  $K_P$  and  $K_I$  coefficients in speed estimation block

$$\hat{\omega}_m = K_P (\tilde{i}_{s\alpha} \hat{\Psi}'_{r\beta} - \tilde{i}_{s\beta} \hat{\Psi}'_{r\alpha}) + K_I \int (\tilde{i}_{s\alpha} \hat{\Psi}'_{r\beta} - \tilde{i}_{s\beta} \hat{\Psi}'_{r\alpha}) dt \quad (4.34)$$



# Chapter 5

## Matrix Converter Induction Motor Drive Control Strategies

The induction motors (IM) becomes recently spread ones in the area of regulated drives [1–3]. Main advantage of the IM is its robustness, low maintenance, low cost and high reliability. However the speed regulation is more complicated compared to DC machines. Because of its principle the speed of IM depends directly on the frequency applied to its terminals. Also there will be always small difference between the angular speed of the supply voltage and angular speed of the rotor, because so called slip is required to produce torque.

The generation of the voltage with variable frequency was the main limiting problem of IM application at the beginning. This problem was eliminated by arrival of power electronics and utilisation of frequency converters.

Nowadays there are many known methods how to control IM resp. produce required variable frequency [2, 108–109]. Generally control methods can be divided into scalar and vector.

### 5.1 Scalar Control Methods for IM

The scalar control strategies control only magnitude and frequency of selected control variable. These methods are simple and robust. They can work in open loop - without speed sensor. These methods offer good steady state performance, but they are not suitable for applications where is required high dynamics of the controlled drive or the efficiency of the drive is taken into account. Scalar control methods can be further divided into voltage (Fig. 5.1) or current (Fig. 5.2) type. Because these methods aims to keep the IM flux constant (avoid saturation), the ratio between voltage and frequency is kept constant, therefore these methods are also known as U/f or Volt per Hertz control.

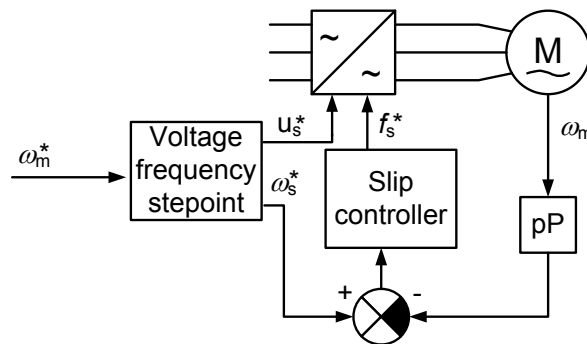


Figure 5.1. Voltage type scalar control

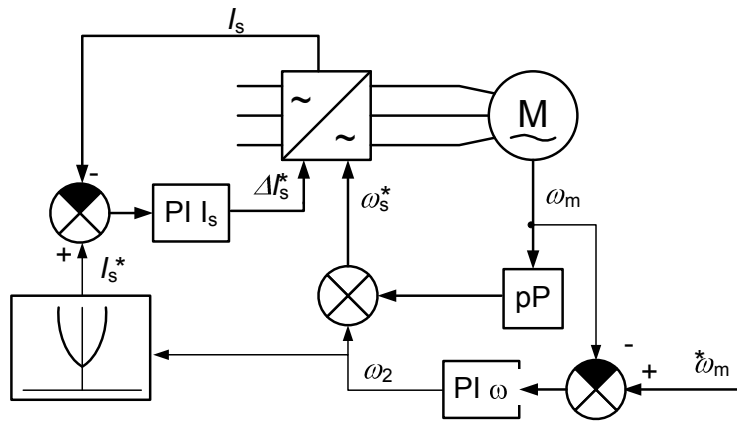


Figure 5.2. Current type scalar control

## 5.2 Vector Control Methods for IM

The aim of vector control is not only the control of magnitude and frequency but also the control of orientation of the controlled variables in machine. Methods of vector control can be further divided according to many criterions e.g. if the flux is controlled directly or indirectly, or if the controlled variable is stator resp. rotor or air gap flux, according to incorporated type of modulator, etc. But all methods offers high dynamics of regulation and tries to decouple control of flux and torque, thus they can be controlled independently like separately excited DC machine. The vector control aims to split current space vector into flux producing current component  $i_{sd}$  and torque producing component  $i_{sq}$  and regulate these components separately. The flux producing component  $i_{sd}$  is always oriented with the reference flux vector (stator resp. rotor) and therefore the decomposition of the current space vector into current components depends on selected reference flux. Simple block schematics of the vector control structure is in Fig. 5.3. The block with motor model is used for calculation of actual position of the flux, that is further used in transformations. Current components are separately regulated, decoupled, then transformed into values acceptable by modulator.

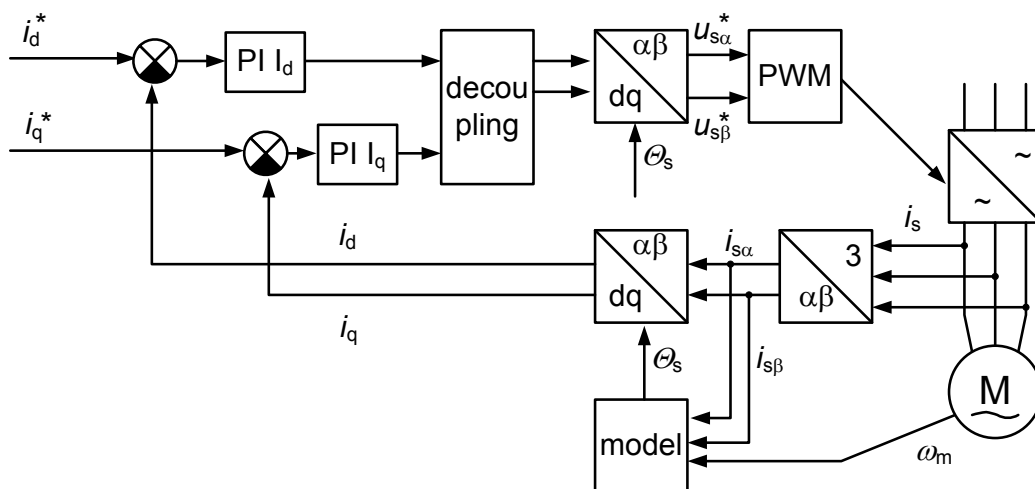


Figure 5.3. Block diagram of the FOC

Theory of field oriented control was firstly presented in Germany at the end of seventies in work of two authors Hasse [110] and Blaschke [92]. Since then there were developed various methods, however all of them are according to method used to determine flux vector position divided into

- Direct Field Oriented Control
- Indirect Field Oriented Control

Direct FOC schemes mostly mean that the flux vector position is calculated from other quantities that can be measured e.g. voltage, current, rotor speed. The indirect FOC schemes refer to control strategies that calculates flux vector position from reference values and measured mechanical speed.

### ■ 5.2.1 Indirect Rotor Field Oriented Control

The block diagram of indirect rotor field oriented control (IRFOC) is depicted in Fig. 5.4. It has got its name because the synchronous speed is calculated as sum of mechanical speed and slip speed. The angle that correspond to the actual rotor flux position is obtained by integration of the synchronous speed. Based on the equations stated in chapter 4 the reference values for the flux producing current and torque producing current can be calculated as

$$i_{sd}^* = \frac{\Psi_r^*}{L_m} \tag{5.1}$$

$$i_{sq}^* = \frac{1}{k_{\alpha\beta} p P} \cdot \frac{L_m}{L_r} \cdot \frac{T_e^*}{\Psi_r^*}$$

the slip speed can be then calculated as

$$\omega_{sl} = \frac{L_m R_r}{L_r} \cdot \frac{i_{sq}^*}{\Psi_r^*} \tag{5.2}$$

From (5.2) is obvious that because of  $\Psi_r^*$  in denominator, it have to be always to some nonzero value otherwise the slip speed calculation will not work properly.

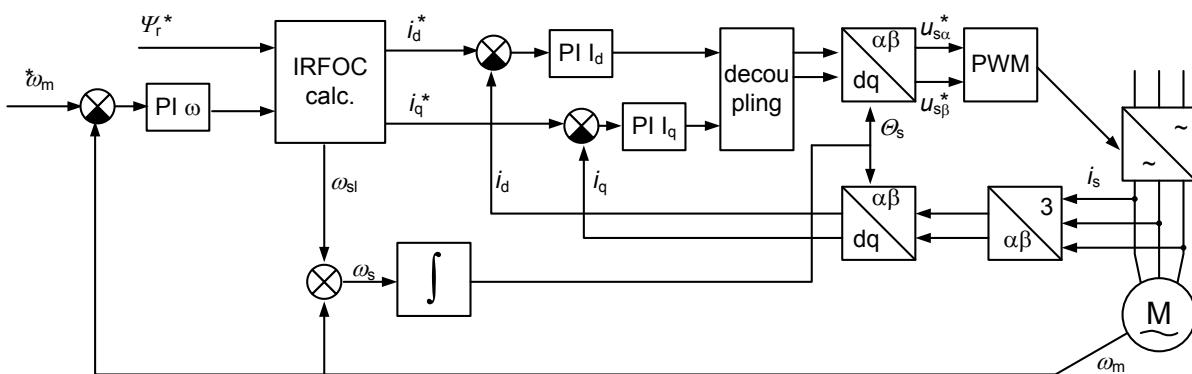


Figure 5.4. Block diagram of the IRFOC

### ■ 5.2.2 Direct Rotor Field Oriented Control

The direct rotor flux oriented control derive transformation angle (rotor flux space vector position) from the components of the flux space vector calculated in flux estimator. The reference value of the flux producing current component  $i_{sd}^*$  is calculated from the

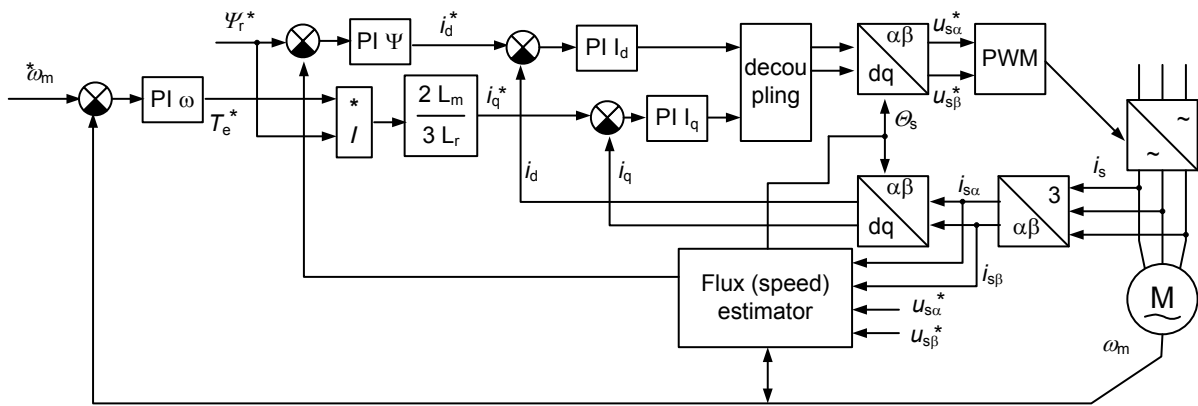


Figure 5.5. Block diagram of the DRFOC

output of the flux controller. The torque producing component of the current  $i_{sq}^*$  can be calculated from (5.1). Advantageous is that changes of the reference flux value in the field weakening region are automatically compensated.

For both methods IRFOC and DRFOC is important to have information about flux value and position as precise as possible. Methods used for estimation of IM flux were discussed in chapter 4. There are also another methods field oriented control they can be found in [2, 38].

### 5.2.3 Direct Torque Control

In the direct torque control (DTC) methods are the decoupled controllers replaced by the bang-bang (hysteresis) controllers. Fundamentals of DTC methods were firstly presented in eighties by Depenbrock in Germany [111–112] and Takahashi and Noguchi in Japan [113]. The principle of DTC is depicted in Fig. 5.6. The structure consists of two hysteresis controllers, where the stator flux controller influences the time duration of switched active vector, that moves stator flux space vector along the reference trajectory. The torque hysteresis controller determines time duration of zero voltage vector, that holds the IM produced torque in defined range. Every switching period is selected proper combination of inverter switching state ( $S_A, S_B, S_C$ ) in order to minimize instantaneous errors of flux and torque. Compared to FOC the DTC has following features

- no current control loops - current is not controlled directly
- regulation is performed in stationary  $\alpha\beta$  coordinate system
- no PWM, switching is done based on preprepared switching table
- requires torque and flux estimator

Based on the switching table realisation the stator flux has either circular path (Takahashi) or hexagonal path (Depenbrock). Main disadvantage of DTC is the fact, that switching frequency depends on width of hysteresis bands, that means harmonics spectra of output current is varying. Another problem appear in range below 20% of nominal speed, where the voltage drop across the stator resistance can not be neglected. Also operation of DTC can be problematic when narrow switching pulses are required, because the minimal switching on and off times of IGBT's have to be respected. That is why the DTC strategies have gone through great development since eighties. There are strategies, that aims to reduce flux and torque ripples by incorporation of SVM like

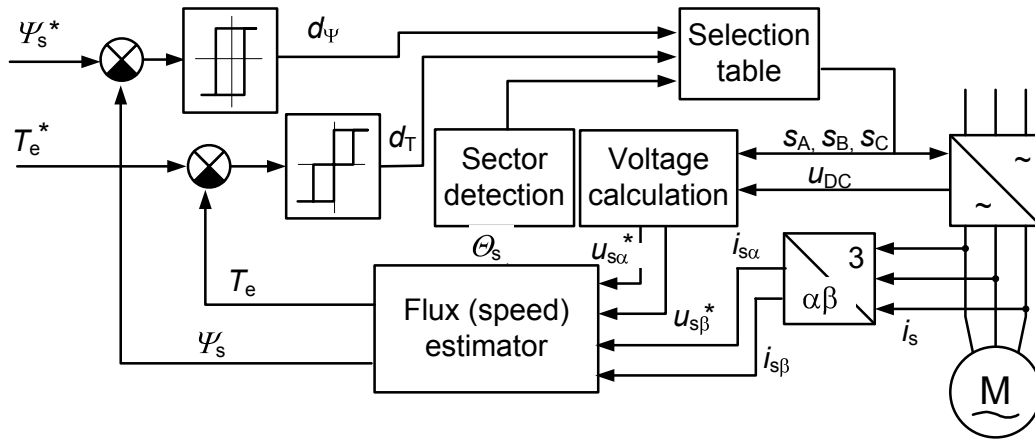


Figure 5.6. Block diagram of the DTC proposed by Takahashi

DTC-SVM operating in polar coordinates, dead-beat DTC-SVM, or DTC strategies with prediction, fuzzy or neural network controllers [108]. There exists modified DTC strategies for matrix converter [38] or for multilevel inverters [114–117].

#### 5.2.4 Predictive Control

The predictive control belongs to the one of most intelligent control methods of nonlinear control [118–122]. The idea of predictive control is to choose the control action by repeatedly solving an optimal control problem. Controller predicts future behaviour of the IM drive based on the knowledge of past and current state. The optimal output of the controller is then selected based on chosen criteria. In every regulation step the controller calculates possible trajectories of the current vector for each of seven possible voltage vector. The trajectories can be calculated as

$$\begin{aligned} \underline{i}_s^*(t) &= \underline{i}_s^*(t_0) + \frac{d\underline{i}_s^*}{dt} \\ \underline{i}_s(t) &= \underline{i}_s(t_0) + \frac{d\underline{i}_s}{dt} \end{aligned} \quad (5.3)$$

The currents  $\underline{i}_s^*(t_0)$  and  $\underline{i}_s(t_0)$  are known, the derivative of reference value can be calculated by numerical method and derivative of actual current can be calculated as

$$\frac{d\underline{i}_s(k)}{dt} \approx \frac{\underline{u}_s(k) - \underline{u}_i(t = t_0)}{L_{\sigma s}} \quad (5.4)$$

where  $k$  represents each of available voltage vectors and  $\underline{u}_i$  is e.m.f voltage calculated by observer.

Such type of control for IM drive fed by matrix converter was presented in [89]. The controller was designed based on the mathematical analysis of the IM reaction to applied voltage vector. The torque and flux reference values are compared with actual ones and based on their difference one from four action vector is selected. The required action vector is then compared with the vectors that can be produced by the converter and the most suitable one is switched on (see Fig. 5.7). Risks of such control strategy are discussed in the paper [89] too.







# Chapter 6

## Compact Matrix Converter Realization

Based on the theory presented in previous chapters the components of the matrix converter prototype were selected and designed. This chapter aims to summary and explain important steps of the design. Design is based partly on the knowledge from [37] and [39]. The design of all parts followed up from the prerequisites:

- nominal power approx. 20 kW
- damped input filter
- clamp circuit protection
- measurement of all input voltages
- measurements of all output currents and two input currents
- power contactor controlled only from SW
- separate power source for control part
- universal measurement interface for ADC with outputs  $\pm 5$  V

Based on these requirements was created diagram with block interconnections that was adapted to wiring diagram (see Apendix C). From this diagram followed interconnections of anther components and power sources, etc. Following parts describes only important components of MC.

### 6.1 Power Part Design

As was mentioned in Sec. 2.5 there are several topologies or modules for realisation of the bidirectional switch. The first step of the design is choosing of nominal voltage and current of the semiconductor switch. This can be simply done from the assumed power of the converter. The output power of the converter was chosen to be approximately 20 kW (When selecting this value also parameters of the input filter were taken into account). When we suppose common supply grid voltage  $u_N = 400$  V we can calculate the nominal current to be approx. 25 A.

$$\frac{P}{\sqrt{3}U_n} = \frac{20000}{\sqrt{3} \cdot 400} = 28 \text{ A} \quad (6.1)$$

Another criteria for selecting of the transistor device is required switching frequency. In this case the maximal value of the switching frequency was selected  $f_{sw} \leq 20$  kHz.

The IGBT modules GD401-70-12 (Tab. 6.1) from the manufacturer Polovodiče Inc. were chosen, because they fit the calculated parameters. Those are IGBT with anti parallel diode in package SOT227 (Fig. 6.1).

The transistor endures continuous current 70A, when we consider proposed current 25 A, the power reserve is adequate. The blocking voltage of the transistor  $U_{CES} = 1200$  V is twice bigger then required blocking voltage. Both parameters secure the transistor from destruction in case of sudden failure. The module of this type of package was selected because converter is built as a laboratory prototype and discreet modules are easily and cheaply exchangeable.



**Figure 6.1.** GD401-70-12 module

Parameter	Symbol	Value	Unit
Voltage collector-emitter	$U_{CES}$	1200	V
Continuous collector current	$I_{C25}$	70	A
	$I_{C75}$	35	A
Allowable short-circuit time	$t_{sc}$	10	$\mu\text{s}$
Maximal power loss	$P_D$	250	W
On delay time	$t_{d(\text{ON})}$	80	ns
Rise time	$t_r$	150	ns
Fall time	$t_f$	500	ns
Switch off energy	$W_{\text{off}}$	6	mJ
Off delay time	$t_{d(\text{OFF})}$	200	ns
Overlapping time		850	ns

**Table 6.1.** Transistor Modules Parameters

Disposition of the IGBT modules on the radiator and their connection is in Fig. 6.2. The transistors are divided into three groups. Each group represents one output phase. This solution assures at least partial symmetry of the input phases and suppresses parasitic inductances of the input phases. Because of the requirements for the modularity of the converter it was decided to use printed circuit board for the connections between modules (Fig. 6.3).

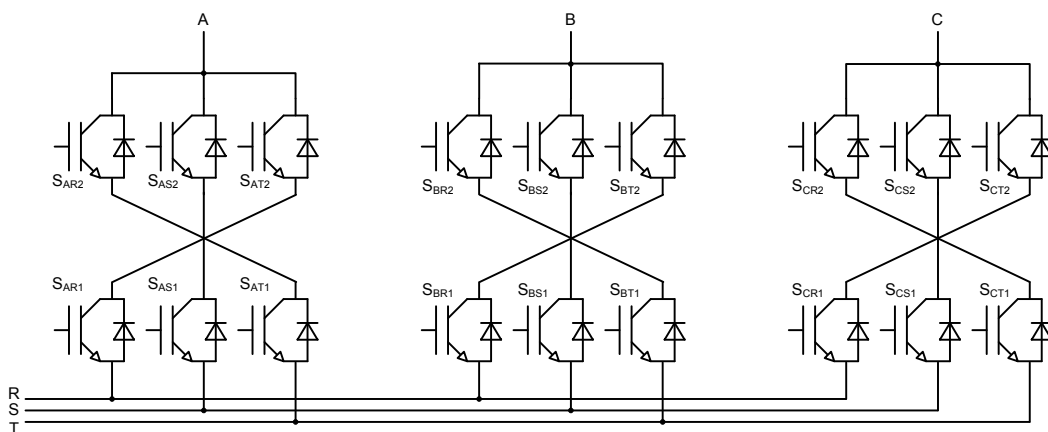


**Figure 6.2.** Interconnections between IGBT modules

The next step in power part design is design of the radiator. Current conduction and switching of the transistors cause power losses and warming of the modules. This heat must be taken away from the transistors. Losses in IGBT modules were estimated from

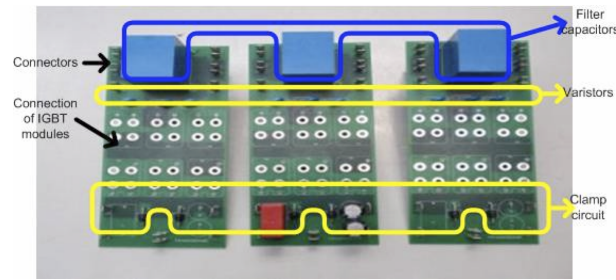


Figure 6.3. Interconnections boards

measured losses of the old converter. Measured efficiency was around 96%, therefore rough losses of the new converter were calculated as:

$$P_{\text{loss}} = (1 - \eta)P_{\text{in}} = (1 - 0.96) \cdot 20 \text{ kW} \approx 800 \text{ W} \quad (6.2)$$

The capability of the radiator to dissipate the heat describes coefficient  $R_{\text{thha}}$ . This coefficient is given by the properties of the radiator (dimensions, area, and mass). The radiator Q180 with length 300 mm from the manufacturer Polovodiče Inc. was chosen. This length of the radiator is not capable to dissipate the heat naturally, therefore it was equipped with auxiliary fan. The value of  $R_{\text{thha}}$  for radiator with fan is  $R_{\text{thha}} = 0.032 \frac{\text{K}}{\text{W}}$ , it was given by the manufacturer. The whole system module – radiator – ambient can be for steady state modelled as an alternative electric circuit Fig. 6.4.

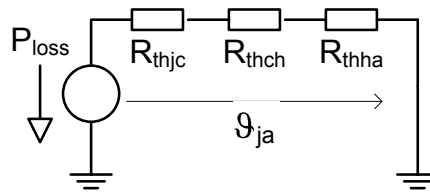


Figure 6.4. Equivalent circuit modelling of the radiator

$$\vartheta_{\text{ja}} = P_{\text{loss}}(R_{\text{thjc}} + R_{\text{thch}} + R_{\text{thha}}) = \frac{800}{18}(0.5 + 0.05 + 0.032) = 25^{\circ}\text{C} \quad (6.3)$$

Equation (6.3) shows that relative warming of the junction is going to be approx.  $25^{\circ}$  for assumed nominal values of the converter. Heat transfer resistances were obtained from the datasheet of the transistor and heater manufacturer.

## 6.2 Input Filter

The input filter is very important part of the converter because especially power converters belong to the category of worse supply network polluters. Therefore were defined limits of interferences that can not be exceeded. That is why the devices, that contain electronic, are also equipped with filters. The basic technical regulations that are concerned with the problematic of EMC are:

- environment: IEC 1000-2-x resp. EN 61000-2-x
- low frequency emission: IEC 1000-3-x resp. EN 61000-3-x

- lf, hf resistance: IEC 1000-4-x resp. EN 61000-4-x
- hf emission and resistance: CISPR 16-x

It was decided that the filter will have two parts, the first part will be a high frequency filter for elimination of the interference in frequency range from 150 kHz to 30 MHz and the second part will be filter for suppression of low frequency interference.

### 6.2.1 High Frequency Filter

High frequency interference is not related to the quality of the power supply. Its impact presents itself mostly in communication circuits of the device. The interference signal can superpose itself on another signal, which can be distorted. As a filter was selected the filter ELFIS 3ELF25ET from manufacturer ELFIS. Parameters of chosen device are in Tab. 6.2. The filter should suppress the interferences according to the Standards SN EN 50081-1, 50081-2, 55011, 55014 a 55022. Input current of the filter is 25 A, therefore it will be also the maximal current of the converter.

$I_n$ (A)	$U_n$ (V)	$I_{\text{sink}}$ (mA)	$P_{\text{loss}}$ (W)	$\sum L$ (mH)
25	440	0.3	3.6	6
$\sum C_x$ ( $\mu\text{F}$ )	$\sum C_y$ ( $\mu\text{F}$ )	$R_x$ (M $\Omega$ )	$R_y$ (M $\Omega$ )	
1.3	0.022	2	4	

Table 6.2. 3ELF25ET parameters

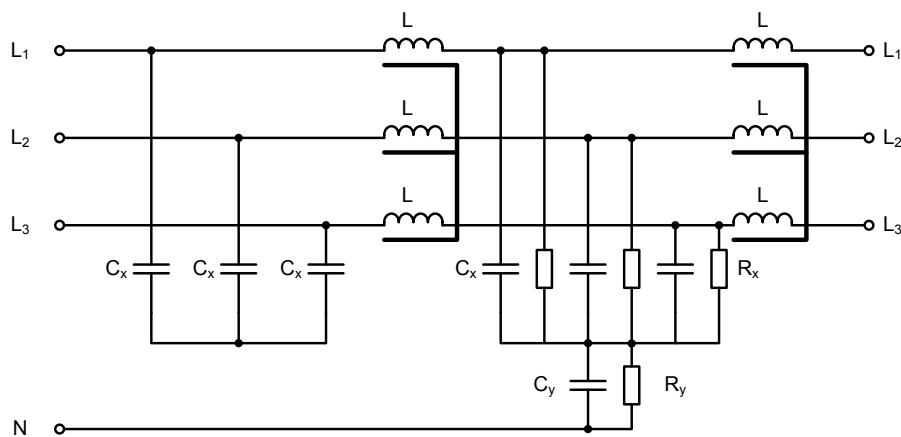


Figure 6.5. High frequency filter topology

The function of the filter can be explained with help of the Fig. 6.6. Inductors connected in series have insignificant effect on the current with low frequency but they have high impedance for the high frequency signals, therefore they limit penetration of the high frequency signals. Capacitor  $C_1$  acts as a short circuit for the high frequency signals. Therefore differential mode (DM) interference flows through the capacitor and returns through the second wire back to the network. The common mode (CM) interference flows through the capacitors  $C_3$  or  $C_4$  back to the ground.

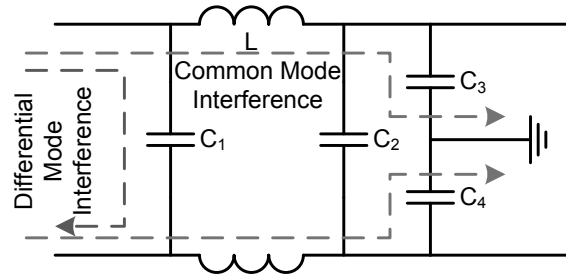


Figure 6.6. DM and CM interference suppression principle

## 6.2.2 Low Frequency Filter

The theory of low frequency filter was analysed in Section 2.6. The resonant frequency must be in enough distance from the switching frequency of the converter. Control part of the converter is designed to output switching frequency of the converter up to 20 kHz. From this point of view seems selection of filter's resonant frequency as 1 kHz suitable. Based on this knowledge other parameters of the filter can be calculated employing equation for resonant frequency (2.6). The value of the filter's inductance should be small enough to ensure low voltage drop on it. Therefore inductor with inductance  $L_F = 1 \text{ mH}$  was selected. Using (2.6) we reach

$$C_F = \frac{1}{4\pi \cdot L_F \cdot f_0^2} = \frac{1}{4\pi \cdot 1 \cdot 10^{-3} \cdot 1000^2} = 25.4 \mu\text{F} \quad (6.4)$$

Based on the capacitors offered at the market the filter capacitors with capacity  $C_F = 3\mu\text{F}$  were selected and hereby filter is realized as  $\Delta$  connection of three parallel connected capacitors. This slightly modifies resonant frequency of the filter

$$f_0 = \frac{1}{2\pi\sqrt{L_F C_F}} = \frac{1}{2\pi\sqrt{1 \cdot 10^{-3} \cdot 27 \cdot 10^{-6}}} = 986.7 \text{ Hz} \quad (6.5)$$

Necessity of damping of the filter was also discussed in Section 2.6. Therefore both types of the damping were considered. Parameters were calculated according to equations initiated in Section 2.6.

$$R_{SD} = \sqrt{\frac{L_F}{C_F}} = \sqrt{\frac{1 \cdot 10^{-3}}{9 \cdot 10^{-6}}} = 10.98 \Omega \quad (6.6)$$

$$L_{SD} = nL_F = \frac{2}{15}L_F = \frac{2}{15} \cdot 1 \cdot 10^{-3} = 133.3 \mu\text{H} \quad (6.7)$$

$$R_{PD} = \sqrt{\frac{L_F}{C_F}} = \sqrt{\frac{1 \cdot 10^{-3}}{27 \cdot 10^{-6}}} = 6.28 \Omega \quad (6.8)$$

$$C_{PD} = nC_F = 4C_F = 4 \cdot 27 \cdot 10^{-6} = 108 \mu\text{F} \quad (6.9)$$

Designed filters were simulated with the help of Matlab/Simulink software and behaviours of the filter were analysed from the point of efficiency and also losses and behaviour under consideration of other parts of the converter especially clamp circuit protection. Figures Fig. 6.7, Fig. 6.8 and Fig. 6.9 show input voltage and current waveforms of the matrix converter with designed filter and connected clamp circuit. The load is connected at  $t_{\text{sim}} = 0.06 \text{ s}$ . The bottom waveform shows energy dissipated in the damping circuit. The Thermal toolbox of the PLECS was used to perform this analysis. The operation of the filter at no load conditions is considered as the worse case

operation, because discharging resistor  $R_{CL}$  of the clamp circuit excite oscillations of the filter [124].

Fig. 6.7 shows that operation of the filter without damping is not possible due to filter vulnerability to oscillations caused by the clamp circuit. From Fig. 6.8 and Fig. 6.9 and also Fig. 2.38 and (2.16) is obvious that parallel damped filter has better efficiency (better transfer function), however losses in the added damping circuit are greater. Less current is flowing through the series damping circuit of the filter and also damping combination of the resistor  $R_{SD}$  and  $L_{SD}$  can be easily connected to the terminals of the filter inductor  $L_F$ . The simulation results of the possible losses in damping circuit are compared in Fig. 6.10. Because the losses and implementation method were also taken into account during design of the filter [39] series damped filter was selected as final filter for designed MC.

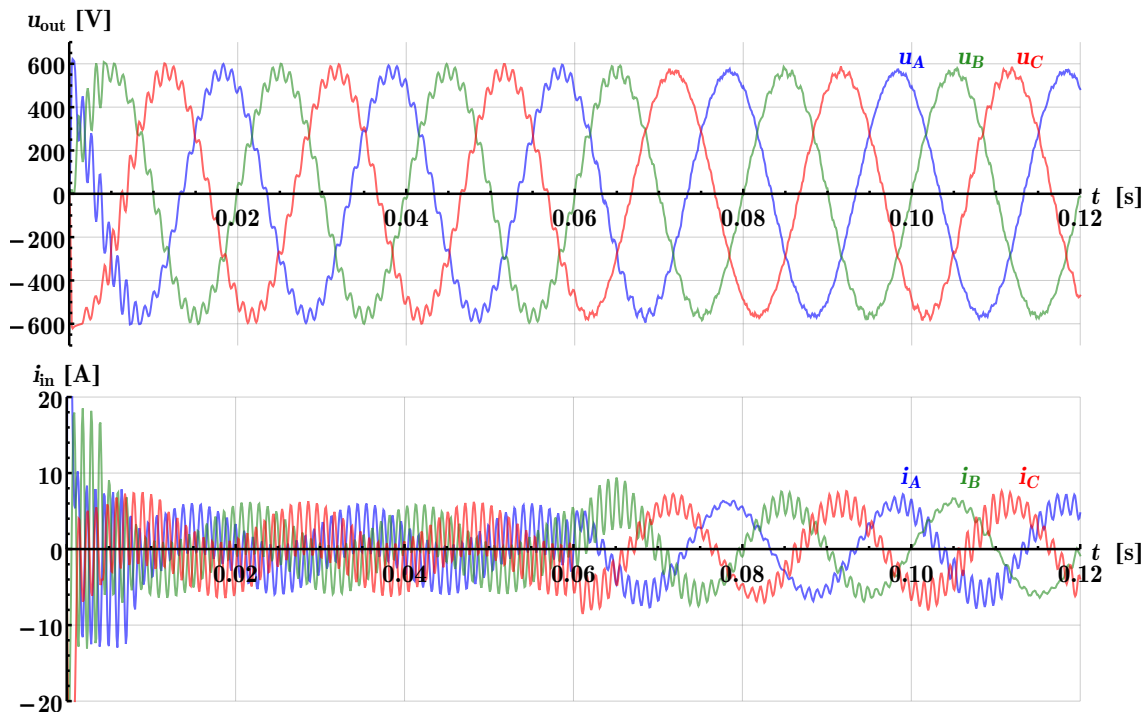


Figure 6.7. LC filter without damping

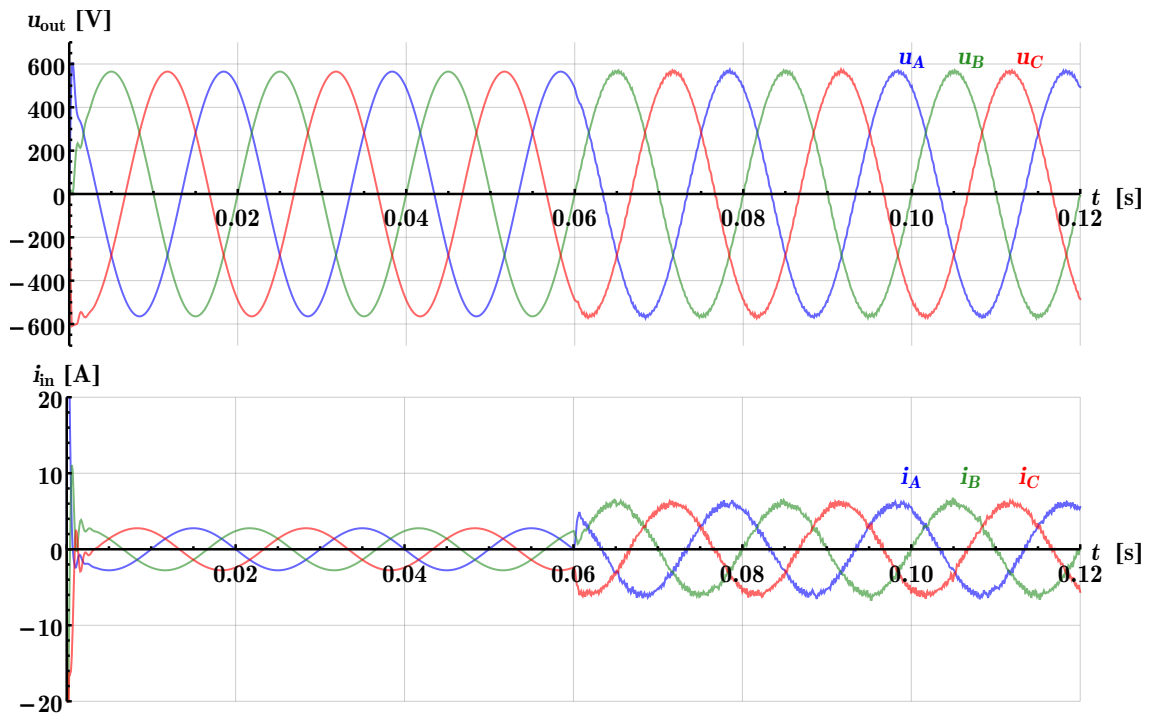


Figure 6.8. LC filter with series damping

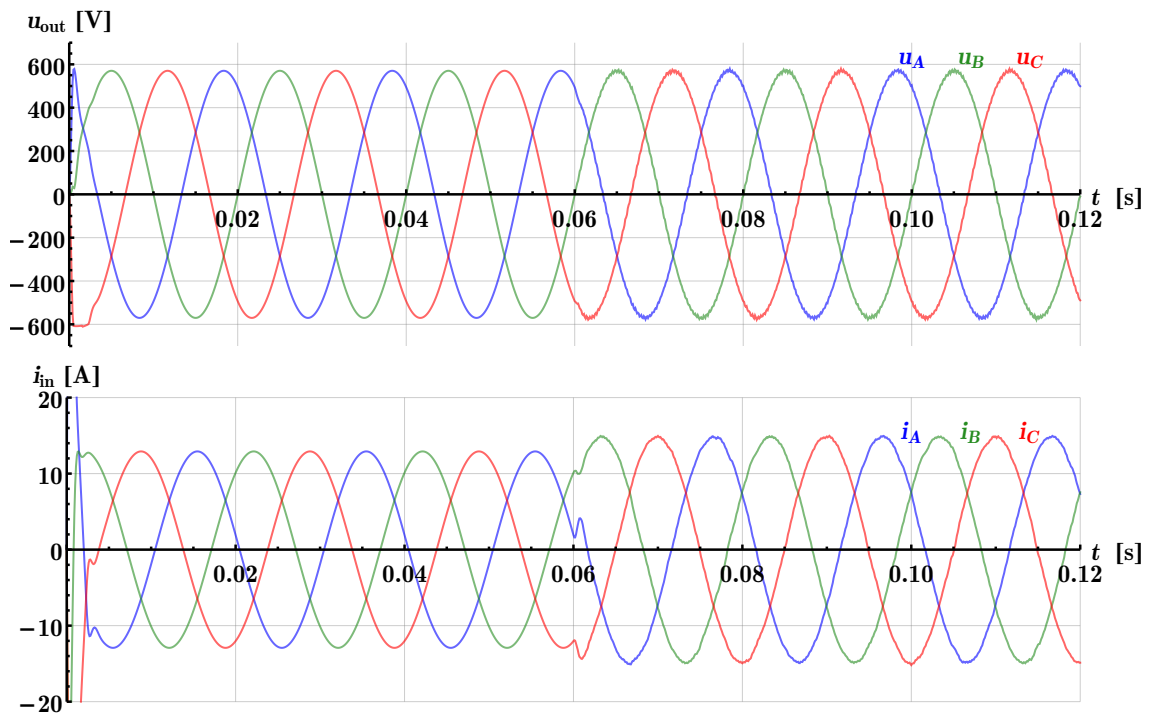


Figure 6.9. LC filter with parallel damping

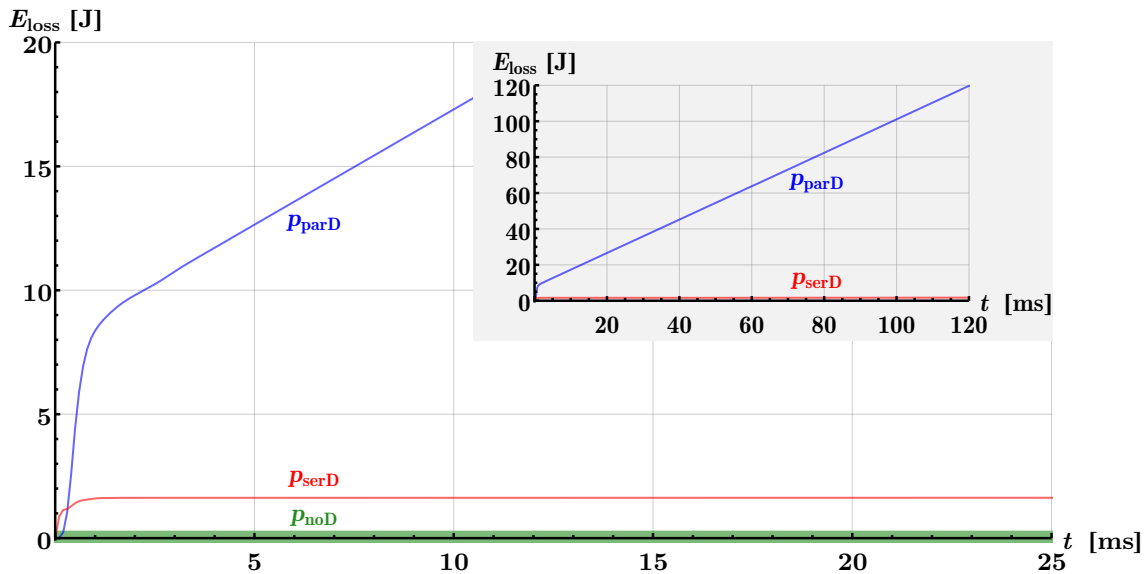


Figure 6.10. Losses in damping circuit

## 6.3 Protections

Protection circuits were also included in the design of the converter in order to protect the IGBT modules. The protection circuits are not necessary for the work of the converter. It can work properly without them. Both types of protection were selected for the converter, hardware and software too. Clamp circuit, varistors, driver boards, circuit breakers ranks to the hardware protection circuits used for the prototype of the matrix converter.

### 6.3.1 Circuit Breaker

The power part of the converter is protected by 3 phase circuit breaker with permitted current 32A, characteristic B. Control part of the converter is fast fuse protected. Both control part and power part have their own contactors. The power part contactor can be switched on only from the control software. The converter is also equipped with safety-stop button that disconnects both contactors.

### 6.3.2 Varistors

The experiences with the old converter have shown, that neither circuit breakers nor clamp circuit are fast enough to protect other transistors in case of any transistor breakdown. Therefore the bidirectional switches of a new converter are also protected by parallel connected varistors, Fig. 2.41. I chose varistor ERZC10DK681 with breakdown voltage  $U_{\text{var}} = 612 - 748V$ . When the voltage reaches level of  $U_{\text{var}}$ , the varistor begins to open and takes over the current from the module. The energy, which can dissipate this varistor, is approximately 70J.

### 6.3.3 Clamp Circuit

Meaning of the clamp circuit and its design was discussed in Sec. 2.7. Because we are dealing with the experimental prototype of the converter, the clamp circuit, that is not necessary for the converter function, is included to the converter design too. The output rectifier part and the capacitors of the clamp circuit are located on the interconnection

boards (Fig. 6.3). The input rectifier part is made by common 3 phase bridge rectifier module, that is mounted on the radiator of the power part of the converter. During the test of the converter was found out, that varistor in DC-link of the floating protection circuits works well in case of sudden power cut of the voltage on the input of the converter. However in case of errors on the output of the converter (long term bad switching) utilisation of the varistor is not working very good.

#### Example of problematic situation:

The converter is fed from common supply network and it is feeding induction machine. Due to some long term switching errors the voltage in DC-link of the floating protection is slowly increasing. Until the voltage reach break down voltage of the varistor (650V in this case). Varistor structure decrease its resistance in order to discharge the DC-link. However there is present voltage on the input of the converter, that continuously charges the DC-link trough the input rectifier. The varistor structure is now fully open dissipating energy from DC-link. When the voltage in the DC-link falls below the  $\sqrt{3} \cdot \sqrt{2} \cdot u_{in}$  more current is flowing to the DC-link from the supply. This will definitely overload the varistor and it ends with varistor explosion. From this point of view the chopper circuit seems to be better solution for discharging the DC-link of the floating protection circuit.

### 6.3.4 Driver Board

The design of the driver boards follows the design of interconnection boards. That means there are 3 driver boards for the converter, each for 6 transistor, that form bidirectional switches of one output phase. Each IGBT module has its own driver circuit. The task of the driver is to amplify the switching signal and it is also used for monitoring transistor states, like current flow direction, voltage drop on the transistor. This information is sent back to the FPGA on the switching pattern generation board. If an error occurs, the FPGA blocks immediately all pulses. For this purpose were selected drivers HCPL-316 from company Avago Technology [125]. Recommended connection 6.11 from the [125] was used for driving of IGBT gates and implementation of saturation protection.

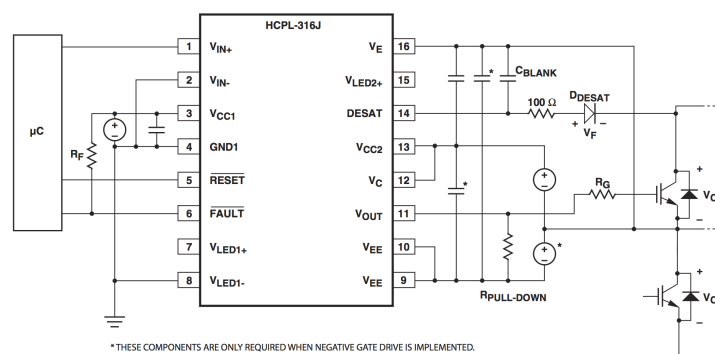
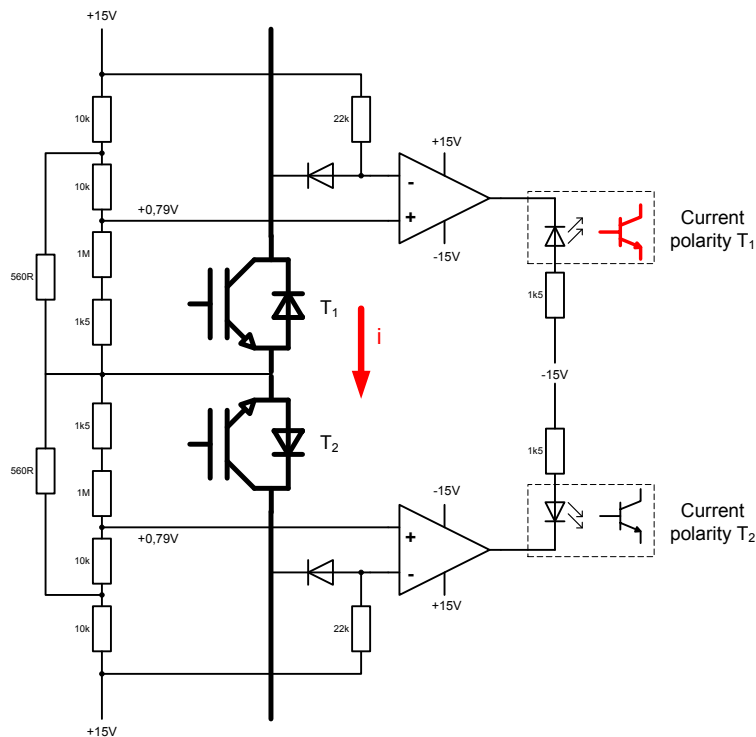


Figure 6.11. HCPL-316J connection [125]

Another task of the driver board is to detect polarity of the current trough the switch. The knowledge of the current direction is necessary for assignment of proper switching pattern during commutation as was discussed in chapter 2.3.1. Because method depicted in Fig. 2.17b require additional semiconductors connected into circuit, the detector based on measurement of voltage drop on the IGBT was developed. The second

method that decides the current direction from value of the voltage across the IGBT leads to measurement of the voltage drop value by A/D converter and would be very ineffective and also the actual information of the voltage is not directly required by the control system.

The realised current polarity detector uses comparator for detection of voltage drop across the IGBT. The circuit Fig. 6.12. Current flowing through the transistor causes voltage drop, that will trigger the comparator and turn on the LED of the optocoupler.



**Figure 6.12.** Current polarity detection circuit

When the voltage drop on a turned-on transistor is lower than defined threshold value  $u_{th}$ , the current is either too small to determine the polarity or the current flows through the diode. When the voltage drop on is higher than  $u_{th}$ , the current flows through the IGBT. This detection circuit also enables to detect possible error in the detection circuit or of the converter. Possible combinations are summarised in Tab. 6.3.

Comparator T <sub>1</sub>	Comparator T <sub>2</sub>	State
0	0	current polarity not detected
0	1	current is flowing through T <sub>2</sub> D <sub>1</sub>
1	0	current is flowing through T <sub>1</sub> D <sub>2</sub>
1	1	current polarity detection error

**Table 6.3.** Current polarity detection states

To the advantages of such solution belongs that no additional resistance is put into the current path. No direct measurement of the voltage drop on the transistor is needed and no further data processing is needed too. Comparator operates in two level logic either YES or NO, that means the galvanic insulation can be simply done by optocoupler.

The propagation delay of this circuit is only settling time of comparator and optocoupler (much faster than ADC). The signal can be easily and immediately processed by FPGA circuit that acts as modulator and generates switching pulses.

### 6.3.5 SW Protections

The hardware protections were already presented, however the reaction time of such protection circuits are very poor in case of long term overload. That is why the software protections were included into control algorithm. The input voltages and input and output currents are periodically measured at the beginning of each control loop. When the measured quantity overcomes the set limit value, the pulses for transistors are immediately blocked and input contactor is disconnected. To prevent malfunction of the converter in case of under voltage on the input there was set limit of minimal voltage too. When the module of the  $\underline{u}_{in}$  space vector is lower than set value the converter is either switched immediately off or the main contactor is prevented to switch on. The trip limits of SW protections are summarised in Tab. 6.4.

Quantity	Normalization	Trip coefficient
$u_{in,max}$	$\sqrt{2} \cdot 230V$	2.45
$u_{in,min}$	$\sqrt{2} \cdot 230V$	0.20
$i_{in}$	$\sqrt{2} \cdot 25A$	1.18
$i_{out}$	$\sqrt{2} \cdot 25A$	1.18
$u_{flprot}$	$\sqrt{3} \cdot \sqrt{2} \cdot 230V$	1.15

Table 6.4. Software protection limits

## 6.4 Control Part

The main tasks of the control part of the MC are to

- generate switching pulses for IGBTs
- in real time calculate implemented control algorithm
- interact with environment

therefore the HW platform for the control part was designed and selected with respect to this. Also when designing the control part of the converter the experiences from the older type of MC controller were respected, too.

The former control system is based on two common personal computers (PC) (see Fig. 6.13)[37]. The first one (Host PC) is equipped with any multitasking operating system as it is usual nowadays. It serves for compilation of the target real-time applications and for monitoring purposes only. The latter PC is equipped with a multi I/O PCI card Meilhaus ME-2600i containing 16 A/D and 4 D/A converters, and a 32 bit bidirectional digital I/O port. This card is connected with an external rack that deals first of all with signal adjusting, pulse generation, and error signal management. A special unit has been developed for the generation of switching pulses. It is connected to the digital output from the I/O card, where a kind of 24 bit parallel bus is implemented. Some of the signals are used for control and synchronization purposes, 12 signals define desired states of the output bits (switch word bus), and another 12 signals define the relative times corresponding to particular switching words. It is possible to define up to 16 switch events on average for every period on any connected card. Of course, the switching unit has to be able to generate exact switching patterns

and be programmed for the next control cycle simultaneously. This is done by means of the dual port-memory based FIFO unit implemented in the Field Programmable Gate Array (FPGA) which is employed in the switching unit. The controller of the switching unit assures that programmed switching events are saved one after the next to the correct positions in the dual port RAM. In this way a First in – first out (FIFO) structure with flexible length is created. The value of the last not yet used time part of the programmed event is continuously compared with the value of the internal timer that is reset at the beginning of every regulation period and when they match, the switching words are applied to drivers of the optical outputs of the switching unit. The above mentioned system works well. However, there are still some main disadvantages:

- the switching pattern must be pre-programmed for the whole modulation cycle,
- the PC processor doesn't communicate directly with switching pulse generating unit but all the commands are transferred through the I/O card,
- the system cannot detect automatically the source and current state of error inputs.

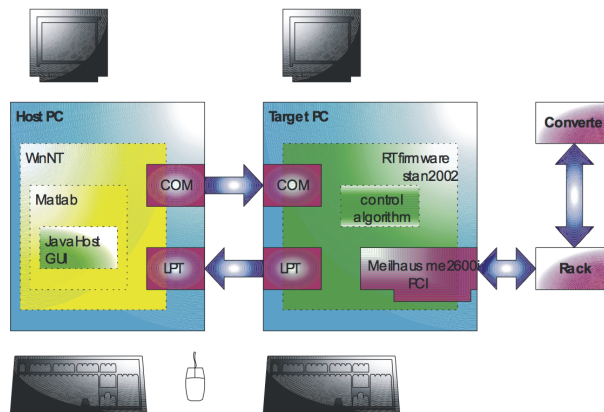


Figure 6.13. Former matrix converter controller [37]

#### 6.4.1 New Matrix Converter Controller

The control part of the compact matrix converter prototype consist of "Switching pattern generator board", that was designed by M. Bednar [40]. CPU module and A/D converter card manufactured by company RTD [126] (see Fig. 6.14).

In order to enable direct communication between the control processor unit and the pulse generator, it was decided to connect the generator forthright to a standard system bus. Industrial Standard Architecture (ISA), Peripheral Component Interconnect (PCI), and PCI Express belong to the most widespread ones. The ISA is the oldest bus, easy to handle and its throughput is sufficient for the above mentioned application. Although nowadays there are almost no mass-market PCs with ISA bus (even though physically not available logically this address space exists; physically devices can be connect via the ISA successor bus – LPC), the situation in the area of industrial computers is completely different. Many producers offer industrial PC boards in PC104, EPIC, and EBX format for embedded applications. For the matrix converter a combination of a custom EBX main board and PC104 processor board has been selected (Fig. 6.15).

In the new proposed system structure, there is only one component between the target PC and drivers – FPGA device (Fig. 6.15). This fact allows implementing of a clear structure of registers mapped directly into the PC memory or input/output (I/O) address space. Also all error signals are connected with the core programmable

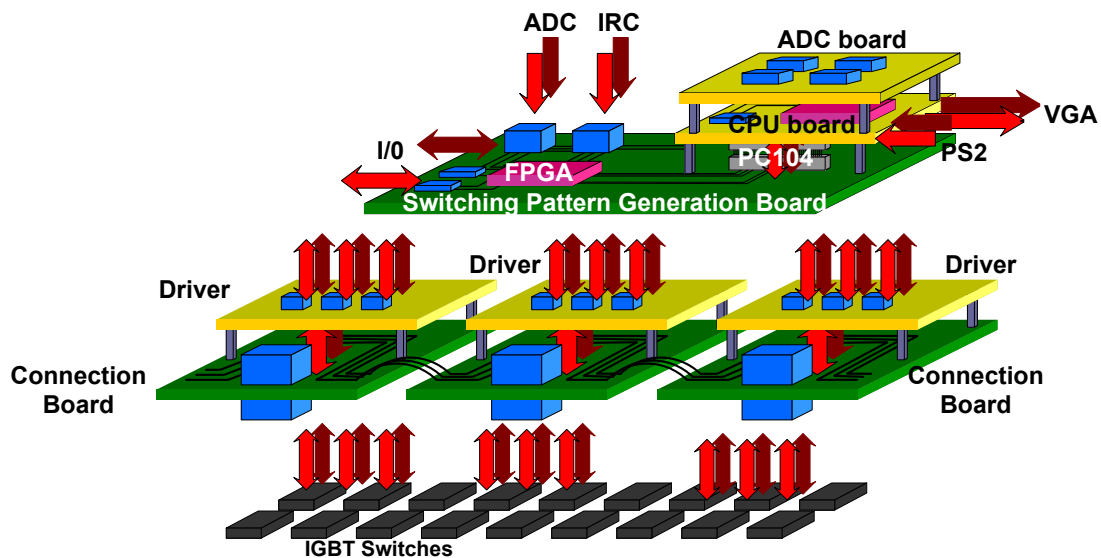


Figure 6.14. Conception of proposed controller

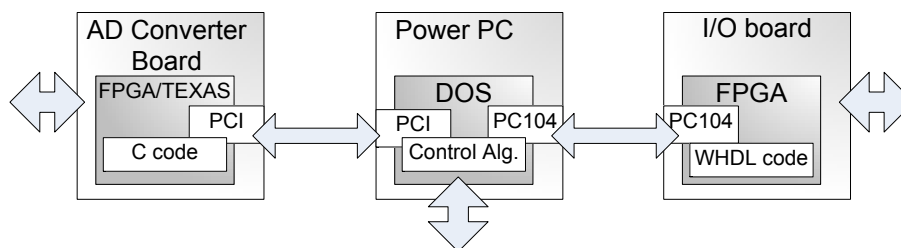


Figure 6.15. Matrix converter control part blocks

device directly. It simplifies the converter start up, shutdown, and diagnostic procedure. Moreover, the device becomes also smaller thanks to the dimensions of the selected industrial PC [126]. In the matrix converter each bidirectional switch needs 2 control signals and it returns 4 signals to indicate the transistor state and current direction. 9 bidirectional switches therefore require 54 signals that have to be accepted by the FPGA based switching pattern board. The FPGA on switching pattern board must be able to handle the communication over the PC 104, too. That is why, there must be many signals for communication with the main controller. The basic requirement set on the control device is exact generation of the switching patterns. Solution of this problem is possible by using some type of FPGA (Field Programmable Gate Array) circuit. If there is an input signal vector the FPGA can apply logical operation on this vector thus large amount of parallel operations can be applied at the same time. Output vector is an issue of all the operations. The clock frequency of modern FPGAs reaches up to 1000 MHz. This system allows implementation of finite state automatons working with current system state and generating switching pattern for the transistors. For this application the Altera Cyclone II circuit has been chosen. The CPU module CML147786CX650HR-128 was selected as a main controller. The CPU has following parameters (Fig. 6.16)

- CPU speed 650 MHz
- 256MByte SDRAM

- multiPort - Advanced Digital I/O (aDIO™) with event/match interrupt modes and bit masking capability
- SVGA display controller
- Bus mastering - 4 Bus Master PCI Add-on Cards Supported (PC/104-Plus modules)

A/D conversion card is connected via PCI Express bus. The card was selected from the same manufacturer because of compatibility (Fig. 6.16)

- Analog input - 12-bit, 1.25 MHz, 8 differential or 16 single-ended, 1K FIFO buffer, 1024 entry channel gain table, pacer, burst clocks data markers, and programmable gain of 1, 2, 4, 8, 16, 32, 64
- Analog output - Two channel, 12 bit, 200 kHz throughput, independent 1 K FIFO buffers
- Timers/Counters - Three 16-bit
- Digital I/O - 16 buffered TTL/CMOS lines. Two independent ports of 8 bits each

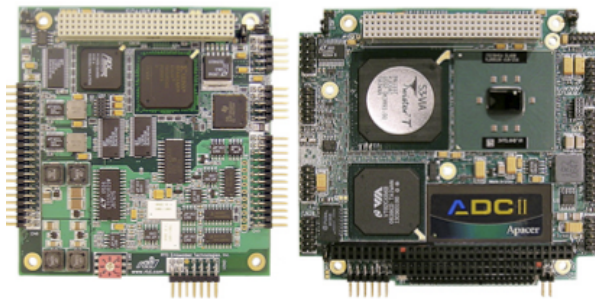


**Figure 6.16.** CPU module and ADC module

RTD offer also board with FPGA (FPGA6800HR) that can be interconnected with CPU module via PC104 [126]. The VHDL code for processing information from IRC and second realisation of modulator for MC was programmed for this board [127]. Because the control part of the converter was designed to be fed from Switching Pattern Generation Board, the interconnection of RTDFPGA6800HR with the driver boards turned to be complicated, so its function was tested and the further development was suspended.

#### ■ 6.4.2 New Matrix Converter Control SW

Control software for the matrix converter can be divided into several modules.

- SW for the modulator
- SW for the CPU (RT-kernel)
- control application

The SW for the modulator is in fact VHDL code for FPGA, that is not accessible to user. It can be treated as kind of firmware, that was developed for the converter and in ideal case the user does not know, that it exists. In our design are in FPGA implemented blocks for safe commutation, switching table and modulator. More information about this SW part can be found in [41–43]. All important registers of the modulator from FPGA are mapped into memory of CPU from.

The SW for the CPU is kind of firmware, too. Although it has futures as standard PC the application there have to fulfil special requirements, because it will be responsible

for calculation of switching commands for the converter [128]. The application (RT-kernel) shall run in two modes:

- non-realtime
- hard realtime

The real time operation means that exact execution of the code is ensured, therefore all HW interrupts have to be disabled and functions that are normally served with interrupts e.g. serial communication, VGA service, keyboard service have to be rewritten so the RT-kernel has full control of the tasks. The time of service tasks execution (VGA, serial communication, keyboard service), should be as low as possible, too. The RT-kernel has to be able to service communication with FPGA modulator via PC104 and with A/D converter board via PCI. Because of this it was decided that the RT-kernel is going to be 32-bit DOS application written in C language [128].

In non real time mode the kernel have to initialise all required peripherals for operation of the control part, disable processor interrupts and loads driver for card with A/D converters [128–129]. Then it waits until it is switched to hard real time mode.

In hard real time mode the RT-kernel locks itself into real time loop with the A/D converter card, that provides synchronisation pulses. The synchronization pulse starts the new control loop and it also triggers the A/D converters conversion. Because even the conversion takes some time and it is done in parallel to the main CPU, the RT-kernel utilizes also this "free" time for some service routines. When the conversion is done, the results are taken and the user defined control action is performed. In the rest of the real time loop the RT-kernel does the rest of the service routines. Flowchart of the real time run is in Fig. 6.17. The screenshot from the application is in Fig. 6.18.

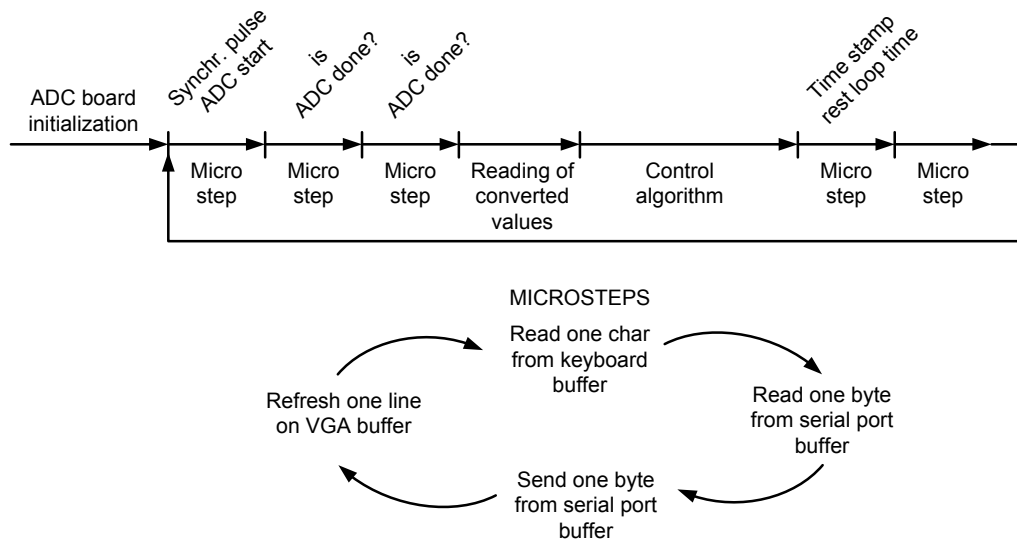


**Figure 6.17.** Real time application flowchart

The control application is part of code, that is written by user and is responsible for control of the converter. The code designed by user is linked together with RT-kernel and driver for the A/D converters card, that are passed to user as libraries. All data between the user control function and RT-kernel are passed via pointers. This solution should shield the end user from unwanted modifications of the RT-kernel. The application is also able to store/record some data to SD card, so the offline analysis of

```

Control screen
Special Flag Register: 000000000000 b  Error register: 0000000000
ETFRO ETFRO ETFRO ETFRO ETFRO ETFRO ETFRO ETFRO ETFRO
Data log info: 00000 00000 00000 00000 00000 00000 00000 00000 00000

FreqSet : 0.000      Modul : 0.010  -
Reg Nr. : 0
Reg Val.: 0.000

PsiReq  0.00      OmMreq  0.00      OmMcalc  0.00      OmScalc  0.00
UZAl    0.000    UZBe    0.000

req      PIpsi    PIiD      PIom      PIiQ
act      0.000    0.000    0.000    0.000    0.000
out      0.000    0.000    0.000    0.000    0.000

req      PIa      PIB      PIC
act      0.000    0.000    0.000
out      0.000    0.000    0.000

```

Figure 6.18. Real time application screenshot

data in Matlab and diagnostics of the system is possible. This functionality should be further extended to transfer selected data via serial line or ethernet.

This section was describing controller design for the matrix converter prototype. The HW for the controller was selected so, that it can be easily incorporated into any control system. Developed RT-kernel can be considered as kind of RT operation system that offers defined interface for any user function. It means arbitrary number of user control functions can be registered into RT-kernel and executed in user defined order. Based on selection of the number of extension cards with A/D converters and with FPGA the system can be modularly assembled and used for control of other converter platform, depending on the codes programmed into FPGA. For communication with FPGA boards is used extended ISA bus (PC104). Only requirement is that the registers of modules written in VHDL have to be mapped in CPU memory or I/O space. To simplify development of the modules and their connection to the system the ISA to Avalon interface was programmed in [127].

### 6.4.3 Development of SW and Simulation of the User Control Application

On the CPU runs operation system DOS. This system was selected because its simple, well documented and its distributions are stable. Developed application can be easily compiled for DOS too. For developing of the application were selected WATCOM C compiler and Eclipse IDE. Watcom was introduced in 1988 for IBM PC. Main advantage is that it offers 32-bit compiler for x86 platforms. In 1999 becomes open source under name of Open Watcom, that offers debugging profiling and other diagnostics tools. Watcom was selected because of its open source licence and compilers that produces very clean and optimised code. Its disadvantage is that its IDE is very simple and looks like text editor. To overcome this problem the IDE of Eclipse was used. Eclipse is known as multi-language development tool, that offers many comfortable functions for code developers as automated code syntax check, fast reading of the source code,

etc. Therefore the combination of Eclipse IDE and Watcom C compiler were used for control application development.

The applications of RT-kernel and driver for A/D converter card are compiled as libraries, that are hidden to user who is writing his control application. They are linked together with the user control application at the end of compilation (see Fig. 6.19). This also enables testing of functionality of the user developed control codes separately from the RT-kernel.

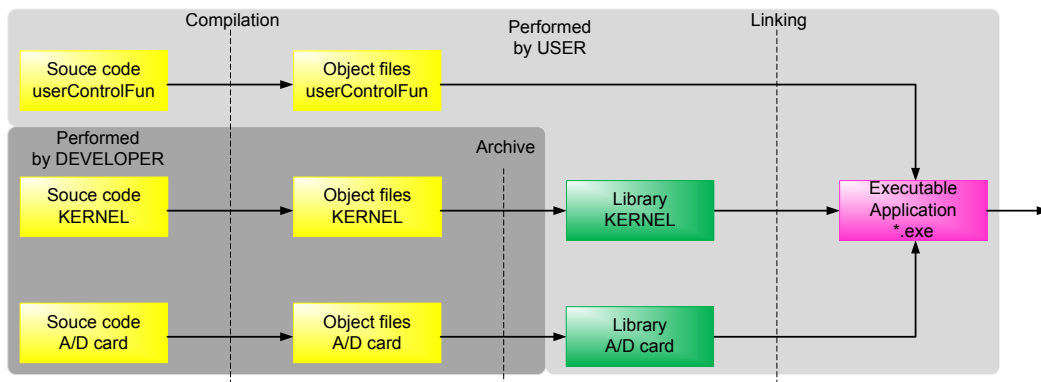
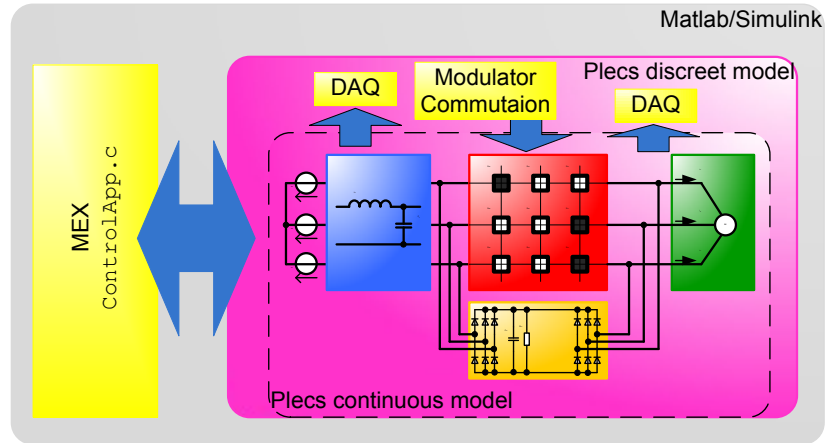


Figure 6.19. Compilation of parts of application

Because developed control application have to run in real time and it calculates switching commands for the transistors, debugging and stoping of the code execution is not possible. Therefore the code have to be tested in another way. For this purpose were used SW Matlab/Simulink and toolbox Plecs (Piece wise Linear Electrical Circuit Simulator). The Plecs is toolbox for simulating of electromechanical components within Matlab environment and is specially developed for simulations of power electronics and drives.

The model of the whole converter including supply, input filter, transistor matrix and load was created at first. The functionality of this model was firstly tested by continuous time solver and with predefined switching patterns. This testing ensures that the ISVM modulator works properly. Then parts of the model that should run with the fixed step e.g. control algorithm, data measurement were put into separate sub model and parts of the code were transformed into Plecs **C-script** block. **C-script** block enables to simulate parts of code written in C-language to be simulated in Plecs. However the interconnections of the code modules are still handled by Simulink "virtual wires". In order to test whole structure of the application with handling of data through pointers the **Mex function** compiler of Matlab was used (Fig. 6.20). In this way were tested all parts of code together. The model of matrix converter was further extended to simulate behaviour of commutation, dead-time and minimal switching times.



**Figure 6.20.** Simulation testing

This sequence of the simulation model development was used further when developing the control strategies. The model of the IM controller was created from Simulink blocks at first, then transformed to the disreet time domain and finally implemented in Eclipse in C-language. The C-code was imported back into Matlab and connected to the model of matrix converter drive created in Plecs. All controller gains were tuned in Matlab/Simulink/Plecs simulations and only then the code put into the converter.

# Chapter 7

## Matrix Converter Drive - Results of Tests

### 7.1 Outline

The design and development of the compact matrix converter was described in chapter 6. This chapter will summarise aspects of control algorithm development. Firstly to test the function of the modulator developed in [43] simple open loop V/f control was developed. Later the two methods of FOC control were developed and tested on the converter.

As the first step when developing the control, simulation models of the drive in Matlab/Simulink, Plects were created. Control algorithms written in C language were translated into Matlab Mex-functions and simulated. The power part of the converter and induction machine were simulated in Plects toolbox.

To test the behaviour of the matrix converter control part two field oriented control strategies were implemented. Diagram of the test bed realised in laboratory is depicted in Fig. 7.1. Induction machine with parameters listed in Appendix B was coupled to separately excited DC machine. Loading torque of the DC machine was controlled by variable resistor connected to armature terminals. Input and output currents are measured directly by the matrix converter. Speed is estimated by the controller and measured by tachogenerator integrated in DC machine with recalculation ratio  $100 \text{ V} = 1000 \text{ rev/min}$ .

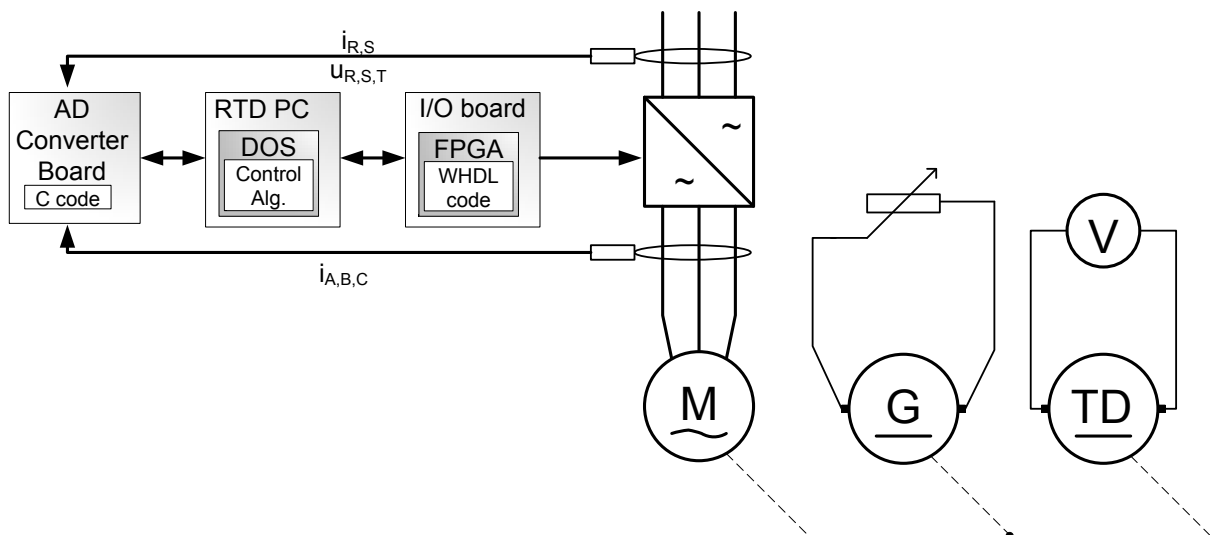


Figure 7.1. Test bed for drive testing

### 7.2 Flux Oriented Control Simulation

Implementation of the field oriented control for the matrix converter drive is same as for drive with VSI. For both converters is the output of controller same - reference

voltage, that is produced by particular modulator. Main difference is in voltage limit of the matrix converter defined in chapter 3. Because the output voltage is limited to 86,6 % of the input voltage amplitude, the matrix converter is from this point of view worse candidate for the FOC implementation.

Control strategy is implemented according to Fig. 5.5. The fluxes and speed are estimated by Luenberger type observer (Fig. 4.4) described in chapter 4. Luenberger observer estimates IM quantities in stator connected reference frame. The estimated value of flux  $\Psi_d$  and currents  $i_{sd}, i_{sd}$  are then transformed into flux connected reference frame. The transformation angle is calculated from the rotor flux components according to (7.1).

$$\Theta_s = \tan^{-1} \frac{\Psi_\beta}{\Psi_\alpha} \quad (7.1)$$

Current set point limitation is implemented according to Fig. 5.9, where the flux producing current component was selected to be preferred. Its allowable maximum is set to 0.5 of  $i_{max}$  and torque producing component is then dynamically limited.

### 7.2.1 Luenberger Observer Speed Estimation

The Luenberger observer (Fig. 4.4) is extended of speed estimation algorithm, because the matrix converter IM drive is not equipped with speed sensor. Its combination of stable flux estimator and speed estimator is in this case very advantageous. Realization of the observer in C language follows

```

1  %Observer
2  tCurrSdDot = (N_sampleTime/(N_sigma*Ls))*tVoltSd+..
3  ..(1-N_sampleTime/N_sigma*(1/N_tauS+((1-N_sigma)/N_tauR)))*..
4  ..tCurrSdEst+tOmegaS*N_sampleTime*tCurrSqEst+(((1-N_sigma)/N_sigma)*..
5  ..N_sampleTime/N_tauR)*tPsiRdEst+((1-N_sigma)/N_sigma)*N_sampleTime*..
6  ..tPsiRqEst*pP*tOmegaEst-(N_k-1)/N_sigma*(1/N_tauR+1/N_tauS)*..
7  ..N_sampleTime*(-tCurrSdMeas+tCurrSdEst)+(N_k-1)*tOmegaEst*pP*..
8  ..N_sampleTime*(-tCurrSqMeas+tCurrSqEst);
9  tCurrSqDot = (N_sampleTime/(N_sigma*Ls))*tVoltSq+..
10 ..(1-N_sampleTime/N_sigma*(1/N_tauS+((1-N_sigma)/N_tauR)))*..
11 ..tCurrSqEst-tOmegaS*N_sampleTime*tCurrSdEst+(((1-N_sigma)/N_sigma)*..
12 ..N_sampleTime/N_tauR)*tPsiRqEst-((1-N_sigma)/N_sigma)*N_sampleTime*..
13 ..tPsiRdEst*pP*tOmegaEst-(N_k-1)/N_sigma*(1/N_tauR+1/N_tauS)*..
14 ..N_sampleTime*(-tCurrSqMeas+tCurrSqEst)-(N_k-1)*tOmegaEst*pP*..
15 ..N_sampleTime*(-tCurrSdMeas+tCurrSdEst);
16 tPsiRdDot = (N_sampleTime/N_tauR)*tCurrSdEst+(1-N_sampleTime/N_tauR)*..
17 ..tPsiRdEst+(tOmegaS-pP*tOmegaEst)*N_sampleTime*tPsiRqEst+..
18 ..(N_k-1)/(1-N_sigma)*(1/N_tauR-N_k/N_tauS)*N_sampleTime*..
19 ..(-tCurrSdMeas+tCurrSdEst)+(N_k-1)/(1-N_sigma)*N_sigma*pP*tOmegaEst*..
20 ..N_sampleTime*(-tCurrSqMeas+tCurrSqEst);
21 tPsiRqDot = (N_sampleTime/N_tauR)*tCurrSqEst+(1-N_sampleTime/N_tauR)*..
22 ..tPsiRqEst-(tOmegaS-pP*tOmegaEst)*N_sampleTime*tPsiRdEst+..
23 ..(N_k-1)/(1-N_sigma)*(1/N_tauR-N_k/N_tauS)*N_sampleTime*..
24 ..(-tCurrSqMeas+tCurrSqEst)-(N_k-1)/(1-N_sigma)*N_sigma*pP*tOmegaEst*..
25 ..N_sampleTime*(-tCurrSdMeas+tCurrSdEst);
26
27 % Transformation angle calculation
28 tThetaS = atan2(tPsiRqDot,tPsiRdDot);
29 tThetaSm = tThetaS;
30

```

```

31 % Storing results for next step
32 tCurrSdEst = tCurrSdDot;
33 tCurrSqEst = tCurrSqDot;
34 tPsiRdEst = tPsiRdDot;
35 tPsiRqEst = tPsiRqDot;
36
37 % Mechanical speed estimation
38 dev = tPsiRqEst*(tCurrSdMeas-tCurrSdEst) -..
39 ..tPsiRdEst*(tCurrSqMeas-tCurrSqEst);
40
41 out = sum + N_Kp*dev;
42 if (out is greater than N_PsatMax)
43 out = N_PsatMax;
44 else if (out is lower than N_PsatMin)
45 out = N_PsatMin;
46
47 sum = sum + N_Ki*dev*N_sampleTime;
48 if (sum is greather than N_IsatMax)
49 sum = N_IsatMax;
50 else if (sum is lower than N_IsatMin)
51 sum = N_IsatMin;
52
53 tOmegaEst = out;
54

```

To test the behaviour of the proposed observer structure model of the induction motor and observer was assembled in SW Matlab/Simulink/Plecs. Parameters of the induction motor used for simulation are in Appendix B. The outputs of the observer were compared with the outputs of the induction motor model that is implemented in Plecs toolbox. Because motor model calculates inner fluxes and other variables in stator fixed coordinate system, the observer works in  $\alpha, \beta$  coordinates too. DRFOC control strategy was used for testing. Fig. 7.2 shows comparison between the value of the flux calculated by the Plecs model of IM (upper part) and estimated flux by observer (bottom part).

Fig. 7.3 shows speed estimation by the LO. Red line represents reference rotor speed in radians, green waveform corresponds to rotor speed calculated by IM model in Plecs and blue waveform is speed estimated by observer. I can be seen that observer tracks the speed mostly without some bigger errors. Some differences are obvious during the transitions and of course there is instability at the beginning where was required zero speed

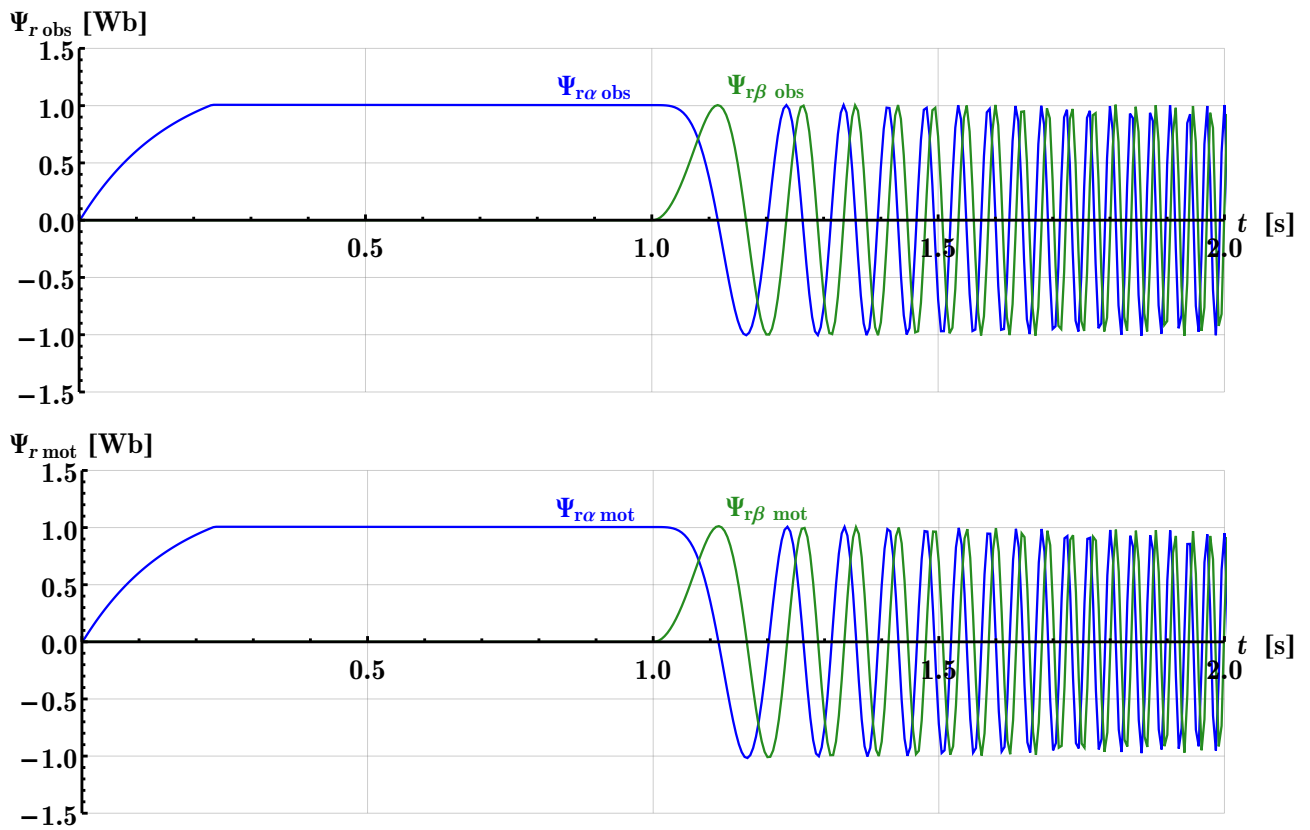


Figure 7.2. Simulation of Luenberger observer rotor flux estimation

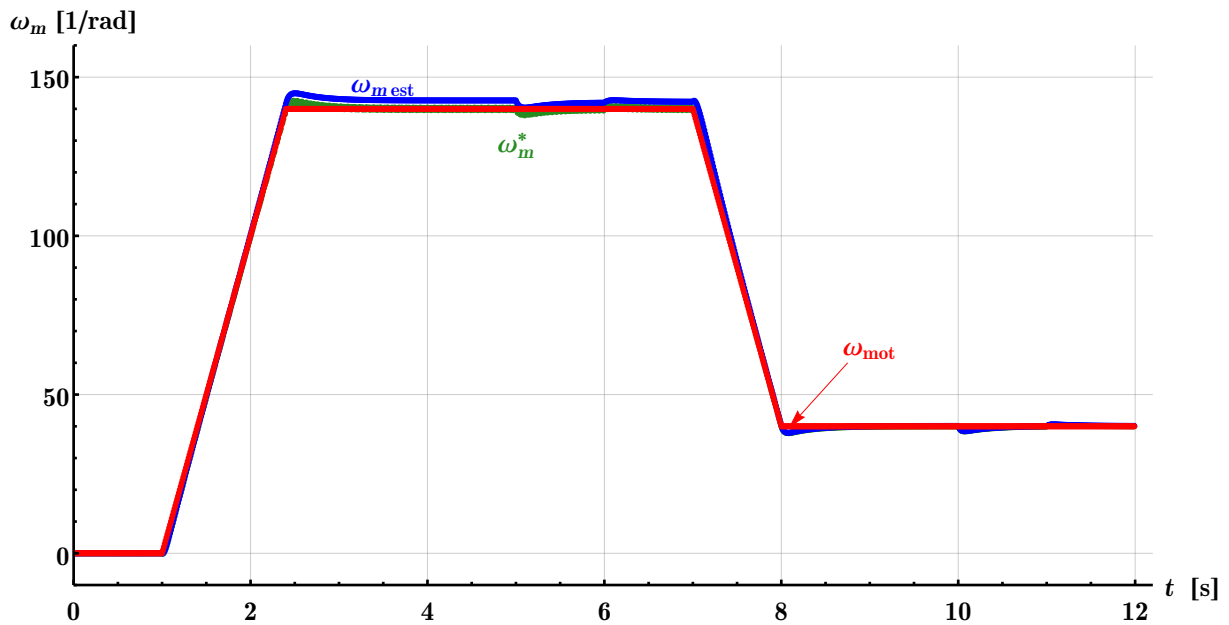
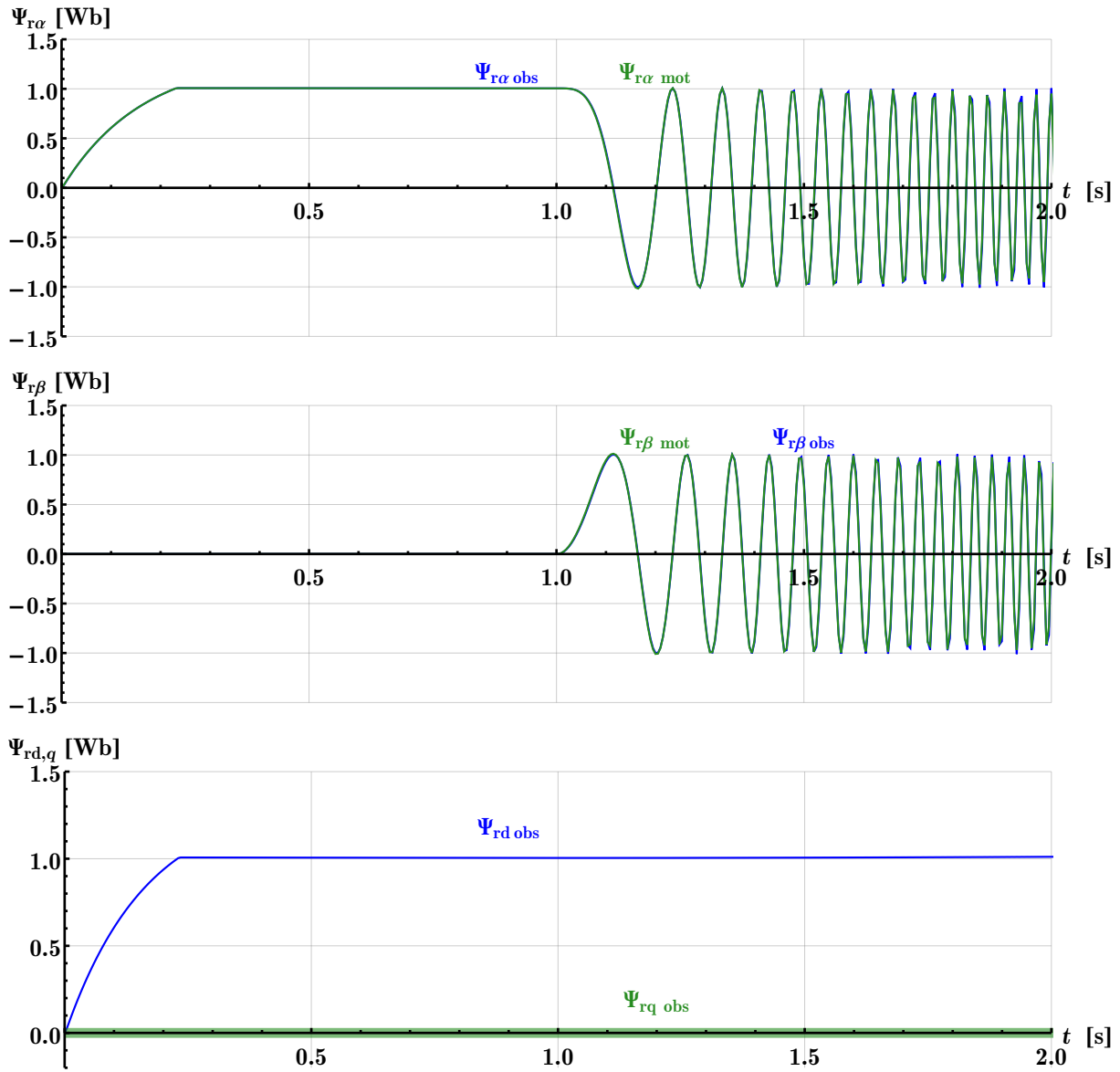


Figure 7.3. Speed estimator simulation

In the Fig. 7.4 are compared estimated and calculated values of flux components in stationary  $\alpha, \beta$  coordinates, in the bottom part of the figure are shown components

of the flux transformed into d,q system, the transformation angle is calculated in the observer.



**Figure 7.4.** Flux components estimator simulation

Figure 7.5 show comparison between current components  $\alpha, \beta$  measured by the model of IM in Plecs and estimated in the observer.

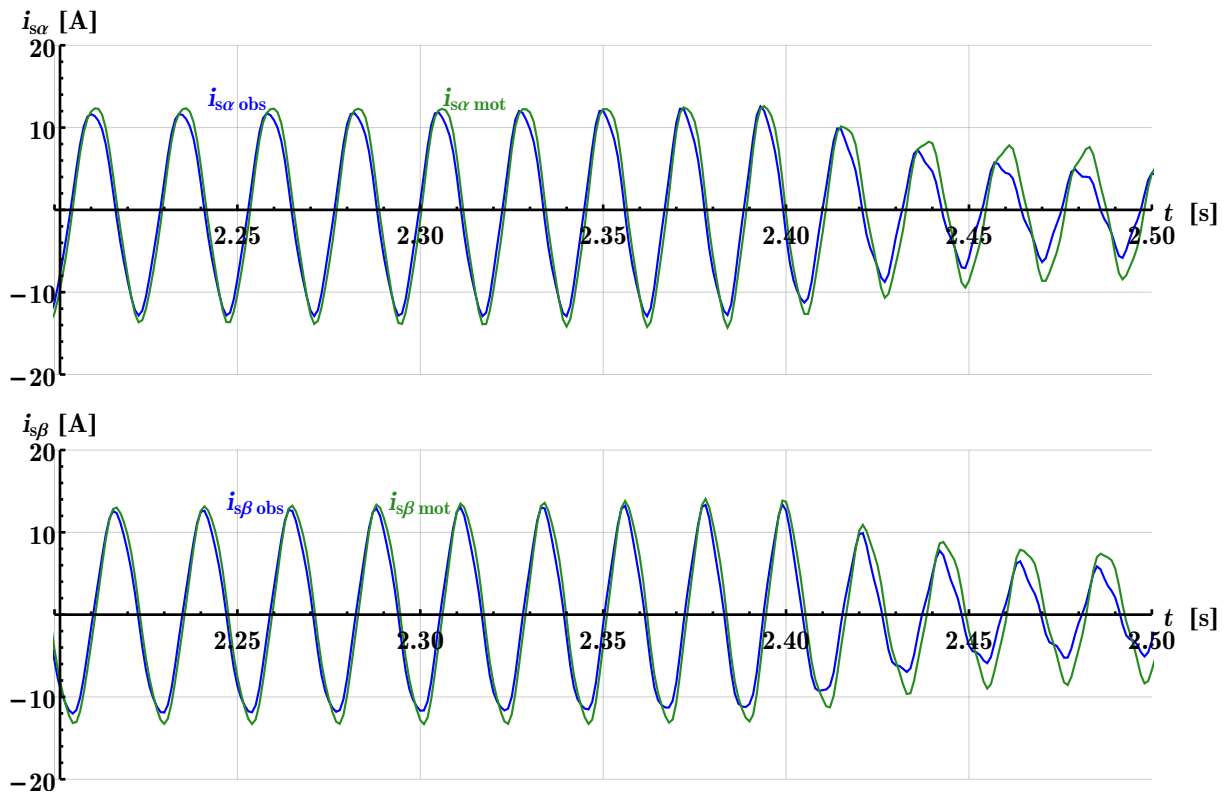


**Figure 7.5.** Current components estimator simulation

Simulations have shown, that designed observer is stable and estimate values of rotor speed and flux without great error. However the stability and accuracy of the observer depends on quality of its inputs (current and voltage). These signals are usually distorted in the real application, because of sensors interference and A/D converters inaccuracy, therefore the resulting accuracy and stability of the observer is slightly lower. In Fig. 7.6 are results of observed and measured speed during DRFOC control of the drive during acceleration and deceleration of the IM. The IM was firstly excited to its nominal flux value and then was slowly increased reference speed to nominal value of IM and back.

Red curve represents required reference speed set from the keyboard, blue waveform is voltage measured on the terminals of the tacho generator by oscilloscope (100 V = 1000 rev/min). The green curve is speed of the induction motor estimated by the observer. It can be seen that estimated speed track reference value of the speed. The amplitude of the estimated speed fluctuations is around  $\pm 5$  rad/s.

During the simulation was also tested the ability of the observer to adapt to change of IM values like stator and rotor resistance. Simulation results have shown that the observer is able to estimate flux and speed without greater error within interval of 50% deviation of the nominal stator resp. rotor resistance value.

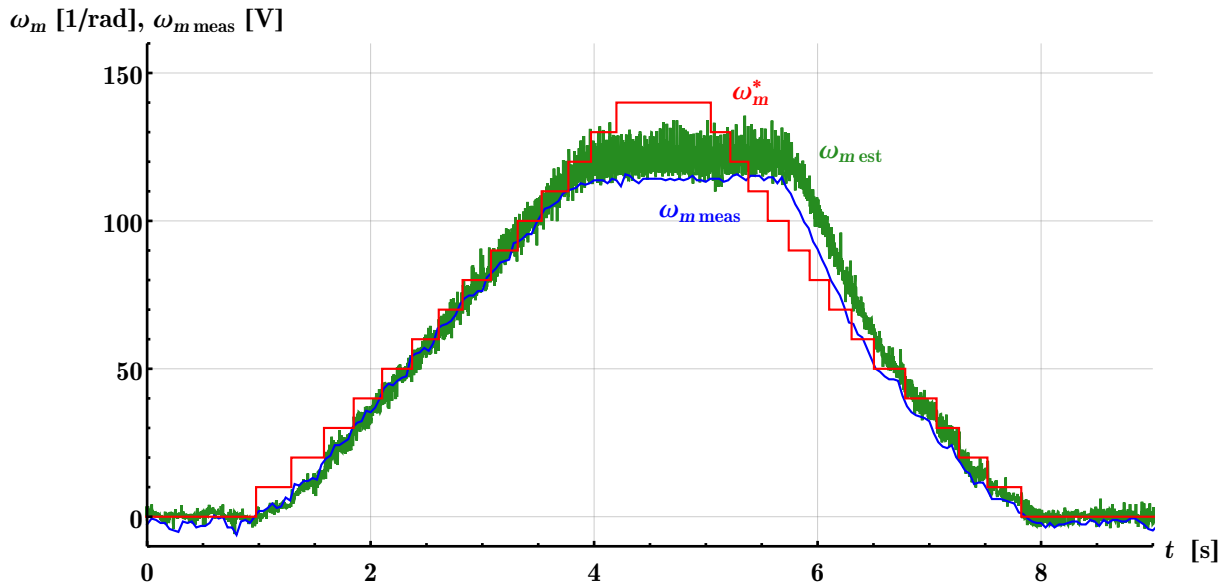


Figure 7.6. Comparison of observed and measured speed

In Fig. 7.7 are depicted waveforms of estimated flux values during the test described above. The IM was firstly excited to value  $\Psi_r = 0.8$  [Wb] and then the speed reference has changed. Upper part of Fig. 7.7 shows estimated rotor flux  $\Psi_r$  in stator fixed coordinate system  $\alpha, \beta$ . In the bottom part of the figure is depicted  $\Psi_r$  in field connected coordinate system  $(d, q)$ . From the figures is obvious that the observer tracks position of the flux space vector accurately, because the  $\Psi_{rd}$  component holds around its reference value and the  $\Psi_{rq}$  value is zero according to FOC control theory.

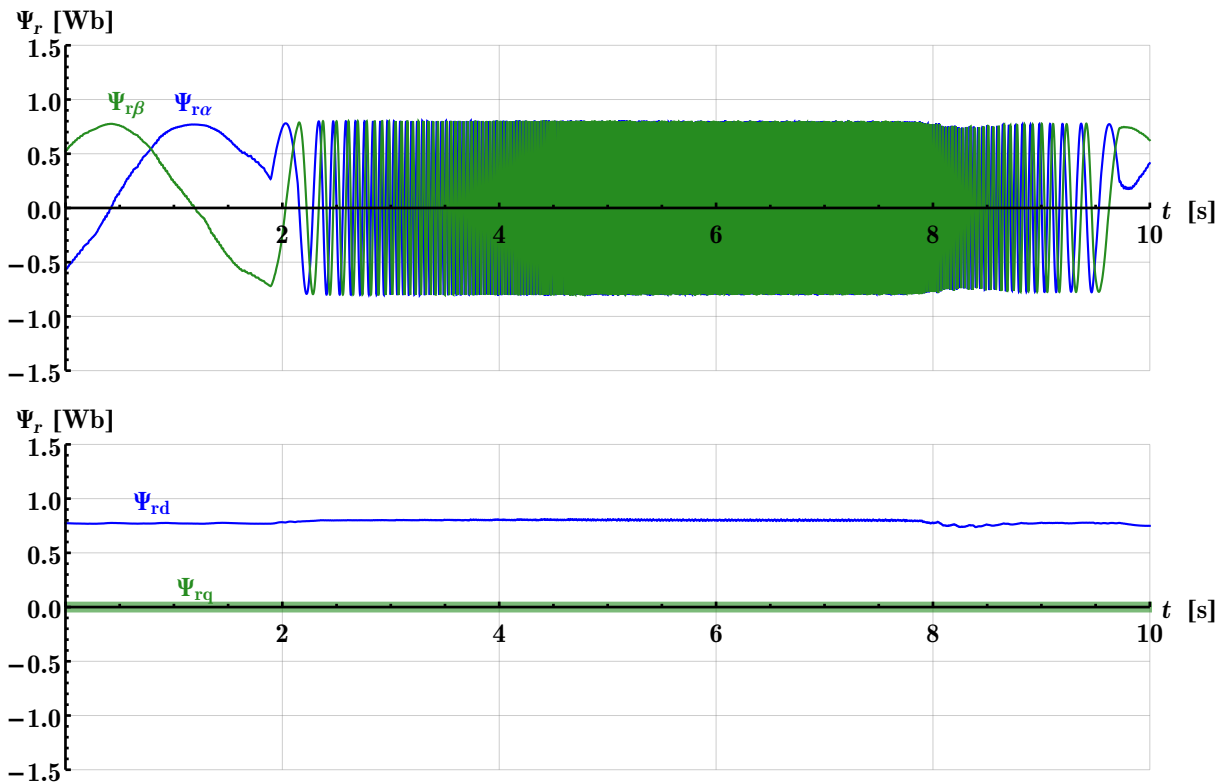


Figure 7.7. Results of the rotor flux estimation on real drive

## 7.2.2 Scalar Control Measurement

Because open loop scalar control is the simplest control strategy for IM drive it was implemented at first for testing of matrix converter drive. However from the measured results it is hard to say something about quality of the control. The measured results are in Fig. 7.8 - 7.9. Converter was supplying induction motor. In the Fig. 7.8 the waveforms of the currents and input voltage are measured directly by LEM sensors, waveform of output voltage are values in  $\alpha, \beta$  coordinate system calculated by modulator. From the figure can be clearly seen the ability of the converter to hold power factor near unity. Nonsinusoidal shape of the input current is caused by supply network in the lab, that contains 5<sup>th</sup>, 7<sup>th</sup>, 11<sup>th</sup>, 13<sup>th</sup> harmonic components. Those harmonics are sucked by the input filter. Fig. 7.9 shows results measure by the NI DAQ box. It show same results measured by independent tool as those measured by the LEM sensors of the converter.

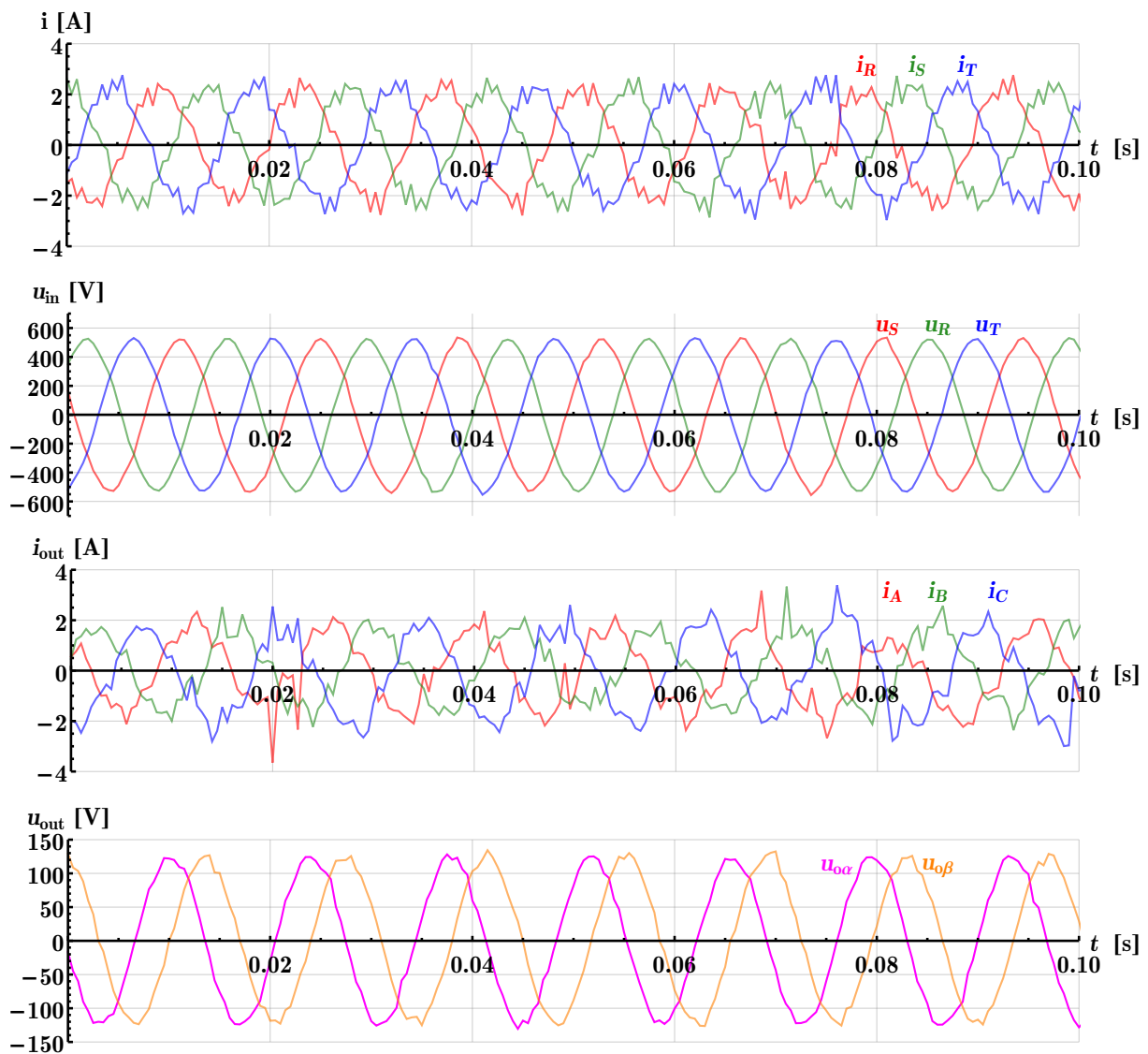


Figure 7.8. Measured input/output waveforms - scalar control

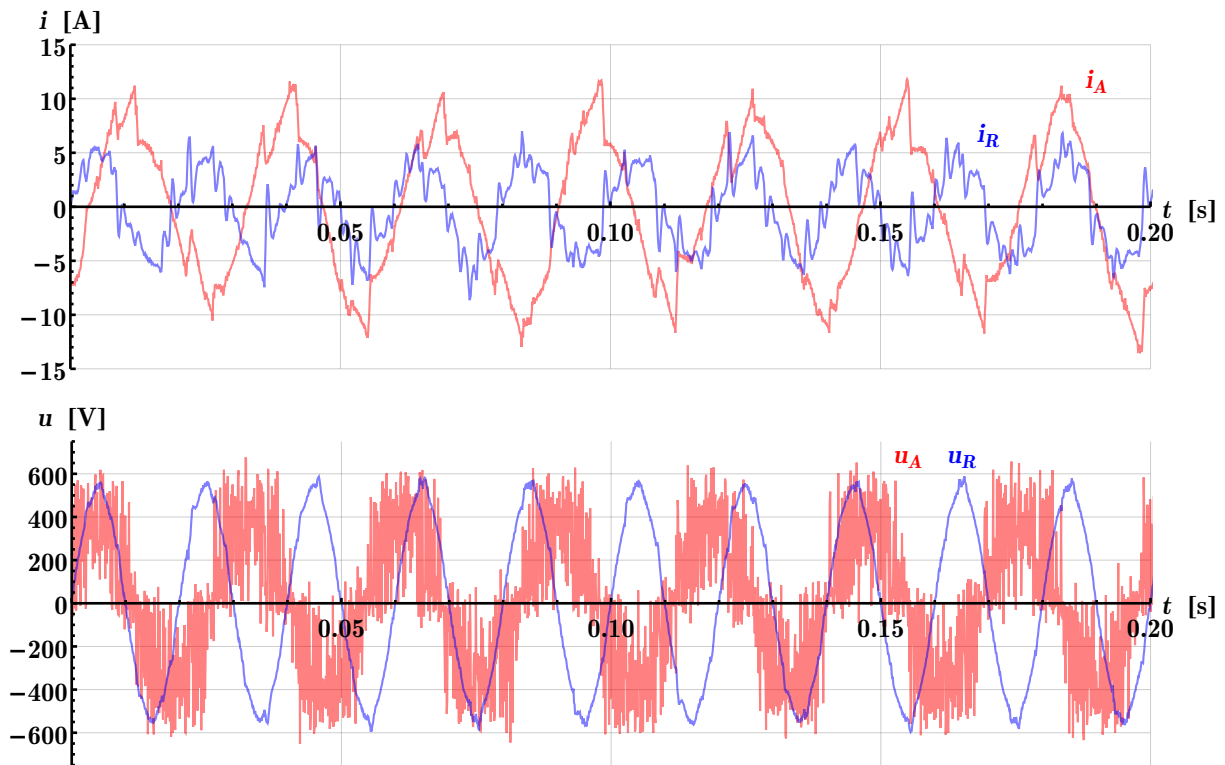


Figure 7.9. Measured input/output waveforms - scalar control

### 7.2.3 Direct Rotor Flux Oriented Control Simulation

The rotor field oriented control model was implemented in Matlab/Simulink and Ples according to structure depicted in Fig. 5.5. Because the real drive test bed is not equipped with speed sensor, the Luenberger observer, that is used for estimation of the flux of IM was extended to estimate the speed information too. Figure 7.10 shows reactions of the flux and speed controllers to change of reference values. In order to test the controller behaviour reference values of the flux and speed were stepwise changed and in each state IM was loaded with different torques. In the Fig. 7.11 are depicted reactions of inner controllers of flux and torque producing current components. Fig. 7.12 shows estimated trajectory of rotor flux space vector. It is obvious, that flux is controlled to have circular path. Also the process of field weakening can be clearly seen. Minimization of the controller's overshoot can be done by better tuning of the controller parameters for specific drive, that is not aim of the simulation in this thesis.

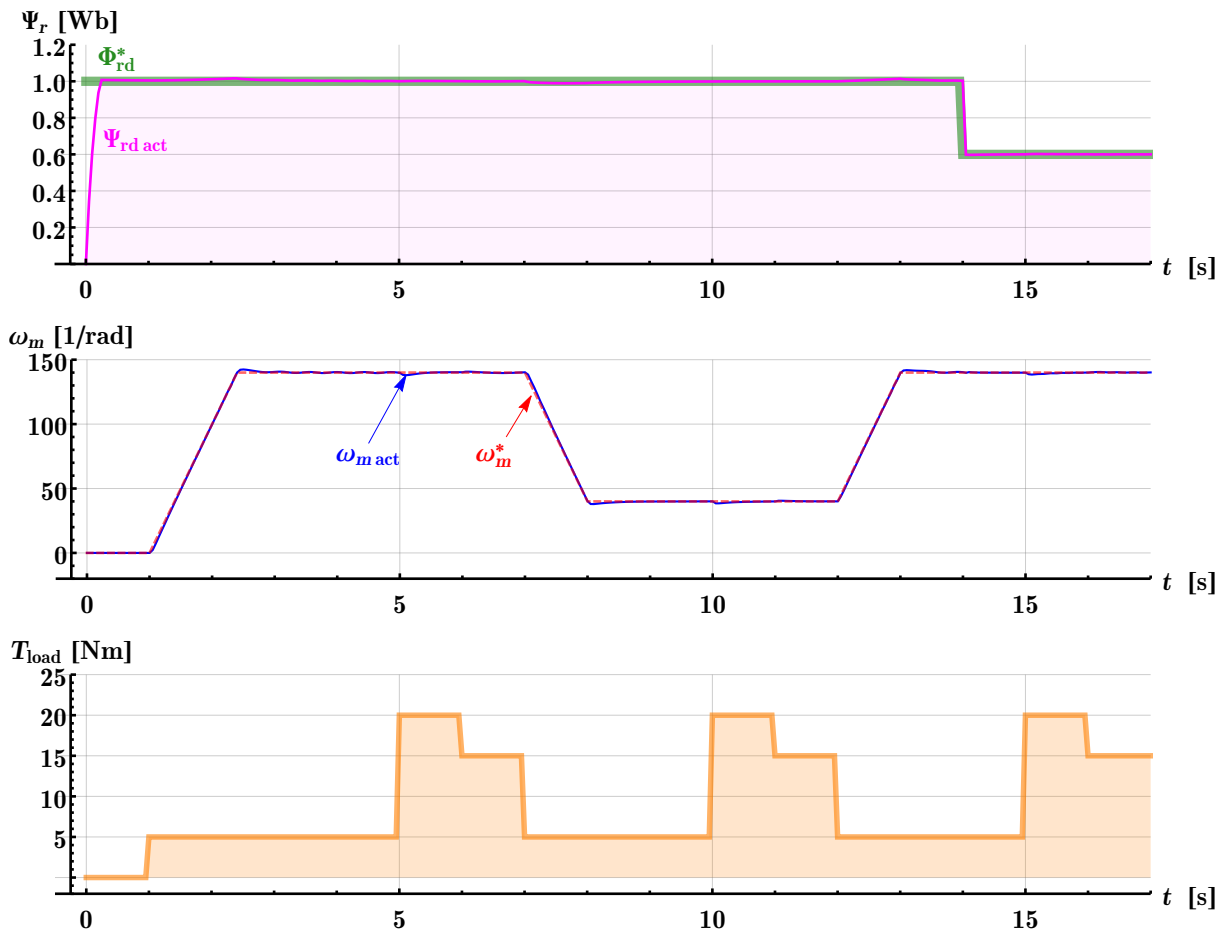


Figure 7.10. DRFOC control - flux and speed controller simulation

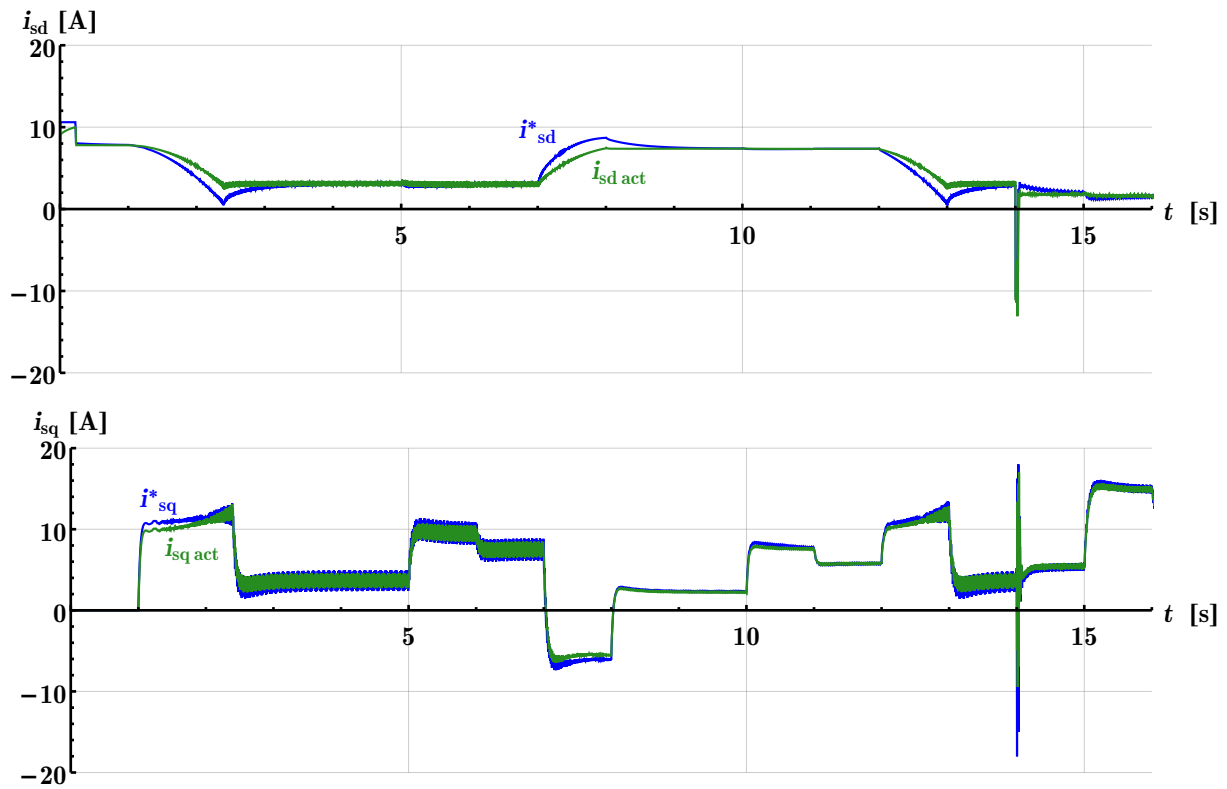
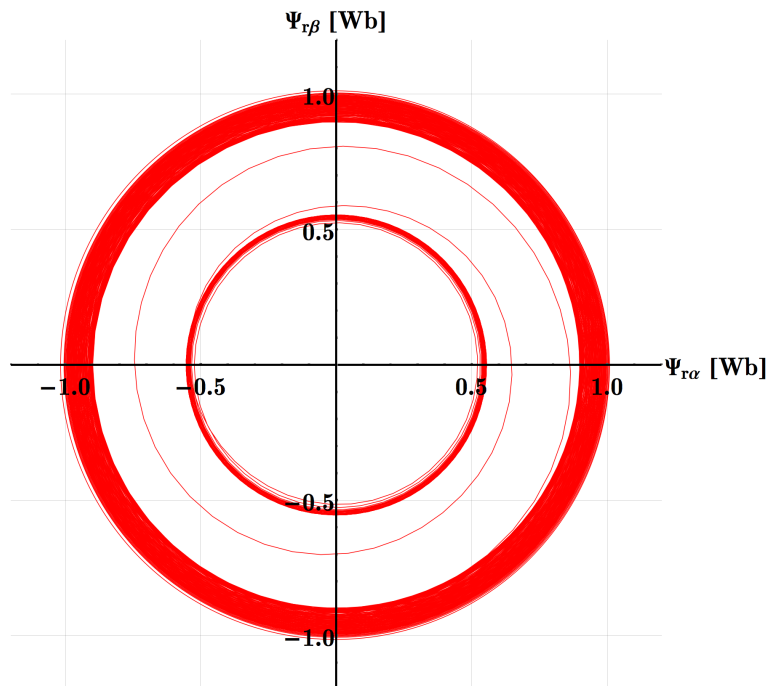


Figure 7.11. DRFOC control - current component controllers reaction

Figure 7.12. DRFOC control -  $\Psi_r$  trajectory

## 7.3 Direct Rotor Flux Oriented Control Realization

Following section shows results of realised DRFOC algorithm on matrix converter IM drive. DRFOC was realized according to Fig. 5.5. Results of the control algorithm

on the real HW are loaded with some errors, because of inaccuracy of measured signals required for the IM model. Performance of the control could be improved by pre filtering of the measured signals and precise tuning of the controller gains, however this task is nearly unsolvable without SW for monitoring and visualisation of the inner variables of the control algorithm, that is still under development. Therefore the constants from the Matlab models were used for the realization.

Fig. 7.13 show reactions of the flux and speed controller. In upper part of the Fig. 7.13 is shown behaviour of the flux controller. During the test of DRFOC the reference value of the flux was set to  $\Psi_r = 0.8$  [Wb]. Reference value of the speed was increased from zero to nominal value and back.

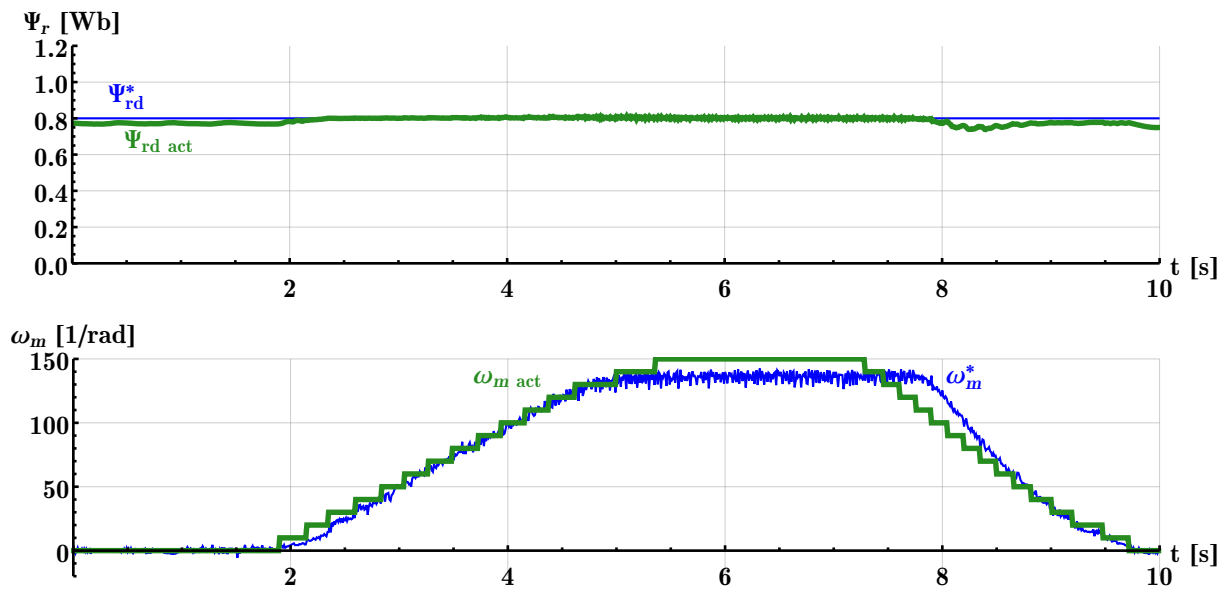


Figure 7.13. DRFOC control - flux and speed controller reaction

In order to test flux and torque current component controllers IM was run up to  $\omega_m = 100 \text{ rad}^{-1}$  and then the IM was abruptly loaded with DC machine with set breaking torque 20 Nm and after some time the IM was unloaded again. Responses of the  $d, q$  current controllers are in Fig. 7.15. From the figure is obvious that decoupling works well, because only torque producing component of the current has changed. Upper part of the Fig. 7.14 shows currents on the input of the matrix converter drive, middle part shows output current. In order to make figure legible RMS values of the currents are visualised. Bottom part of the figure then shows actual values of flux and torque components of the current. Detail of the current reaction is in 7.15. Upper part of the figure shows the reference flux producing current component as output of the rotor flux controller and actual value of  $i_{sd}$  calculated from measured output currents. Bottom part shows same situation for torque producing component of the current.

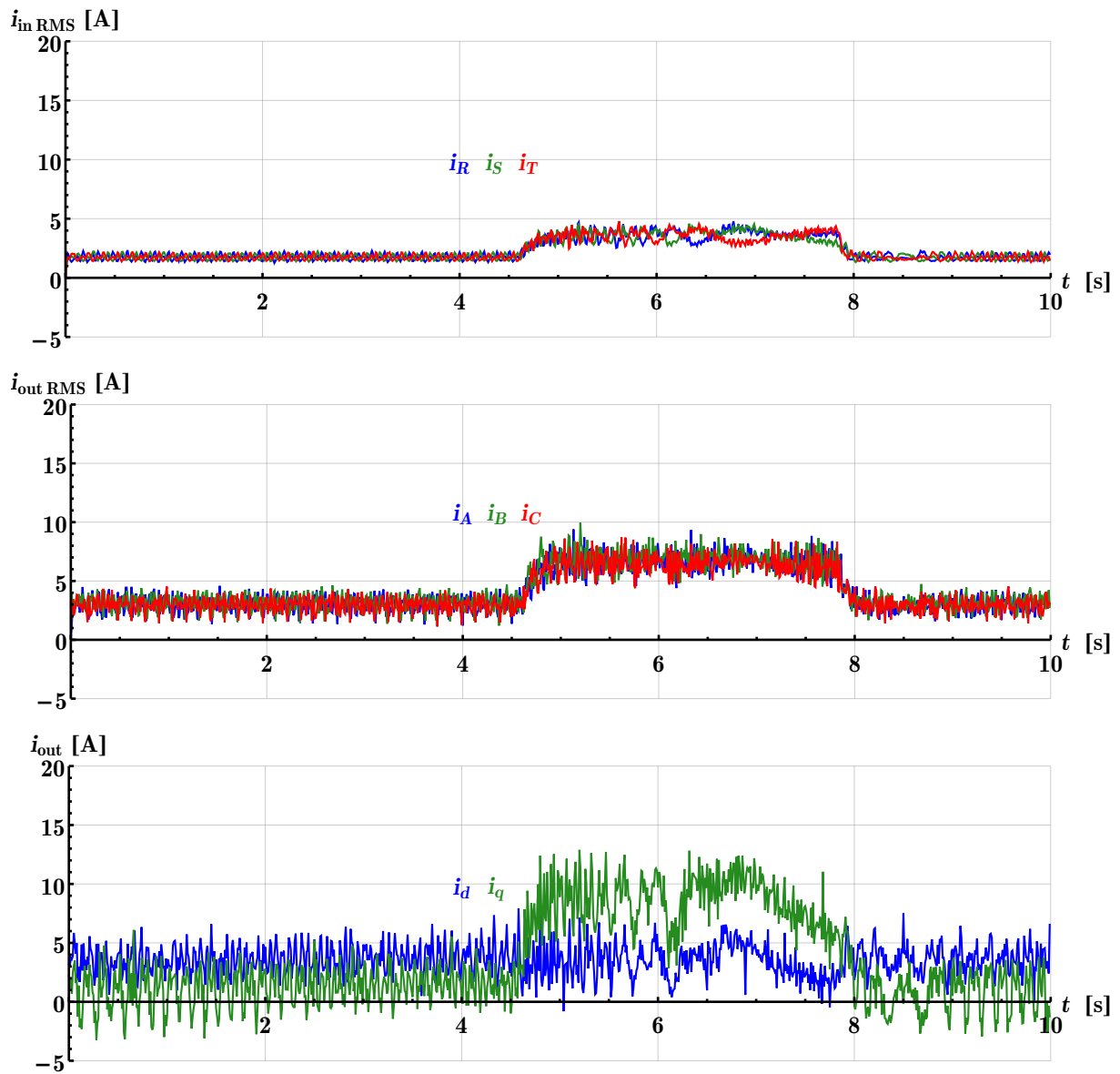


Figure 7.14. DRFOC control - reaction to load step

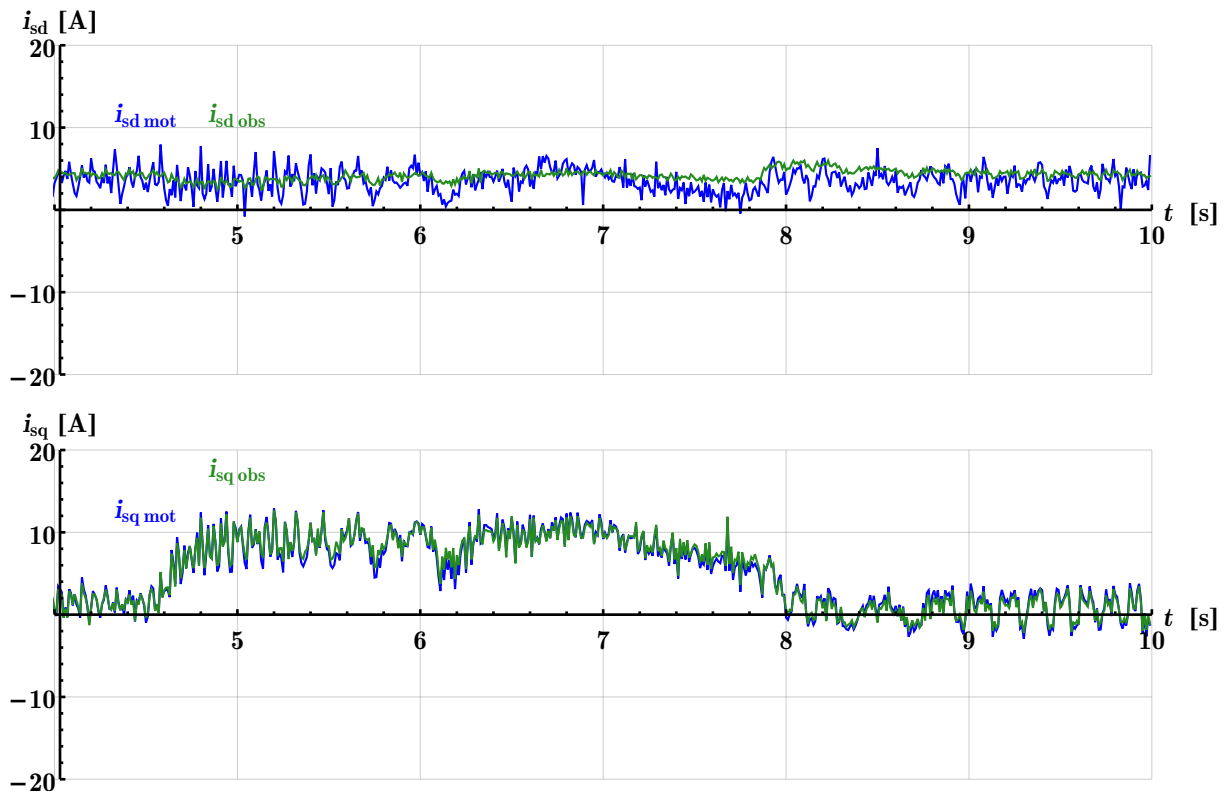


Figure 7.15. DRFOC control - current component controllers reaction

In the Fig. 7.16 is shown trajectory of the rotor flux space vector movement.

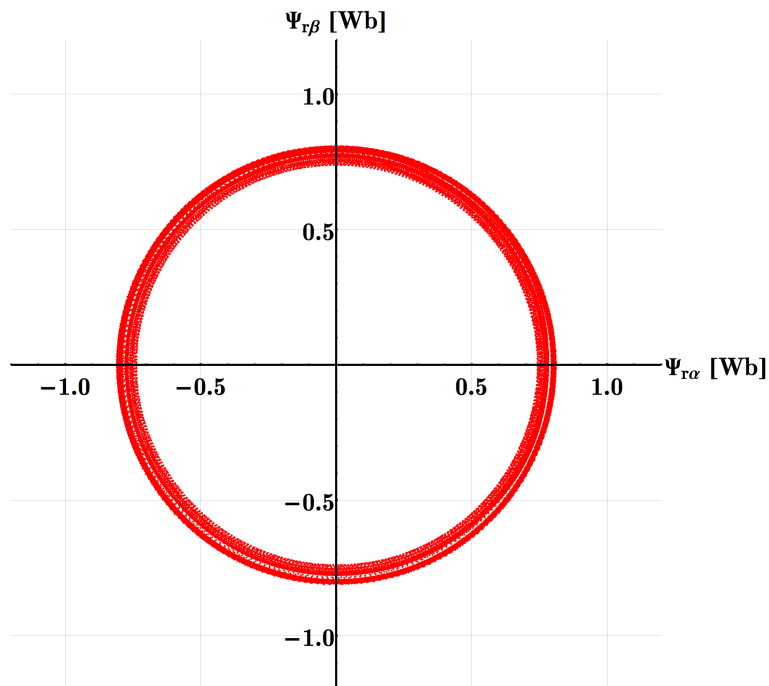


Figure 7.16. DRFOC control -  $\Psi_r$  trajectory

## 7.4 Current PWM Control Simulation

The current PWM control according to Fig. 5.8 was second candidate to be implemented. Principle of the strategy was described in chapter 5. Figure 7.17 shows reactions of the flux and speed controllers changes of reference values. Reactions of the flux controller are depicted in the Fig. 7.17. It is obvious, that actual value of the IM flux (green) tracks required value (blue) very well. Small errors during speed and load torque transitions are partly caused by settling time of the observer and partly by behaviour of current P-controllers. Speed controller reactions show, that required speed of the drive is satisfactorily held. Minimization of the overshoot can be done by better tuning of the controller parameters for specific drive, that is not necessary in the simulation.

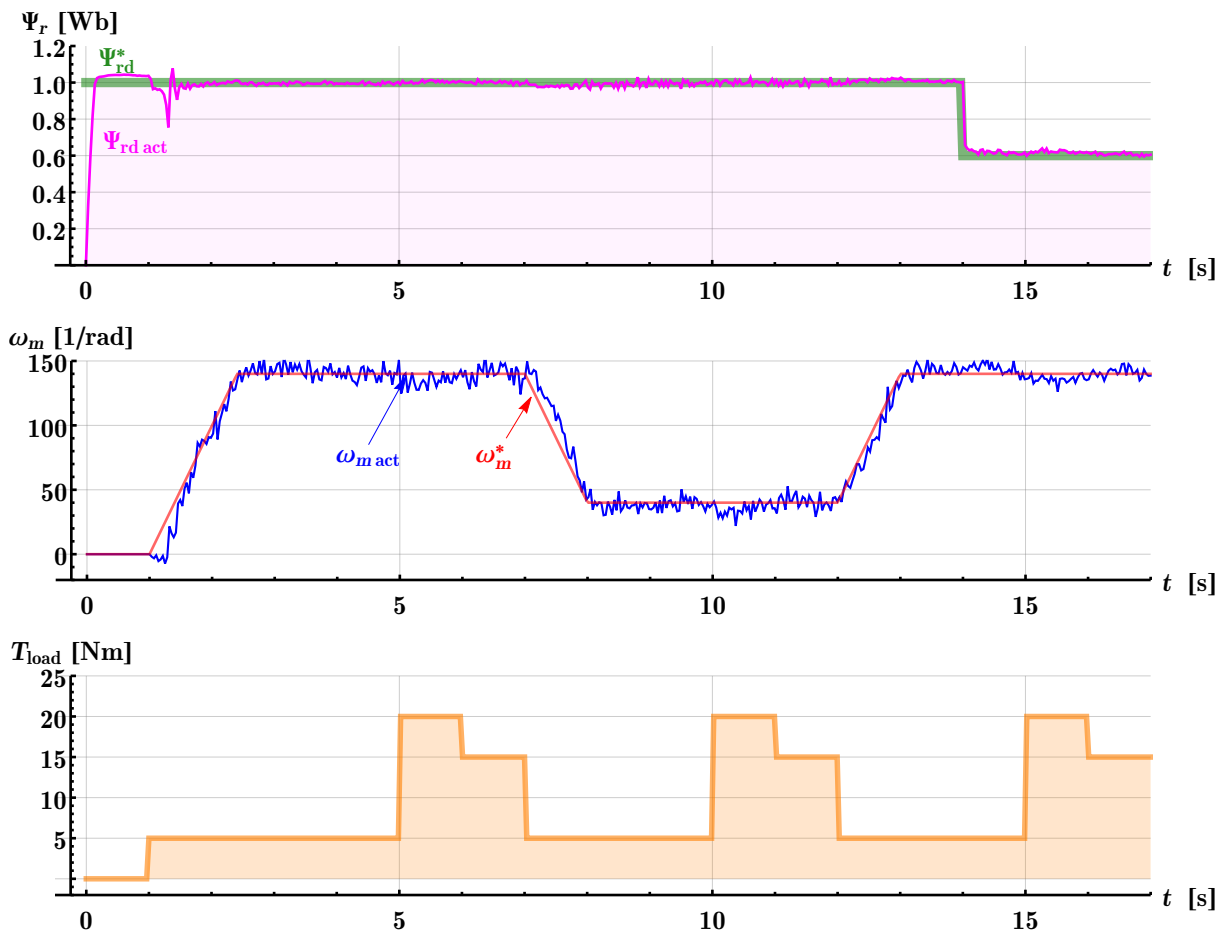


Figure 7.17. Current PWM control - flux and speed controller simulation

Fig. 7.18 shows behaviour of the particular current controllers. As was mentioned in chapter 4, because the input signals are AC quantities only proportional controllers fit this application. Fig. 7.19 shows estimated flux of IM in polar coordinates. It is obvious, that flux is controlled to have circular path. Also the process of field weakening can be clearly seen.

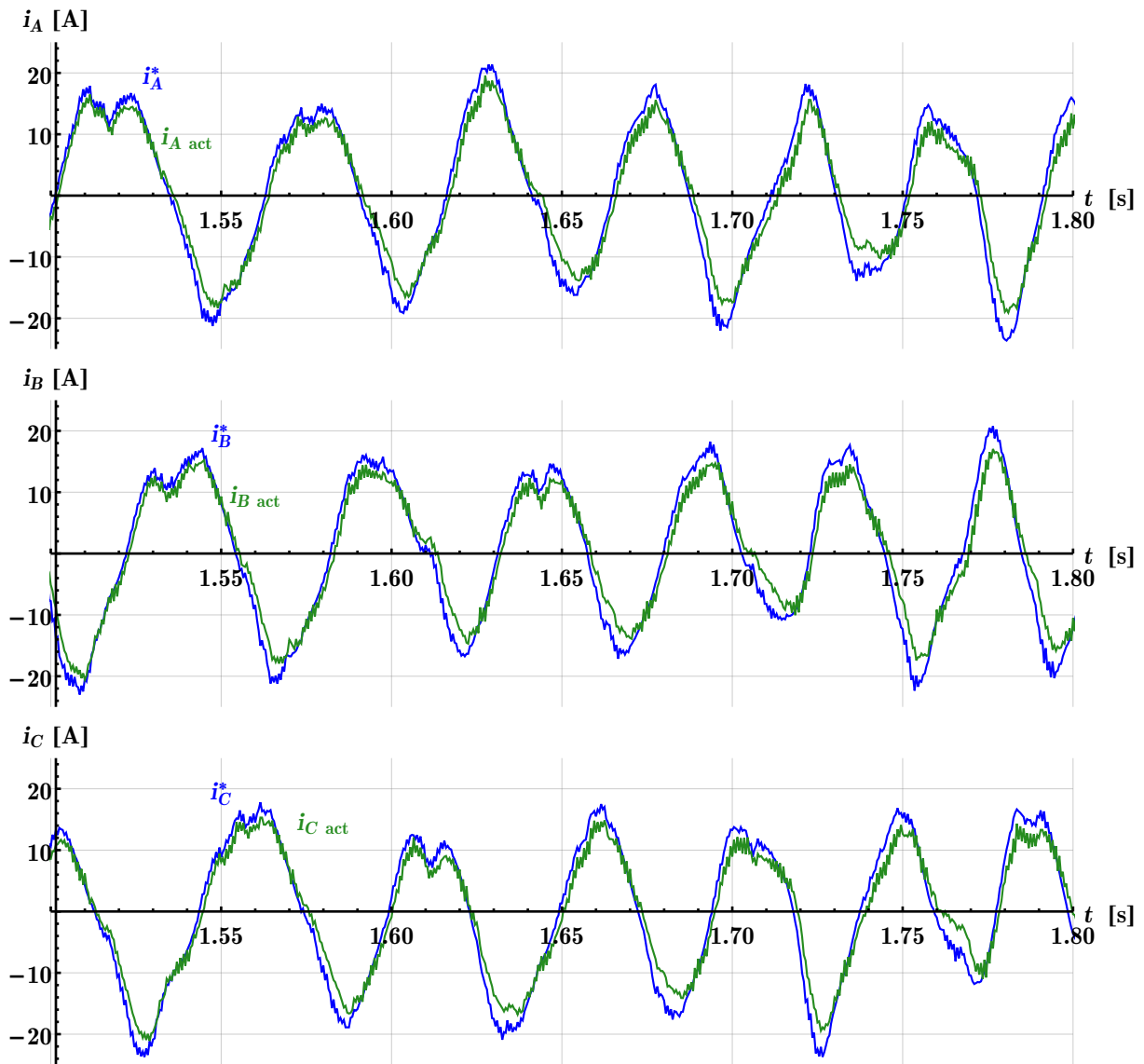
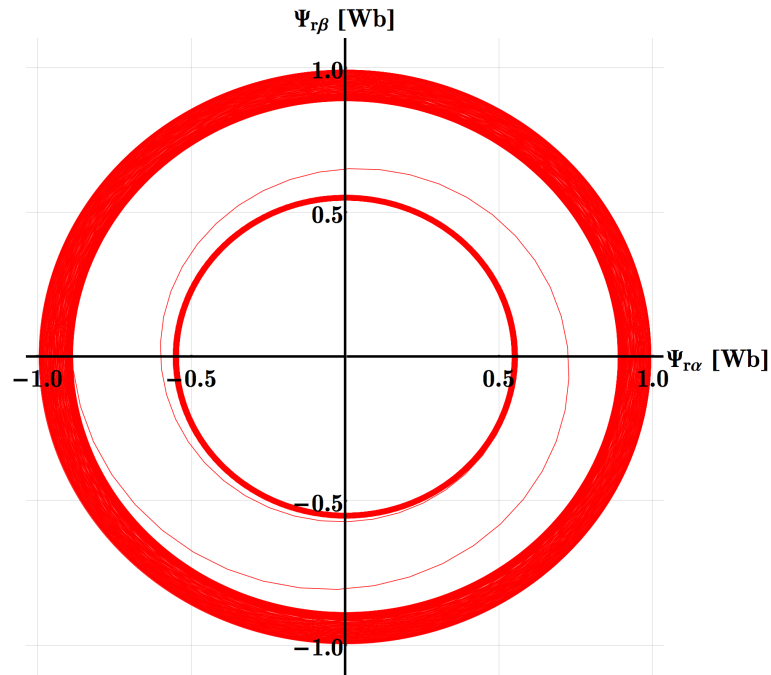


Figure 7.18. Current PWM control - current controllers reaction



**Figure 7.19.** Current PWM control -  $\Psi_r$  trajectory

## 7.5 Current PWM Control Realization

Fig. 7.20 shows behaviour of the particular current controllers during the measurement on the real converter. Compared to 7.18 currents are more rippled. This is caused by lower switching frequency of the real converter and also by inaccuracy of the current sensors. Fig. 7.22 show trajectory of the rotor flux  $\Psi_r$  during current PWM control. Although the currents are more rippled the flux is held on circular path. Fig. 7.21 shows behaviour of the IM drive during acceleration and deceleration. It is obvious that both controllers track their reference values with good accuracy.

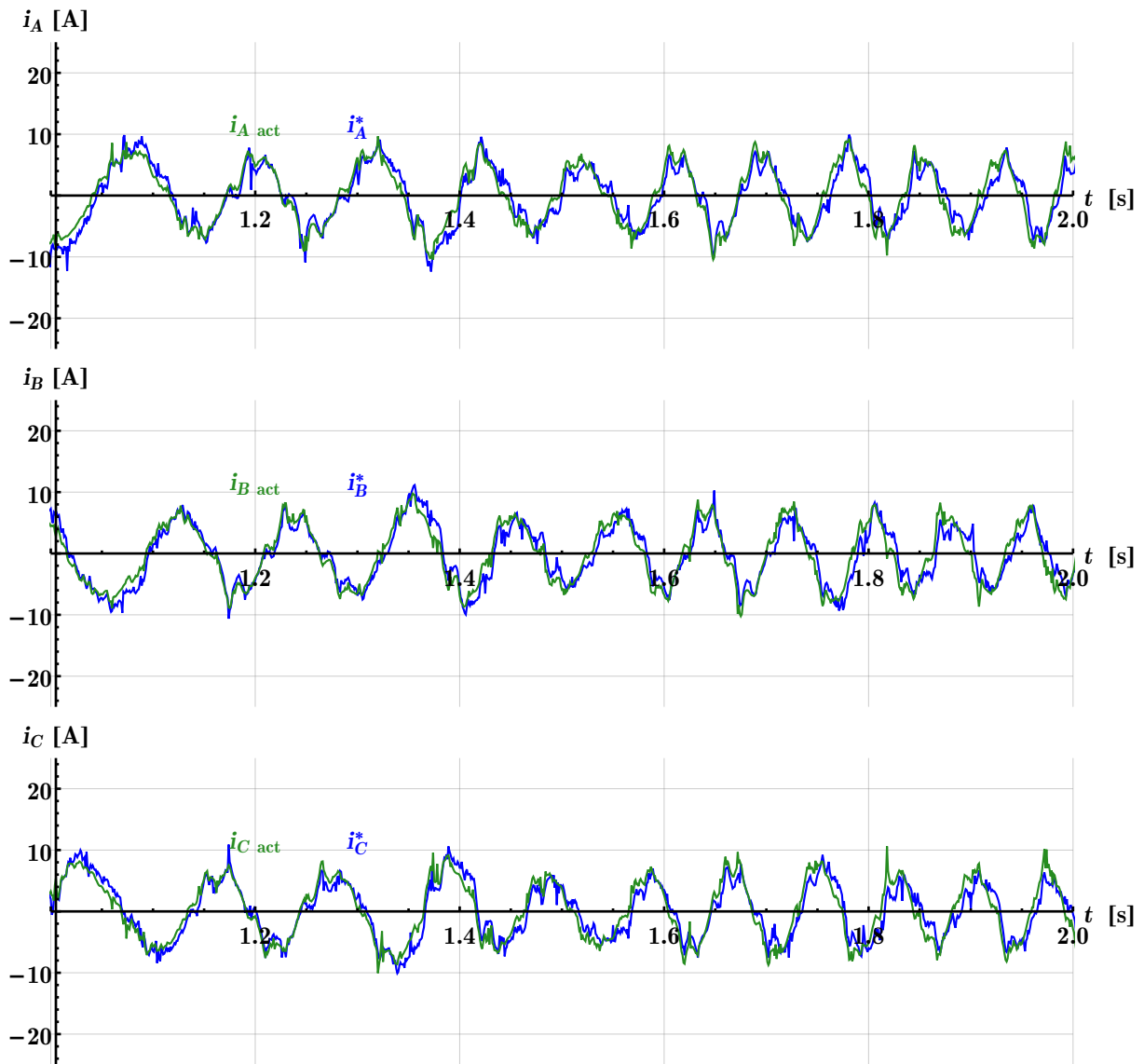


Figure 7.20. Current PWM control - current controllers reaction

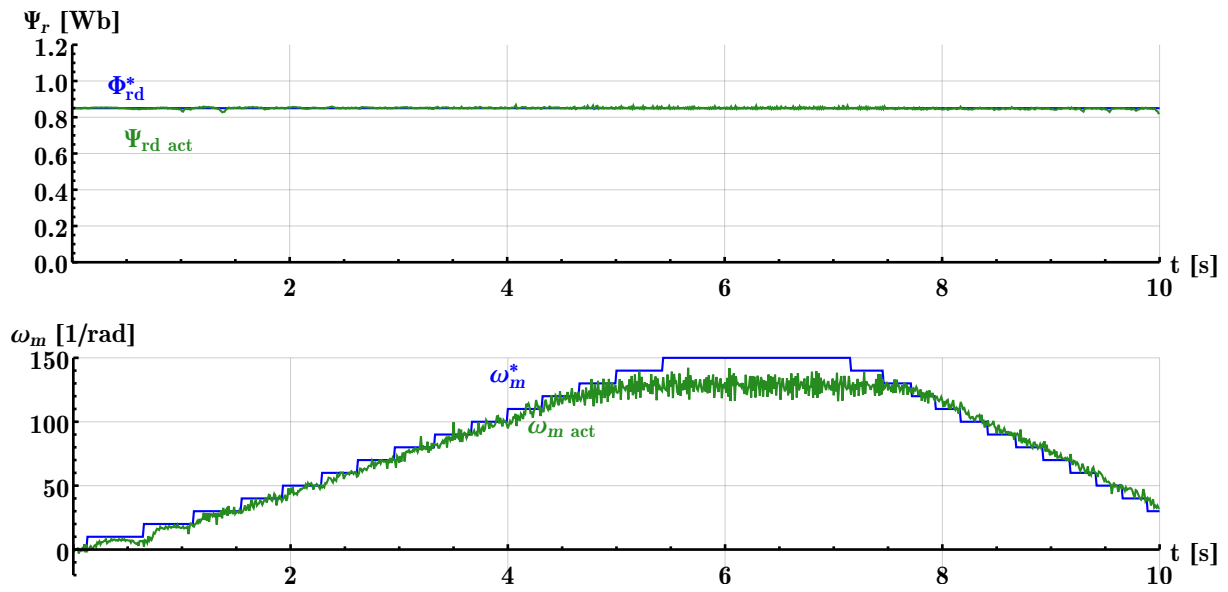


Figure 7.21. Current PWM control - flux and speed controller reaction

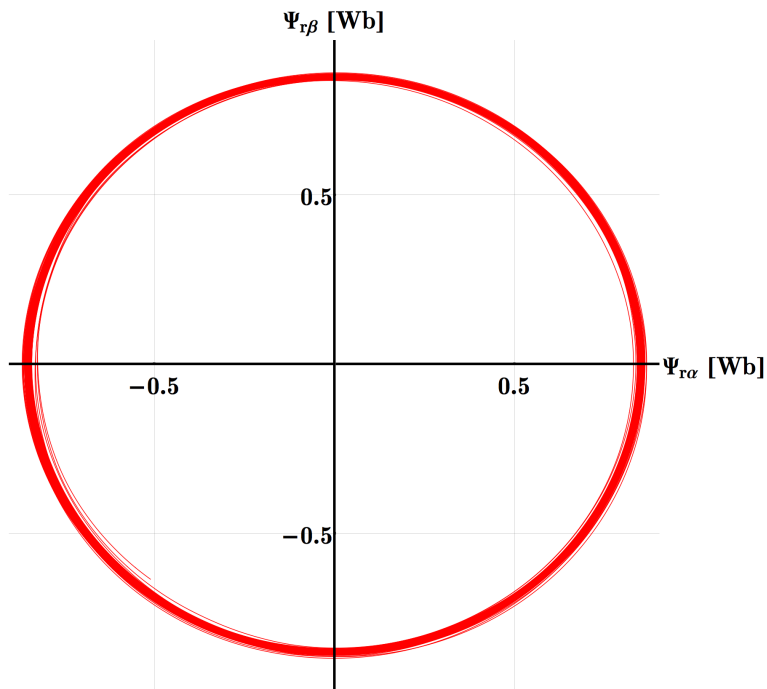


Figure 7.22. Current PWM control -  $\Psi_r$  trajectory



## Chapter 8

# Application of Matrix Converter with Induction Generator

The generation of electrical energy from "green" sources is very popular topic in past decade. Among these sources can be ranked also wind and water energy. These power sources are available also in remote areas, where can be used to drive prime movers for small electric power plants. In the conventional big power plants are usually used synchronous generators. In small power plants driven by renewable energy sources like small hydroplants or wind turbines are increasingly used induction generators. The advantageous features of the IM generator application are low cost, high reliability, ruggedness and low maintenance. Drawbacks as poor voltage regulation have been overcome by development of the static power converters, that enable control go the IM generator output voltage. However, the induction generator needs an external power source to provide its excitation. This is difficult in remote areas where there is no electrical power supply network.

Using of a Self Excited Induction Generator (SEIG), where the three phase capacitor bank is connected to the IM terminals to provide reactive power for the load and generator, can solve the problem with excitation. When SEIG is driven by external source of mechanical power, residual magnetism in the rotor causes that voltage is induced into stator winding. The current starts to flow between the capacitor bank and stator winding and thus the flux in stator is established. The active power required by the load is supplied by the IM generator. The change in the load impedance directly influence excitation of the SEIG, because the reactive power is shared between the load and generator. From this point of view the performance of the SEIG depends on [130]:

- Parameters of induction machine - parameters like rated power, power factor, temperature affects performance of generator.
- Self excitation process - Connection of the capacitors controlled or uncontrolled. influences process of generator self excitation
- Type of load, starting/maximum current affects the excitation process.
- Type of the prime mover.

The main problem of the SEIG system is its poor voltage and frequency regulation under varying load conditions. A change of the load directly influences the machine excitation. It is caused by sharing of the reactive power of the excitation capacitors between the SEIG and the load. Therefore, the voltage on the terminals of the generator drops when the load impedance is increased resulting in poor voltage regulation. On the other hand, the slip of the induction generator increases with increasing load, resulting in a load dependent frequency, even if the speed of the prime mover remains constant. To overcome this problems a power converter has to be connected to the SEIG output.

A sliding mode strategy that aims to control voltage and frequency of a SEIG system was presented in [131]. Regulation of voltage an frequency of the SEIG under varying load conditions was examined in [132]. The controller is based on rectifier circuit and chopped load, that holds SEIG under defined load conditions by varying of the amount

of additional load added by the means of PWM switching. In [133] is presented a method of voltage and frequency regulation of an induction generator working in off grid mode. A PWM converter was used to eliminate the need of a transistor switch placed in the DC side of the converter. This reduces cost and high frequency current components.

In most cases, the control of the voltage across the IM terminals is generally performed by controlling of reactive power source and frequency regulation is achieved by regulating the speed of the prime mover by utilising a mechanical speed governor. However, the regulation of speed and voltage does not result in a satisfactory level of performance due to the high dynamic of the changes of slip of the machine and the difficulties in building a smooth variable reactive power source at low costs.

The structure of the SEIG system is depicted in Fig. 8.1. The system consists of 3 main parts: generator, load, and capacitor bank that supplies reactive power to the generator and to the load.

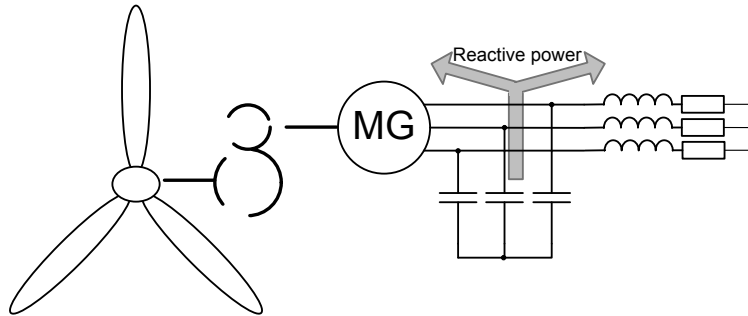


**Figure 8.1.** Self excited induction generator schematics

The value of the capacitor required for self excitation of the generator can be calculated for the given speed as intersection of the capacitive reactance line with magnetising curve (Fig. 8.2). At this point is all reactive power for the generator supplied by the capacitors. For the SEIG is variation of magnetising inductance main factor for voltage build and its stability. From the Fig. 8.2 can be seen that  $L_m$  starts from smaller values, than reaches its peak and finally decrease in saturation. During the self excitation the voltage increases as  $L_m$  do. Beyond the peak  $L_m$  starts to decrease while the voltage rises until it reaches its steady state value. In the interval from the beginning the  $L_m$  maximum (area A) the SEIG operates in unstable region e.g. small decrease of the speed will cause decrease of the  $L_m$  that will lead to decrease of voltage until it falls to zero. In the area marked as B in Fig. 8.2 the SEIG operates in stable region. The decrease of the speed is connected with decrease of the voltage and increase of the  $L_m$  so the SEIG remains in new steady state with lower output voltage.

From the plate data can be required capacitance per phase of  $\Delta$  connected capacitors for IM roughly calculated as:

$$S = \sqrt{3}U_N I_N = 1.73 \cdot 380 \cdot 11.8 = 7757.3 \text{ VA} \quad (8.1)$$

$$P = S \cos \varphi = 7757.3 \cdot 0.8 = 6205 \text{ W} \quad (8.2)$$

$$Q = \sqrt{S^2 - P^2} = 4648 \text{ VAR} \quad (8.3)$$

$$X_C = U_N^2 / (Q/3) = 380^2 \cdot 3 / 4648 = 93.06 \Omega; C_{\text{exc}} = 34.1 \mu\text{F} \quad (8.4)$$

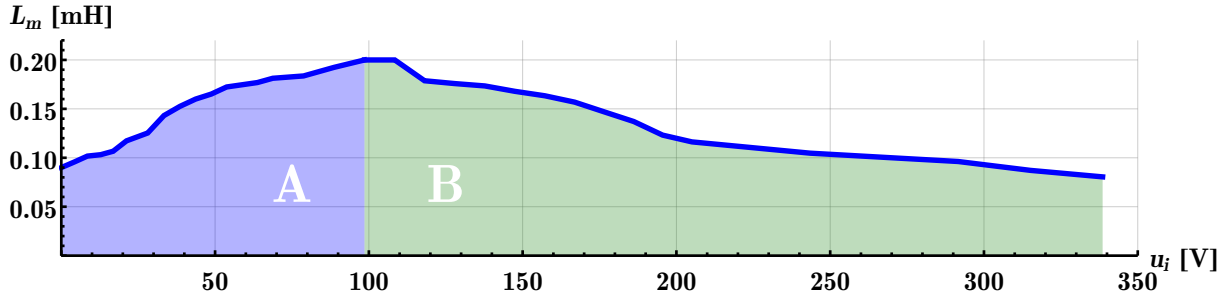


**Figure 8.2.** Variation of magnetising inductance  $L_m$  with phase voltage

In order to analyse the excitation process and behaviour of the generator is often used description based on SEIG equivalent circuit depicted in Fig. 8.3. Under assumption of no load conditions, this circuit can be described by equation (4.13) that have to be extended to respect connected capacitor [134]. In [134] is also performed analytical derivation of minimal value of excitation capacitor controlled by the VSI.

$$\frac{d}{dt}u_C = \mathbf{A}_C u_C(t) + \mathbf{B}_C i_C(t) \quad (8.5)$$

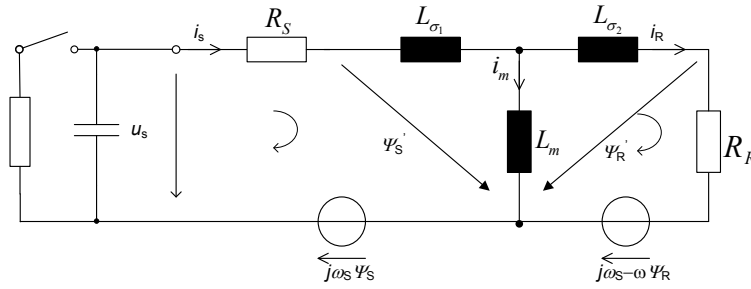


**Figure 8.3.** Equivalent circuit of the SEIG

As was stated above the generator requires source of reactive power, that have to be designed for given load. Any change of the operation conditions of the generator will be connected with the change of the generated output voltage parameters. To avoid changes of the output frequency of the generated voltage the generator is either equipped with gearbox or is used for feeding rectifier and DC load [135]. Moreover the change of the speed will be followed by new operation point and thus change of the generator output voltage. In this place seems to be interesting to analyse possible application of the matrix converter with the SEIG.

Among the mentioned features of the MC in chapter 2 was that it is able to recuperate energy, operate with any input and output frequency and it offers possibility to control power factor too. Implemented ISVM control strategy splits converter into virtual rectifier part (input of the matrix converter) and virtual inverter part (output of the matrix converter), that can be controlled independently. This offers possibility to reverse power flow through the converter and connect the generator to its output (see Fig. 8.4). The output of the converter is therefore controlled to produce reactive power required for the generator and at the input side are switched transistors like sinusoidal



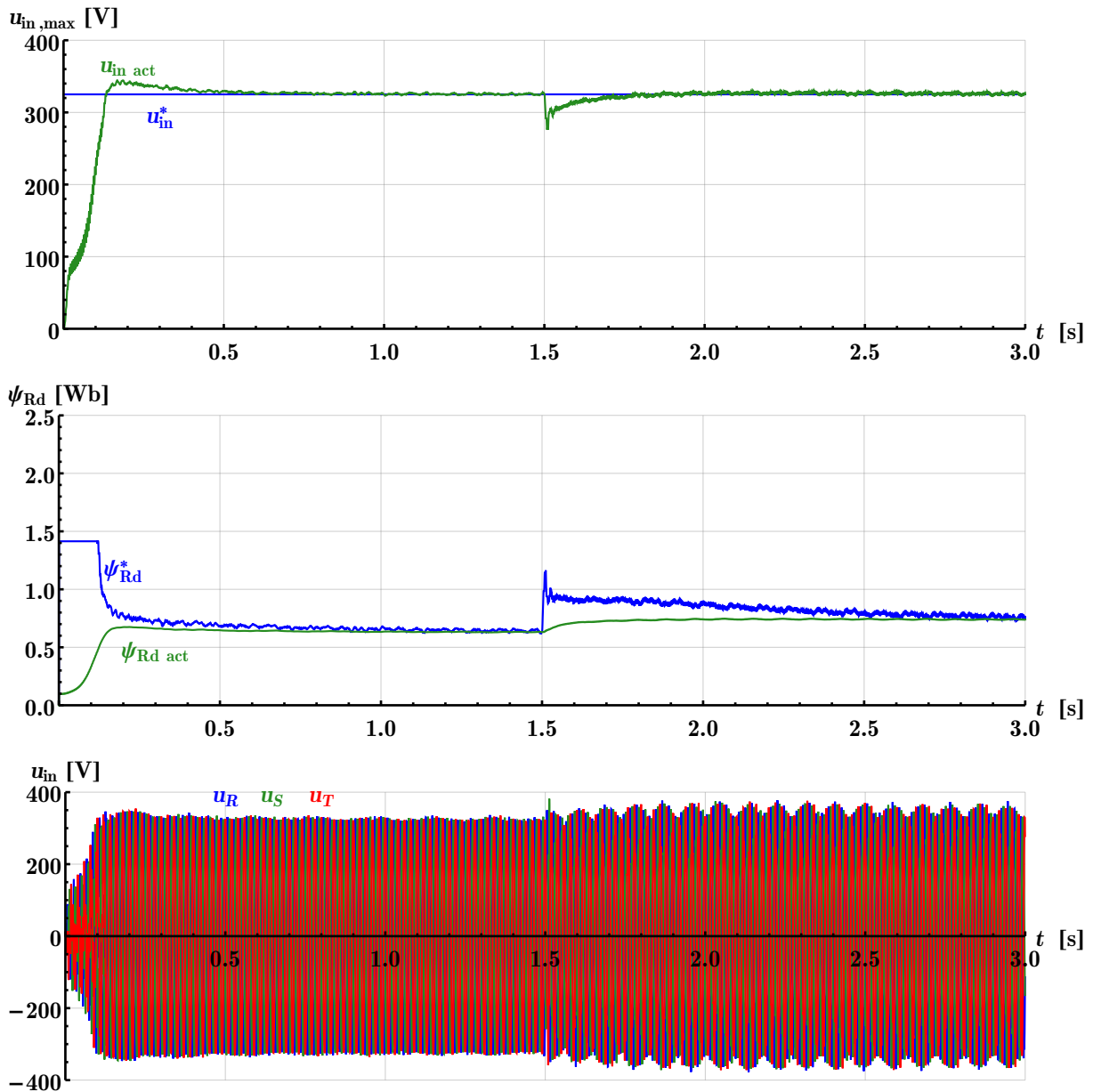


**Figure 8.5.** Controllers reaction during SEIG operation  $C_f = 9 \mu\text{F}$ ,  $\omega_m = 160 \text{ rad}^{-1}$

In the Fig. 8.5 are shown simulation results of the flux and voltage controllers. The bottom waveforms correspond to generated voltage on the matrix converter terminals. In this case the process of excitation takes approximately 0.2 s. Increased load is compensated by increase of IM flux.

Figure 8.6 show induction machine rotor flux  $\Psi_r$  and electrical torque produced by the generator. The rotor of the IM was driven by the source of constant speed  $\omega_m = 160 \text{ rad}^{-1}$

Figures 8.7 and 8.8 show voltages and currents on the output and input terminals of the matrix converter. Fig. 8.7 shows the full waveforms to get an view about the shape of the waveforms and Fig. 8.8 show selected details of excitation process, load step and after stabilisation of the controllers. From the details of the currents  $i_{A,B,C}$  consumed

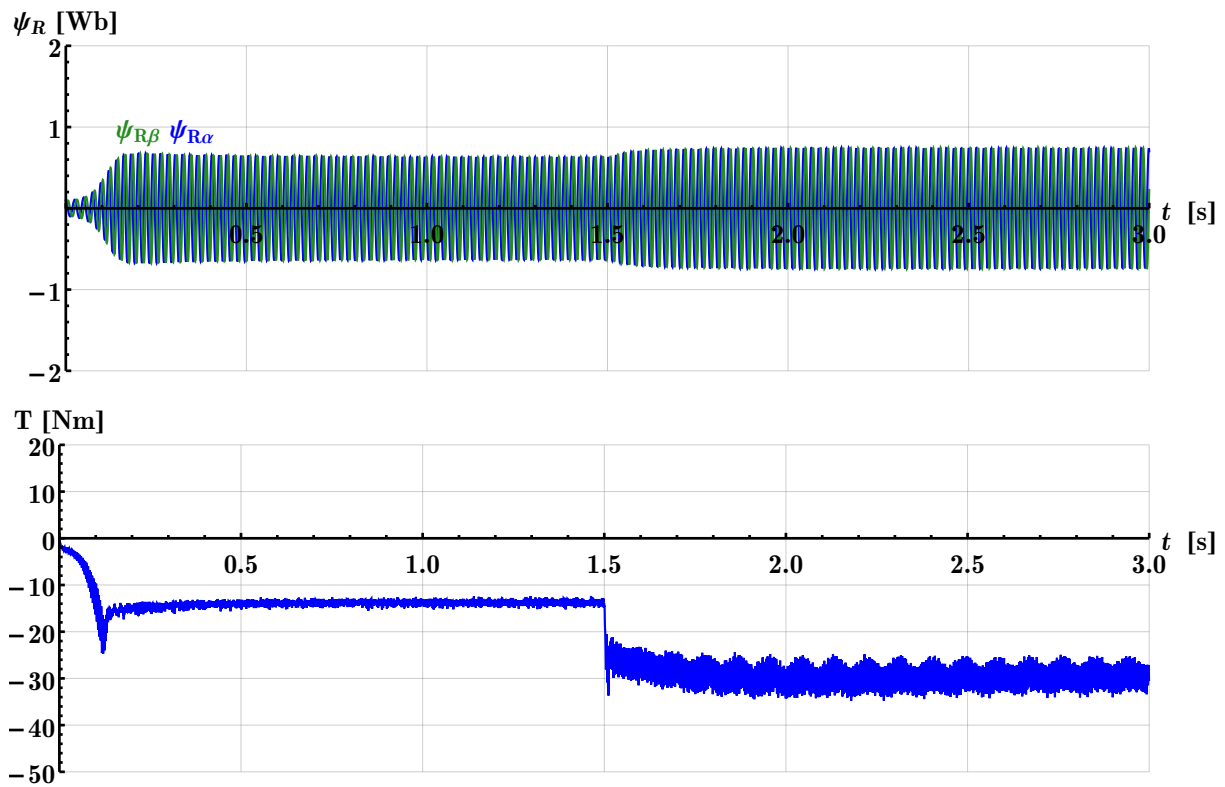


**Figure 8.6.** Generator behaviour simulation  $C_f = 9 \mu\text{F}$ ,  $\omega_m = 160 \text{ rad}^{-1}$

by the output of the converter in Fig. 8.8 is obvious that after the increase of the load is the induction generator already working on its maximum, because the shape of the currents is very close to square wave. Fig. 8.9 and 8.10 show behaviour of the generator with decreased filter capacity. From the figures is obvious, that the generated voltage is more rippled, but the system is still functional.

When we look at all details of the generated voltages and currents in Fig. 8.8, 8.10, 8.12 it can be seen that currents are opposite to voltages, that means matrix converter takes energy from the machine connected on its output and feeds load connected to its input terminals. The frequency on the input of the converter does not depend on the speed of the SEIG prime mover, therefore expensive gearbox can be omitted. Moreover the matrix converter is able to excite the IM with much smaller capacitor connected to its terminals than requires SEIG system with phase connected capacitors.

In the Fig. 8.11 and 8.12 are depicted behaviours of the SEIG with driving speed  $\omega_m = 100 \text{ rad}^{-1}$ , that means matrix converter is producing on its input higher frequency than on its output. From the figures is obvious that process of self excitation takes more time and the shape of waveforms generated on the input of the converter is more distorted and the transient states take longer times. It can be also seen that although the frequency of the generated voltage is required 50 Hz, the converter is not able to produce required voltage at this speed.

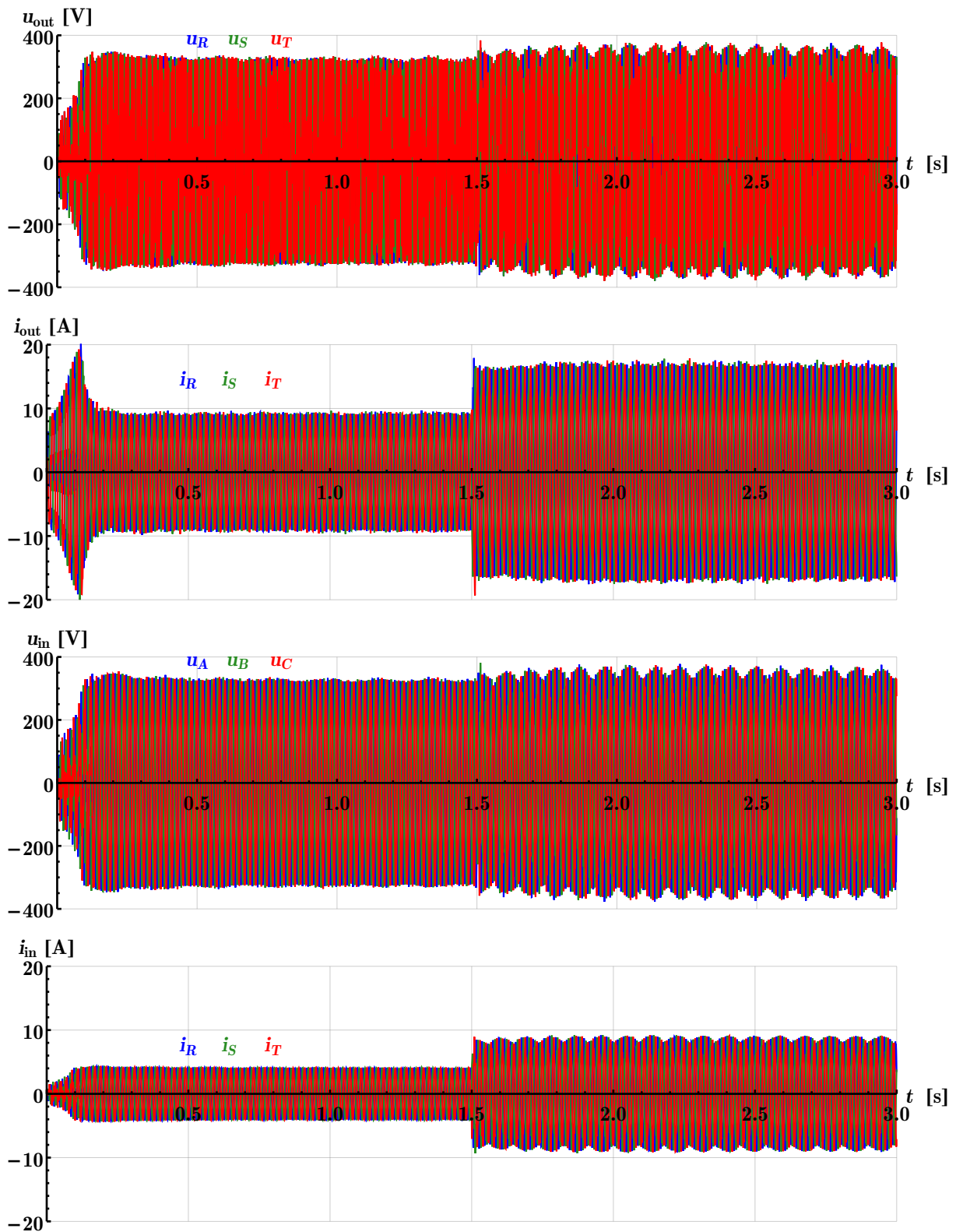


**Figure 8.7.** Matrix converter output and input voltage and current waveforms  $C_f = 9 \mu\text{F}$ ,  $\omega_m = 160 \text{ rad}^{-1}$

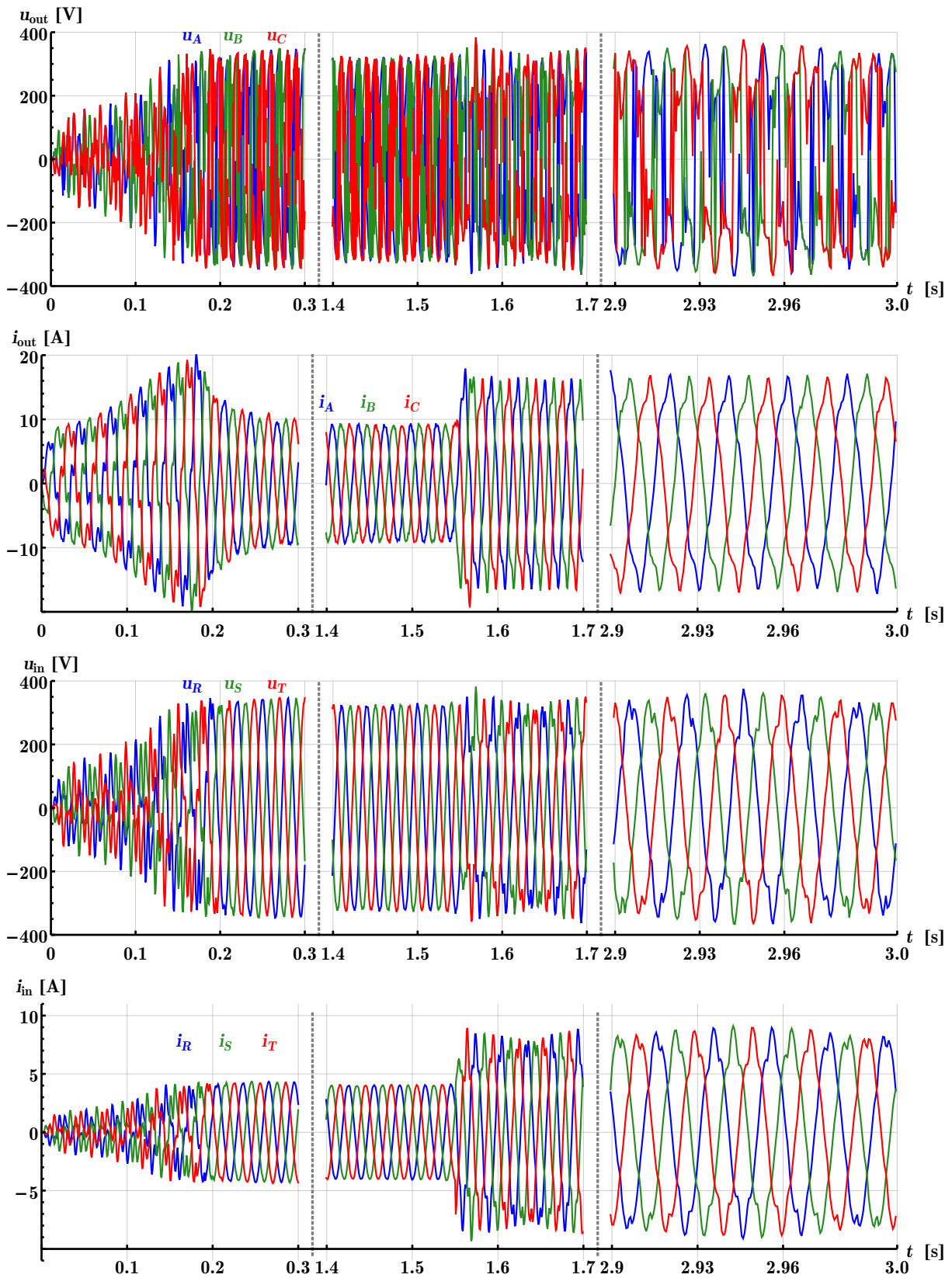


**Figure 8.8.** Matrix converter output and input voltage and current waveforms details  
 $C_f = 9 \mu\text{F}$ ,  $\omega_m = 160 \text{ rad}^{-1}$

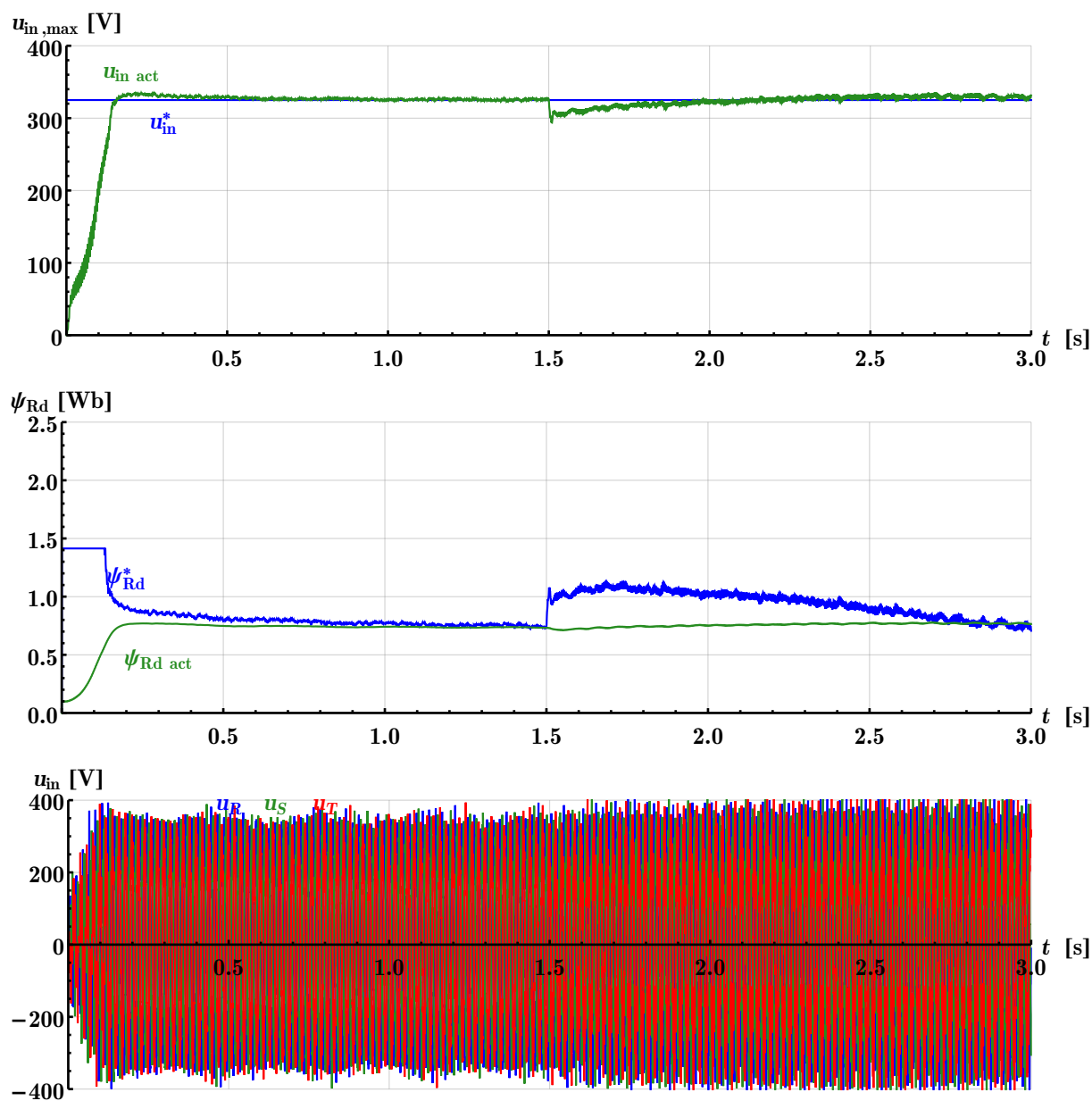


**Figure 8.9.** Controllers reaction during SEIG operation  $C_f = 1 \mu\text{F}$ ,  $\omega_m = 160 \text{ rad}^{-1}$

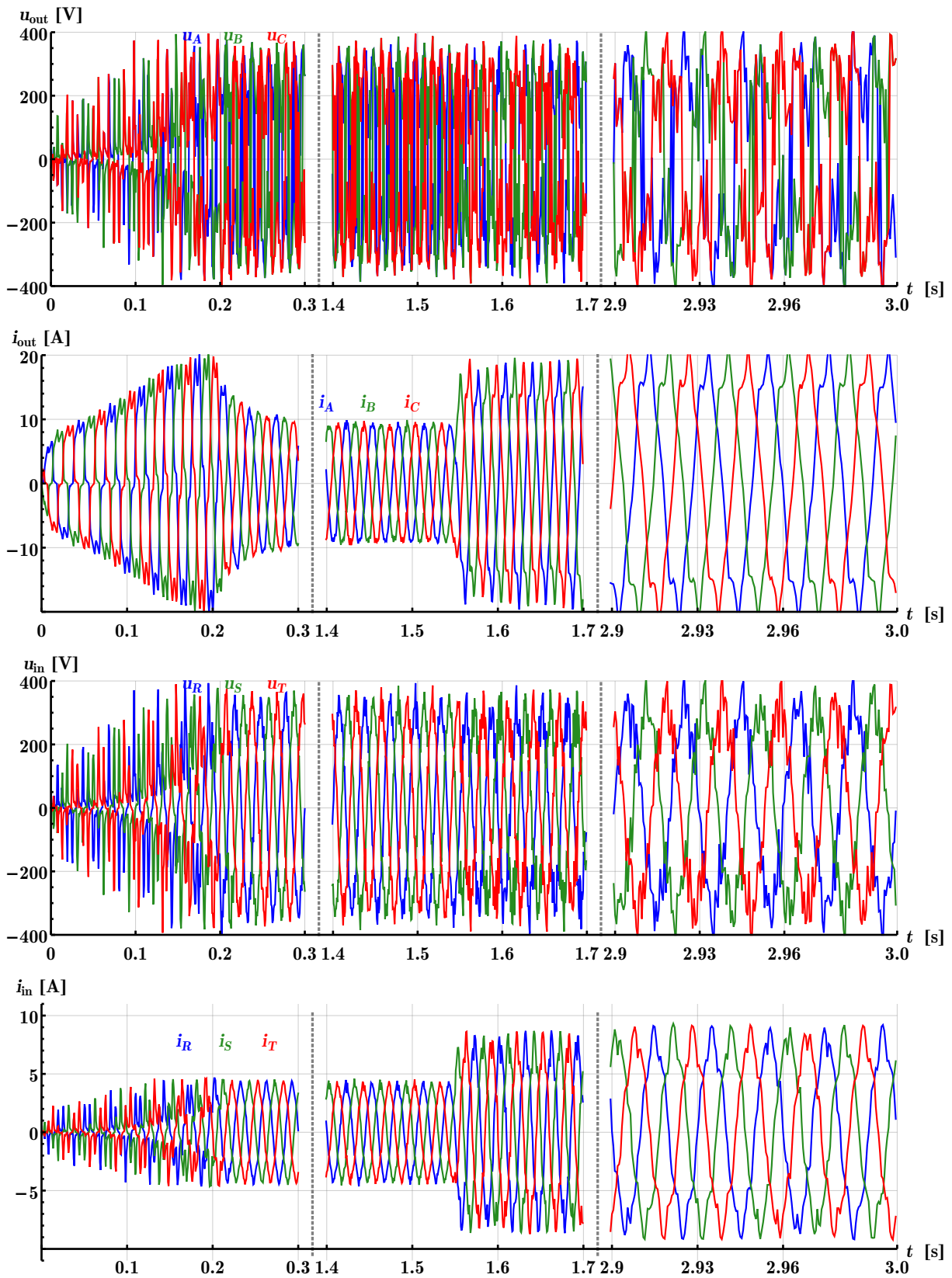


**Figure 8.10.** Matrix converter output and input voltage and current waveforms details  
 $C_f = 1 \mu\text{F}$ ,  $\omega_m = 160 \text{ rad}^{-1}$

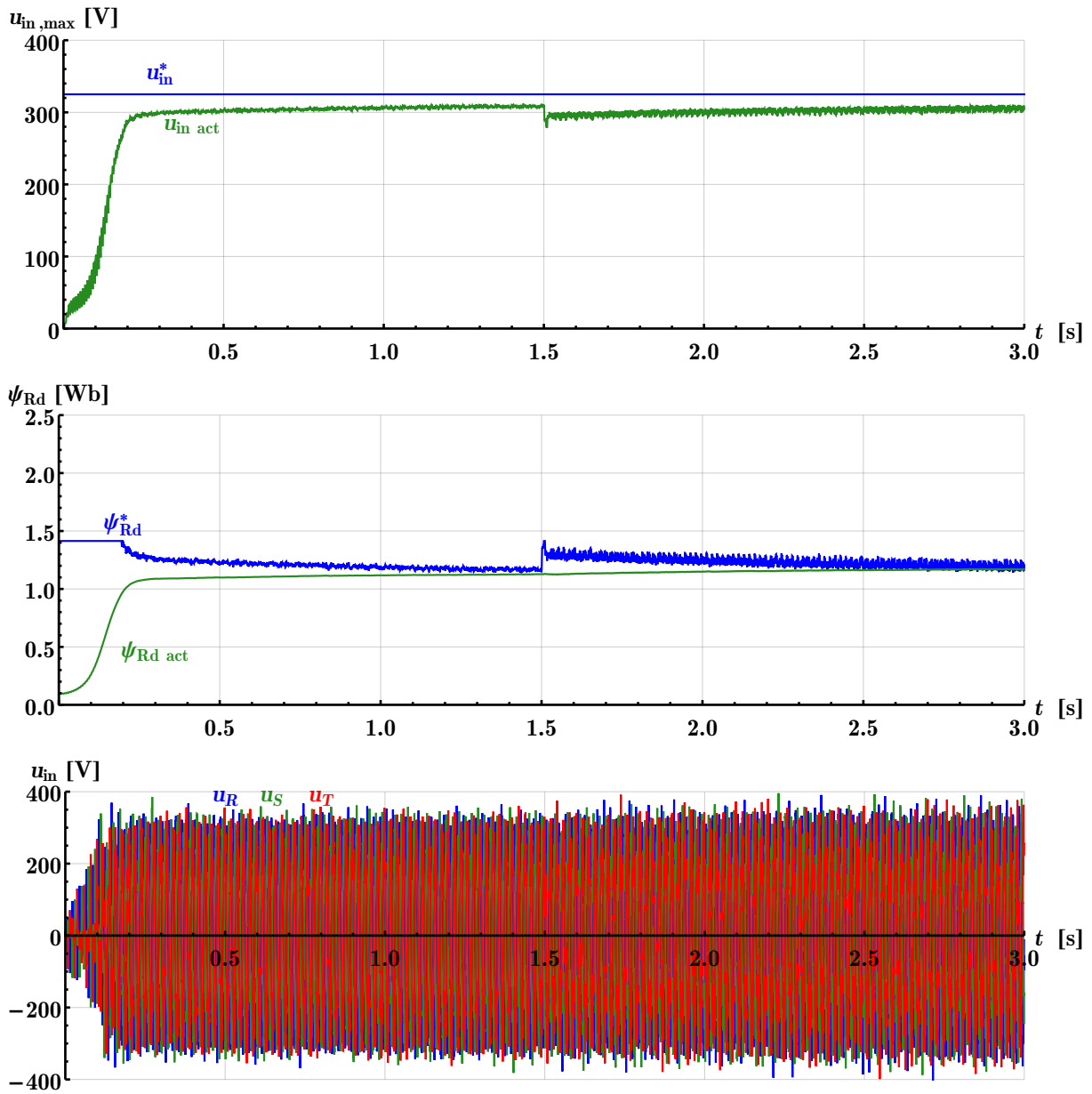
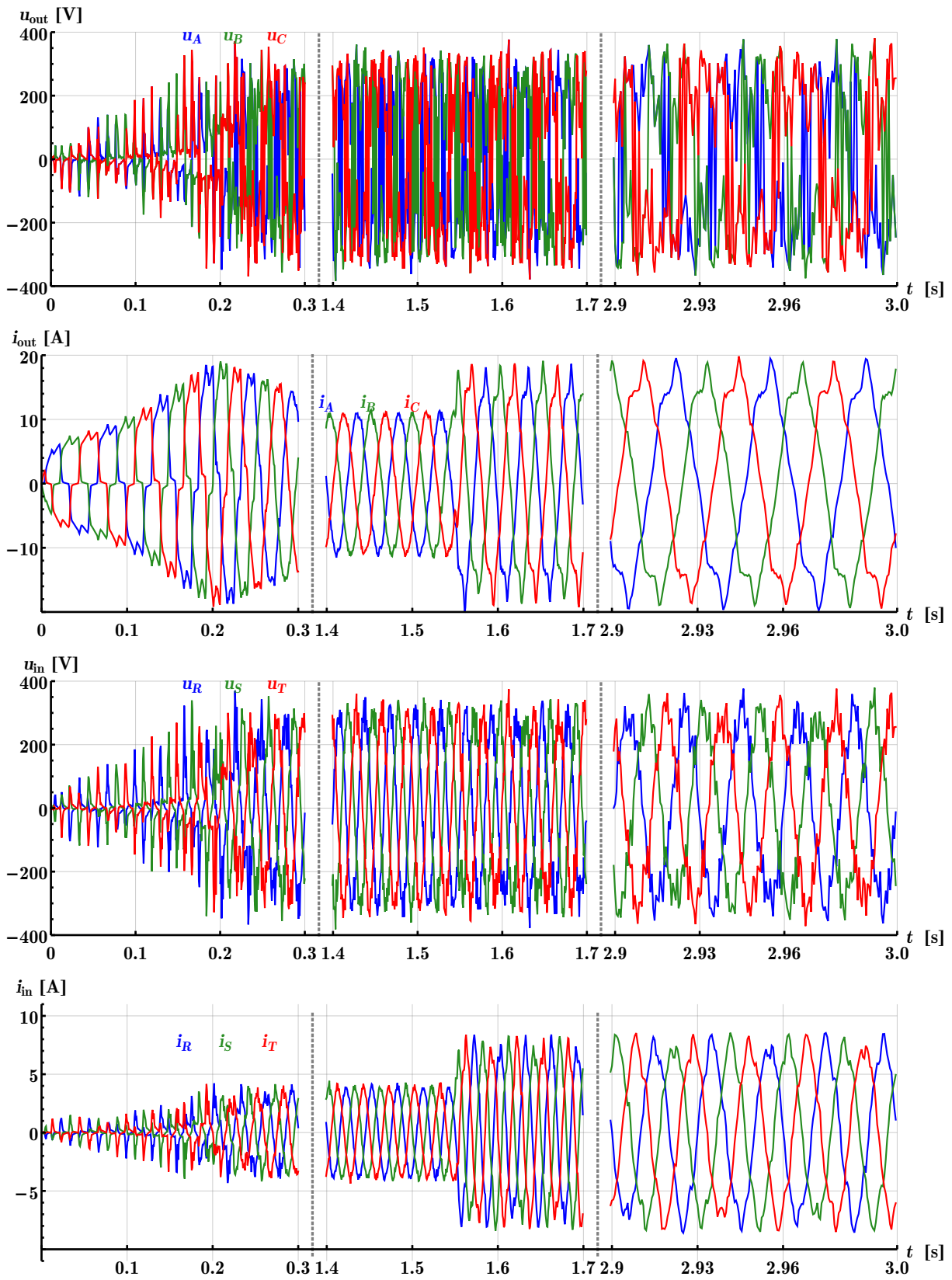


Figure 8.11. Controllers reaction during SEIG operation  $C_f = 9 \mu\text{F}$ ,  $\omega_m = 100 \text{ rad}^{-1}$



**Figure 8.12.** Matrix converter output and input voltage and current waveforms details  
 $C_f = 9 \mu\text{F}$ ,  $\omega_m = 100 \text{ rad}^{-1}$

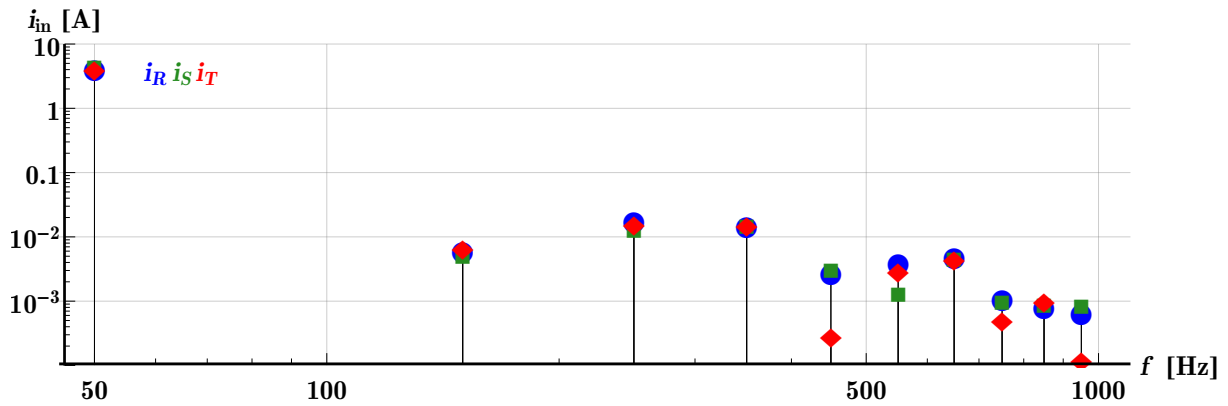


Figure 8.13. Harmonics analysis of generated current  $C_f = 9 \mu\text{F}$ ,  $\omega_m = 100 \text{ rad}^{-1}$

Harmonics analysis of the currents generated on the input of the matrix converter were performed. In Fig. 8.13 is harmonics analysis for the generator operating at speed  $\omega_m = 160 \text{ rad}^{-1}$ , with nominal input filter capacity. From the analysis is obvious that only 1<sup>st</sup> harmonics is present and has frequency of 50 Hz. Fig. 8.14 shows analysis when the generator was operating at speed  $\omega_m = 100 \text{ rad}^{-1}$ . The harmonics content is nearly same and produced frequency is 50 Hz too. In Fig. 8.15 is analysis for matrix converter with reduced input filter capacity  $C_f = 1 \mu\text{F}$ . From the analysis is obvious that harmonics content is worse than for the designed filter, that means although in both cases the IM is excited the harmonics content of the produced current is influenced by the type and parameters of the input filter.

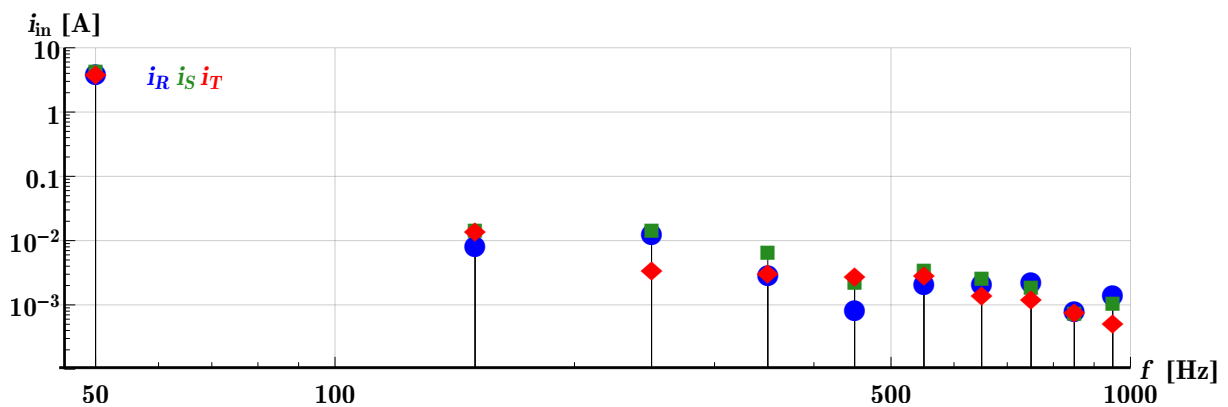


Figure 8.14. Harmonics analysis of generated current  $C_f = 9 \mu\text{F}$ ,  $\omega_m = 100 \text{ rad}^{-1}$

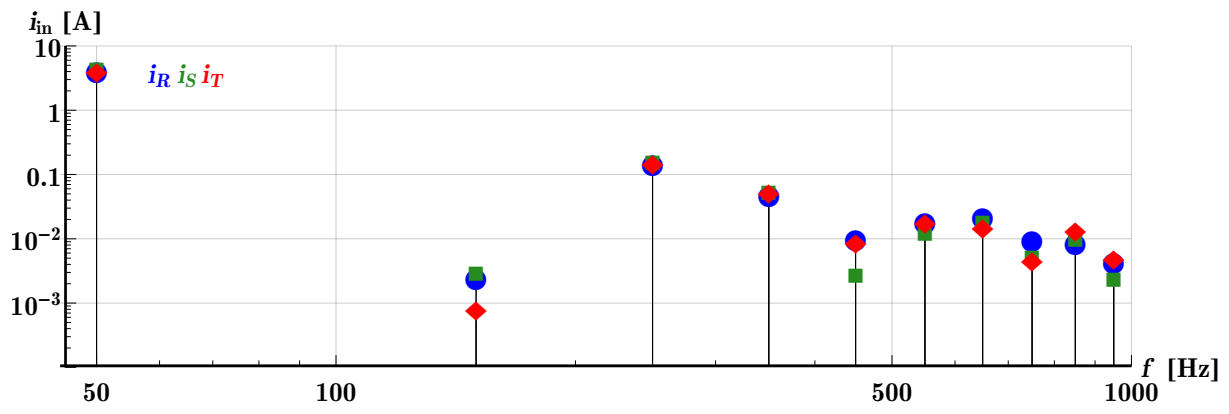


Figure 8.15. Harmonics analysis of generated current  $C_f = 1 \mu\text{F}$ ,  $\omega_m = 160 \text{ rad}^{-1}$

# Chapter 9

## Conclusion

The main goal of this thesis was to design, build and finally test the assembled sample of the matrix converter, including bringing it into operation. The damping of filter oscillations is discussed in detail in this work also. Selected control strategies have been instrumented to the direct converter and implemented. First, the functionality was tested under a simple scalar approach (Voltage/Hertz), later current PWM and then at last the rotor flux oriented vector control was employed. Since the absence of the speed sensor, the extended Luenberger observer was used to estimate both speed and rotor flux required for the controller.

The power part and the control unit have been designed with respect to extensibility and sustainability in order to enable further improvements of commutation, modulation, control or diagnostic part in future works later on in the years.

### 9.1 Overview of the results

Chapter 2 provides an overview through various topologies of direct converters. Among others, the behavior and limitations of the matrix converter, as allowable switching states even including the problems appearing during commutation (current take-over from one IGBT to another) and known commutation strategies are mentioned, although this thesis does not focus directly to these topics. But each commutation strategy sets different requirements on the control part and measurement interface, therefore commutation strategy (or a group of them to be supported) had to be selected at the beginning of the design. Finally, at the end of this chapter there are also described all important blocks of power part of the classical 3x3 matrix converter as bi-directional switches, filter topologies, protection circuits, etc.

Chapter 3 is considered as an overview of control and modulation strategies that were developed for the matrix converter. Special attention is paid to indirect space vector modulation, which is used for developed prototype of the converter. ISVM is based on virtual splitting of the matrix converter into rectifier part and inverter part followed by application of known control strategies from conventional VSR and VSI, connected together into one consecutive mutual combination. The only difference is absence of DC link which limits the amplitude of the output voltage to 86.6% of the input voltage. Possible ways of switching optimization are briefly presented here too. At the end of the chapter there are also mentioned control strategies that produce output voltage by the means of direct selection of switching combination (DTC, predictive control, etc.).

In chapters 4 and 5 there are discussed problems connected with mathematical description of an induction machine and control strategies that can be used for a matrix converter drive. Both scalar and vector control strategies are mentioned. Special attention is paid to the description of induction machine in state variables and discretization of created machine model. The methods for estimation of induction machine flux and rotational speed are introduced too. From a broaden variety of methods that can be used for estimation of induction machine mechanical speed, the extended Luenberger

observer was selected. It is not as complicated to implement it in the **C language** compared to other methods e.g. Kalman filter and it can estimate both the speed and the rotor flux at the same time.

Chapter 6 is devoted to the description of the particular design steps of the converter prototype leading to its realization and testing. The choice of suitable IGBTs, their spatial arrangement on the heat sink and the corresponding realization of needed interconnections are presented. The selection procedure and the design of converter input filter with considering of power losses in the damping circuit is demonstrated here also. Rather briefly then the design of the protection circuit for the whole converter system, including switches, is introduced. The challenges of selected clamping circuit discharge method in context of input circuit breaker are discussed. However, no easy applicable design rules safeguarding a proper selective protection system are provided here. Thus experimental verification of this design step is always very advisable. Further, the realization of the control part including test methods of developed SW is mentioned. Obviously, the sample converter consists of many other circuits and boards, such as: supply for measurement sensors, their signal adjustment, interconnection board etc. They are essential for the converter operation. They were designed during the construction of the converter, however they are mostly not mentioned in detail in this thesis, because it is out of the scope and the design typically only follows the manufacturer's guidelines from their data sheets. In contrast, the design and testing of the circuit for the current polarity detection is to be highlighted, since its existence is crucial for some commutation methods. This has been employed for implementing the current controlled four step commutation strategy.

Chapter 7 then shows results of the converter testing. Simple method of scalar control (Voltage/Hz control) was implemented at first in order to test the functionality of both, the converter power part and its controller including the RT-kernel. Consequently more complex control strategies were implemented, inclusive the rotor flux oriented vector control (DRFOC) and current PWM control. Firstly, all selected algorithms were simulated in Matlab/Simulink environment in continuous mode, secondly then, they were discretized, re-implemented into **C language** and in the form of a mex-function simulated and tested once more. Finally, the **C code** was compiled with the RT-kernel for the target platform and tested on the real converter prototype. All developed models and source codes have been archived in an up-to-date manner in form of Mercurial DVCS repository.

Obtained results of the simulations and measured results were compared together. It is seen that models created with the help of Plecs toolbox in Matlab and the implemented C-codes are in good accordance with the measured results including the designed observer. On the matrix converter drive, the estimated speed was compared with a measured one provided by tachogenerator. From this comparison, it is obvious that the designed observer estimates speed with good accuracy in the area of middle and higher speeds. However for speed lower than approx. 5% of the nominal one its accuracy drops significantly.

Already during testing of the drive under the scalar control, several issues had been detected, but they all were solved. Firstly, there was a problem with tripping level of the floating protection of the converter. Here the output current and input voltage SW protections have to be adjusted accordingly. Secondly the EMI caused by transistor's switching caused malfunction of VGA controller of the embedded CPU. Measurements were showing that there is problem caused by the induced voltage into grounding and shielding wires of the VGA cable. The problem was solved by supplying the diagnostic

LCD monitor via an isolation transformer. Last issue was caused by increased energy consumption of the CPU controller boards reaching values exceeding the nominal data-sheet values and has been resolved by adding an ordinary PC power source. Overall, we can state, there had appeared problems that are common for prototypes. As usually the current temporary solutions shall be beneficial for a future redesign.

Chapter 8 is focusing on a system consisting of a matrix converter connected to a self excited induction machine. The main drawback of an off-grid induction generator in the classical configuration is the need for a big capacitor bank supplying the required reactive power. Moreover, the parameters of its output are heavily dependent on mechanical speed of the shaft. The simulations presented in chapter 8 show that matrix converter can be used to control the excitation of an induction machine, i.e. amplitude of generated voltage. The frequency is held constant by the converter and thus higher quality of the generator's output is reached, here even with lower energy accumulated in external components. This kind of matrix converter application was tested only by the means of simulations, because proposed control structure requires information about voltage on terminals between the induction motor and matrix converter and corresponding sensors have not been incorporated into the initial design. However, since the simulation and measured results of the matrix converter drive with FOC were in a good accordance, we can legitimately regard the simulation results to be near to the reality in this case as well.

## 9.2 Suggestions for the Future Work

The presented compact matrix converter was designed with the aim to build a prototype based on a relatively modern converter topology, which would have some scientific potential for further research. The development and assembly of the converter began 7 years ago. However, during this period the area of power converters (switching devices, control HW etc.) has experienced a rapid development. The current state of art shows that the classical 3 x 3 topology as replacement of VSI has not spread as much as expected. However, its derivatives as sparse, multilevel or more phase topologies have attracted significantly more attention. From the point of view of semiconductor parts itself, the promising approach shall be the replacement of the classical IGBTs with new parts based on SiC, because of their lower resistance, higher allowable switching frequency and higher working temperature. These features can help to further increase the quality of generated outputs and decrease the volume of the converter too. This would be the next important step on the way to an almost all-silicon solution.

From the point of view of the controller part, the further advances in the utilization of the present FPGA, faster A/D converters and implementation of IRC or resolver IPs would improve converter's performance. Implementation of a faster commutation strategy fully utilizing the current polarity detectors carried out in the presented prototype would improve the performance too.

The research in the area of predictive control strategies and their implementation, deployment of the matrix converter in the area of power generation, as wind energy converter systems (WECS) or self excited induction generators (SEIG), seems to be logical direction of a further development also. In these areas, the advantages of the direct converter, as consumption and production of sinusoidal current, possibility of power factor control, lower content of power passive components would definitely stand out. In this case the additional tree voltage sensors shall be added at the output terminals of the existing prototype or they should be taken as one of new requirements in case of a potential new redesigning the matrix converter.

## 9.3 Fulfillment of the Objectives Defined in Section 1.3

I consider all objectives of this thesis to be satisfied.

- The design and configuration of the power part is presented in the section 6.1. Selection of the components to be adopted in the compact matrix converter prototype was conducted with emphasis on the predefined requirements defining the rated power of the converter, switching frequency of the IGBTs and intended laboratory use of the converter.
- The input filter topology selection with the aim of minimization of the power losses in the damping branches and sizing approach for the particular components are to be found in the section 6.2.
- Design of suitable protections for the power part of the converter prototype is completed in the section 6.3. The whole matrix of IGBT switches is covered by a clamp circuit and subsequently each and every individual bi-directional switch is protected against overvoltage by its own varistor. The protections based on measurements of actual values of voltages and currents carried out in control software are included also.
- Selection procedure of a platform for the control part of the converter drive is mentioned in the section 6.4. It is to emphasize that in the control part, which contains also the driver boards, a circuit for current polarity detection is tightly integrated with the bidirectional switch.
- The control strategies for the induction machine drive and matrix converter are briefly summarized in the chapter 5. Results of the implementation of the selected strategies are shown in the chapter 7.
- Methods for identification of induction machine's speed and flux values and implementation of IM model are presented in the chapter 4. Code snippet of the C program implementing the selected Luenberger observer is to be found in the chapter 7.
- After the control part and the power part of the compact matrix converter had been assembled together and integration period was closed, the field oriented control algorithm for the matrix converter drive was successfully implemented using the RT-kernel. Thus the functionality of the converter was verified.
- Finally the analysis of the possible use of matrix converters in off-grid systems with induction generator was performed in the chapter 8. An appropriate controller for this special use case was proposed and a model of the complete SEIG system was created in Matlab/Simulink/Plecs. Simulation results forebode that the matrix converter is able to control reactive power delivered to the generator and thus control also the amplitude of generated voltage. Moreover no additional capacitor bank is need in this configuration.

## References

- [1] D. W. Novotny, and T. A. Lipo. *Vector Control and Dynamics of AC Drive*. 1st edition. Oxford: Oxford University Press, 1996. ISBN 0-19-856439-2.
- [2] P. Vas. *Sensorless vector and direct torque control*. Oxford: Oxford University Press, 1998. ISBN 0-19-856465-1.
- [3] B. K. Bose. *Power electronics and motor drives: advances and trends*. Amsterdam: Academic Press, 2006. ISBN 0-12-088405-4.
- [4] R. W. Erickson, and D. Maksimovic. *Fundamentals of power electronics*. 2 edition. Norwell: Springer, 2001. ISBN 0-792-37270-0.
- [5] M. H. Rashid. *Power electronics handbook*. 3rd edition. Burlington: Butterworth-Heinemann, 2011. ISBN 978-0-12-382036-5.
- [6] M. Pfeifer, and G. Schroder. *New commutation method of a matrix converter*. In: *Industrial Electronics, 2009. ISIE 2009. IEEE International Symposium on*. 2009. 1516-1519.
- [7] T. Schulte, and G. Schroder. *Power loss comparison of different matrix converter commutation strategies*. In: *Power Electronics and Motion Control Conference (EPE/PEMC), 2012 15th International*. 2012. DS2c.9-1-DS2c.9-6.
- [8] X. Liu, P. - Ch. Loh, Wang. P., F. Blaabjerg, J. Tang, and E. A. Al-Ammar. *Distributed Generation Using Indirect Matrix Converter in Reverse Power Mode*. *Power Electronics, IEEE Transactions on*. 2013, 28 (3), 1072-1082.
- [9] X. Liu, P. Wang, P. Ch. Loh, and F. Blaabjerg. *A Three-Phase Dual-Input Matrix Converter for Grid Integration of Two AC Type Energy Resources*. *Industrial Electronics, IEEE Transactions on*. 2013, 60 (1), 20-30.
- [10] K. Park, K.-B. Lee, and F. Blaabjerg. *Improving Output Performance of a Z-Source Sparse Matrix Converter Under Unbalanced Input-Voltage Conditions*. *Power Electronics, IEEE Transactions on*. 2012, 27 (4), 2043-2054.
- [11] X. Liu, P. Wang, P. Ch. Loh, and F. Blaabjerg. *A Compact Three-Phase Single-Input/Dual-Output Matrix Converter*. *Industrial Electronics, IEEE Transactions on*. 2012, 59 (1), 6-16.
- [12] T. Friedli, and J. W. Kolar. *Milestones in Matrix Converter Research*. *IEEEJ Journal of Industry Application*. 2012, 1 (1), 2-14.
- [13] T. Friedli, J. W. Kolar, J. Rodriguez, and P. W. Wheeler. *Comparative Evaluation of Three-Phase AC-AC Matrix Converter and Voltage DC-Link Back-to-Back Converter Systems*. *Industrial Electronics, IEEE Transactions on*. 2012, 59 (12), 4487-4510.
- [14] M. Rivera, J. Rodriguez, J. R. Espinoza, T. Friedli, J. W. Kolar, A. Wilson, and C. A. Rojas. *Imposed Sinusoidal Source and Load Currents for an Indirect Matrix Converter*. *Industrial Electronics, IEEE Transactions on*. 2012, 59 (9), 3427-3435.
- [15] F. Schafmeister, and J. W. Kolar. *Novel Hybrid Modulation Schemes Significantly Extending the Reactive Power Control Range of All Matrix Converter Topologies*

- With Low Computational Effort. *Industrial Electronics, IEEE Transactions on*. 2012, 59 (1), 194-210.
- [16] M. Jussila. *Comparison of Space Vector Modulated Direct and Indirect Matrix Converter in Low Power Applications*. Ph.D. Thesis, Tampere University of Technology. 2007.
- [17] M. A. Sayed, and T. Takeshita. *Novel PWM technique for three-to-five phase matrix converter*. In: *Renewable Energy Research and Applications (ICRERA), 2013 International Conference on*. 2013. 644-649.
- [18] W. Xinyu, L. Jinjun, X. Taotao, and W. Xiaojian. *Research of three-phase single-stage matrix converter for power electronic transformer*. In: *Power Electronics and Motion Control Conference (IPEMC), 2012 7th International*. 2012. 599-603.
- [19] W. Xiaohong, H. Yuan, and T. Lianfang. *Research of control strategy for matrix converter based on space vector modulation*. In: *Computing, Communication, Control, and Management, 2009. CCCM 2009. ISECS International Colloquium on*. 2009. 354-357.
- [20] Y. Shi, X. Yang, Q. He, and Z. Wang. Research on a novel capacitor clamped multilevel matrix converter. *Power Electronics, IEEE Transactions on*. 2005, 20 (5), 1055-1065.
- [21] X. Qin, B. Zhou, J. Wei, J. Lei, X. Liu, and N. Han. Distortion analysis and duty ratio correction algorithm for asymmetric modulation of two-stage matrix converter. *Industrial Electronics, IEEE Transactions on*. 2014, (99), 1-1.
- [22] N. X. Bac, D.M. Vilathgamuwa, and U.K. Madawala. A SiC-Based Matrix Converter Topology for Inductive Power Transfer System. *Power Electronics, IEEE Transactions on*. 2014, 29 (8), 4029-4038.
- [23] Ch. Xia, J. Zhao, Y. Yan, and T. Shi. A Novel Direct Torque Control of Matrix Converter-Fed PMSM Drives Using Duty Cycle Control for Torque Ripple Reduction. *Industrial Electronics, IEEE Transactions on*. 2014, 61 (6), 2700-2713.
- [24] P. W. Wheeler, J. Rodriguez, J. C. Clare, L. Empringham, and A. Weinstein. Matrix converters: a technology review. *Industrial Electronics, IEEE Transactions on*. 2002, 49 (2), 276-288.
- [25] J. W. Kolar, T. Friedli, J. Rodriguez, and P. W. Wheeler. Review of Three-Phase PWM AC-AC Converter Topologies. *Industrial Electronics, IEEE Transactions on*. 2011, 58 (11), 4988-5006.
- [26] J. Rodriguez, M. Rivera, J. W. Kolar, and P. W. Wheeler. A Review of Control and Modulation Methods for Matrix Converters. *Industrial Electronics, IEEE Transactions on*. 2012, 59 (1), 58-70.
- [27] L. de Lillo, L. Empringham, M. Schulz, and P. W. Wheeler. *A high power density SiC-JFET-based matrix converter*. In: *Power Electronics and Applications (EPE 2011), Proceedings of the 2011-14th European Conference on*. 2011. 1-8.
- [28] L. de Lillo, L. Empringham, M. Schulz, and P. Wheeler. *Pushing Power Density Limits using SiC-JFet-based Matrix Converter Pushing Power Density Limits using SiC-JFet based Matrix Converter*. . Infineon Technologies report.
- [29] J. Riedemann, R. Pena, R. Cardenas, J. C. Clare, P. W. Wheeler, and M. Rivera. *Switching strategies for an indirect matrix converter fed open-end load*. In: *IEEE International Symposium on Industrial Electronics*. 2013.

- [30] S. Safari, A. Castellazzi, and P. W. Wheeler. Experimental and Analytical Performance Evaluation of SiC Power Devices in the Matrix Converter. *Power Electronics, IEEE Transactions on*. 2014, 29 (5), 2584-2596.
- [31] S. Safari, A. Castellazzi, and P. Wheeler. *Influence of commutation delay on waveform distortion in high frequency SiC matrix converter*. In: *IET Conference Publications*. 2014.
- [32] *SML300AT06*. <http://products.semelab-tt.com/>. 2006.  
<http://products.semelab-tt.com/pdf/power/SML300MAT06.pdf>.
- [33] D. Domes, and W. Hofmann. *SiC JFET in Contrast to High Speed Si IGBT in Matrix Converter Topology*. In: *Power Electronics Specialists Conference, 2007. PESC 2007. IEEE*. 2007. 54-60.
- [34] J. K. Hayes, A. Escobar-Mejia, J. C. Balda, A. Dutta, and S. S. Ang. *Realization of a SiC module-based indirect matrix converter with minimum parasitic inductances*. In: *Applied Power Electronics Conference and Exposition (APEC), 2014 Twenty-Ninth Annual IEEE*. 2014. 587-594.
- [35] <http://www.yaskawa.eu.com/cz/drives-motion/pohon-s-menicem/varispeed-ac/liceni.html>.
- [36] <http://www.yaskawa.eu.com/cz/drives-motion/pohon-s-menicem/medium-voltage/-inverter-drives/mx1s.html>.
- [37] S. Fligl. *Matrix Converter in Hybrid Drives*. Ph.D. Thesis, CTU in Prague. Prague, 2006.
- [38] D. Kuzmanovic. *Field Oriented Control and Direct Torque Control of Matrix Converter-Fed Induction Motor*. Ph.D. Thesis, CTU in Prague. Prague, 2009.
- [39] J. Bauer. *Konstrukce kompaktniho maticoveho menice a jeho dimenzovani*. Master's Thesis, CTU in Prague. Prague, 2007.
- [40] M. Bednar. *Deska generatoru spinacich pulzu pro kompaktni maticovy menic*. Master's Thesis, CTU in Prague. Prague, 2007.
- [41] P. Posta. *Stavovy automat modulatoru pro kompaktni maticovy menic*. Master's Thesis, CTU in Prague. Prague, 2007.
- [42] L. Linhart. *Modulacni strategie maticoveho menice*. Master's Thesis, CTU in Prague. Prague, 2008.
- [43] P. Posta. *Modulator maticoveho menice*. Ph.D. Thesis, CTU in Prague. Prague, 2014.
- [44] L. Gyugyi, and B. R. Pelly. *Static power frequency changers; theory, performance and applicationl*. New York: John Wiley and Sons, 1976.
- [45] L. Huber, and D. Borojevic. *Space vector modulator for forced commutated cycloconverters*. In: *Industry Applications Society Annual Meeting, 1989., Conference Record of the 1989 IEEE*. 1989. 871-876 vol.1.
- [46] L. Huber, and D. Borojevic. *Space vector modulation with unity input power factor for forced commutated cycloconverters*. In: *Industry Applications Society Annual Meeting, 1991., Conference Record of the 1991 IEEE*. 1991. 1032-1041 vol.1.
- [47] M. Venturini. *A new sine wave in sine wave out, conversion technique which eliminates reactive elements*. In: *POWERCON, 1980. In Proc.* 1980.

- [48] M. Venturiny, and A. Alesina. *The generalized transformer: A new bidirectional sinusoidal waveform frequency converter with continuously adjustable input power factor*. In: *IEEE PESC'80, 1980*. 1980.
- [49] J. W. Kolar, M. Baumann, F. Schafmeister, and H. Ertl. *Novel three-phase AC-DC-AC sparse matrix converter*. In: *Applied Power Electronics Conference and Exposition, 2002. APEC 2002. Seventeenth Annual IEEE*. 2002. 777-791 vol.2.
- [50] L. Wei, T. A. Lipo, and H. Chan. *Matrix converter topologies with reduced number of switches*. In: *Power Electronics Specialists Conference, 2002. IEEE 33rd Annual*. 2002. 57-63 vol.1.
- [51] N.-S. Choi, Y. Li, B.-H. Han, J.-S. Ko, and E.-Ch. Nho. *Matrix converter with a novel general commutation strategy*. In: *Power Electronics, 2007. ICPE '07. 7th International Conference on*. 2007. 1038-1043.
- [52] N. Burany. *Safe control of four-quadrant switches*. In: *Industry Applications Society Annual Meeting, 1989., Conference Record of the 1989 IEEE*. 1989. 1190-1194 vol.1.
- [53] L. Wei, T. A. Lipo, and H. Chan. *Robust voltage commutation of the conventional matrix converter*. In: *Power Electronics Specialist Conference, 2003. PESC '03. 2003 IEEE 34th Annual*. 2003. 717-722 vol.2.
- [54] J. Mahlein, J. Igney, J. Weigold, M. Braun, and O. Simon. *Matrix converter commutation strategies with and without explicit input voltage sign measurement*. *Industrial Electronics, IEEE Transactions on*. 2002, 49 (2), 407-414.
- [55] M. Ziegler, and W. Hofmann. *Semi natural two steps commutation strategy for matrix converters*. In: *Power Electronics Specialists Conference, 1998. PESC 98 Record. 29th Annual IEEE*. 1998. 727-731 vol.1.
- [56] M. Ziegler, and W. Hofmann. *Implementation of a two steps commutated matrix converter*. In: *Power Electronics Specialists Conference, 1999. PESC 99. 30th Annual IEEE*. 1999. 175-180 vol.1.
- [57] L. Hao, N. Ziling, and Z. Ye. *A New Controlled Commutation Strategies for Matrix Converter*. In: *Computer Science and Computational Technology, 2008. ISCSCCT '08. International Symposium on*. 2008. 242-245.
- [58] L. Empringham, P. W. Wheeler, and J. C. Clare. *Matrix converter bi-directional switch commutation using intelligent gate drives*. In: *Power Electronics and Variable Speed Drives, 1998. Seventh International Conference on*. 1998. 626-631.
- [59] D. Zhou, K. Sun, L. Huang, and K. Sasagawa. *A novel commutation method of matrix converter fed induction motor drive using RB-IGBT*. In: *Industry Applications Conference, 2005. Fourtieth IAS Annual Meeting*. 2005. 2347-2354 Vol. 4.
- [60] M. Ziegler, and W. Hofmann. *New one-step commutation strategies in matrix converters*. In: *Power Electronics and Drive Systems, 2001. Proceedings., 2001 4th IEEE International Conference on*. 2001. 560-564 vol.2.
- [61] X.- H. Ma, G. -J. Tan, X.-I. Wu, Y. Fang, X. Z, and Y.-F. Han. *Research on Improved Four-step Commutation Strategy of Matrix Converter Based on Two Line Voltage Synthesis*. In: *Innovative Computing, Information and Control, 2007. ICICIC '07. Second International Conference on*. 2007. 503-503.
- [62] B. He, X. Wang, H. Lin, and H. She. *Research on two-step voltage-controlled commutation strategies for Matrix Converter*. In: *Power Electronics and Motion Control Conference, 2009. IPEMC '09. IEEE 6th International*. 2009. 1745-1751.

- [63] C. -T. Pan, C. -T. Chen, and J. -J. Shieh. *A zero switching loss matrix converter*. In: *Power Electronics Specialists Conference, 1993. PESC '93 Record., 24th Annual IEEE*. 1993. 545-550.
- [64] S. Schulz, A. Ecklebe, and A. Lindemann. Influence of Parasitic Elements on the Commutation of a Resonant Matrix Converter. *Integrated Power Systems (CIPS), 2008 5th International Conference on*. 2008, 1-6.
- [65] R. Mecke, C. Rathge, A. Ecklebe, and A. Lindemann. *Bidirectional switches for matrix converter in contactless energy transmission systems*. In: *Power Electronics and Applications, 2005 European Conference on*. 2005. 10 pp.-P.10.
- [66] M. J. Bland, P. Wheeler, J. C. Clare, and L. Empringham. *Comparison of bi-directional switch components for direct AC-AC converters*. In: *Power Electronics Specialists Conference, 2004. PESC 04. 2004 IEEE 35th Annual*. 2004. 2905-2909 Vol.4.
- [67] *IGBT Bi-Directional Switch Module*. 2010.  
<http://www.dynexpowersemiconductors.com/>.
- [68] M. Hornkamp, M. Loddenkoetter, M. Münzer, O. Simon, and M. Bruckman. *EconoMAC the first all-in-one IGBT module for matrix converters*. . EUPEC technical report.
- [69] *The development of a reverse-blocking IGBT for use in matrix converters*. [www.dataweek.co.za/](http://www.dataweek.co.za/). 2005.  
<http://www.dataweek.co.za/news.aspx?pklnnewsid=18413>.
- [70] H. She, H. Lin, X. Wang, and L. Yue. *Damped input filter design of matrix converter*. In: *Power Electronics and Drive Systems, 2009. PEDS 2009. International Conference on*. 2009. 672-677.
- [71] A. Trentin, P. Zanchetta, J. Clare, and P. W. Wheeler. Automated Optimal Design of Input Filters for Direct AC/AC Matrix Converters. *Industrial Electronics, IEEE Transactions on*. 2012, 59 (7), 2811-2823.
- [72] K. Yamada, T. Higuchi, E. Yamamoto, H. Hara, T. Sawa, M. M. Swamy, and T. Kume. *Filtering techniques for matrix converters to achieve environmentally harmonious drives*. In: *Power Electronics and Applications, 2005 European Conference on*. 2005. 10 pp.-P.10.
- [73] A. Alesina, and M. Venturini. Analysis and design of optimum-amplitude nine-switch direct AC-AC converters. *Power Electronics, IEEE Transactions on*. 1989, 4 (1), 101-112.
- [74] P. Nielsen, F. Blaabjerg, and J. K. Pedersen. *Novel solutions for protection of matrix converter to three phase induction machine*. In: *Industry Applications Conference, 1997. Thirty-Second IAS Annual Meeting, IAS '97., Conference Record of the 1997 IEEE*. 1997. 1447-1454.
- [75] P. Nielsen, F. Blaabjerg, and J. K. Pedersen. New protection issues of a matrix converter: design considerations for adjustable-speed drives. *Industry Applications, IEEE Transactions on*. 1999, 35 (5), 1150-1161.
- [76] J. Mahlein, M. Bruckmann, and M. Braun. Passive protection strategy for a drive system with a matrix converter and an induction machine. *Industrial Electronics, IEEE Transactions on*. 2002, 49 (2), 297-303.
- [77] J. Mahlein, and M. Braun. *A matrix converter without diode clamped over-voltage protection*. In: *Power Electronics and Motion Control Conference, 2000. Proceedings. IPEMC 2000. The Third International*. 2000. 817-822 vol.2.

- [78] G. Roy, and G. - A. April. *Cycloconverter operation under a new scalar control algorithm*. In: *Power Electronics Specialists Conference, 1989. PESC '89 Record., 20th Annual IEEE*. 1989. 368-375 vol.1.
- [79] J. Vadillo, J. M. Echeverria, L. Fontan, M. Martinez-Iturralde, and I. Elosegui. *Modeling and simulation of a direct space vector modulated Matrix Converter using different switching strategies*. In: *Power Electronics, Electrical Drives, Automation and Motion, 2008. SPEEDAM 2008. International Symposium on*. 2008. 944-949.
- [80] P. Nielsen, F. Blaabjerg, and J. K. Pedersen. *Space vector modulated matrix converter with minimized number of switchings and a feedforward compensation of input voltage unbalance*. In: *Power Electronics, Drives and Energy Systems for Industrial Growth, 1996., Proceedings of the 1996 International Conference on*. 1996. 833-839 vol.2.
- [81] D. Casadei, G. Serra, and A. Tani. The use of matrix converters in direct torque control of induction machines. *Industrial Electronics, IEEE Transactions on*. 2001, 48 (6), 1057-1064.
- [82] S. Kouro, P. Cortes, R. Vargas, U. Ammann, and J. Rodriguez. Model Predictive Control, a Simple and Powerful Method to Control Power Converters. *Industrial Electronics, IEEE Transactions on*. 2009, 56 (6), 1826-1838.
- [83] S. Yusoff, L. de Lillo, P. Zanchetta, and P. W. Wheeler. *Predictive control of a direct AC/AC matrix converter power supply under non-linear load conditions*. In: *Power Electronics and Motion Control Conference and Exposition, 2012. EPE-PEMC 2012. 15th International*. 2012.
- [84] K. Zhou, and D. Wang. Relationship between space-vector modulation and three-phase carrier-based PWM: a comprehensive analysis three-phase inverters. *Industrial Electronics, IEEE Transactions on*. 2002, 49 (1), 186-196.
- [85] D. Casadei, G. Serra, A. Tani, and L. Zarri. Matrix converter modulation strategies: a new general approach based on space-vector representation of the switch state. *Industrial Electronics, IEEE Transactions on*. 2002, 49 (2), 370-381.
- [86] S. Fligl. *Contribution to the mathematical description of the matrix converter power electronic topology*. In: *Applied Electronics (AE), 2011 International Conference on*. 2011. 1-4. ISBN 1803-7232.
- [87] T. Takeshita, and H. Fukagawa. *Output Current Signs-Based PWM Strategy of Matrix Converters for Reducing Input Current Harmonics*. In: *Power Electronics and Motion Control Conference and Exposition, 2012. EPE-PEMC 2012. 15th International*. 2012.
- [88] M. Popescu. *Improved direct and inverse gamma models for vector controlled induction machines*. In: *Power Electronics and Variable Speed Drives, 2000. Eighth International Conference on (IEE Conf. Publ. No. 475)*. 2000. 147-153.
- [89] S. Fligl, J. Bauer, and S. Ryvkin. *Matrix converter sliding mode based control for induction motor drive*. In: *Optimization of Electrical and Electronic Equipment (OPTIM), 2012 13th International Conference on*. 2012. 393-402.
- [90] N. P. Quang, and J. A. Dittrich. *Vector Control of Three-Phase AC Machines*. Springer, 2008.
- [91] S. Fligl, J. Bauer, M. Vlcek, and J. Lettl. *Analysis of induction machine T and G circuit coequality for use in electric drive controllers*. In: *Optimization of Electrical and Electronic Equipment (OPTIM), 2012 13th International Conference on*. 2012. 659-664.

- [92] F. Blaschke. *The principle of Field Orientation as Applied to the New "Transvektor" Closed-loop Control System for Rotating-Field Machines*. In: *Siemens Review*. 1972. 217-219.
- [93] P. Vas. *Parameter Estimation, Condition Monitoring, and Diagnosis of in Electrical Machines*. Clarendon Press, 1993.
- [94] P.L. Jansen, R.D. Lorenz, and D.W. Novotny. Observer-based direct field orientation: analysis and comparison of alternative methods. *Industry Applications, IEEE Transactions on*. 1994, 30 (4), 945-953.
- [95] M.R. Khan, and A. Iqbal. *Model reference adaptive system with simple sensorless flux observer for induction motor drive: MRAS with simple sensorless flux observer for induction motor drive*. In: *Power Electronics, Drives and Energy Systems (PEDES), 2012 IEEE International Conference on*. 2012. 1-6.
- [96] M. A. Gallegos, R. Alvarez, and C. A. Nunez. *A survey on speed estimation for sensorless control of induction motors*. In: *International Power Electronics Congress, 10th IEEE*. 2006. 1-6.
- [97] M. Comanescu, and V. Utkin. *A sliding mode adaptive MRAS speed estimator for induction motors*. In: *Industrial Electronics, 2008. ISIE 2008. IEEE International Symposium on*. 2008. 634-638.
- [98] M. Dybkowski, and T. Orłowska-Kowalska. *Application of the stator current-based MRAS speed estimator in the sensorless induction motor drive*. In: *Power Electronics and Motion Control Conference, 2008. EPE-PEMC 2008. 13th*. 2008. 2306-2311.
- [99] M. N. Marwali, and A. Keyhani. *A comparative study of rotor flux based MRAS and back EMF based MRAS speed estimators for speed sensorless vector control of induction machines*. In: *Industry Applications Conference, 1997. Thirty-Second IAS Annual Meeting, IAS '97., Conference Record of the 1997 IEEE*. 1997. 160-166 vol.1.
- [100] M. Rashed, F. Stronach, and P. Vas. *A stable MRAS-based sensorless vector control induction motor drive at low speeds*. In: *Electric Machines and Drives Conference, 2003. IEMDC'03. IEEE International*. 2003. 139-144.
- [101] M. N. Gayathri, S. Himavathi, and R. Sankaran. *Performance of vector controlled induction motor drive with reactive power based MRAS rotor resistance estimator*. In: *Recent Advancements in Electrical, Electronics and Control Engineering (ICONRAEeCE), 2011 International Conference on*. 2011. 352-356.
- [102] M. N. Gayathri, S. Himavathi, and R. Sankaran. *Comparison of rotor flux and reactive power based MRAS rotor resistance estimators for Vector Controlled Induction Motor drive*. In: *Advances in Engineering, Science and Management (ICAESM), 2012 International Conference on*. 2012. 183-189.
- [103] A. Larabi, and M. S. Boucherit. *Robust speed-sensorless induction motor with the rotor time constant adaptation*. In: *Electrical Systems for Aircraft, Railway and Ship Propulsion (ESARS), 2010*. 2010. 1-6.
- [104] J. Hu, B. R. Duggal, and M. Vilathgamuwa. *A MRAS-based speed sensorless field oriented control of induction motor with on-line stator resistance tuning*. In: *Power Electronic Drives and Energy Systems for Industrial Growth, 1998. Proceedings. 1998 International Conference on*. 1998. 38-43 Vol.1.
- [105] R. Isermann. *Identifikation dynamischer systeme*. Springer-Verlag, 1988.

- [106] K. Kubota, K. Matsuse, and T. Nakano. DSP-based speed adaptive flux observer of induction motor. *Industry Applications, IEEE Transactions on*. 1993, 29 (2), 344-348.
- [107] K. Kubota, and K. Matsuse. *Speed sensorless field oriented control of induction machines using flux observer*. In: *Industrial Electronics, Control and Instrumentation, 1994. IECON '94., 20th International Conference on*. 1994. 1611-1615 vol.3.
- [108] G.S. Buja, and M.P. Kazmierkowski. Direct torque control of PWM inverter-fed AC motors - a survey. *Industrial Electronics, IEEE Transactions on*. 2004, 51 (4), 744-757.
- [109] M.P. Kazmierkowski. *Control strategies for PWM rectifier/inverter-fed induction motors*. In: *Industrial Electronics, 2000. ISIE 2000. Proceedings of the 2000 IEEE International Symposium on*. 2000.
- [110] K. Hasse. Drehzahlregelverfahren für schnelle Umkehrantriebe mit stromrichter-geschpisten Asynchron-Kurzschlusslaufermotoren. *Regelungstechnik*. 1972, 20
- [111] M. Depenbrock. Direct self-control (DSC) of inverter-fed induction machine. *Power Electronics, IEEE Transactions on*. 1988, 3 (4), 420-429.
- [112] U. Baader, M. Depenbrock, and G. Gierse. Direct self control (DSC) of inverter-fed induction machine: a basis for speed control without speed measurement. *Industry Applications, IEEE Transactions on*. 1992, 28 (3), 581-588.
- [113] I. Takahashi, and T. Noguchi. A New Quick-Response and High-Efficiency Control Strategy of an Induction Motor. *Industry Applications, IEEE Transactions on*. 1986, IA-22 (5), 820-827.
- [114] M.F. Escalante, J.-C. Vannier, and A. Arzande. Flying capacitor multilevel inverters and DTC motor drive applications. *Industrial Electronics, IEEE Transactions on*. 2002, 49 (4), 809-815.
- [115] C. A. Martins, X. Roboam, T. A. Meynard, and A. S. Carvalho. Switching frequency imposition and ripple reduction in DTC drives by using a multilevel converter. *Power Electronics, IEEE Transactions on*. 2002, 17 (2), 286-297.
- [116] S. Kouro, R. Bernal, H. Miranda, C. A. Silva, and J. Rodriguez. High-Performance Torque and Flux Control for Multilevel Inverter Fed Induction Motors. *Power Electronics, IEEE Transactions on*. 2007, 22 (6), 2116-2123.
- [117] F. Khoucha, S. M. Lagoun, K. Marouani, A. Kheloui, and M. El Hachemi Benbouzid. Hybrid Cascaded H-Bridge Multilevel-Inverter Induction-Motor-Drive Direct Torque Control for Automotive Applications. *Industrial Electronics, IEEE Transactions on*. 2010, 57 (3), 892-899.
- [118] J. Holtz, and S. Stadtfeld. *A predictive controller for the stator current vector of AC machines fed from a switched voltage source*. In: *International Power Electronics Conference*. 1983.
- [119] B. Abdeldjebar, and B. Khier. *Generalized predictive control: Application of the Induction Motor*. In: *Smart Manufacturing Application, 2008. ICSMA 2008. International Conference on*. 2008. 526-529.
- [120] A. Diab, and V.V. Pankratov. *Model predictive control of vector controlled induction motor drive*. In: *Strategic Technology (IFOST), 2012 7th International Forum on*. 2012. 1-6.

- [121] J. Scoltock, T. Geyer, and U. Madawala. *A comparison of Predictive Current Control schemes for MV induction motor drives*. In: *IECON 2011 - 37th Annual Conference on IEEE Industrial Electronics Society*. 2011. 1680-1685.
- [122] J. Guzinski, and H. Abu-Rub. *Predictive current control implementation in the sensorless induction motor drive*. In: *Industrial Electronics (ISIE), 2011 IEEE International Symposium on*. 2011. 691-696.
- [123] T. M. Rowan, R. J. Kerkman, and T. A. Lipo. Operation of Naturally Sampled Current Regulators in the Transition Mode. *Industry Applications, IEEE Transactions on*. 1987, IA-23 (4), 586-596.
- [124] J. Bauer, S. Fligl, and A. Steimel. Design and Dimensioning of Essential Passive Components for the Matrix Converter Prototype. *Automatika*. 2012, 53 (3), 225-235.
- [125] *HCPL-316J datasheet*. <http://www.avagotech.com/>. 2011.
- [126] <http://www.rtd.com/>.
- [127] J. Kucka. *Modulation Strategies for Voltage Converters*. Master's Thesis, CTU in Prague. Prague, 2014.
- [128] R. Martinek. *RT rozsireni OS DOS pro platformu PC104*. Master's Thesis, CTU in Prague. Prague, 2013.
- [129] L. Klik. *Ovladac PC104 I/O modulu s moznosti ukladani sad zaznamu merenych dat*. Master's Thesis, CTU in Prague. Prague, 2013.
- [130] R.C. Bansal. Three-phase self-excited induction generators: an overview. *Energy Conversion, IEEE Transactions on*. 2005, 20 (2), 292-299.
- [131] E. Suarez, and G. Bortolotto. Voltage-frequency control of a self-excited induction generator. *Energy Conversion, IEEE Transactions on*. 1999, 14 (3), 394-401.
- [132] B. Singh, S.S. Murthy, M. Madhusudan, M. Goel, and AK. Tandon. *A Steady State Analysis on Voltage and Frequency Control of Self-Excited Induction Generator in Micro-Hydro System*. In: *Power Electronics, Drives and Energy Systems, 2006. PEDES '06. International Conference on*. 2006. 1-6.
- [133] K.H. Youssef, M.A Wahba, Hasan A Yousef, and O.A Sebakhy. *A new method for voltage and frequency control of stand-alone self-excited induction generator using PWM converter with variable DC link voltage*. In: *American Control Conference, 2008*. 2008. 2486-2491.
- [134] S. Ryvkin, M. Valiyev, S. Fligl, and J. Bauer. *Control of Island Mode Working Induction Generator Based on State Space Controller*. In: *PEMC 2014 Proceedings of*. 2014.
- [135] B. Mohamed, A. Ahmed, and col. *General study of self excited induction generator used in isolated renewable energy conversion source*. In: *Proceedings of the 2014 International Conference on Circuits, Systems, Signal Processing, Communications and Computers (CSSCC '14)*.
- [136]
- [137]



# Appendix A

## Nomenclature

### A.1 Notation of Mathematical Symbols

$x$	instantaneous scalar value
$x^*$	reference value
$\underline{x}$	space vector
$\mathbf{x}$	vector
$\mathbf{X}$	matrix

### A.2 Glossary of Symbols and Variables

$t$	[s]..time
$f$	[Hz]..frequency
$\omega$	[rad/s]..angular speed
$\omega_s$	[rad/s]..synchronous angular speed
$\omega_m$	[rad/s]..mechanical angular speed
$\omega_{slip}$	[rad/s]..slip angular speed, rotor angular speed
$i, I$	[A]..current
$u, U$	[V]..voltage
$\Psi$	[Wb]..flux
$\Psi_s$	[Wb]..stator flux
$\Psi_r$	[Wb]..rotor flux
$T$	[Nm]..torque
$p, P$	[W]..power
$pP$	[-]..number of pole pairs
$R$	[ $\Omega$ ]..resistance
$R_s$	[ $\Omega$ ]..stator resistance
$R_r$	[ $\Omega$ ]..rotor resistance
$L$	[H]..inductance
$L_{s\sigma}$	[H]..stator leakage inductance
$L_{r\sigma}$	[H]..rotor leakage inductance
$L_m$	[H]..magnetizing inductance
$\sigma$	[-]..total leakage factor
$C$	[F]..capacitance
$m$	[kg]..mass
$J$	[kgm <sup>2</sup> ]..moment of inertia
$\theta_s$	[rad/s]..angle of IM field
$j$	[-]..imaginary unit
$\alpha, \beta$	[-]..real and imaginary part of the space vector in stationary reference frame

- d, q [-]..real and imaginary part of the space vector in synchronously rotating reference frame  
 e [-]..Euler's number

### A.3 Subscripts

- RMS root means square / effective value  
 AVG average value  
 MAX maximal value  
 A first output phase  
 B second output phase  
 C third output phase  
 R first input phase  
 S second input phase  
 T third input phase  
 P virtual rectifier positive terminal  
 N virtual rectifier negative terminal

### A.4 Abbreviations

- MC matrix converter  
 IM induction machine  
 SVM space vector modulation  
 ISVM indirect space vector modulation  
 DTC direct torque control  
 FOC field oriented control  
 VSI voltage source inverter  
 CSC current source converter  
 PWM pulse width modulation  
 FPGA field programable gate array  
 IGBT insulated gate bipolar transistor  
 RBIGBT reverse blocking IGBT  
 AC, DC alternating value, direct value  
 HW hardware  
 SW software  
 RT real time  
 PC 104 ISA type communication bus

# Appendix B

## Parameters Set in Models

### B.1 Matrix Converter Parameters

$L_f = 1$	[mH]	..input filter inductance
$C_f = 9$	[ $\mu$ F]	..input filter capacity
$L_{SD} = 150$	[ $\mu$ H]	..damping inductance
$R_{SD} = 10$	[ $\Omega$ ]	..damping resistance
$f_s = 5000$	[Hz]	..switching frequency
$C_{CL} = 1000$	[ $\mu$ F]	..clamp circuit capacity
$R_{CL} = 10$	[k $\Omega$ ]	..clamp circuit discharge resistance

### B.2 Induction Motor Parameters

$U_n = 230$	[V]	..nominal voltage
$I_n = 11.8$	[A]	..nominal current
$P_n = 5.5$	[kW]	..nominal power
$\omega_n = 145$	[rad $^{-1}$ ]	..nominal speed
Y	[-]	..stator winding connection
pP = 2	[-]	..number of pole pairs
$R_s = 0.952$	[ $\Omega$ ]	..stator resistance
$L_{s\sigma} = 0.0093$	[H]	..stator leakage inductance
$R_r = 0.952$	[ $\Omega$ ]	..rotor resistance
$L_{r\sigma} = 0.0072$	[H]	..rotor leakage inductance
$L_m = 0.129$	[H]	..magnetizing inductance

### B.3 DC Motor Parameters

$U_n = 220$	[V]	..nominal voltage - armature
$I_n = 19.0$	[A]	..nominal current - armature
$P_n = 7.5$	[kW]	..nominal power
$\omega_n = 210$	[rad $^{-1}$ ]	..nominal speed
$U_n = 220$	[V]	..nominal voltage - excitation
$I_n = 1.2$	[A]	..nominal current - excitation

### B.4 Simulation Settings

$T_s = 100 \cdot 10^{-6}$	[s]	..sample time
---------------------------	-----	---------------

## B.5 Luenberger Observer Settings

$k = 1.3$  [-] ..correction constant  
 $K_P = 0.25$  [-] ..proportional gain of speed adaptation  
 $K_I = 100$  [-] ..integral gain of speed adaptation

## B.6 Current PWM Controllers Setting

$i_{\max} = 17$  [A] ..maximal allowable module of stator current space vector  
 $K_P = 0.25$  [-] ..proportional gain of speed controller  
 $K_I = 100$  [-] ..integral gain of speed controller  
 $K_P = 100$  [-] ..proportional gain of flux controller  
 $K_I = 75$  [-] ..integral gain of flux controller  
 $K_P = 46$  [-] ..proportional gain of phase A current controller  
 $K_I = 0$  [-] ..integral gain of phase A current controller  
 $K_P = 46$  [-] ..proportional gain of phase B current controller  
 $K_I = 0$  [-] ..integral gain of phase B current controller  
 $K_P = 46$  [-] ..proportional gain of phase C current controller  
 $K_I = 0$  [-] ..integral gain of phase C current controller

## B.7 DRFOC Controllers Setting

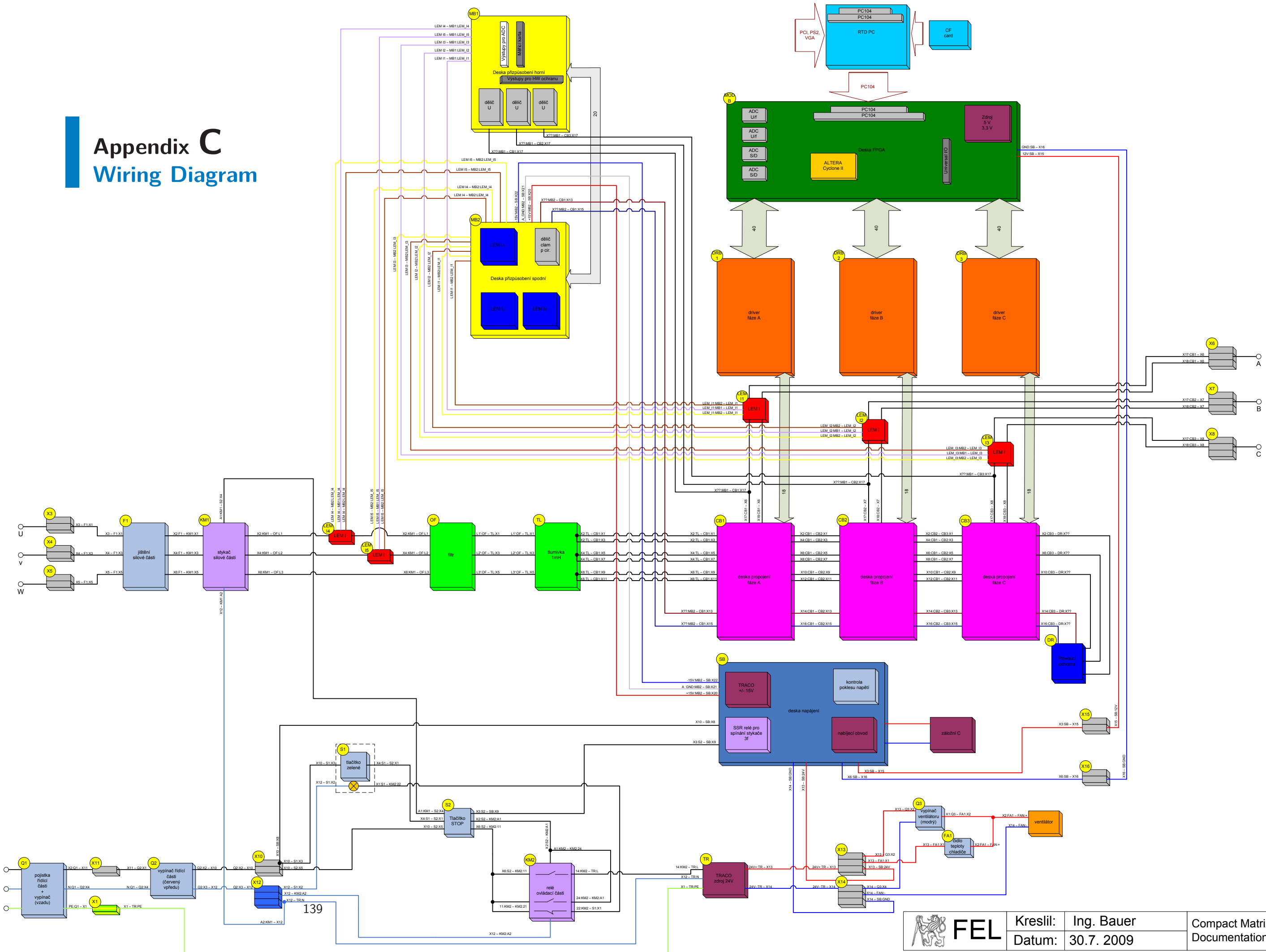
$i_{\max} = 17$  [A] ..maximal allowable module of stator current space vector  
 $K_P = 1.15$  [-] ..proportional gain of speed controller  
 $K_I = 2.5$  [-] ..integral gain of speed controller  
 $K_P = 350$  [-] ..proportional gain of flux controller  
 $K_I = 250$  [-] ..integral gain of flux controller  
 $K_P = 11.5$  [-] ..proportional gain of flux producing current controller  
 $K_I = 2.3$  [-] ..integral gain of phase flux producing current controller  
 $K_P = 11.5$  [-] ..proportional gain of torque producing current controller  
 $K_I = 2.3$  [-] ..integral gain of phase torque producing controller

## B.8 Self Excited Generator Model Parameters

$R_l = 80$  [ $\Omega$ ] ..load resistance  
 $L_l = 10$  [mH] ..load inductance  
 $C_f = 1$  [ $\mu\text{F}$ ] ..input filter capacity  
 $C_f = 9$  [ $\mu\text{F}$ ] ..input filter capacity  
 $K_P = 0.01$  [-] ..proportional gain of voltage controller  
 $K_I = 0.08$  [-] ..integral gain of voltage controller  
 $K_P = 18$  [-] ..proportional gain of flux controller  
 $K_I = 25$  [-] ..integral gain of flux controller  
 $K_P = 115$  [-] ..proportional gain of phase A current controller  
 $K_I = 0$  [-] ..integral gain of phase A current controller  
 $K_P = 115$  [-] ..proportional gain of phase B current controller  
 $K_I = 0$  [-] ..integral gain of phase B current controller  
 $K_P = 115$  [-] ..proportional gain of phase C current controller  
 $K_I = 0$  [-] ..integral gain of phase C current controller

# Appendix C

## Wiring Diagram



## Appendix D

### Space Vector Definition

The space vector represents a three phase system of time variant quantities (voltage, current, flux) in a complex plane. Originally they were used to describe dynamics behaviour of the IM. However space vectors can be advantageously used to describe behaviours of power converters and their modulation too. Furthermore nowadays space vectors are used in control of AC machines. In order to refresh knowledge about the space vector basic definitions and transformations are listed below.

Let  $x_a, x_b, x_c$  are instantaneous values of three phase variables forming the space vector  $\underline{x}$ .

$$\underline{x} = \frac{2}{3}(x_a + \mathbf{a}x_b + \mathbf{a}^2x_c) \quad (9.1)$$

where  $\mathbf{a} = \mathbf{e}^{j2\pi/3}$  and  $\mathbf{a}^2 = \mathbf{e}^{-j2\pi/3}$ . If the variables are sinusoidal, symmetric and rotate with constant angular frequency, the space vector  $\underline{x}$  can be then expressed as

$$\underline{x} = |\underline{x}| \mathbf{e}^{j\omega_k t} \quad (9.2)$$

where  $|x|$  is the magnitude of the space vector  $\underline{x}$ . The  $\underline{x}$  can be then easily split in two orthogonal components, i.e. into projection to the real and imaginary axis components (Re and Im).

$$\underline{x} = \text{Re}\{\underline{x}\} + j\text{Im}\{\underline{x}\} = x_\alpha + jx_\beta \quad (9.3)$$

If the three phase system contains a zero sequence component, it is taken into account separately

$$x_0 = (x_a + x_b + x_c)/3 \quad (9.4)$$

To simplify the transformation it is useful to use matrix form of expression. The transformation from three phase system to two axis system is sometimes called Clark's transformation and can be expressed as

$$\begin{bmatrix} x_\alpha \\ x_\beta \\ x_0 \end{bmatrix} = k_{\alpha\beta} \begin{bmatrix} 1 & -\frac{1}{2} & -\frac{1}{2} \\ 0 & \frac{\sqrt{3}}{2} & -\frac{\sqrt{3}}{2} \\ \frac{1}{2} & \frac{1}{2} & \frac{1}{2} \end{bmatrix} \begin{bmatrix} x_a \\ x_b \\ x_c \end{bmatrix} \quad (9.5)$$

inverse

$$\begin{bmatrix} x_a \\ x_b \\ x_c \end{bmatrix} = \begin{bmatrix} 1 & 0 & 1 \\ -\frac{1}{2} & \frac{\sqrt{3}}{2} & 1 \\ -\frac{1}{2} & -\frac{\sqrt{3}}{2} & 1 \end{bmatrix} \begin{bmatrix} x_\alpha \\ x_\beta \\ x_0 \end{bmatrix} \quad (9.6)$$

Sometimes emerge the necessity to use another reference frame. In this case let us assume that  $\theta_k$  is the angle of the reference frame and  $\theta_x$  is the instantaneous angle of the space vector  $\underline{x}$  in stationary reference frame. The space vector can be then expressed as

$$\underline{x}_k = |\underline{x}| \mathbf{e}^{j(\theta_x - \theta_k)} \quad (9.7)$$

Then transformation from stationary reference frame to arbitrary reference frame  $u, v$  (Park's transformation) can be expressed as

$$\begin{bmatrix} x_u \\ x_v \\ x_0 \end{bmatrix} = \begin{bmatrix} \cos \theta_k & \sin \theta_k & 0 \\ -\sin \theta_k & \cos \theta_k & 0 \\ 0 & 0 & 1 \end{bmatrix} \begin{bmatrix} x_\alpha \\ x_\beta \\ x_0 \end{bmatrix} \quad (9.8)$$

$$\begin{bmatrix} x_u \\ x_v \\ x_0 \end{bmatrix} = \frac{2}{3} \begin{bmatrix} \cos \theta_k & \cos(\theta_k - \frac{2\pi}{3}) & \cos(\theta_k - \frac{4\pi}{3}) \\ -\sin \theta_k & \sin(\theta_k - \frac{2\pi}{3}) & \sin(\theta_k - \frac{4\pi}{3}) \\ \frac{1}{2} & \frac{1}{2} & \frac{1}{2} \end{bmatrix} \begin{bmatrix} x_a \\ x_b \\ x_c \end{bmatrix} \quad (9.9)$$

Inverse transformation from the arbitrary reference frame into stationary, three phase respectively

$$\begin{bmatrix} x_\alpha \\ x_\beta \\ x_0 \end{bmatrix} = \begin{bmatrix} \cos \theta_k & -\sin \theta_k & 0 \\ \sin \theta_k & \cos \theta_k & 0 \\ 0 & 0 & 1 \end{bmatrix} \begin{bmatrix} x_u \\ x_v \\ x_0 \end{bmatrix} \quad (9.10)$$

$$\begin{bmatrix} x_a \\ x_b \\ x_c \end{bmatrix} = \begin{bmatrix} \cos \theta_k & -\sin \theta_k & 1 \\ \cos(\theta_k - \frac{2\pi}{3}) & -\sin(\theta_k - \frac{2\pi}{3}) & 1 \\ \cos(\theta_k - \frac{4\pi}{3}) & -\sin(\theta_k - \frac{4\pi}{3}) & 1 \end{bmatrix} \begin{bmatrix} x_u \\ x_v \\ x_0 \end{bmatrix} \quad (9.11)$$

Another important equation is for representation of the instantaneous values of the active power  $p$  using space vector theory. Let us consider three phase system with phase voltages  $u_{(a,b,c)}$  and currents  $i_{(a,b,c)}$  the power can be then expressed as

$$p = u_a i_a + u_b i_b + u_c i_c = \frac{3}{2} \text{Re}\{\underline{u}\underline{i}^*\} = \frac{3}{2} (u_\alpha i_\alpha + u_\beta i_\beta) = \frac{3}{2} (u_u i_u + u_v i_v) \quad (9.12)$$

with  $\underline{u}$  and  $\underline{i}$  are voltage resp. current space vectors formed by  $u_{(a,b,c)}$  and  $i_{(a,b,c)}$ ,  $\underline{i}^*$  means complex conjugate value of  $\underline{i}$  and  $u_{(\alpha,\beta)}$ ,  $i_{(\alpha,\beta)}$  and  $u_{(u,v)}$ ,  $i_{(u,v)}$  are two axis components of  $\underline{u}$  and  $\underline{i}$  obtained with the help of (9.5) and (9.8) respectively.

Finally just for clarification let us describe the space vectors for the matrix converter. There are two space vectors on the input of the converter  $\underline{u}_i$  and  $\underline{i}_i$  defined as

$$\begin{aligned} \underline{u}_i &= \frac{2}{3} (u_R + \underline{a}u_S + \underline{a}^2u_T) = |\underline{u}_i| \mathbf{e}^{j\omega_i t} \\ \underline{i}_i &= \frac{2}{3} (i_R + \underline{a}i_S + \underline{a}^2i_T) = |\underline{i}_i| \mathbf{e}^{j(\omega_i t + \varphi_{i,1})} \end{aligned} \quad (9.13)$$

and two space vectors on the output of the converter  $\underline{u}_o$  and  $\underline{i}_o$  defined as

$$\begin{aligned} \underline{u}_o &= \frac{2}{3} (u_A + \underline{a}u_B + \underline{a}^2u_C) = |\underline{u}_o| \mathbf{e}^{j\omega_o t} \\ \underline{i}_o &= \frac{2}{3} (i_A + \underline{a}i_B + \underline{a}^2i_C) = |\underline{i}_o| \mathbf{e}^{j(\omega_o t + \varphi_{o,1})} \end{aligned} \quad (9.14)$$

where  $\underline{u}_{i(R,S,T)}$  represents input phase voltages and  $\underline{i}_{i(R,S,T)}$  represents input currents,  $\underline{u}_{o(A,B,C)}$  refers to the output phase voltages and  $\underline{i}_{o(A,B,C)}$  refers to the output currents. All phase quantities are treated as purely sinusoidal and symmetric, with angular frequencies  $\omega_i$  for input and  $\omega_o$  for the output. The  $\varphi_{(i,o),1}$  represents phase shift between the corresponding voltage space vector and corresponding current space vector.

Just at the end it is good to refresh the knowledge of relations goniometric form and exponent form of sine and cosine functions

---

$$\begin{aligned}\sin x &= \frac{\mathbf{e}^{jx} - \mathbf{e}^{-jx}}{2j}, \quad x \in \Re \\ \cos x &= \frac{\mathbf{e}^{jx} + \mathbf{e}^{-jx}}{2j}, \quad x \in \Re\end{aligned}\tag{9.15}$$

## Appendix E

# Representation of Induction Machine in Three Phase System

In Fig. E.1 is depicted the structure of the three phase asynchronous machine. When we assume symmetrical stator and rotor winding, it can be easily described by equations

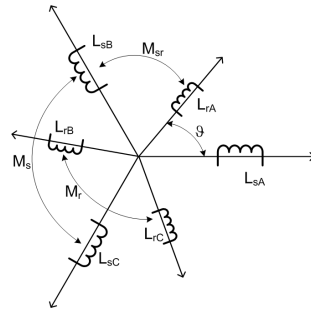


**Figure E.1.** 3 phase representation of IM

$$\begin{aligned}
 u_{sA} &= R_{sA}i_{sA} + \frac{d}{dt}\Psi_{sA} & u_{rA} &= R_{rA}i_{rA} + \frac{d}{dt}\Psi_{rA} \\
 u_{sB} &= R_{sB}i_{sB} + \frac{d}{dt}\Psi_{sB} & u_{rB} &= R_{rB}i_{rB} + \frac{d}{dt}\Psi_{rB} \\
 u_{sC} &= R_{sC}i_{sC} + \frac{d}{dt}\Psi_{sC} & u_{rC} &= R_{rC}i_{rC} + \frac{d}{dt}\Psi_{rC}
 \end{aligned} \tag{9.16}$$

where values of corresponding fluxes are calculated as

$$\begin{aligned}
 \Psi_{sA} &= L_{sA}i_{sA} + L_m i_{rA} & \Psi_{rA} &= L_{rA}i_{rA} + L_m i_{sA} \\
 \Psi_{sB} &= L_{sB}i_{sB} + L_m i_{rB} & \Psi_{rB} &= L_{rB}i_{rB} + L_m i_{sB} \\
 \Psi_{sC} &= L_{sC}i_{sC} + L_m i_{rC} & \Psi_{rC} &= L_{rC}i_{rC} + L_m i_{sC}
 \end{aligned} \tag{9.17}$$

where  $L_s$  and  $L_r$  are equivalent stator resp. rotor inductances that can be calculated as

$$L_s = L_{sA} + \frac{1}{2}M_s \quad L_r = L_{rA} + \frac{1}{2}M_r \tag{9.18}$$

and equivalent mutual inductance between stator and rotor winding  $L_m$  as

$$L_m = \frac{3}{2} M_{sr} \quad (9.19)$$

(9.16) and (9.17) forms system of 12 equations that need to be solved. In order to simplify the analysis the three phase quantities can be replaced by space vector defined D. The equation (9.5) represents so called Clark transformation (from three phase system into two axis orthogonal system) Fig. E.2. The transformation coefficient  $k_{\alpha\beta}$  has usually value of  $\frac{2}{3}$ , however for modelling of IM are sometimes used other values (see Tab. E.1). This transformation removes magnetic coupling between the inductors  $M_s$  and  $M_r$  in transformed system too.

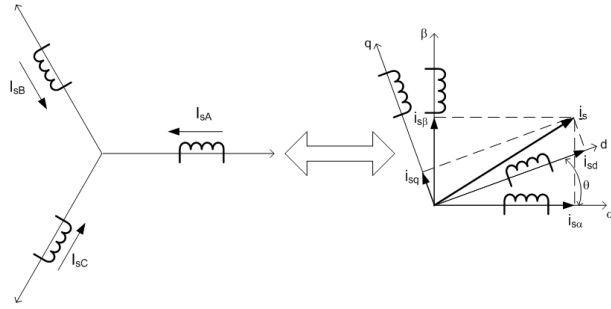


**Figure E.2.** Stator current in three phase / orthogonal system

$k_{\alpha\beta}$	Effect
1	Module of space vector has its physical value ( $\frac{3}{2}$ of phase value amplitude)
$\sqrt{\frac{2}{3}}$	Transformation is power invariant - power values correspond to their physical values
$\frac{2}{3}$	Space vector module has same value as amplitude of variable in $x - axis$ direction

**Table E.1.** Coefficients used in Clark's transformation

The components of the space vector can be then calculated as

$$\begin{aligned} i_{s\alpha} &= \Re(\underline{i}_s) = k_{\alpha\beta} \left( i_{sA} - \frac{1}{2} i_{sB} - \frac{1}{2} i_{sC} \right) = \frac{3}{2} k_{\alpha\beta} i_{sA} \\ i_{s\beta} &= \Im(\underline{i}_s) = \frac{\sqrt{3}}{2} k_{\alpha\beta} (i_{sB} - i_{sC}) \end{aligned} \quad (9.20)$$

If we consider coordinate system rotating with angular speed  $\omega_k$  the components of the space vector in such system can be calculated as

$$\begin{aligned} i_{su} &= i_{s\alpha} \cos \theta_k + i_{s\beta} \sin \theta_k \\ i_{sv} &= -i_{s\alpha} \sin \theta_k + i_{s\beta} \cos \theta_k \end{aligned} \quad (9.21)$$

## E.1 IM Equations in Different Coordinate Systems

3 variants of angular speeds  $\omega_k$  are used. First one is coordinate system connected with stator (stationary) where  $\omega_k = 0$ . This system is noted with  $\alpha, \beta$  coordinates.

$$\begin{aligned}
 u_{s\alpha} &= R_s i_{s\alpha} + \frac{d}{dt} \Psi_{s\alpha} \\
 u_{s\beta} &= R_s i_{s\beta} + \frac{d}{dt} \Psi_{s\beta} \\
 0 = u_{r\alpha} &= R_r i_{r\alpha} + \frac{d}{dt} \Psi_{r\alpha} + \omega_r \Psi_{r\beta} \\
 0 = u_{r\beta} &= R_r i_{r\beta} + \frac{d}{dt} \Psi_{r\beta} - \omega_r \Psi_{r\alpha} \\
 \Psi_{s\alpha} &= L_s i_{s\alpha} + L_m i_{r\alpha} \\
 \Psi_{s\beta} &= L_s i_{s\beta} + L_m i_{r\beta} \\
 \Psi_{r\alpha} &= L_r i_{r\alpha} + L_m i_{s\alpha} \\
 \Psi_{r\beta} &= L_r i_{r\beta} + L_m i_{s\beta}
 \end{aligned} \tag{9.22}$$

Second coordinate system is connected with rotor, therefore rotates with angular speed  $\omega_k = \omega_r$ . This system is noted with  $x, y$  coordinates.

$$\begin{aligned}
 u_{sx} &= R_s i_{sx} + \frac{d}{dt} \Psi_{sx} - \omega_r \Psi_{sy} \\
 u_{sy} &= R_s i_{sy} + \frac{d}{dt} \Psi_{sy} + \omega_r \Psi_{sx} \\
 0 = u_{rx} &= R_r i_{rx} + \frac{d}{dt} \Psi_{rx} \\
 0 = u_{ry} &= R_r i_{ry} + \frac{d}{dt} \Psi_{ry} \\
 \Psi_{sx} &= L_s i_{sx} + L_m i_{rx} \\
 \Psi_{sy} &= L_s i_{sy} + L_m i_{ry} \\
 \Psi_{rx} &= L_r i_{rx} + L_m i_{sx} \\
 \Psi_{ry} &= L_r i_{ry} + L_m i_{sy}
 \end{aligned} \tag{9.23}$$

Third coordinate system is connected with flux space vector, therefore rotates with angular speed  $\omega_k = \omega_s$ . This system is noted with  $d, q$  coordinates.

$$\begin{aligned}
 u_{sd} &= R_s i_{sd} + \frac{d}{dt} \Psi_{sd} - \omega_s \Psi_{sq} \\
 u_{sq} &= R_s i_{sq} + \frac{d}{dt} \Psi_{sq} + \omega_s \Psi_{sd} \\
 0 = u_{rd} &= R_r i_{rd} + \frac{d}{dt} \Psi_{rd} - (\omega_s - \omega_r) \Psi_{rq} \\
 0 = u_{rq} &= R_r i_{rq} + \frac{d}{dt} \Psi_{rq} + (\omega_s - \omega_r) \Psi_{rd} \\
 \Psi_{sd} &= L_s i_{sd} + L_m i_{rd} \\
 \Psi_{sq} &= L_s i_{sq} + L_m i_{rq} \\
 \Psi_{rd} &= L_r i_{rd} + L_m i_{sd} \\
 \Psi_{rq} &= L_r i_{rq} + L_m i_{sq}
 \end{aligned} \tag{9.24}$$



# Appendix F

## List of Author's Publications

### F.1 Publications Related to Thesis

#### F.1.1 Publications in Journals with Impact Factor

- [1] J. Bauer, S. Flígl, and A. Steimel. Design and Dimensioning of Essential Passive Components for the Matrix Converter Prototype. *Automatika*, 53(3):225–235, 8 2012. Contribution **33%**.

#### F.1.2 Publications in Reviewed Journals

- [1] J. Bauer. Development of a Compact Matrix Converter. *Acta Polytechnica*, 49(2):64–69, November 2009. Contribution **100%**.
- [2] J. Bauer. Simulation of a Matrix Converter Fed Drive With Sliding Mode Control. *Acta Polytechnica*, 52(5):8–16, 2012. Contribution **100%**.
- [3] J. Bauer and J. Lettl. Compact Matrix Converter Prototype. *ElectroScope*, 2009(2009):60–64, November 2009. Contribution **50%**.

#### F.1.3 Patents

---

#### F.1.4 Publications Excerpted in Web of Science

- [1] J. Bauer and S. Flígl. Comparison of Fuzzy Logic Based and Sliding Mode Based Controller for IM Drive Fed by Matrix Converter. In *Advances in Intelligent Systems and Computing*, pages 411–420, Heidelberg, 2013. Springer. Contribution **50%**.
- [2] J. Bauer, J. Lettl, and L. Linhart. Comparison of Different Filter Types for Grid Connected Inverter. In *PIERS 2011 Marrakesh Proceedings*, pages 1426–1429, Cambridge, MA, 2011. The Electromagnetics Academy. Contribution **33%**.
- [3] J. Bauer, J. Lettl, L. Linhart, and S. Flígl. Contribution to the Matrix Converter Overmodulation Strategies Based on the Virtual DC-Link Concept. In *Proceedings of the 14th EPE-PEMC Conference 2010*, pages T3–46–T3–52, Skopje, 2010. International Council on Large Electric Systems Macedonian National Committee. Contribution **25%**.
- [4] J. Lettl, S. Flígl, J. Bauer, and S. Ryvkin. Simulation of the Matrix Converter Drive with Sliding Mode Control. In *Proceedings of PIERS 2012*, pages 929–933, Cambridge, 2012. Electromagnetics Academy. Contribution **25%**.
- [5] J. Lettl, D. Kuzmanovič, J. Bauer, and S. Flígl. Possibilities of Control Method Application to Matrix Converter Induction Motor Drive. In *2012 International*

*Conference on Applied Electronics*, pages 171–174, Pilsen, 2012. University of West Bohemia. Contribution **25%**.

- [6] J. Lettl, L. Linhart, and J. Bauer. Matrix Converter Commutation Time Reduction. In *PIERS 2011 Marrakesh Proceedings*, pages 1406–1410, Cambridge, MA, 2011. The Electromagnetics Academy. Contribution **33%**.
- [7] L. Linhart, J. Lettl, and J. Bauer. Matrix Converter Two-Step Commutation Method Limitations. In *Proceedings of the 14th EPE-PEMC Conference 2010*, pages T3–53–T3–58, Skopje, 2010. International Council on Large Electric Systems Macedonian National Committee. Contribution **33%**.

### ■ F.1.5 Other Publications

- [1] J. Bauer and S. Flígl. Comparison of Fuzzy Logic Based and Sliding Mode Based Controller for IM Drive Fed by Matrix Converter. In *Advances in Intelligent Systems and Computing*, pages 411–420, Heidelberg, 2013. Springer. Contribution **50%**.
- [2] J. Bauer, J. Lettl, L. Linhart, and S. Flígl. Contribution to the Matrix Converter Overmodulation Strategies Based on the Virtual DC-Link Concept. In *Proceedings of the 14th EPE-PEMC Conference 2010*, pages T3–46–T3–52, Skopje, 2010. International Council on Large Electric Systems Macedonian National Committee. Contribution **25%**.
- [3] J. Lettl, S. Flígl, J. Bauer, and S. Ryvkin. Simulation of the Matrix Converter Drive with Sliding Mode Control. In *Proceedings of PIERS 2012*, pages 929–933, Cambridge, 2012. Electromagnetics Academy. Contribution **25%**.
- [4] J. Lettl, D. Kuzmanovič, J. Bauer, and S. Flígl. Possibilities of Control Method Application to Matrix Converter Induction Motor Drive. In *2012 International Conference on Applied Electronics*, pages 171–174, Pilsen, 2012. University of West Bohemia. Contribution **25%**.
- [5] J. Lettl, L. Linhart, and J. Bauer. Matrix Converter Commutation Time Reduction. In *PIERS 2011 Marrakesh Proceedings*, pages 1406–1410, Cambridge, MA, 2011. The Electromagnetics Academy. Contribution **33%**.
- [6] L. Linhart, J. Lettl, and J. Bauer. Matrix Converter Two-Step Commutation Method Limitations. In *Proceedings of the 14th EPE-PEMC Conference 2010*, pages T3–53–T3–58, Skopje, 2010. International Council on Large Electric Systems Macedonian National Committee. Contribution **33%**.

## ■ F.2 Other Publications

### ■ F.2.1 Publications in Journals with Impact Factor

- [1] J. Bauer and J. Lettl. Solar Power Station Output Inverter Control Design. *Radioengineering*, 20(1):258–262, duben 2011. Contribution **80%**.
- [2] J. Sláma, J. Bauer, S. Flígl, and V. Kříha. Active Control of Atmospheric Pressure Discharges. *Problems of Atomic Science and Technology. Series: Plasma Physics*, 83(1):246–248, 2013. Contribution **25%**.

## ■ F.2.2 Publications in Reviewed Journals

- [1] J. Bauer. Single-Phase Pulse Width Modulated Rectifier. *Acta Polytechnica*, 48(3/2008):84–87, říjen 2008. Contribution **100%**.
- [2] J. Bauer. Single Phase Voltage Source Inverter Photovoltaic Application. *Acta Polytechnica*, 50(4/2010):7–11, 2010. Contribution **100%**.
- [3] J. Bauer. Simulation of a Matrix Converter Fed Drive With Sliding Mode Control. *Acta Polytechnica*, 52(5):8–16, 2012. Contribution **100%**.
- [4] J. Bauer, J. Lettl, P. Pichlík, and J. Zděnek. Low Power Photovoltaic Converter Control and Development. *Transaction on Electrical Engineering*, 1(3):80–85, 2012. Contribution **25%**.
- [5] J. Zděnek, J. Lettl, and J. Bauer. Structured System and Software Design of Distributed Control Computer of Mechatronic Facility for Space Research. *Transaction on Electrical Engineering*, 1(2):60–65, 2012. Contribution **33%**.

## ■ F.2.3 Patents

---

## ■ F.2.4 Publications Excerpted in Web of Science

- [1] J. Bauer, S. Flígl, M. Vlček, and J. Lettl. Comparison of Alternative Equivalent Circuits of Induction Motor. In *Proceedings of the 13th International Scientific Conference EPE 2012*, pages 1081–1086, Brno, 2012. Vysoké učení technické v Brně, Fakulta elektrotechniky a komunikačních technologií. Contribution **25%**.
- [2] S. Flígl, J. Bauer, and J. Lettl. Analytical Derivation of Induction Machine Efficiency Map. In *Proceedings of 2013 fourth international conference International Conference on Power Engineering, Energy and Electrical Drives (POWERENG2013)*, pages –, Red Hook, 2013. Curran Associates, Inc. Contribution **33%**.
- [3] S. Flígl, J. Bauer, J. Lettl, and S. Ryvkin. Reduced State Space Induction Motor Analysis. In *Proceedings of the 13th International Scientific Conference EPE 2012*, pages 1087–1092, Brno, 2012. Vysoké učení technické v Brně, Fakulta elektrotechniky a komunikačních technologií. Contribution **25%**.
- [4] J. Lettl and J. Bauer. Compatibility of Different Types of Frequency Converters with Supply Network. In *Proceedings of PIERS 2010 in Cambridge*, pages –, Cambridge, MA, 2010. The Electromagnetics Academy. Contribution **50%**.
- [5] J. Lettl, S. Flígl, J. Bauer, and M. Vlček. Comparison of Gamma and T Models for Converter Controlled Induction Machine Drives. In *Proceedings of PIERS 2012*, pages 925–928, Cambridge, 2012. Electromagnetics Academy. Contribution **25%**.

## ■ F.2.5 Other Publications

- [1] J. Bauer. Single-Phase Pulse Width Modulated Rectifier. In *Poster 2008*, pages –, Prague, 2008. CTU, Faculty of Electrical Engineering. Contribution **100%**.
- [2] J. Bauer. Single Phase Voltage Source Inverter Photovoltaic Application. In *POSTER 2010 - Proceedings of the 14th International Conference on Electrical Engineering*, pages –, Praha, 2010. ČVUT v Praze, FEL. Contribution **100%**.

- [3] J. Bauer, T. Haubert, S. Flígl, and J. Lettl. Mapa účinnosti asynchronního motoru - analytické odvození. In *XXXIII. celostátní konference o elektrických pohonech*, pages –, 2013. Contribution **25%**.
- [4] J. Bauer, P. Karlovský, and J. Lettl. Analysis of the Influence of the Rotor Losses on the IM Control. In *XX. International Symposium on Electric Machinery In Prague*, pages 6–10, Prague, 2013. CTU, Faculty of Electrical Engineering, Department of Electric Drives and Traction. Contribution **33%**.
- [5] J. Bauer and J. Koupený. Simulation of the Drive with the Permanent Magnet Synchronous Motor. In *POSTER 2011 - 15th International Student Conference on Electrical Engineering*, pages 1–5, Prague, 2011. CTU, Faculty of Electrical Engineering. Contribution **50%**.
- [6] J. Bauer, J. Koupený, and J. Lettl. Permanent Magnet Synchronous Drive Vector Control Modeling. In *XIX. International Symposium On Electric Machinery In Prague*, pages 45–50, Prague, 2011. CTU, Faculty of Electrical Engineering, Department of Electric Drives and Traction. Contribution **33%**.
- [7] J. Bauer and J. Lettl. EMC Comparison Of Controlled Rectifiers and PWM Rectifiers. In *Sborník konference ELEN 2008*, pages –, Prague, 2008. CTU, Faculty of Electrical Engineering, Department of Electroenergetics. Contribution **50%**.
- [8] J. Bauer and J. Lettl. PWM Rectifier Realization. In *Electronics Devices and Systems Proceedings*, pages 472–477, Brno, 2008. Vysoké učení technické v Brně. Contribution **50%**.
- [9] J. Bauer and J. Lettl. Design of Inverter for Photovoltaic Application. In *EDS 2010 Electronic Devices and Systems*, pages 16–23, Brno, 2010. VUT v Brně, FEL, Ústav mikroelektroniky. Contribution **50%**.
- [10] J. Bauer and J. Lettl. Possibilities of frequency converter side effects on the supply network reduction. In *XVIII. International Symposium on Electric Machinery in Prague*, pages –, Prague, 2010. CTU, Faculty of Electrical Engineering, Department of Electric Drives and Traction. Contribution **50%**.
- [11] J. Bauer and J. Lettl. Simulace střídače malého výkonu pro solární panel. In *Sborník z XXXII. celostátní konference o elektrických pohonech*, pages 166–171, Praha, 2011. Česká elektrotechnická společnost. Contribution **50%**.
- [12] J. Bauer, J. Lettl, M. Bednář, and L. Linhart. PWM Rectifier Control Algorithm. In *TRANSCOM 2009*, pages 17–20, Žilina, 2009. Technical University of Žilina. Contribution **25%**.
- [13] J. Bauer, J. Lettl, and P. Pichlík. Problematics of the High Compatible Semiconductor Power Converters. In *Workshop 2011, CTU Student Grant Competition in 2010 (SGS 2010)*, pages –, Praha, 2011. ČVTVS. Contribution **33%**.
- [14] J. Bauer, J. Lettl, and P. Pošta. Řízení usměrňovače s pulzně šířkovou modulací. In *XXXI. celostátní konference o elektrických pohonech*, pages –, Praha, 2009. Česká elektrotechnická společnost. Contribution **33%**.
- [15] J. Bauer, L. Linhart, P. Pošta, and J. Lettl. Experimental Results Measured on PWM Rectifier and their Comparison with Thyristor Rectifier. In *Workshop 09 CTU REPORTS*, pages 284–285, Prague, 2009. CTU. Contribution **25%**.
- [16] J. Bauer, J. Zděnek, and J. Lettl. Photovoltaic Inverter Control and Development. In *Proceedings of EDPE 2011*, pages 1–6, Košice, 2011. Technická univerzita

Košice, Fakulta elektrotechniky a informatiky, Katedra počítačů a informatiky. Contribution **33%**.

- [17] J. Bradna, J. Bauer, S. Flígl, and V. Hlinovský. Comparison of Alternative Equivalent Circuits of Induction Motor with Real Machine Data. In *Advances in Mechanisms Design*, pages 13–19, Heidelberg, 2012. Springer. Contribution **25%**.
- [18] S. Flígl, J. Bauer, and J. Lettl. Analytical Derivation of Induction Machine Efficiency Map. In *Proceedings of 2013 fourth international conference International Conference on Power Engineering, Energy and Electrical Drives (POWERENG2013)*, pages –, Red Hook, 2013. Curran Associates, Inc. Contribution **33%**.
- [19] S. Flígl, J. Bauer, M. Vlček, and J. Lettl. Analysis of induction machine T and G circuit coequality for use in electric drive controllers. In *Book of Abstracts of the 13th Conference on Optimization of Electrical and Electronic Equipment*, pages 659–664, Brasov, 2012. Transilvania University of Brasov. Contribution **25%**.
- [20] T. Haubert, J. Bauer, and P. Mindl. Using of dSpace DS1103 for Electric Vehicle Power Consumption Modeling. In *21th Annual Conference Proceedings Technical Computing Prague 2013*, page 24, Prague, 2013. HUMUSOFT. Contribution **33%**.
- [21] V. Hlinovský, T. Haubert, and J. Bauer. Automatizovaný PXI systém pro měření parametrů náhradního schématu asynchronního motoru použitelných v matematických modelech. In *XXXIII. celostátní konference o elektrických pohonech*, pages –, 2013. Contribution **33%**.
- [22] J. Lettl and J. Bauer. Measured Properties of Realized PWM Rectifier. In *XVI. International Symposium On Electric Machinery In Prague*, pages 178–184, Prague, 2008. CTU, Faculty of Electrical Engineering, Department of Electric Drives and Traction. Contribution **50%**.
- [23] J. Lettl and J. Bauer. Filter Design for Photovoltaic Application with Voltage Source Inverter. In *Sborník konference ELEN 2010*, pages –, Prague, 2010. CTU, Faculty of Electrical Engineering, Department of Electroenergetics. Contribution **50%**.
- [24] J. Lettl, S. Flígl, and J. Bauer. Comparison of DTC and Sliding Mode Control of IM Drive. In *PIERS 2013 Taipei Proceedings*, pages –, Cambridge, 2013. Electromagnetics Academy. Contribution **33%**.

## F.3 Responses to Published Works

Citation of F.1.4 [2] in [2] and F.2.4 [4] in [1]

- [1] Pavel Koblík and Jiri Pavelka. Possibility of MV Multilevel Inverter Use as Active Filter. In *2012 IEEE INTERNATIONAL SYMPOSIUM ON INDUSTRIAL ELECTRONICS (ISIE)*, pages 1052–1057, 2012. 21st IEEE International Symposium on Industrial Electronics (ISIE), Hangzhou, PEOPLES R CHINA, MAY 28-31, 2012.
- [2] Tuan Ngo and Surya Santoso. Grid-connected photovoltaic converters: Topology and grid interconnection. *JOURNAL OF RENEWABLE AND SUSTAINABLE ENERGY*, 6(3), MAY 2014.



# Appendix G

## CV



### Curriculum Vitae

#### PERSONAL INFORMATION

Name Jan Bauer  
Address Masarykova 205, 250 88, Čelákovice  
Telephone **+420606789553**  
Fax  
E-mail [bauerja2@fel.cvut.cz](mailto:bauerja2@fel.cvut.cz)

Nationality Czech Republic

Date of birth 14.1.1983

#### WORK EXPERIENCE

- Dates (from – to) 2008- present
- Name and address of employer Faculty of Electrical Engineering, Czech Technical University in Prague, Department of Electric Drives and Traction
  - Main activities and responsibilities assistant professor
- Dates (from – to) 10/2013- 12/2013
- Name and address of employer Mongolian University of Science and Technology, School of Power Engineering
  - Main activities and responsibilities hosting lecturer
- Dates (from – to) 2001 – 2006
- Name and address of employer Blumenbecker Prag s.r.o.
  - Main activities and responsibilities auxiliary technical work – AutoCAD

**EDUCATION AND TRAINING**

Dates (from – to)	9/2007 – present
• Name and type of organisation providing education and training	<i>Faculty of Electrical Engineering, Czech Technical University in Prague, study program Electrical Machines, Apparatuses and Drives – PhD study program</i>
Dates (from – to)	6/2007
	<b>ING. degree</b> <i>Faculty of Electrical Engineering, Czech Technical University in Prague, study program Electrical Machines, Apparatuses and Drives</i>
Dates (from – to)	10/2005 – 9/2006
• Name and type of organisation providing education and training	<i>Electrical Engineering and Computer Science, Leibnitz University of Hannover, Germany</i> Erasmus student in master program
Dates (from – to)	10/2001- 6/2007
• Name and type of organisation providing education and training	<i>Faculty of Electrical Engineering, Czech Technical University in Prague, study program Electrical Machines, Apparatuses and Drives – Ing. study program</i>
Dates (from – to)	1993 – 2001
• Name and type of organisation providing education and training	<i>Grammar school Karla Sladkovského, Prague</i> Final examination in: Czech language and literature, English language, Mathematics, Physics

<p><b>PERSONAL SKILLS AND COMPETENCES</b>  <i>Acquired in the course of life and career but not necessarily covered by formal certificates and diplomas.</i></p>	
MOTHER TONGUE	<b>Czech language</b>
OTHER LANGUAGES	
<ul style="list-style-type: none"> <li>• Reading skills</li> <li>• Writing skills</li> <li>• Verbal skills</li> </ul>	<p><b>English language</b>            Fluent            Intermediate            Advance</p>
<ul style="list-style-type: none"> <li>• Reading skills</li> <li>• Writing skills</li> <li>• Verbal skills</li> </ul>	<p><b>German Language</b>            Intermediate            Intermediate            Advance</p>
<p><b>ORGANISATIONAL SKILLS AND COMPETENCES</b>  <i>Coordination and administration of people, projects and budgets; at work, in voluntary work (for example culture and sports) and at home, etc.</i></p>	<p>one year as rowing trainer            leader of youth summer camps</p>
<p><b>TECHNICAL SKILLS AND COMPETENCES</b>  <i>With computers, specific kinds of equipment, machinery, etc.</i></p>	<p>AutoCAD, OrCAD, MatLab, Simulink, Plecs, VHDL, C, EAGLE            Pascal, Basic, Html, Asembler            MS Office – Word, Excel, Powerpoint, Visio</p>
<p><b>HOBBIES AND INTERESSTS</b></p>	<p>rowing, cycling</p>
<p><b>OTHER SKILLS AND COMPETENCES</b>  <i>Competences not mentioned above.</i></p>	<p>willingness to learn new things            an ability to quick learn and adapt to new process</p>
DRIVING LICENCE(S)	B

**PUBLICATIONS AND RESEARCH  
ACTIVITIES**

Papers in journals with IF: 3  
Papers in other journals: 5  
Conference papers: > 30

supervisor of 3 diploma and 8 bachelor theses  
solver of 3 internal university grants

**5 MOST IMPORTANT PAPERS**

- [1] Lettl, J., Bauer, J.: Compatibility of Different Types of Frequency Converters with Supply Network. Progress in Electromagnetics Research Symposium PIERS 2010 Proceedings, pp. 434-438, July 05-08, 2010, Cambridge, MA, USA.
- [2] Bauer, J., Lettl, J.: Solar Power Station Output Inverter Control Design. Radioengineering, Volume 20, Issue 1, pp. 258-262, April 2011.
- [3] Slama, J; Bauer, J; Fligl, S; Kriha, V: ACTIVE CONTROL OF ATMOSPHERIC PRESSURE DISCHARGES, PROBLEMS OF ATOMIC SCIENCE AND TECHNOLOGY Issue: 1 Pages: 246-248 Published: 2013
- [4] Bauer, Jan; Fligl, Stanislav: Comparison of Fuzzy Logic Based and Sliding Mode Based Controller for IM Drive Fed by Matrix Converter, Conference: 7th Int Conf on Soft Comp Models in Industrial and Environm Applications/5th Computational Intelligence in Security for Information Syst/3rd Int Conf on EUropean Transnational Educ Location: Ostrava, CZECH REPUBLIC Date: SEP 05-07, 2012
- [5] Bauer, Jan; Fligl, Stanislav; Steimel, Andreas Design and Dimensioning of Essential Passive Components for the Matrix Converter Prototype, AUTOMATIKA Volume: 53 Issue: 3 Pages: 225-235 DOI: 10.7305/automatika.53-3.134 Published: JUL-SEP 2012

**COOPERATION ON RESEARCH PROJECTS**

- [1] Research and development of progressive technologies for electric drives (TAČR ALFA - TA01011408, 01/2011 - 12/2014) – member of the team
- [2] Problematics of compatibility of semiconductor power converters (CTU internal grant, 2010)
- [3] Control of the IM drive fed by Matrix converter (CTU internal grant, 2011)

Date: 25.9. 2013

Signature: 